The deviatoric behaviour of peat: a route between past empiricism and future perspectives

Muraro, Stefano

DOI
10.4233/uuid:ffbea4e0-2e97-4d41-819d-beec42120b29

Publication date
2019

Document Version
Final published version

Citation (APA)
Muraro, S. (2019). *The deviatoric behaviour of peat: a route between past empiricism and future perspectives*. [Dissertation (TU Delft), Delft University of Technology]. https://doi.org/10.4233/uuid:ffbea4e0-2e97-4d41-819d-beec42120b29

The deviatoric behaviour of peat: a route between past empiricism and future perspectives

The deviatoric behaviour of peat: a route between past empiricism and future perspectives

Dissertation

for the purpose of obtaining the degree of doctor
at Delft University of Technology
by the authority of the Rector Magnificus prof. dr ir. T. H. J. J. van der Hagen
chair of the Board for Doctorates
to be defended publicly on
Wednesday 27 February 2019 at 17:30 o'clock

by

Stefano MURARO

Master Degree in Environmental and Land Engineering,
Università degli Studi di Trento, Trento, Italy,
born in Marostica, Italy

This dissertation has been approved by the promotor.

Composition of the doctoral committee:

Rector Magnificus,	chairperson
Prof. dr. C. Jommi,	Delft University of Technology, promotor

Independent members:

Prof. dr. F. Cotecchia,	Politecnico di Bari
Prof. dr. A. Gens,	Universitat Politècnica de Catalunya
Dr. V. Magnanimo,	University of Twente
Ir. H. van Hemert,	Rijkswaterstaat, STOWA
Prof. dr. K. Gavin,	Delft University of Technology
Prof. dr. M. Hicks,	Delft University of Technology

Keywords: Organic soils, peats, field stress-test, laboratory tests, constitutive modelling, numerical modelling, kinematic compatibility, end restraint.

Printed by: Ipskamp Printing

Front: Micrograph of the tested peat fabric from polarised microscopy.

ISBN 978-94-028-1389-0

An electronic version of this dissertation is available at
http://repository.tudelft.nl/.

dedicated to whom it may concern

Contents

Preface

"Any physical theory is always provisional, in the sense that it is only a hypothesis: you can never prove it. No matter how many times the results of experiments agree with some theory, you can never be sure that the next time the result will not contradict the theory. On the other hand, you can disprove a theory by finding even a single observation that disagrees with the predictions of the theory. As philosopher of science Karl Popper has emphasized, a good theory is characterized by the fact that it makes a number of predictions that could in principle be disproved or falsified by observation. Each time new experiments are observed to agree with the predictions the theory survives, and our confidence in it is increased; but if ever a new observation is found to disagree, we have to abandon or modify the theory. At least that is what is supposed to happen, but you can always question the competence of the person who carried out the observation."

Professor Stephen Hawking

Stefano MURARO
Delft, February 2019

1

Introduction

1

1.1. Problem statement

Transport and flood defence infrastructure are crucial assets for the mobility and the safety of people. A relevant part of these geotechnical infrastructure in Europe and overseas, especially in the northern hemisphere, are built on soft organic soils, including a variety of soft organic clays, estuarine sediments deposits and peats. Within the European context, the Netherlands is maybe the most important country where soft soils commonly serve as foundation layers. Flood protection is assured by a vast system of primary and secondary dykes, of which 14000 km are regional dykes. Most of these dykes lie on extensive deposits of peat, organic clay and silt. Of these, 7000 km of dykes may suffer from excessive settlements and shear deformations, including 3500 km that are estimated to be constructed purely of peat. The social and economic relevance of this problem is dramatic. Every five years, the entire dykes system needs to be re-assessed to assure the required safety standard and around 1 billion euros are invested every year to maintain, repair and upgrade the Dutch dykes network.

The assessment of these dykes is not straightforward, especially due to the lack of adequate geotechnical knowledge of the behaviour of peats at the engineering scale, which represents one of the greatest concerns that public water authorities and geotechnical engineers are currently facing. Water content up to 800%-900%, organic content of 80%-90%, low unit weight around 10 kN/m^3, multiple levels of fibrous structures, time dependent behaviour and bio-degradation of the organic fraction with production of bio-genic gas are the characteristics that make peat a rather unique soil. Particularly challenging is the deviatoric behaviour of peat. Contrasting results and knowledge gaps still remain first in interpreting, and secondly in modelling, field and laboratory stress-strain response of peats upon deviatoric loads. Lack of systematic studies in this direction, increases the knowledge uncertainties on the short-term performance and the long-term durability of earth embankments.

Laboratory tests on the one side and field stress-tests on the other, seem to provide a rather diverging picture of the shear strength of peat. Contrarily to the common statement that "peat is a weak soil", exceptional shear strength parameters as friction angles in the range of 50°-70° were found in the laboratory by many researchers (Adams, 1961; Oikawa & Miyakawa, 1980; Landva & La Rochelle, 1983; Yamaguchi et al., 1985b; Cola & Cortellazzo, 2005; Cheng et al., 2007; Hendry et al., 2012; O'Kelly, 2017). On the contrary, recent field stress-tests on both existing and trial embankments on peats, suggested a much lower mobilised shear strength at failure (Rowe et al., 1984; Zwanenburg et al., 2012; Zwanenburg & Jardine, 2015). This discrepancy contributed to generate diffuse prejudices towards traditional experimental tests on peats such as triaxial tests. Hence, severe overly conservative approaches dominate the current engineering practice where high material reduction factors are adopted, resulting in inevitable high costs for maintenance (€100K/km per year) and reinforcement (€8M/km per year).

As suggested by numerous authors, the exceptional friction angles obtained in standard undrained triaxial compression tests on peat derive to the additional reinforcement offered by the fibrous inclusions in the peat fabric (Landva & La Rochelle,

1983; Yamaguchi et al., 1985b; Cola & Cortellazzo, 2005; Hendry et al., 2012). Uncertainties on the magnitude of this contribution when passing from the laboratory scale to the field scale lead to the conclusion that ring shear and direct shear are more reliable to determine the shear strength of peat by limiting the fibres stretching (Farrell & Hebib, 1998). On this base, the simple shear apparatus has been recently re-introduced in the current practice in the Netherlands (Zwanenburg et al., 2012). The current assessment procedure for dykes on peat are based on ultimate limit states, in spite of the fact that in many geotechnical applications where peats are encountered serviceability limit states should be the major concern. The well-known limitations of the direct shear and simple shear apparatuses (Wood et al., 1979; Budhu, 1988) preclude the access to the complete state of stresses and strains of the soil, hence limiting the knowledge on the pre-failure behaviour and a rational development of constitutive models. These considerations call for the necessity of re-evaluating the applicability of triaxial tests on peats.

To evaluate the representativeness of different shear apparatuses for peats, a consortium composed by STOWA, Dutch waterboards and provinces, proposed to set up a full scale breach test on a regional historical dyke in the Netherlands. The test was designed by TU Delft within the project Reliable Dykes. The results from the stress-test suggest that the pre-failure response of peat is extremely important in the overall behaviour of the dyke system and that the mobilised shear strength of peat at failure is lower than the value attainable from laboratory tests. Field observations also reveal the presence of gas bubbles released systematically from the peat foundation layer which raise concerns about their potential impact on the peat response both in terms of deformability and shear strength.

This investigation aims to advance the current knowledge of the deviatoric behaviour of peats, including pre-failure and failure, by means of a holistic research approach including observation on the field stress-test, laboratory testing and simple constitutive modelling. The field stress-test on a historical rural dyke on peat at the Leendert de Boerspolder site is the starting point. The role played by the peat layer in the pre-failure and failure mechanisms is analysed, and the result confirms that peat is a deformable soil, but not a weak soil. The high deformability of the peat layer turns to play a fundamental role in relation with the kinematic compatibility of the deformations with adjacent soil layers.

From the field observations, the attention is then transferred to the laboratory scale to characterise the failure and the pre-failure stress-strain response. Current concerns on triaxial tests on peats are thoroughly tackled to avoid misconceptions on the applicability of the results. To the author's opinion, before asserting the drawbacks that any shear apparatus inevitably has, a basic but fundamental question must be answered: is the observed behaviour from the laboratory test the true material response? Attempts of discerning the material behaviour from the sample behaviour are pursued by clarifying the dramatic influence of end restraint on the shear strength (i.e. ultimate limit state) and on the plastic deformation mechanism of peats (i.e. serviceability limit states). The experimental research focuses on reconstituted peat samples in an attempt to reveal the fundamental behaviour

of peat by limiting the influence of natural variability on the observed response, and excludes the big fibrous inclusions sometimes included in undisturbed peat samples. Few other isolated contributions on reconstituted peats can be found in the literature (Ogino et al., 2002; Cola & Cortellazzo, 2005; Komatsu et al., 2011; O'Kelly & Zhang, 2013). However, they concentrated on shear strength and did not analyse in detail the pre-failure deviatoric behaviour. To minimise the differences in the stress-strain response coming from the rate dependency of peat, uniform axial strain rate is adopted in each test series. Possible time dependent effects are verified to be negligible on the main conclusions of the study.

The experimental observations are assisted by the development of a simple elastic-plastic modelling approach for the deviatoric behaviour of fully saturated peats, which is implemented in a Finite Element code. The development of the constitutive model follows a hierarchical approach, where each constitutive ingredient is derived from direct experimental evidence. The model capabilities are tested against experimental tests modelled as a boundary value problem. Good qualitative and quantitative agreement with the experimental results is found for a wide range of deviatoric strains up to 20%. However, the model adopted shows limitations, which are eventually discussed. To elevate the model capabilities to a predictive level, further ingredients must be included. The experimental results show relevant fabric effects which introduce a directional response in the plastic deformation mechanism, and an additional contribution to shear strength at high deviatoric strain levels. To translate this experimental evidence into the proposed constitutive model, ingredients as induced anisotropy and matrix-fibres interaction should be introduced. Rate dependency can also be easily introduced in the proposed model within the framework of visco-elasto-plasticity.

Starting from the field observation of gas bubbles in the peat foundation layer at the Leendert de Boerspolder dyke, the thesis concludes with an experimental attempt to quantify for the first time the implications of biogenic gas bubbles on the mechanical behaviour of peats serving as foundation layer for dykes and embankments. The results show the potential effects on serviceability limit states, with gas exsolution and expansion increasing the compressibility of the soil skeleton and of the pore fluid. The presence of gas becomes also extremely relevant during shear, with the compressibility of the gas phase reducing the mobilised shear strength for given axial strain levels. The effects appear to become dramatic at low total stresses, which is often the case for peat foundation layers, and suggest that the influence of gas bubbles should not be disregarded.

1.2. Research objectives

The key objectives of this thesis are as follows:

- Describe the pre-failure and the failure mechanism of a rural dyke on peat. Special attention is given to identify the triggering mechanism and the role of kinematic compatibility between the different soil layers;
- Characterise the shear strength of peat by ruling out the misconceptions introduced by the end restraint effect in standard undrained triaxial tests;
- Examine the implications of end restraint on the definition of the stress-dilatancy rule of peat from drained compression tests;
- Propose a simple constitutive model for the deviatoric behaviour of peat based on the previous experimental data;
- Assess the implications of gas bubbles in the geotechnical response of foundation peat layers on both serviceability and ultimate limit states.

1.3. Thesis organisation

The thesis organisation reflects the ambition to have chapters as self-consistent pieces of work, which could be eventually translated into research papers.

Chapter 2 presents the field stress-test at the Leendert de Boerspolder historical dyke where the pre-failure and failure mechanisms are reconstructed from the field measurements.
Chapter 3 analyses the results of the experimental investigation on the end restraint effect on the shear strength of reconstituted peat in undrained triaxial compression tests.
Chapter 4 reports a numerical and experimental approach to quantify the impact of end restraint on the plastic deformation mode of reconstituted peat samples and the consequences in terms of constitutive stress-dilatancy rule (paper accepted for publication on Canadian Geotechnical Journal).
Chapter 5 introduces a simple constitutive model based on the previous experimental results for the deviatoric behaviour of peat.
Chapter 6 reports an experimental comparison between natural and reconstituted peat samples from undrained triaxial compression tests. A simple constitutive approach to model natural peat as a fibres-reinforced soil is also derived at the element scale.
Chapter 7 summarises the first experimental attempt to quantify the geotechnical impact of gas bubbles in the pre-failure and failure response of foundation peat layers (paper accepted for publication on Géotechnique).
Chapter 8 summarises the conclusions and the recommendations of this work.

Two appendixes complete this work. Appendix A reports the first attempt to adapt an existing hypoplastic model to reproduce the experimental results on peat, at the

1

element scale. The results reveal the merits of hypoplasticity to model the non-linearity of the pre-failure behaviour and the directional response of peats, which are of great importance when assessing the serviceability limit states of geotechnical structures founded on peats. (The content of this appendix has been published as a research paper on the International Journal for Numerical and Analytical Methods in Geomechanics). Eventually, appendix B reports the calibration of the triaxial apparatus used in the experimental campaign.

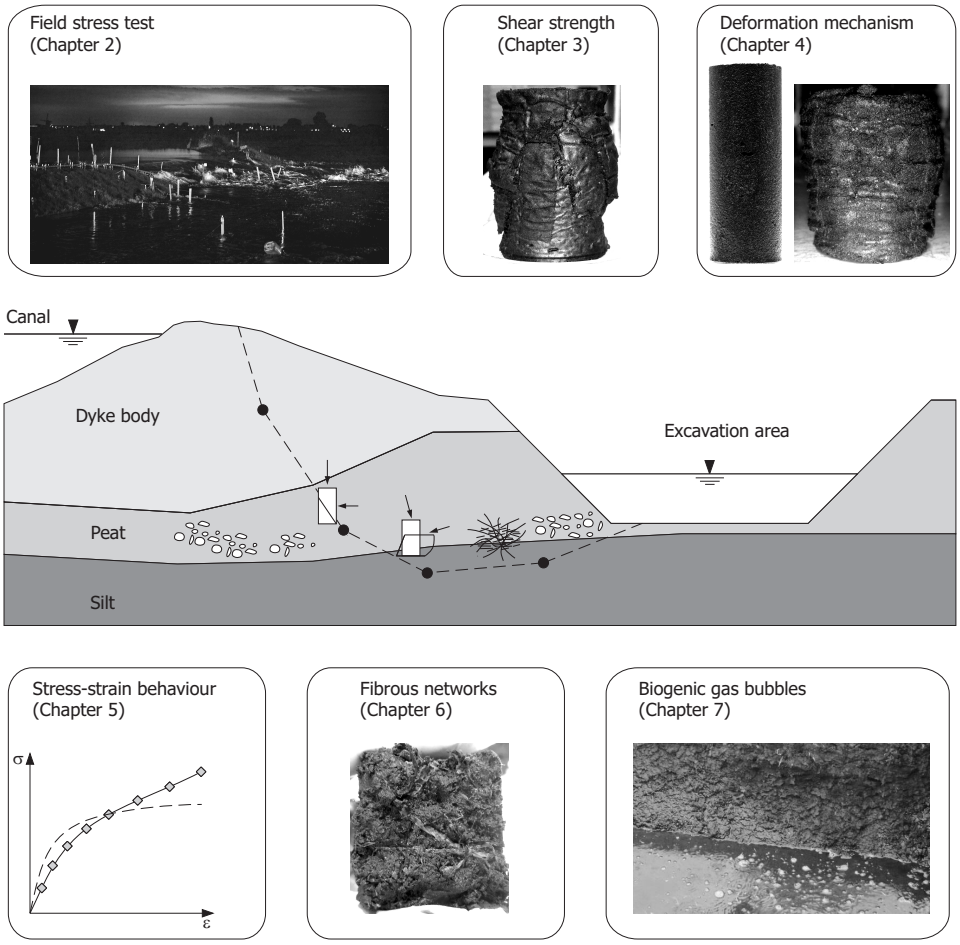

Figure 1.1: Illustrative organisation of the thesis

2

Failure of the Leendert de Boerspolder rural dyke: revealing the role of peat

Siempre adelante, ni un paso atrás y lo que fuere menester sea.

Carlos Fernando Galán

Thanks are due to Tom de Gast, who manged the design of the stress test in the field as part of his PhD research (de Gast, 2019), and for providing the photographs in Figure 2.7, 2.8, 2.9. Figure 2.1 is reported by courtesy of Hoogheemraadschap van Rijnland (https://www.rijnland.net/).

2.1. ABSTRACT

A historical 500 years old rural dyke on peat was brought to failure in the Netherlands. The test had a twofold scope to describe the role of each soil formation in the failure mechanism and to assess the existing approaches used in the assessment of regional dykes in the Netherlands. The failure mechanism occurred as a progressive failure, with significant outward bulging of the peat at the toe, followed by a global lateral displacement and sinking of the crest of the dyke. Contrarily to the common expectation, failure was not triggered in the peat but in the organic silt formation underneath. However, the large deformability of peat represented the trigger for the inception of failure. The kinematic compatibility between the peat and the silt restricted the shear strains at failure at 5%, well below the attainable strains to mobilise the ultimate shear strength of peat. The results of this test call for the necessity of describing the pre-failure behaviour of peats often neglected in the current practice.

2.2. INTRODUCTION

More than half of the Netherlands lies below the sea and the rivers level. The protection against flooding is assured by multiple levels of dykes and embankments: 3200 km of primary dykes and 14000 km of secondary dykes protect the country from the sea and from the inner water. Every five years, the entire dykes system needs to be re-assessed to assure the required safety standard. Despite the considerable advances in investments, knowledge and technology (monitoring systems and early warning systems), occasional dykes failures cannot be excluded a priori (Van Baars, 2005; Van Meindert et al., 2008). Concerns about dykes stability in the Netherlands have led in the recent years to a series of field stress-tests both on existing and trial embankments (Koelewijn et al., 2014; Zwanenburg et al., 2012; Zwanenburg & Jardine, 2015). These tests aimed to reduce the discrepancy between the shear strength actually mobilised in the field during failure and the one assumed in design and assessment procedures. Among the foundation layers, particularly critical is the behaviour of peat, which often serves as foundation layer for many dykes in the Netherlands (Den Haan & Kruse, 2007); 7000 km of dykes have peat-related issues, including 3500 km that are estimated to be constructed purely of peat. Several difficulties arise from the peculiar characteristics of this material, such as exceptional water content up to 800%-900% and organic content 80%-90%, multiple levels of fibrous structures, time dependent behaviour and biodegradation of the organic fraction with generation of bio-genic gas bubbles (Jommi et al., 2017).

Extensive experimental research on the shear strength of peat already elucidated its frictional nature, with high friction angles, 50°-70°, and small apparent intercept cohesion (Adams, 1961; Oikawa & Miyakawa, 1980; Yamaguchi et al., 1985b; Cheng et al., 2007). The presence of multiple fibrous networks not entirely decomposed within the peat fabric is recognised to provide additional reinforcement to the material, especially at the laboratory scale (Landva & La Rochelle, 1983; Cola & Cortellazzo, 2005). However, the adoption of such high shear strength parameters leads to unrealistic factor of safety in many geotechnical applications, with potential unsafe situations for both serviceability and ultimate limit states. As a result, in common engineering practice high material reduction factors are often applied, which on the contrary, introduce severe overly conservative approaches with high economic and social costs. This over-conservatism contrasts with the actual performances of the vast majority of these dykes, self-standing for many decades or centuries.

Previous stress-tests on trial embankments on peat indicated a typical failure mode showing a combined mechanism of vertical settlement and rotation of the crest of the dykes (active side) and horizontal sliding of the peat at the toe (shear section). In details, vertical and sub-vertical cracks were observed within the dyke body. Squeeze of the embankment filling inside the foundation layers (punching mechanism at early stage) caused horizontal displacement of the peat layers at the toe with a sliding plane at the contact between the peat and the underlying layer (Zwanenburg et al., 2012). In the vast majority of the previous field stress-tests, failure was induced by increasing the vertical load on the crest and/or by excavating

the toe of the dyke, thus reducing the horizontal stabilising force. With the intent of increasing the unit weight of the embankment filling, artificial increase of pore pressure inside the dyke body was also adopted.

Successful attempts of back-analysing the previous field tests by means of Finite Element Analysis are reported in the literature. However, uncertainties about the most appropriate laboratory test to obtain reliable shear strength parameters for peat remain. Good agreement between the observed and the predicted behaviour was obtained by Den Haan & Feddema (2013) and Tashiro et al. (2015), by adopting shear strength parameters from undrained triaxial compression tests (TxCU). On the contrary, Rowe et al. (1984) and Zwanenburg et al. (2012) found that peak shear strength derived from triaxial compression tests overestimate the mobilised strength along the sliding plane in peat. Therefore, they suggested the adoption of direct shear (DS) and direct simple shear (DSS) tests for reproducing the field observations.

Without entering in this debate, it is worth mentioning that for many earth structures on soft soils, design and assessment criteria are often ruled by serviceability limit states rather than ultimate limit states. This implies the necessity of taking into account not only the failure but also and especially the pre-failure behaviour of the soil layers and the kinematic compatibility between them. The high deviatoric strain levels attained in the laboratory tests by peat samples before reaching failure (20%-30% Tsushima & Mitachi (1985) and O'Kelly & Zhang (2013)), are well above the strains at the onset of failure for the other foundation layers. As a result even if in the last decades, many efforts have been devoted to identify the shear strength of peats with different shear apparatuses, it seems still complicate to estimate the true resistance of existing dykes as whole geotechnical structures.

Within this context, this contribution describes the most recent failure test conducted in the Netherlands on an existing historical regional dyke at the Leendert de Boerspolder site, a small polder located in the Kagerplassen south of the Haarlemmermeer (Figure 2.1).

Figure 2.1: View of the Leendert de Boerspolder dyke before the start of the failure test (September 2015)

The area was designated to become a natural reserve as a compensation measurement for land reclamation. To this mean, the area had to undergo controlled flooding, and STOWA, the foundation for research on regional dykes in the Netherlands, together with TU Delft decided to exploit the opportunity to perform a unique failure test on a historical dyke. The test was used to assess the existing approaches used in the assessment of regional dykes in the Netherlands. The description of the assumptions and the procedures adopted in the design of the failure test are not reported herein. On the contrary, in the following pages, the attention is given to reconstruct the pre-failure and failure mechanism by combining multiple measurements from the field instrumentation and the laboratory tests. The role of each foundation layer is clarified in the attempt to identify the critical aspects of each soil formation.

2.3. SUBSOIL PROPERTIES

An extensive in-situ investigation programme was performed to characterise the soils layers at the embankment site consisting in: 18 cone penetration tests with pore pressure measurements (CPTUs), 6 soil borings and multiple geophysical surveys (ERT, GPR, EM), conducted in the summer 2014 and 2015. Undisturbed samples were taken from the boreholes using a Shelby tube-type piston with a diameter of 106 mm in three different verticals as reported in Figure 2.2, below the crest of the dyke, at the toe and in the polder area.

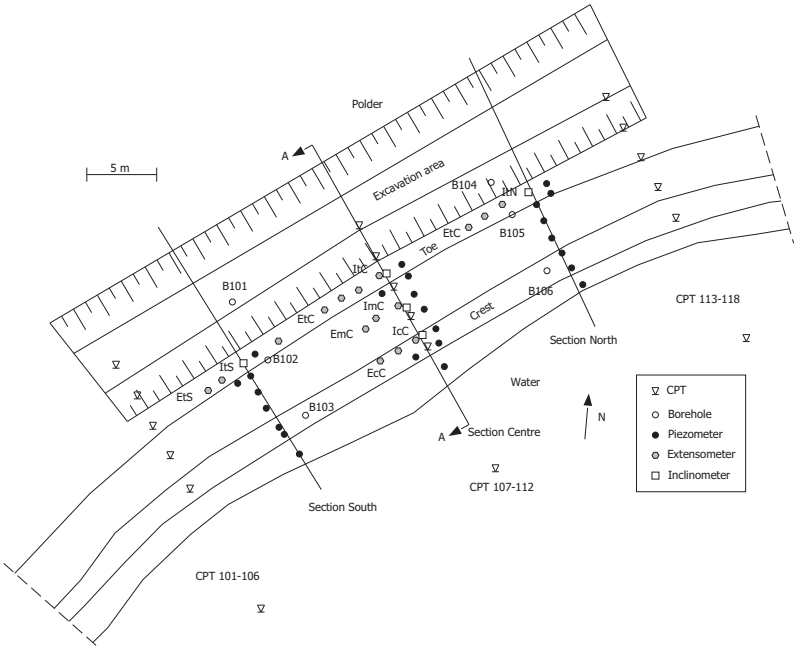

Figure 2.2: Plan view of Leendert de Boerspolder embankment test site showing the location of the soil borings and the location of the monitoring instrumentation

The general stratigraphy of the soil layers determined during the in-situ campaign is reported in Figure 2.3 in correspondence of the cross section A-A (Figure 2.2).

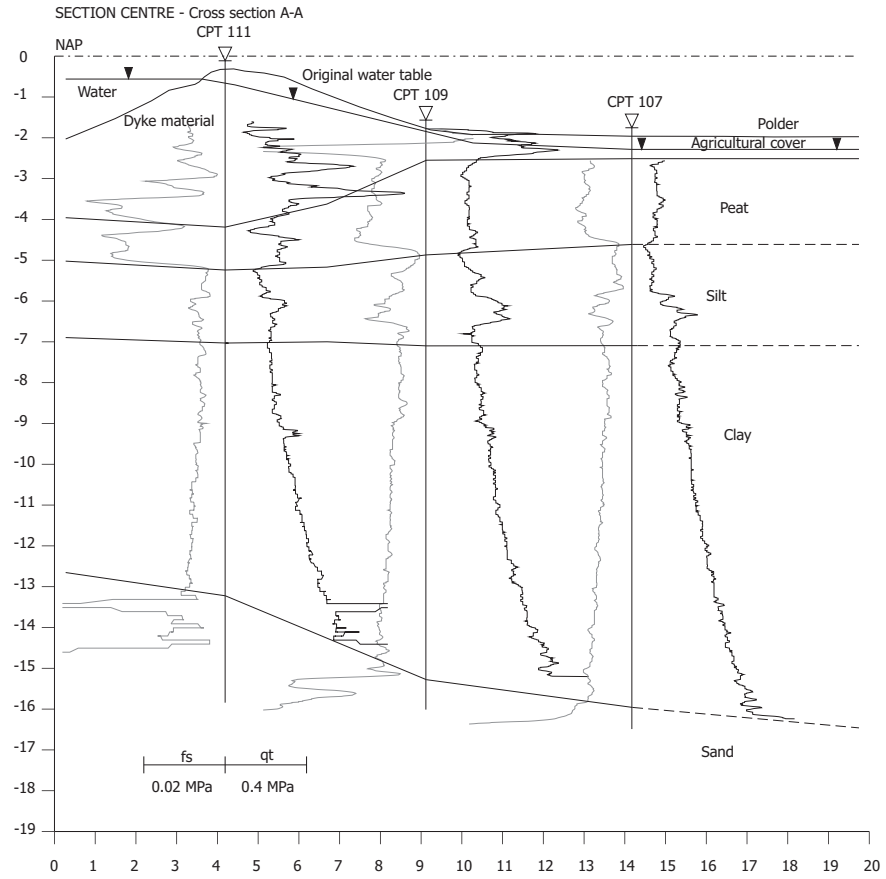

Figure 2.3: Cross sectional profile of Section Centre showing the soil stratigraphy inferred from the site investigation

The dyke body was found to be extremely heterogeneous, mainly made of cohesive layers mixed with recycled materials such as potteries, shells, glass and cast-iron pieces, available at the time of the construction 500 years ago. The stratigraphy of the foundation layers consisted of: a) peat layer with a thickness between 1 m below the crest of the dyke and 2.5 m at the polder side; b) silt deposit approximately 2 m thick characterised by a variable organic content; c) thick deep clay layer; and d) Pleistocene sand layer downward inclined from the canal to the polder side (Figure 2.3). The water level in the canal and in the polder was artificially regulated with very little variations during all the monitoring period. The NAP (Normaal Amsterdam Peil) is assumed as reference for the elevations. The original phreatic surface, before the stress-test, was located 0.3 m under the crest of the dyke (-0.7

m NAP), 0.2 m (-2 m NAP) and 0.4 m (-2.3 m NAP) below the ground level at the toe and in the polder, respectively. The dyke material ranged from a silty sand with traces of gravel and clay to a clayey silt with traces of sand. The silt deposit below the peat layer ranged from a silt with traces of sand and clay to a clayey sandy silt (Ponzoni, 2017). The general soil properties of the different layers are summarised in Figure 2.4. Based on the expected location of the failure surface, the geotechnical characterisation focused on the soil layers until the silt deposit. The deep clay layer, not interested by the shear surface, is then excluded from the following discussion.

As shown in Figure 2.4 significant variations of the properties of the dyke body were found due to several interpositions of different materials. The average specific gravity, Gs (D5550-14, 2014), was about 2.6 while an average bulk unit weight of 18 kN/m^3 was determined. The water content profile within the dyke, Figure 2.4(b), increased with depth ranging from 0.19 to 1.1. The organic content (D2974-14, 2014) also increased with depth from 3% to 7%, at the bottom of the dyke body. A clear transition with the peat layer is visible in Figure 2.4(a) for the vertical profile below the crest of the dyke. The high abundance of organic matter which characterises the peat matrix is reflected in a dramatic drop of the specific gravity, Gs=1.5, and an increase in the water content up to 8. The organic content was about 80%-90%. Remains of plants, roots and reeds were systematically found in peat samples below -4 m NAP both on the polder side and below the crest of the dyke while the upper part of the peat being more amorphous. The foundation silt layer was characterised by an average specific gravity of 2.6 and with a natural water content decreasing with depth from 0.83 (-6.5 m NAP) to 0.48 (-7.1 m NAP) below the crest of the dyke. This tendency was reflected also in the organic content which decreased from 7.5% to 5% with depth. Atterberg's limits calculated on samples at -6.67 m NAP below the crest of the dyke gave a limit liquid of 77.4% and a plastic limit of 40.8%. Finally, the bulk unit weight seemed to increase almost linearly with depth both under the crest and at the polder side.
The profile of the in situ void ratio, e_0 and overconsolidation ratio OCR, from oedometer and triaxial tests on undisturbed samples, are displayed in Figure 2.5(a) and Figure 2.5(b) respectively (Ponzoni, 2017). The dyke material was slightly overconsolidated (maximum OCR equal to 1.9) in the surficial part while the OCR decreased with depth towards the normal consolidated state at -3.5 m NAP at the interface with the peat layer. The underneath peat layer and organic silt resulted slightly overconsolidated or normally consolidated (Figure 2.5(b)). Moving to the polder side, both the peat and the organic silt presented an OCR between 3 and 4.

Indications about the vertical saturated hydraulic conductivity, k_v, for the dyke material and the organic silt layer were obtained from oedometer tests according to the Taylor's method (Ponzoni, 2017). For the dyke material k_v was found in order of 3e-08 m/s in the upper part and 2e-09 m/s in the deeper part. In the silt layer, the hydraulic conductivity decreased with depth, passing from 1e-08 m/s to 4e-09 m/s. For the peat layer a special oedometer cell equipped with a pore pressure transducer was adopted (Zhao & Jommi, 2018). Dramatic reduction in the hydraulic conductivity occurs for peat upon compression (Mesri & Ajlouni, 2007).

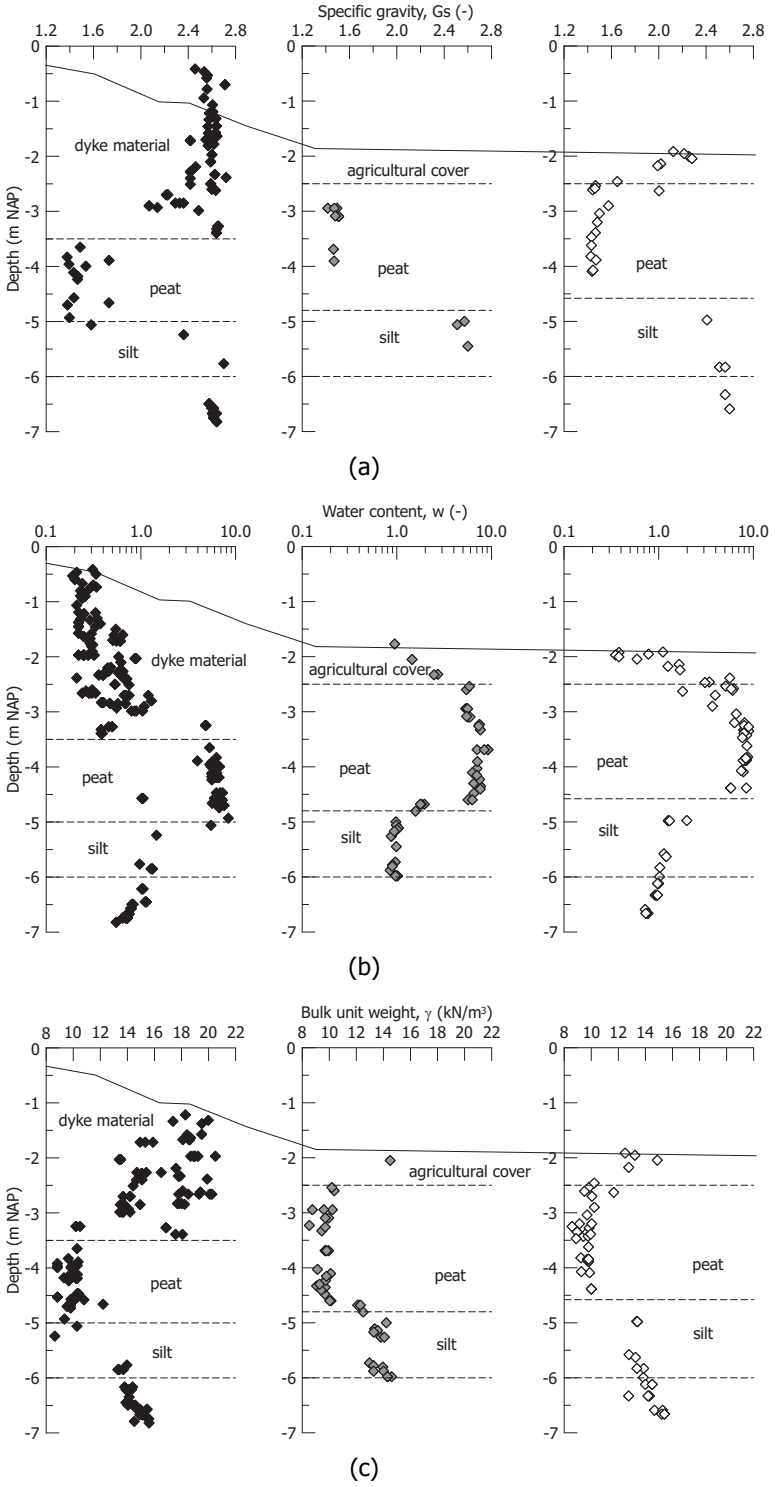

Figure 2.4: Profiles of (a) specific gravity, (b) water content and (c) bulk unit weight along three verticals for a typical cross section of the Leendert de Boerspolder embankment test site

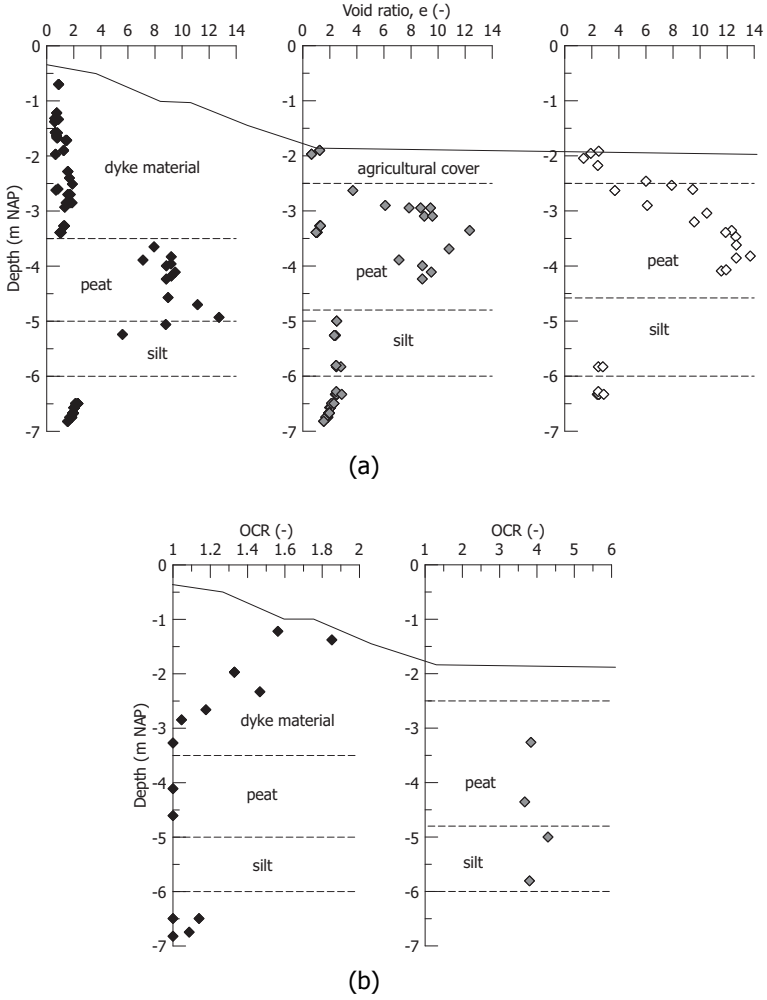

Figure 2.5: Profiles of (a) void ratio and (b) overconsolidation ratio along three verticals for a typical cross section of the Leendert de Boerspolder embankment test site

Accounting for the initial void ratio and organic content of the peat below the dyke body and at the polder side, e_0=10 and e_0=12 respectively, k_v=1e-06-1e-07 m/s was expected.

2.4. MONITORING INSTRUMENTATION

The in-situ instrumentation was designed with the two primary purposes of providing sufficient data of the pre-failure response of the system and to collect as much information as possible during the failure. All measurements were automated and constantly monitored during the test. Three cross sections (Section North, Centre, South) were instrumented as displayed in Figure 2.2. Section Centre was the most instrumented considering the likelihood of the occurrence of failure at this location due to the restraint offered by the two extremities of the dykes. The instrumentation included:

- 25 piezometers installed in the dyke body and in the foundation layers with accuracy ±0.1 kPa. Eight piezometers were installed in the Section North and South while nine piezometers in the Section Centre. The intended function of the piezometers was to characterise the different hydraulic behaviour of the subsoil in response to the operations throughout the entire stress-test (i.e. excavation, dewatering, refilling). The cross-sectional position of the piezometers was chosen based on preliminary stability analyses carried out to predict the probable location of the failure zone;
- 5 automatic two axis inclinometers. In the Section North and South, one inclinometer was placed at the toe of the dyke while three in the Section Centre, at the toe, at the centre and at crest of the dyke respectively. Each in-place inclinometer rod was equipped with inclination transducers 0.5 m of vertical spacing each, which automatically logged the inclination profile of the tube at set time intervals with an accuracy of ±0.5°;
- 5 vertical boreholes rod type extensometers installed in the foundation layers. Each vertical rod was equipped with three extensometer bases apart from the one installed at the toe of the dyke at the Section Centre which had 4 bases. The extensometers rods were anchored at the interface of the different subsoil allowing to automatically record the settlement or heave of the entire soil column above with an accuracy of ±2 mm. The change in thickness of each soil layer was then obtained from the difference between the readings of consecutive extensometers.

Figure 2.6 reports the location of the instrumentation installed in the Section Centre together with the excavation stages performed in the stress-test as described in the following paragraph.

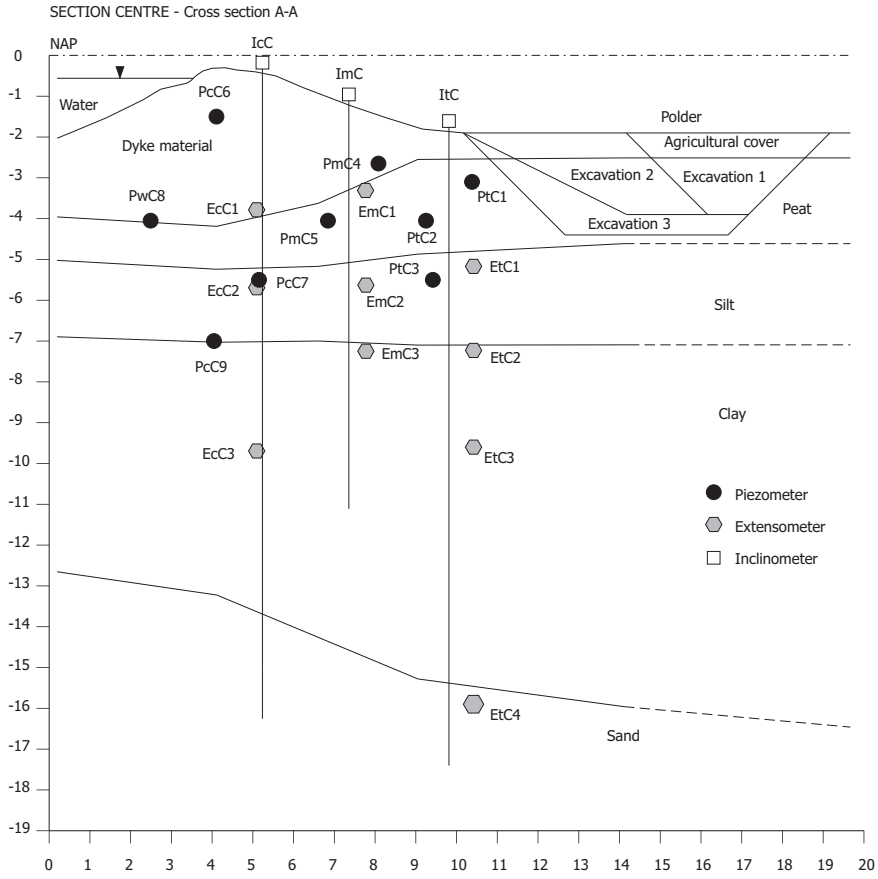

Figure 2.6: Cross sectional profile of Section Centre with the instrumentation and the excavation stages

2.5. TEST LAYOUT

A wetting system was placed on the crest of the dyke on 21 September 2015 to saturate the dyke body, (Figure 2.7), in order to increase its weight and reduce the uncertainty related to possible unsaturated conditions.

Figure 2.7: Wetting system placed at the crest of the dyke

Three excavation stages were executed at the toe of the embankment in a progressive series: September 28 excavation 1; October 5 excavation 2; October 12 excavation 3. The first excavation started 10 m away from the toe of the dyke (Figure 2.8(a)) and removed the first 2 m of surficial soils consisting in the agricultural cover, approximately 0.6 m thick and 1.4 m of peat (Figure 2.6). With the second stage, the excavation front was extended to 1 m from the toe of the dyke while keeping the excavation depth 2 meters below the ground surface. Eventually, the third excavation (Figure 2.8(b)) deepened the depth to the final value of 2.5 m below the ground surface. Each excavation took approximately half a day and the water level in the excavated area was left free to reach its steady condition for the next two days. After this interval, with the intent of stressing the entire system without reaching failure (i.e. pre-failure response), the water in the ditch was lowered down of 1 meter and kept in this position for 1 day. Afterwards, it was restored to the original position. The excavation then proceeded to the next stage. During the last dewatering (October 14) the water level was eventually lowered down under controlled conditions until failure was triggered. Table 2.1 reports the chronological sequence of the entire operations.

2.6. OBSERVED FAILURE

2.6.1. Shear mechanism

At 06:25 am of October 14 with a constant water level in the excavated area of 1.5 m (-3.5 m NAP) the dyke failed (Figure 2.9). The failure interested the

(a)

(b)

Figure 2.8: Operations during the excavation 1, 10 meters from the toe of the dyke (a) and (b) excavation 3 completed (the monitoring instrumentation along the dyke is visible)

2

Table 2.1: Chronological sequence of the operations to bring the dyke to failure

Date (2015)	Operation	Date (2015)	Operation
21/09, 15:25	Start wetting system	08/10, 08:00	Water filling 2 on
28/09, 09:20	Excavation 1 on	08/10, 10:05	Water filling 2 off
28/09, 16:25	Excavation 1 off	12/10, 07:20	Excavation 3 on
30/09, 09:20	Dewatering 1 on	12/10, 16:45	Excavation 3 off
30/09, 12:00	Dewatering 1 off (-1 m)	14/10, 00:38	Dewatering 3.1 on
01/10, 12:45	Water filling 1 on	14/10, 02:17	Dewatering 3.1 off (-0.5 m)
01/10, 14:00	Water filling 1 off	14/10, 02:47	Dewatering 3.2 on
05/10, 08:00	Excavation 2 on	14/10, 04:13	Dewatering 3.2 off (-1.0 m)
05/10, 17:30	Excavation 2 off	14/10, 04:43	Dewatering 3.3 on
07/10, 09:05	Dewatering 2 on	14/10, 06:06	Dewatering 3.3 off (-1.5 m)
07/10, 13:20	Dewatering 2 off (-1 m)	14/10, 06:25	Failure

portion of the dyke between Section Centre and Section South (Figure 2.2) for a width of about 15 m. The Section North did not fail.

Figure 2.9: The moment of the failure of the dyke at the Leendert de Boerspolder in correspondence of Section Centre and Section South

The failure appeared as a combined mechanism of a translational movement of the soil layers located at the toe of the dyke followed by a progressive rotational mechanism of the dyke body. The maximum horizontal displacement, perpendicular to the embankment, was recorded in the lower part of the peat layer at the toe and it was approximately 2.6 m in the Section Centre and 2 m in the Section South. The central portion of the dyke and the crest in the Section Centre followed the movement of the toe with maximum horizontal displacement of 2.4 m and 1.8 m respectively. To reconstruct the failure mechanism, Figure 2.10 displays the horizontal displacements measured by the inclinometers located in the Section Centre during the last dewatering on October 14. The inclinometer at the mid of the slope, ImC, presented a malfunctioning at -6 m NAP. For the sake of clarity, in the following graphs, data have been cut at 06:20 am of October 14 when the dyke was at imminent failure.

At the toe of the dyke (ItC), the shear mechanism was composed apparently by two shear planes: the first one at the interface between the peat and the silt layer (-4.8 m NAP) and the second one developing within the peat itself (-3.9 m NAP) (Figure 2.10). Also in the central line (ImC) two shear planes might be recognised, one inside the silt layer and a minor one at the contact between the dyke body and the peat (-3 m NAP). To clarify the instant when the shear mechanism was fully activated, Figure 2.11 reports the relative horizontal displacements recorded by the inclinometer ItC and ImC at the toe and centre of the Section Centre respectively, recorded during October 14.

The shear mechanism was fully activated along the entire cross section at 05:49 am during the dewatering 3.3, with a water table in the excavated area decreasing from -1 m to -1.5 m from the ground surface. It is interesting to notice that at the toe, significant acceleration in the horizontal direction started occurring within

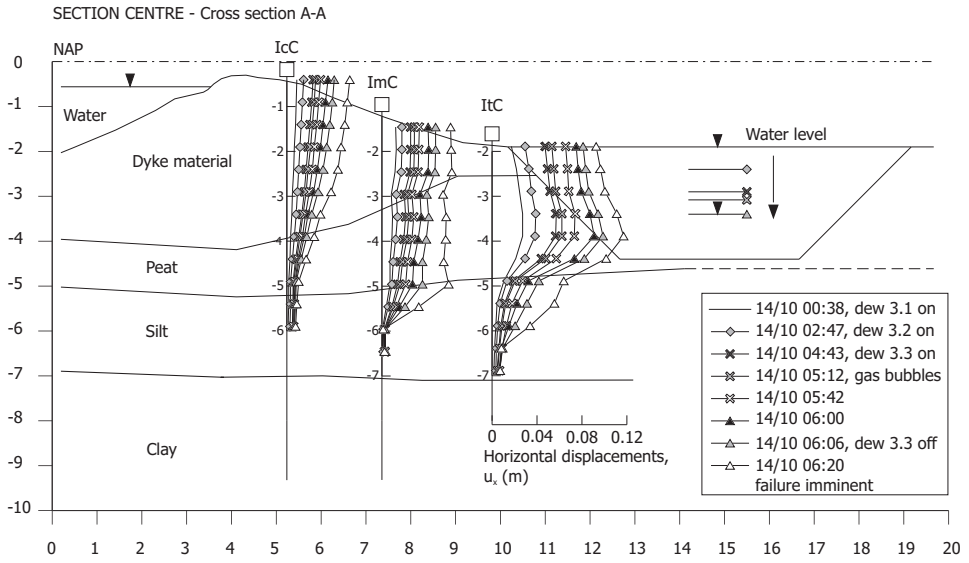

Figure 2.10: Horizontal displacements perpendicular to the embankment recorded during October 14 by the three inclinometers installed in the Section Centre

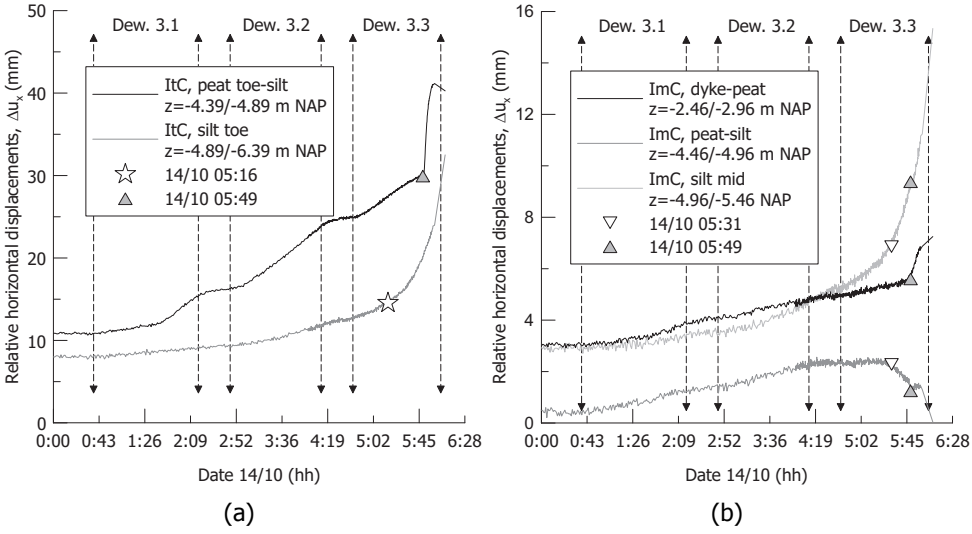

Figure 2.11: Relative horizontal displacements recorded at different depths during October 14 from the inclinometers (a) ItC and (b) ImC

the silt layer (Figure 2.11(a)) at 05:16 am (33 minutes before the shear surface formed at the interface with the peat). Moving to the central line (Figure 2.11(b) light grey) the silt layer began to accelerate horizontally at 05:31 am. Exactly at this time, the relative displacement between the peat and the silt (Figure 2.11(b) dark grey) stopped and reversed the trend. It is worth remembering that based on the distance between each transducer along the rod, the position of the shear plane can be inferred only with an accuracy of ±0.25 m.

2.6.2. Piezometric response

Furhter details of the shear mechanism during the last dewatering 3.3 are provided in Figure 2.12 where the horizontal displacements are combined with the data recorded by the extensometers and piezometers. The horizontal displacements of each soil layer have been averaged in the vertical direction for the sake of simplicity. The axes of each figure indicate the sensors which were considered. All the displacement measurements have been zeroed at midnight of October 14. Positive vertical displacements indicate heave.

The shear mechanism initiated in the silt at the toe of the dyke at 05:16 am, when the ratio between the horizontal and vertical displacement showed an increase in the horizontal direction (Figure 2.12(a)). The piezometer in the silt layer PtC3 (Figure 2.12(b)) measured a sudden decrease in the hydraulic head denoting a dilatant behaviour. Slightly later, at 05:29 am, in the lower part of the peat layer just above the silt the horizontal displacement rate started to increase (Figure 2.12(c)) compared to the vertical one, accompanied by a decrease in the hydraulic head from the PtC2 located in the lower part of peat (Figure 2.12(d)). On the contrary, in the upper portion of the peat layer, PtC1, nothing was recorded at 05:29 am. In the central line of the slope, at 05:31 am the upper part of the silt layer accelerated horizontally (Figure 2.12(e) light grey), while the peat layer above increased its vertical displacement component. It is worth noticing that, differently from the toe, the silt in the central portion of the slope settled, thus promoting also the vertical compression of the peat above. The corresponding piezometer in the peat layer PmC5 (Figure 2.12(f)) starting at 05:31 am showed a progressive decrease in the hydraulic head. Few minutes after, at 05:36 am (Figure 2.12(e)) horizontal displacements occurred in the dyke material at nearly constant vertical displacements and the piezometer PmC4 (Figure 2.12(f)) recorded a sudden increase in the hydraulic head, probably shear induced. Along the vertical section below the crest of the dyke, only at 05:49 am, the piezometers PcC6 and PcC7 (Figure 2.12(h)) decreased and increased respectively when the shear mechanism was activated along the entire cross section. The evolution of the entire shear mechanism is displayed in Figure 2.13 (vectors are not in scale).

2.6.3. Volumetric and distortional strains

To reconstruct the volumetric behaviour of the single layers, blocks of single materials have been defined based on the location of the inclinometers and extensometers as schematised in Figure 2.14. For each block the net vertical and horizontal displacements were estimated as difference between consecutive exten-

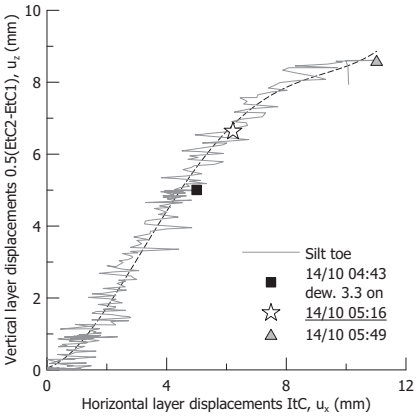
Vertical layer displacements 0.5(EtC2-EtC1), u_z (mm)
Horizontal layer displacements ItC, u_x (mm)
Silt toe
14/10 04:43
dew. 3.3 on
14/10 05:16
14/10 05:49

(a)

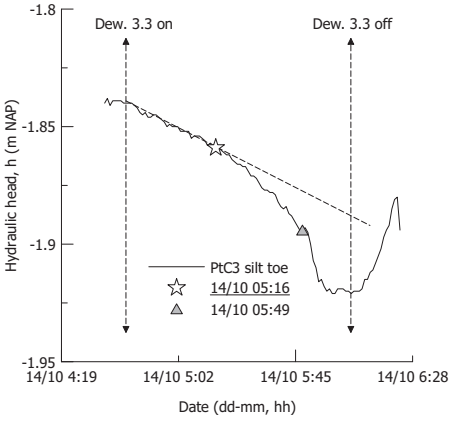
Hydraulic head, h (m NAP)
Dew. 3.3 on
Dew. 3.3 off
PtC3 silt toe
14/10 05:16
14/10 05:49
Date (dd-mm, hh)

(b)

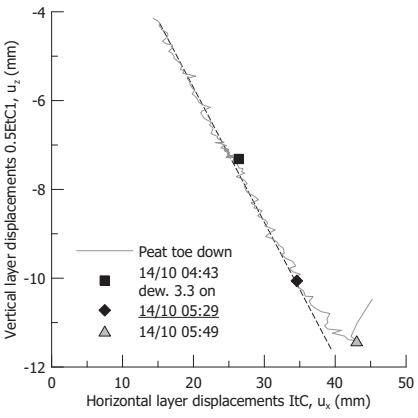
Vertical layer displacements 0.5EtC1, u_z (mm)
Horizontal layer displacements ItC, u_x (mm)
Peat toe down
14/10 04:43
dew. 3.3 on
14/10 05:29
14/10 05:49

(c)

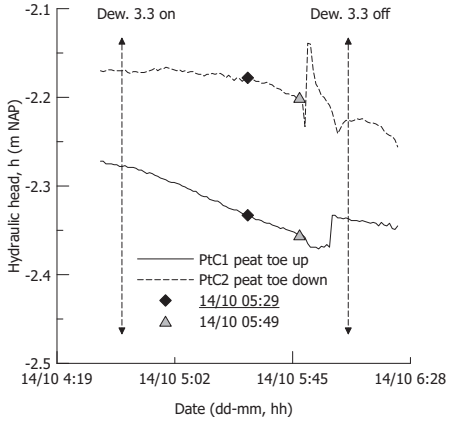
Hydraulic head, h (m NAP)
Dew. 3.3 on
Dew. 3.3 off
PtC1 peat toe up
PtC2 peat toe down
14/10 05:29
14/10 05:49
Date (dd-mm, hh)

(d)

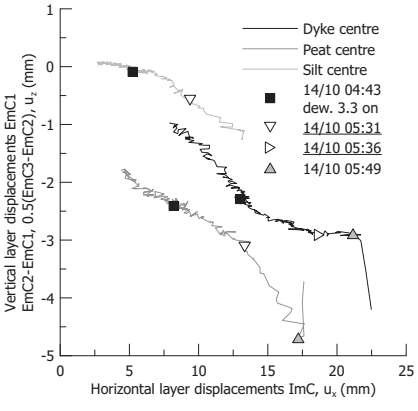
Vertical layer displacements EmC1
EmC2-EmC1, 0.5(EmC3-EmC2), u_z (mm)
Horizontal layer displacements ImC, u_x (mm)
Dyke centre
Peat centre
Silt centre
14/10 04:43
dew. 3.3 on
14/10 05:31
14/10 05:36
14/10 05:49

(e)

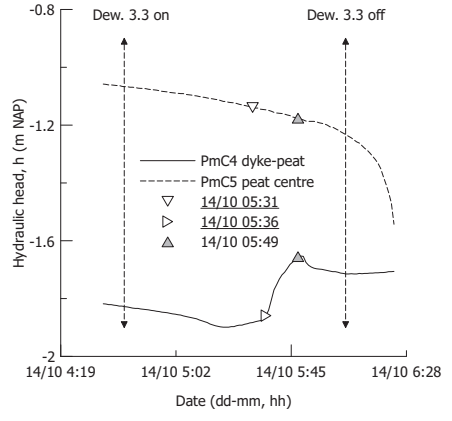
Hydraulic head, h (m NAP)
Dew. 3.3 on
Dew. 3.3 off
PmC4 dyke-peat
PmC5 peat centre
14/10 05:31
14/10 05:36
14/10 05:49
Date (dd-mm, hh)

(f)

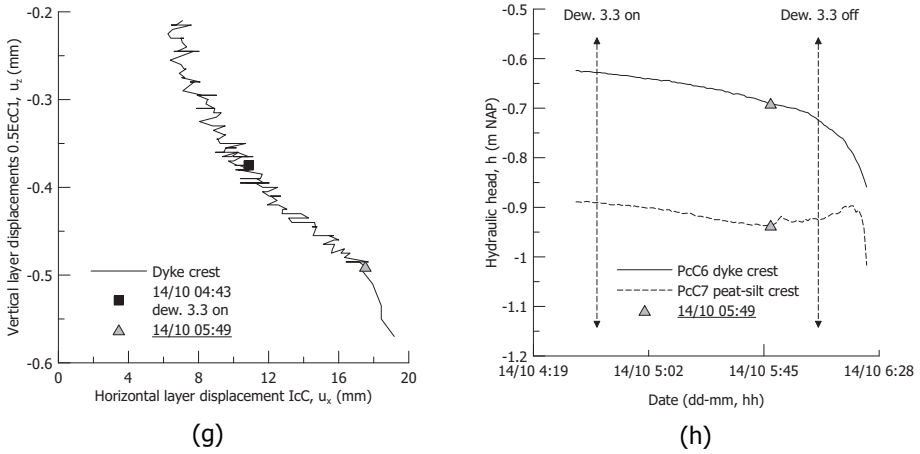

(g) (h)

Figure 2.12: Horizontal and vertical displacement components (a), (c), (e), (g) and hydraulic head (b), (d), (f), (h) measured during the dewatering 3.3 on October 14

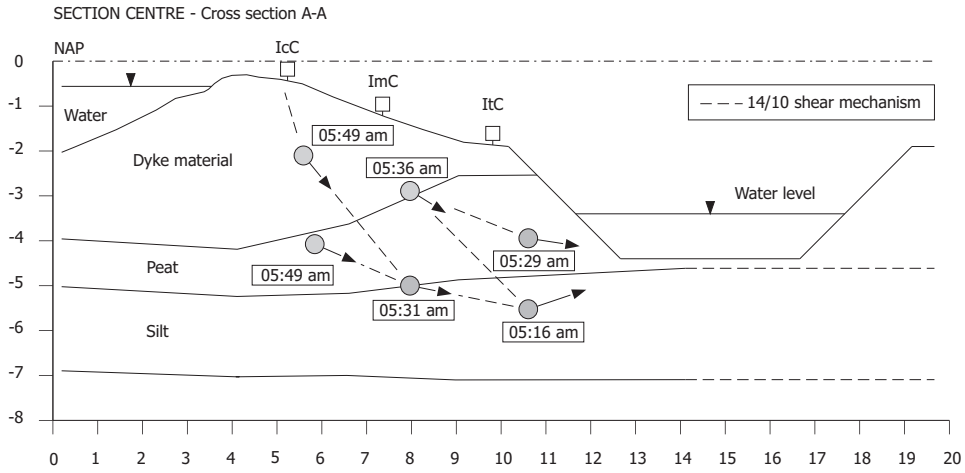

Figure 2.13: Evolution of the shear mechanism during October 14

someters and inclinometers. The volumetric strains were calculated for each block based on the initial size. For the vertical strain, the extensometers at the right and the left of each block were averaged. Figure 2.15 reports the development of volumetric strain for each soil block of Figure 2.14 during the night of October 14.

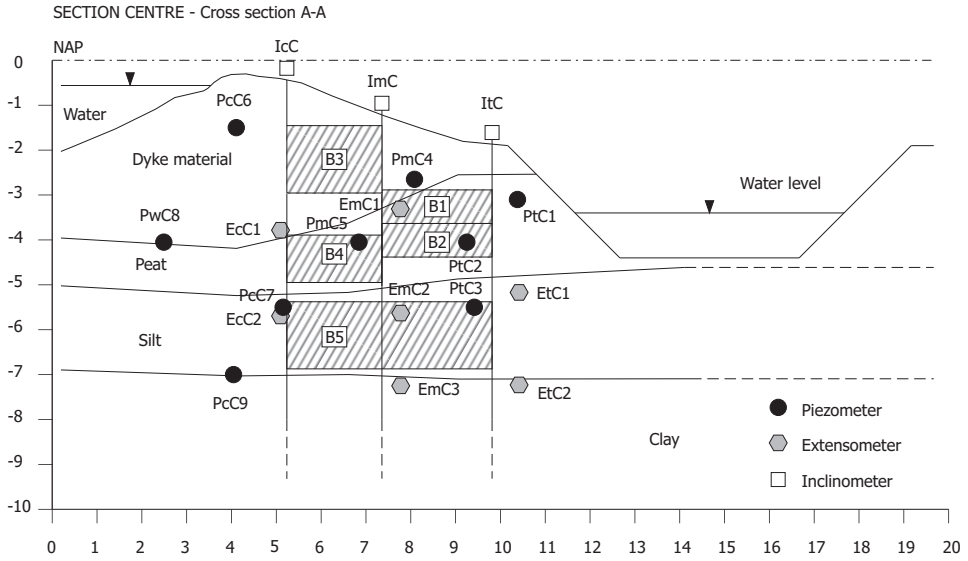

Figure 2.14: Definition of the blocks of single material used for computing the volumetric strains based on the inclinometers and extensometers readings

Comparison between Figure 2.15 and the hydraulic response in Figure 2.12 allows to define the volumetric response of the different soil layers involved in the failure mechanism. In actual field situations, distinguishing between drained and undrained behaviour is rather striking considering that the true response is neither perfectly undrained nor drained. The organic silt at the toe of the dyke showed volumetric dilation as displayed in Figure 2.15 in agreement with a reduction of the hydraulic head measured in the piezometer PtC3 in Figure 2.12(b). The behaviour of the peat at the toe deserves some attention. Two sub-blocks were distinguished in Figure 2.14 based on the horizontal displacement profile in Figure 2.10. The upper peat dilated, despite less than the silt below, while the lower peat presented only a small tendency to dilate. This difference could derive from the shear mechanism experienced by the two peat blocks: the lower peat B2 was sheared while the upper one B1 was substantially dragged by the lower block. As a result, the average net horizontal displacements of the two blocks differed substantially. The horizontal bulging and stretching of the upper peat not only compensated the vertical compression but resulted in a dilatant volumetric strain. On the contrary, for peat block B2 the axial and horizontal strains almost equated in magnitude. Moving to the central part of the slope, peat B4 denoted contractive volumetric strain despite no excess of pore pressure being recorded by the piezometer PtC5 (Figure 2.12(f)). Nonetheless, the position of this piezometer close to the interface with the dyke

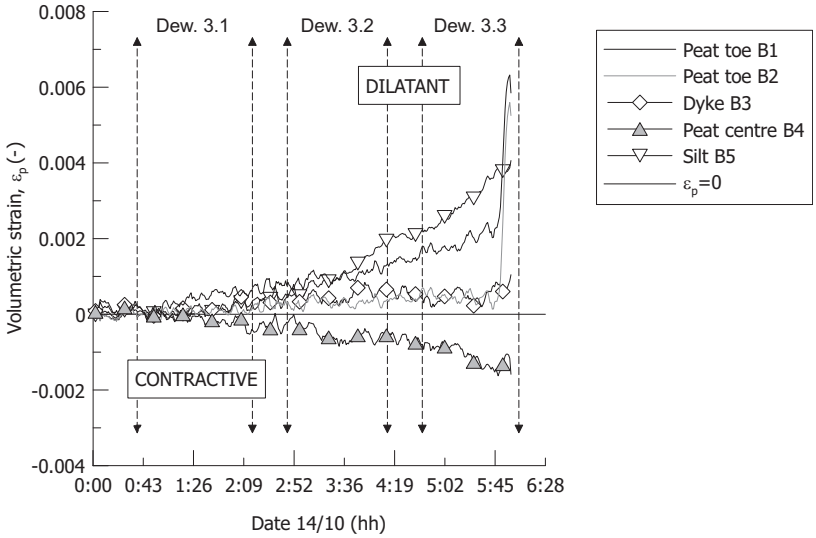

Figure 2.15: Volumetric strains representative of each soil block calculated during the last stage of dewatering on October 14

material may not represent faithfully the average behaviour of the peat block B4. The dyke material in the block B3 slightly dilated in accordance with the hydraulic response in Figure 2.12(h) (piezometer PcC6). The local increase in the hydraulic head measured at the piezometer PmC4 may have been induced by localised shear displacements occurring at the interface between the dyke material and the peat beneath.

To complete the description of the hydro-mechanical response of the soils, the distortional behaviour is considered. Figure 2.16 reports the horizontal net displacements perpendicular to the dyke as the difference between the three different inclinometers (Figure 2.10) for the silt and the peat layers at the toe of the dyke in the Section Centre. The shear mechanism for the silt layer can be faithfully represented by a simple shear mode with a shear strain, γ, at 06:20 am (imminent failure) of about 5%. The mechanism in the peat layer was more complex, with the lower part (Peat B2) approximately experiencing a simple shear mechanism (γ=6% 06:20 am imminent failure) together with bulging, while the upper one (Peat B1), was horizontally dragged and stretched.

Simple shear tests performed during the experimental laboratory characterisation on undisturbed samples collected in the summer 2014 are here presented to validate the conclusions on the hydro-mechanical behaviour observed in the field during the stress-test. Attention is given to the crucial role of peat and silt at the toe of the dyke. Figure 2.17 reports the results of constant height simple shear tests on two undisturbed samples of silt at the toe of the embankment from the borehole B102 (Figure 2.2). The first sample was taken at -5.10 m (NAP), close to the interface with the peat, and contains peat and wood traces. The second

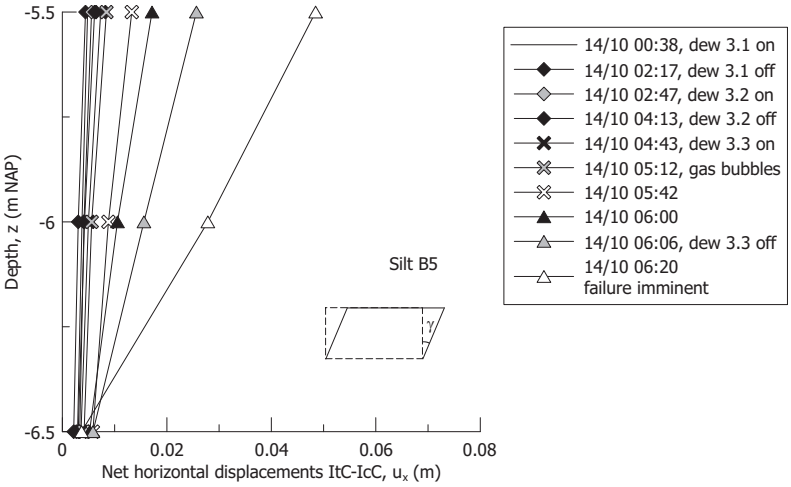

(a)

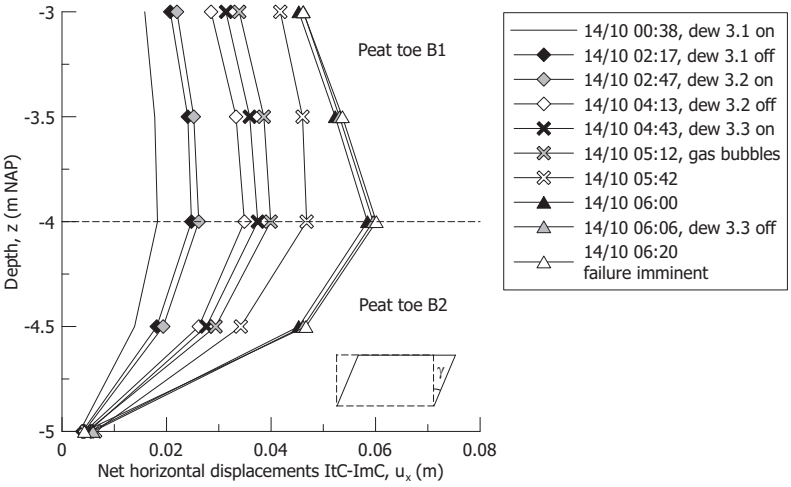

(b)

Figure 2.16: Net horizontal displacements perpendicular to the dyke in the Section Centre for (a) the silt layer and (b) the peat layer during October 14

one, collected at greater depth -5.8 m (NAP), was located in the middle of the silt formation. The in situ vertical effective stress before the stress-test, calculated from the average unit weight and the position of the water table at the toe (-0.2 from the ground), ranges between 10 kPa and 15 kPa. The experimental results are presented in terms of stress ratio, τ_h/σ'_v (where τ_h is the shear stress and σ'_v is the vertical effective stress at the top boundary of the sample) and excess pore pressure (Δu_w) normalised with the preconsolidation vertical effective stress, σ'_c. The shear strains have been cut before the ultimate state for the sake of clarity.

The experimental results in Figure 2.17 confirm the volumetric behaviour reconstructed from the field for the silt layer with a dilatant response (Figure 2.17(b)(d)) for shear strain of 5% experienced by the silt soil block before the imminent failure (Figure 2.16(a)). It is worth noticing the impact of peat traces in the upper silt sample in terms of operative stress ratio (i.e. shear strength) compared to the deeper sample. The abundance of organic traces in the silt matrix close to the interface with the peat layer not only influence the ultimate stress ratio (0.95 for the B102-7 sample, 0.8 for the deeper sample B102-8) but also leads to a more ductile pre-failure stress-strain response with a significant increase in the required shear strain to mobilise the same shear strength (Figure 2.17(a)(b)), as explained in the following. The results on undisturbed peat samples at the toe of the dyke from the borehole B102-5 at a depth of -4.15 m (NAP) are displayed in Figure 2.18.

For an estimated in situ vertical effective stress within the peat of about 9 kPa, a dilatant behaviour was observed for shear strain of about 5% (Figure 2.18(b)), confirming the observations obtained from the field for the peat at the toe B1 and B2 in Figure 2.14. It is worth reminding that the shear mechanism for the upper peat block B1 (Figure 2.14) was not truly represented by a simple shear, but rather by a horizontal stretching leading to a higher dilatant response than that observed in the experimental tests. On the contrary, for the peat B4 (Figure 2.14) below the mid slope of the dyke a contractive behaviour was obtained from the experimental results (Figure 2.18) on a sample (B103-9 in Figure 2.2) consolidated at σ'_c=26 kPa representative of the in situ stress state at -4.7 m (NAP) below the crest of the dyke.

2.7. 3D FAILURE DISPLACEMENTS

2.7.1. Section South

As previously mentioned, the failure occurred between the Section Centre and the Section South for an approximate length of about 15 m. As for the Section Centre, also in the Section South the shear mechanism was initiated within the first meter of silt at the toe of the dyke (-4.78/-5.78 m NAP) where significant acceleration in the horizontal displacements occurred at 05:16 am on October 14, simultaneously with the Section Centre as reported in Figure 2.19(a). However, differently from the latter, in this case the shear mechanism involved both the silt and the peat without a localised shear surface at the interface (Figure 2.20). Above, the peat layer was then crossed by a shear plane at -3.7 m (NAP) as for the Section Centre.

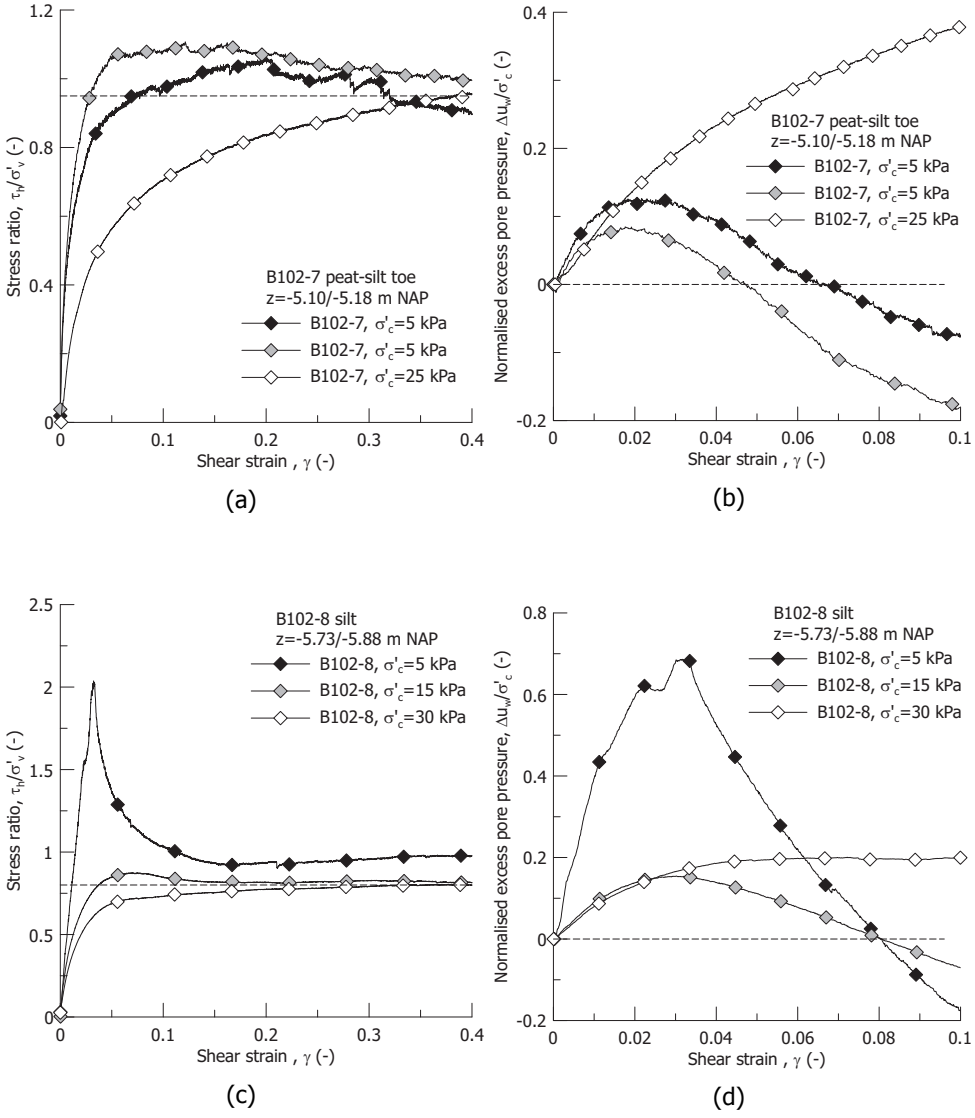

Figure 2.17: Stress ratio (a), (c) and excess pore pressure (b), (d) during simple shear tests at constant height for silt samples B102-7 and B102-8 at the toe of the dyke

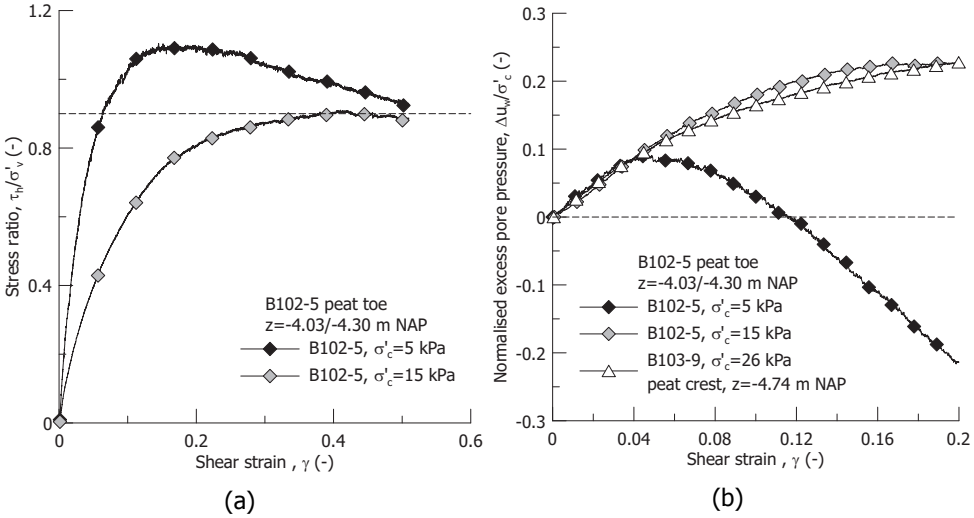

Figure 2.18: Stress ratio (a) and excess pore pressure (b) during simple shear tests at constant height for peat samples B102-5 at the toe of the dyke (in the latter the sample B103-9 below the crest of the dyke is added)

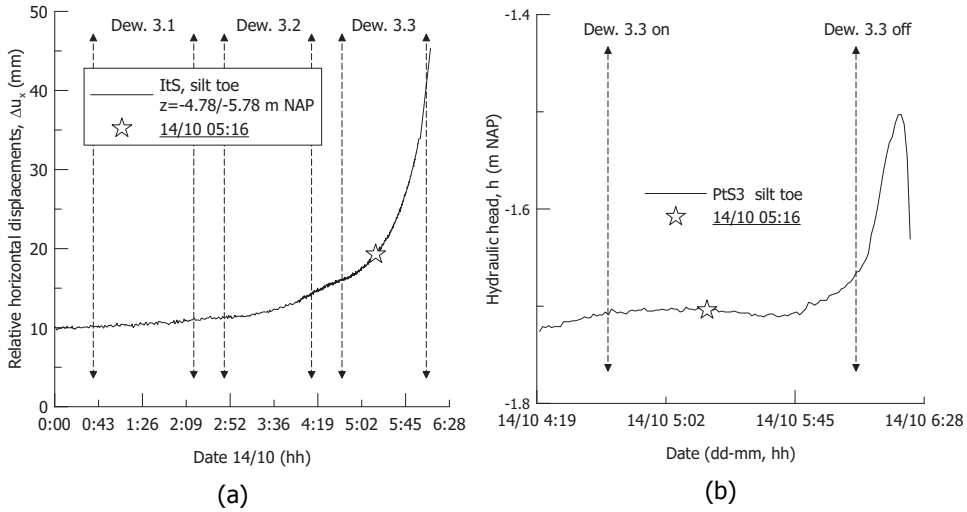

Figure 2.19: Relative horizontal displacements recorded at different depths during October 14 from the inclinometer ItS (a) and (b) hydraulic head recorded by the piezometer PtS3 located in the silt layer at the toe of the dyke

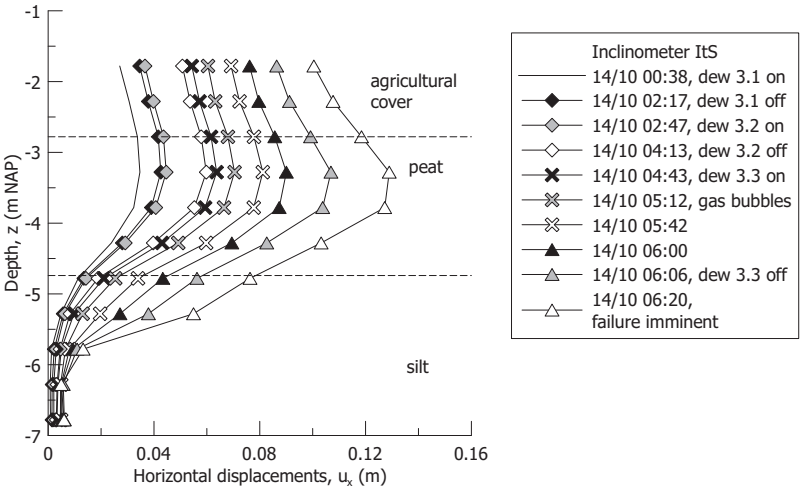

Figure 2.20: Horizontal displacements perpendicular to the dyke recorded by the inclinometer ItS during October 14

Contrarily to the response of the piezometer PtC3 located in the silt layer in the Section Centre, the analogous in the Section South, PtS3, recorded an increase in the hydraulic head as displayed in Figure 2.19(b). This difference may be explained by considering Figure 2.20 where the kinematic mechanism at the toe of the dyke involved both the silt layer and the peat as unique soil block (-3.7 m to -5.7 m NAP). Analysing the extensometer response, vertical compression of both the peat and the silt accompanied the horizontal displacement contrarily to the response in the Section Centre where the silt layer experienced heave while shearing (Figure 2.12(a)).

2.7.2. Section North

Section North did not fail. The inclinometer at the toe of the dyke indicated a sharp shear plane at the interface between the silt and the peat layer. However the horizontal displacements in the peat attained values of about half compared to the other two sections (Figure 2.21(a)), 6 cm compared with 12 cm at 06:20 am on October 14 (Figure 2.20). Following the philosophy adopted in Figure 2.11(a) and Figure 2.19(a), Figure 2.21(b) reports the relative horizontal displacement at the interface between the peat and the silt and within the silt layer.

As displayed in Figure 2.21(b), the silt layer accumulated only 5 mm of relative horizontal displacement in two meters of thickness (-4.92/-6.92 m NAP) while in both Section South and Centre, 5 and 3 cm were measured (Figure 2.11(a) and Figure 2.19(a)). An insight into the deformation mode of the peat at the toe of Section North is offered in Figure 2.22. The horizontal displacement profile from the inclinometer ItN is overlapped with the net profile (Figure 2.16(b)) obtained from the Section Centre (location of the failure) by subtracting the readings of the inclinometer ImC from the inclinometer ItC, at the mid and toe of the dyke

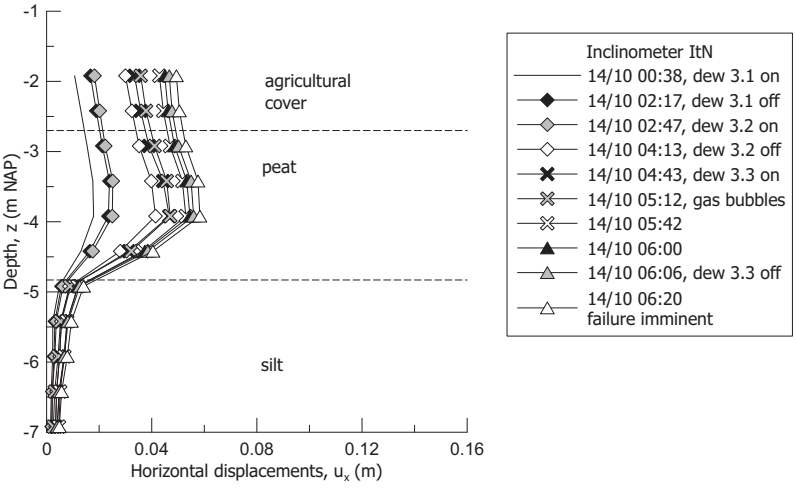

(a)

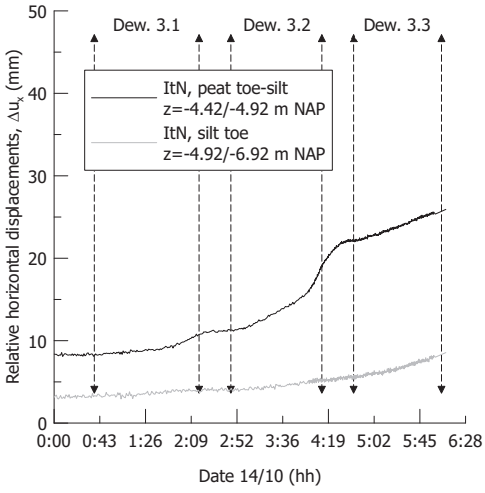

(b)

Figure 2.21: Horizontal displacements recorded by the inclinometer ItN at the toe of the dyke (a) and (b) relative horizontal displacements recorded at different depths during October 14 from the inclinometer ItN

respectively. In Figure 2.22 it is assumed that no horizontal displacements occurred in the peat at the centre of the dyke slope along Section North. In the absence of an inclinometer and considering that Section North did not fail, this assumption can be considered acceptable, though conservative.

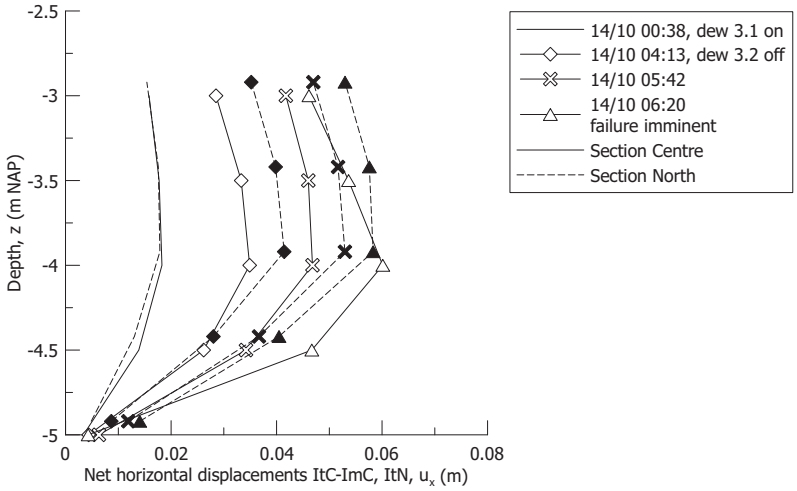

Figure 2.22: Net horizontal displacements in the peat layer at the toe of the dyke in the Section North and Section Centre during October 14

The two profiles substantially coincide despite the fact that Section Centre failed while Section North did not, which allows to state that the silt layer and not the peat was indeed the critical soil for the failure. If the hypothesis on null displacement of the peat at the centre of the dyke is released, then a perfect match would be obtained in Figure 2.22. The map of the maximum horizontal displacement vectors obtained from the inclinometers reading at the end of the second dewatering (October 7) and at the end of the third dewatering performed on the night of October 14 is reported in Figure 2.23. At the toe of the dyke between the Sections South and Centre, outward displacements directed towards the excavated area occurred. The spreading mechanism thus caused converging movement of the mid slope and the crest in between the two sections.

2.8. PRE-FAILURE RESPONSE

The previous considerations on the shear mechanism allow to state the critical role played by the silt layer underneath the peat in bringing the dyke to failure. However, the triggering mechanism, which induced the failure in the silt layer, has to be determined. To help answering this question, it is worthwhile to analyse the pre-failure response during the second dewatering performed on October 7 after the second excavation (Table 2.1). The horizontal displacements perpendicular to the dyke recorded by the inclinometers at the toe (ItN, ItC and ItS) are compared in Figure 2.24.

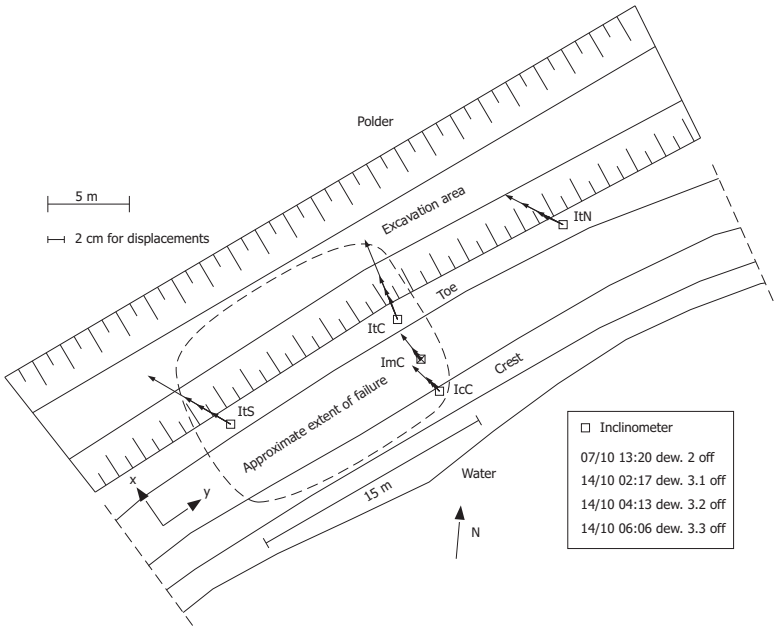

Figure 2.23: Maximum horizontal displacement vectors reconstructed from the inclinometers reading (the approximate area of failure is also shown)

In all the three sections, the peat at the toe of the dyke significantly bulged due to the on-going dewatering, which reduced the stabilizing thrust exerted by the water. Lateral bulging is a characteristic deformation mode of peat (Landva & La Rochelle, 1983). As a dragging mechanism, the displacements propagated from the peat to the silt underneath. However, significant differences are visible for the silt layer in the Section North compared to the other two sections in Figure 2.24. In Section South and Centre the dragging action exerted by the peat induced visible lateral displacement in the 2 m of silt below. In the Section North the displacements of peat layer did not transfer in depth within the silt formation, but on the contrary, remained localised at the interface. As discussed in Figure 2.22 with reference to the net horizontal displacement of the peat at the toe during October 14, also in this case, accounting for higher displacement in the silt formation in the Section North, the three profiles in Figure 2.24 would basically coincide. Following this reasoning, it can be asserted that the silt layer at the toe of the dyke in the Section South and Centre was brought to failure by the overlying peat layer, which moved significantly in the horizontal direction. Indeed, the different stress-strain response of peat and silt played the major role in the shear mechanism. Figure 2.25 compares the results of constant height simple shear tests on a peat and silt undisturbed samples retrieved from the borehole B102 (Figure 2.2). Both the samples were consolidated at 5 kPa.

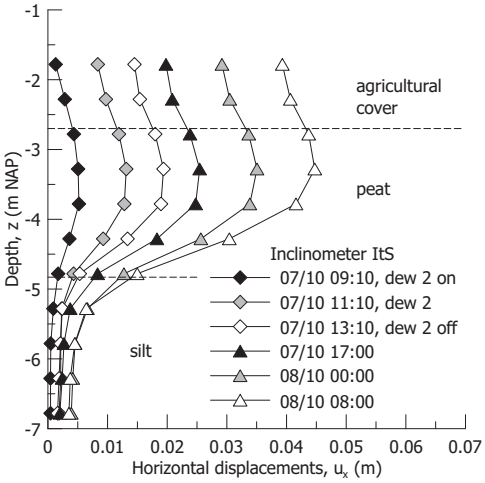

(a)

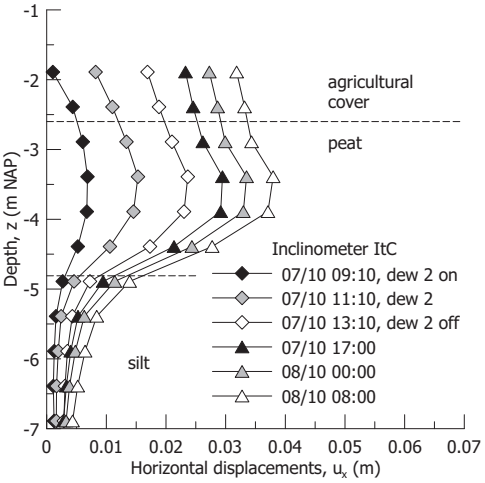

(b)

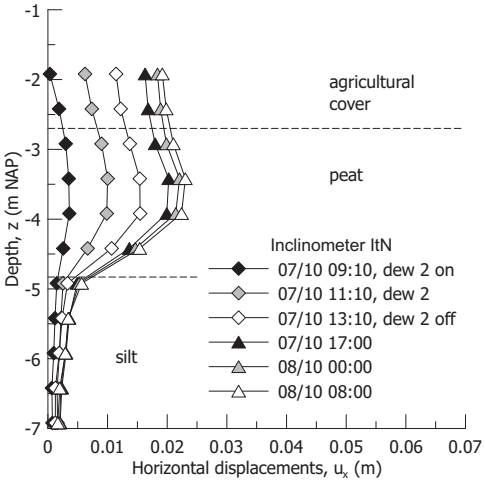

(c)

Figure 2.24: Horizontal displacements perpendicular to the dyke recorded by the inclinometers at the toe of the dyke during October 7: (a) Section South, (b) Section Centre and (c) Section North

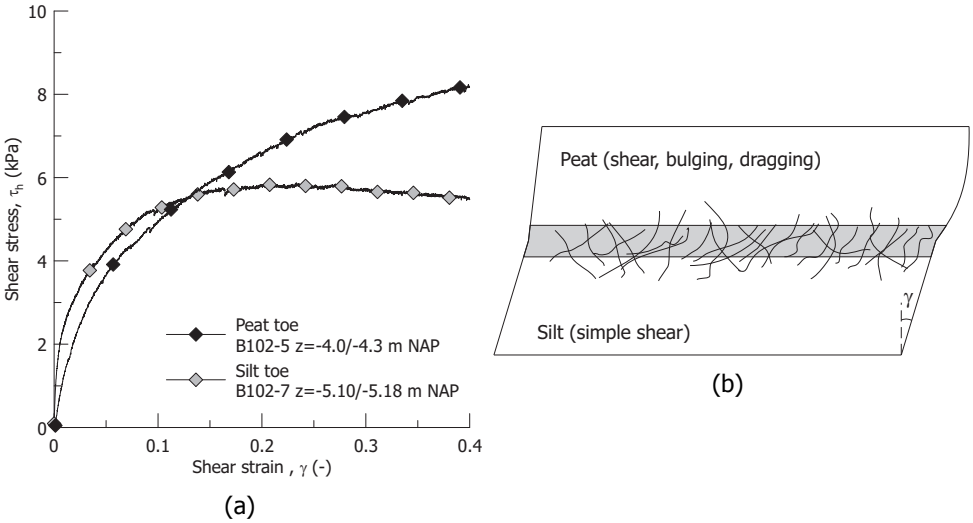

Figure 2.25: Comparison between the shear stress-strain response obtained from constant height simple shear tests on peat and silt undisturbed samples (a) and (b) shear mechanism at the interface between silt and peat

Continuous strain hardening dominate the shear response of peat even for shear strain higher than 30%, with the silt approaching failure well before. The comparison in Figure 2.25 underlines the key role played by the interface between these two materials. Kinematic compatibility at the interface imposes the continuity of the displacements from the peat to the silt formation, resulting in much higher mobilised shear strength in the latter. However the actual interface conditions in the field are essential in defining the degree of the kinematic compatibility before displacement localisation and discontinuity occur.

An undisturbed peat sample (B102-6) taken at the interface between peat and silt along the borehole B102 (Section South Figure 2.2) is displayed in Figure 2.26. Closer detail on the peat formation above the interface revealed abundant randomly oriented fibres, also present within the interface with the silt formation (Figure 2.26(b)). To the author's interpretation the presence of this fibrous network is believed to have played the role of a structural frame, bonding together the peat and the underlying silt formation. The high kinematic constraint exerted by this additional reinforcement assured that the bulging of peat dragged and sheared the silt formation underneath according to the scheme in Figure 2.25(b). The different stress-strain response of these two layers justifies then the occurrence of failure in the silt soil rather than in peat. On the contrary, the inclinometer ItN in Figure 2.21(a) suggests a lower degree of constraint at the interface between the peat and the silt, leading to a localised mechanism without dragging the silt formation, which indeed did not fail.

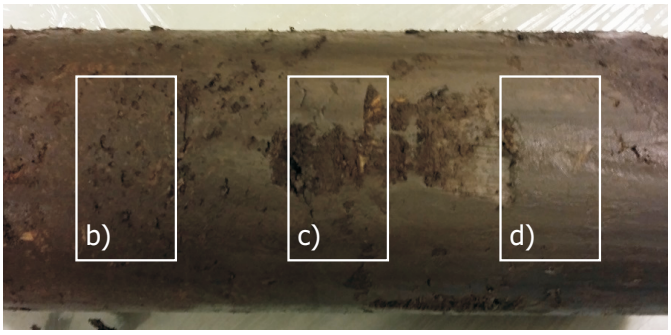

(a)

(b)

(c)

(d)

Figure 2.26: Sample B102-6 taken at the interface between peat and silt at the toe of Section South: (a) 50 cm sample, (b) detail of the fibrous peat, (c) presence of fibres within the interface and (d) silt with horizontally aligned fibres

2.9. CONCLUSIONS

The Leendert de Boerspolder test was designed to investigate the full scale behaviour of regional historical dykes on peats in relation with the current assessment approaches used in the Netherlands. The test allowed to clarify the role of the different foundation layers in the pre-failure and failure mechanism with special attention to the peat. The main conclusions from the field data interpretation are listed below.

- The cause of shear failure for the Leendert de Boerspolder dyke was due to the soft organic silt underneath the peat layer rather than the peat itself. However, the large deformability of peat represented the trigger for the inception of the failure in the silt.
- The failure mechanism was composed by a spreading failure at the toe of the dyke and a consequent sinking of the crest of the dyke. The failure was originated within the first meter of silt underneath the peat as a result of the significant bulging of the peat layer at the toe of the dyke. Taking into account the kinematic compatibility at the peat-silt interface, small shear strains of about 5% were enough to mobilise the ultimate shear strength of the silt.
- Kinematic compatibility between the foundation layers reduced significantly the shear strains required to induce the failure of the system (5%), well below the shear strain attainable by peat at its failure state (15%). For assessment and design criteria based on operational shear strength for peats, shear strength parameters at large strains do not represent the actual field conditions.
- Accounting for the low vertical effective stress of the soils layers at the toe of dyke and the failure mechanism, failure was accompanied by a dilatant response both in the silt and peat, though of different magnitude.
- Gas bubbles release was observed in the excavated area at the toe of the dyke just before the imminent failure, confirming previous field observations. Total stress reduction and pore pressure decrease are triggering factors for gas exsolution and breakthrough. Hence, the influence of gas bubbles must be evaluated and accounted for in the assessment of geotechnical structures on peats.
- The monitoring instrumentation revealed the benefits of installing extensometers rods, still not currently used in the Netherlands, for reconstructing the volumetric and distortional behaviour of the soil layers involved in the shear mechanism.

LIST OF SYMBOLS

Gs	specific gravity
OC	organic content
e	void ratio
w	water content
γ_b	bulk unit weight
k_v	hydraulic conductivity in the vertical direction
σ_v'	vertical effective stress
σ_c'	preconsolidation vertical effective stress
τ_h	horizontal shear stress
OCR	overconsolidation ratio
u_x	horizontal displacement
u_z	vertical displacement
Δu_w	excess pore pressure
ε_p	volumetric strain
ε_q	deviatoric strain
γ	shear strain

3

Are standard undrained triaxial tests on peat wrong? An experimental study aimed to avoid current misinterpretation of the data

원숭이도 나무에서 떨어진다

Even monkeys may fall from trees

Korean saying

The content of this chapter has been submitted as a research article to Géotechnique.

3.1. ABSTRACT

Triaxial tests on peats are strongly criticised due to the difficulty to obtain reliable shear strength parameters applicable in the design and assessment procedures of geotechnical structures. This contribution wants to re-establish the applicability of triaxial tests on peats showing that when end restraint effects on the observed behaviour are ruled out, part of the long-lasting misconceptions on the shear failure of peats can be overcome. Undrained triaxial compression tests have been carried out on reconstituted peat to examine the influence of end restraint on the observed shear strength and on the relationship between deviatoric stress, excess pore pressure and deviatoric strain. Samples have been tested with standard rough end platens and with modified platens to reduce the friction between the sample extremities and the porous stones. Four different initial height to diameter ratio have been examined. The results indicate that end restraint contributes dramatically to the apparent shear strength of the tested samples. Overestimation in the calculated deviatoric stress and in the measured excess pore pressure at the bottom of the sample occur for the typical height to diameter ratio 2 and rough end platens. These effects decrease only for a height to diameter ratio of about 3, although this choice hinders the geometrical stability of the sample. On the contrary, end platens with reduced friction and short specimens allow to reveal the true material behaviour. Overestimation in the ultimate friction angle of 12° is found, passing from 43° to 55°, if the end restraint is not reduced or accounted for when performing triaxial tests on the tested peat.

3.2. INTRODUCTION

Design and assessment procedures in geotechnical engineering require reliable shear strength parameters for the soils. Although obvious, this requirement is still an open issue when organic soils as peats are encountered. Direct shear and ring shear apparatuses have been used in some experimental investigation of natural fibrous peats (Landva & La Rochelle, 1983; Stark & Vettel, 1992; Farrell & Hebib, 1998; Ogino et al., 2002; Komatsu et al., 2011), but the well-known stress non-uniformities, which are amplified by the presence of fibres and by the large strains attained by peat samples, make the results rather arguable. The direct simple shear apparatus is widely preferred based on the assumption that it guarantees more uniform stress and strain states (O'Kelly, 2017). However, the assumption is questionable too (Ladd & Edgers, 1972; Wood et al., 1979; Budhu, 1984; Airey, 1984; Budhu, 1988), and clear evidence of non-uniform strains is shown by tracking the specimen deformation as in the videos taken on simple shear tests on large samples by Den Haan & Grognet (2014). In addition, in the common engineering practice direct simple shear tests on peat are performed in undrained conditions, which impose a failure mechanism not necessarily corresponding to what observed in the field. On the contrary, peat layers in the foundation of dykes and railway lines often show failure mechanisms dominated by lateral bulging and vertical compression, which are not necessarily characterised by a constant volume constraint (Landva & La Rochelle, 1983; Tashiro et al., 2015; Acharya et al., 2015).

Triaxial tests are used to obtain more reliable information on the deformation mechanism of soils at failure. However, the use of both drained and undrained triaxial tests on peats has been strongly criticised. High shear strength parameters are often derived from undrained triaxial compression tests with friction angles in the range of 50°-70° (Adams, 1961; Oikawa & Miyakawa, 1980; Landva & La Rochelle, 1983; Yamaguchi et al., 1985b; Farrell & Hebib, 1998; Edil & Wang, 2000; Cola & Cortellazzo, 2005; Cheng et al., 2007). The presence of multiples fibrous networks in the peat fabric stretched during axial compression are claimed to be responsible of the observed high friction angles, as they provide additional reinforcement to the material, thus increasing the observed shear strength. It is not rare that fibrous peat samples develop high excess pore water pressure leading to null effective radial stress, which brings the stress state of the sample towards the tension cut off line, TCO, or above it, before failure is reached (Oikawa & Miyakawa, 1980; Kanmuri et al., 1998; Boulanger et al., 1998; Cola & Cortellazzo, 2005; Hendry et al., 2012). Still, the stress-strain response is typically dominated by strain hardening behaviour, with a deviatoric stress increasing almost linearly with the deviatoric strain at high strain levels, which makes the definition of a failure criterion rather subjective. Drained triaxial compression tests are not considered suitable for peats, due to the fibres reinforcement, which does not allow to reach failure, with the deviatoric stress steadily increasing for axial strain even above 30% (Farrell & Hebib, 1998; O'Kelly & Zhang, 2013; O'Kelly, 2015).

Several criteria have been proposed in the literature to correct the exceptionally high shear strength parameters for peats, derived from a conventional interpretation of triaxial tests, which have scarce applicability in the engineering practice.

Using a strain based approach, failure is identified with the attainment of an arbitrary axial strain threshold (15% in Ogino et al. (2002) and Hayashi et al. (2012), 2% and 5% in Den Haan & Feddema (2013) for undrained compression tests, and 20% in Zhang & O'Kelly (2014) for drained compression tests). Different alternatives have been proposed based on extrapolation of the experimental data in the stress-strain or in the stress path planes, in the attempt to limit the reference deviatoric stress at failure (Kanmuri et al., 1998; Den Haan & Kruse, 2007; Hendry et al., 2012; O'Kelly, 2017). Kanmuri et al. (1998) and more recently Hendry et al. (2012) proposed to associate failure to the start of the ultimate linear strain hardening response in undrained triaxial compression tests. This choice roughly coincides with the proposal by Oikawa & Miyakawa (1980), who suggested to identify failure as the transition between contractive and dilatant response. Despite these approaches being useful in the practice, where reasonable shear strength parameters are required, their mechanical ground is still a matter of debate, which raises doubts on the reliability of these choices.

The current prejudices towards triaxial tests on peats also come from misinterpretation of the experimental results. Data from triaxial tests are traditionally elaborated assuming stresses and strains uniformity implying they give representative information on the true material behaviour. However, the intense experimental efforts in the 1960's to investigate the restraining effects of the cap and base on the response of triaxial specimen clearly showed that the boundary conditions imposed to the sample with standard laboratory devices are far from being uniform (Rowe & Barden (1964), Bishop & Green (1965) for sands; Olson & Campbell (1964), Barden & McDermott (1965) and Duncan & Dunlop (1968) for clays). Therefore, the observed behaviour derived from stress-strain quantities based on averaged external measurements may be significantly different from the true material behaviour and may lead to a fictitious increase in the apparent shear strength of the soil. To limit these problems, samples should be tested by adopting lubricated end platens or with high height to diameter ratio.

Shockley & Ahlvin (1960) warned on the importance of end restraint when failure occurs by bulging rather than with a well-defined shear plane, as typically observed in undrained triaxial compression on peats. To the author's knowledge no dedicated studies are reported on end restraint effects for peat samples tested in triaxial apparatuses, although the high compressibility and the additional reinforcement offered by the fibres allow peat samples to sustain exceptional axial strains upon compression, thus enhancing stresses and strains non-uniformities (Rowe et al., 1984). Paradoxically, only few isolated indications about possible end restraint effects on the observed peat behaviour are reported for ring shear apparatus by Stark & Vettel (1992) and for direct simple shear by Yamaguchi et al. (1987). The latter authors showed that the shear strength of natural peat samples is significantly affected by the height to diameter ratio and that the friction at the top and bottom of the sample increases the observed strength.

The role of end restraint on the coupled hydro-mechanical response of peat tested in undrained triaxial compression is systematically investigated here, in a dedicated experimental study. To isolate the effects of end restraint from the ad-

ditional reinforcement offered by big fibres, reconstituted peat samples with small fibres were used. Samples with different height to diameter ratio were tested, with both standard rough end platens and modified end platens, which reduce the shear stresses at the sample boundaries. Special attention is given to clarify the difference between the sample behaviour and the true material behaviour in terms of deviatoric stress-strain response and excess pore pressure. Adopting modified end platens reveals a dramatic reduction in the estimated ultimate friction angle for the tested peat. The results contribute to re-establish the potential of triaxial tests on peats, provided that stresses and strains non-uniformities are reduced or their effects are taken into account when elaborating the experimental data.

3.3. EXPERIMENTAL PROGRAMME

3.3.1. Material

The peat used in this investigation was collected 1.0 to 1.5 m below the ground surface, at the Leendert de Boerspolder site in the Netherlands. To reduce biodegradation, the material was stored in a climate controlled room at 10±1°C and 90% relative humidity. Reconstituted peat samples were prepared by mixing the material with demineralised water to a slurry with water content of 855%, corresponding to 1.4 times the liquid limit. Afterwards, the material was consolidated in a floating consolidometer under a total vertical stress of 10 kPa for 48 hours, before mounting in the triaxial apparatus. The oven-drying procedures for soil classification were performed at a temperature of 60°C (Head, 2014). The specific gravity of the soil, Gs, was measured with a helium pycnometer in accordance to D5550-14 (2014). The organic content, OC, was assessed by igniting oven-dried samples in a furnace at 500°C (D2974-14, 2014; Den Haan & Kruse, 2007). Table 3.1 reports the index properties of the tested samples. Fibre content determination gave an average value of 0.14 (D1997-13, 2013).

Figure 3.1 displays a picture obtained from x-ray micro CT on the tested peat, after 2 days drying at a temperature of 14°C and relative humidity of 80%. Inorganic soil grains are visible with higher density (white spots) within the fibrous matrix. The fibrous structure is characterised by diffuse small fibres having a maximum length of about 3 mm.

3.3.2. Experimental procedure

The testing programme consisted in a series of conventional undrained triaxial compression tests. To complement the information about the volumetric behaviour, a K_0-consolidation test was carried out. The tested specimens were 38 mm in diameter and with variable height according to the prescribed initial height to diameter ratio, H_0/D_0, as reported in Table 3.1. The choice of testing 38 mm samples was imposed by the limited height of the triaxial apparatus for the tallest specimen. Nonetheless, the representativeness of the tested soil volume is assured, given the short fibres present in the peat matrix (Lade, 2016). The tests were carried out using a GDS load frame triaxial apparatus with back pressure and cell pressure volume controllers and submersible 1 kN load cell, under controlled air

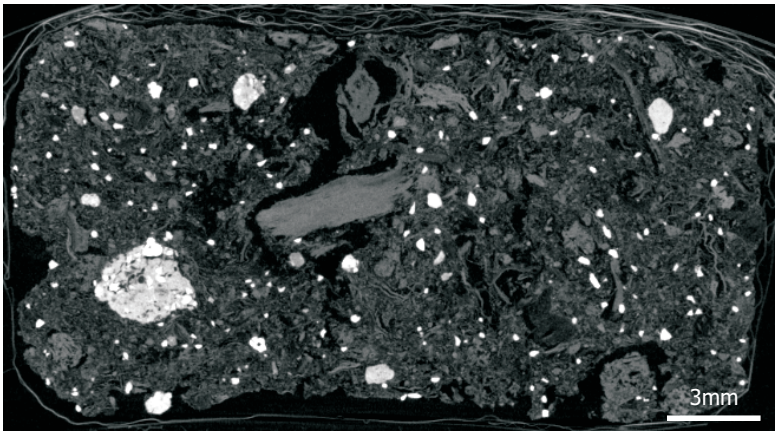

Figure 3.1: Micro CT scan of the reconstituted peat used in the experimental investigation (white spots: denser inorganic constituents)

temperature 14±1°C and relative humidity 80%. The accuracy of the controllers is ±1 kPa on pressure and ±300 mm^3 on volume (0.15% full scale range, FSR). Thin membranes 0.25 mm thick were used. To accelerate the consolidation process, lateral filter paper was placed around the samples. To prevent "short circuit" effects between the back pressure and the pore pressure transducer located at the bottom of the sample, 10 mm of clearance were left between the lower edge of the lateral filter paper and the bottom of the samples (Head & Epps, 2014b). To reduce end restraint effects on the observed behaviour, two approaches were adopted (Figure 3.2):

- increasing the height to diameter ratio for tests with standard rough platens;
- modifying the end platens by interposing a perforated plastic disk and a perforated nitrile membrane 0.1 mm thick between the filter paper and the sample.

No silicone grease was applied between the perforated plastic disk and the nitrile membrane due to the difficulty in preventing contamination of the filter paper and the porous stone. Despite the present solution not assuring the same effectiveness as the one adopted in Rowe & Barden (1964), the lower friction between the nitrile membrane and the plastic disk compared with the one at the interface between the filter paper and the porous stone already improves the uniformity of stresses and strains. Not using enlarged platens was compensated by the significant lateral contraction experienced by the samples during the initial isotropic consolidation. To assure perfect contact between the top cap and the load cell, a suction cap was used.

The samples were isotropically consolidated up to a pre-consolidation mean effective stress p'_c of about 35 kPa (Table 3.1) and then sheared in undrained conditions at constant axial strain rate, $\dot{\varepsilon}_a$= 0.02%/min. Four tests were conducted with standard rough end platens and a height to diameter ratio increasing from

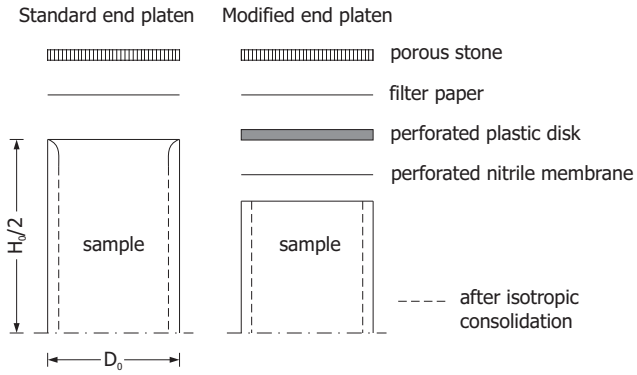

Figure 3.2: Standard and modified end platens adopted in the present experimental investigation to reduce the end restraint

H_0/D_0=1.5 to H_0/D_0=3. Sample 5 with H_0/D_0=1.5, and sample 6 with H_0/D_0=2, were tested with modified end platens. The strain rate was chosen to theoretically assure pore pressure equalisation (Blight, 1963; Lade, 2016). The average axial strain rate experienced by sample 7, tested under drained K_0 stress control, is reported in Table 3.1. The void ratio in Table 3.1 refers to the initial void ratio of the samples before the initial isotropic consolidation.

Table 3.1: Index properties of the tested specimens and specifics of the triaxial tests conducted

Sample	Gs (-)	e (-)	OC (-)	p'_c=p'_0 (kPa)	Path	H_0/D_0 (-)	End platens	$\dot{\varepsilon}_a$ (%/min)
Sample 1	1.49	9.70	0.90	35	TxCU	1.5	Standard	0.02
Sample 2	1.49	9.80	0.90	35	TxCU	2.0	Standard	0.02
Sample 3	1.54	10.39	0.90	34	TxCU	2.5	Standard	0.02
Sample 4	1.49	9.64	0.90	35	TxCU	3.0	Standard	0.02
Sample 5	1.49	9.89	0.90	34	TxCU	1.5	Modified	0.02
Sample 6	1.47	9.59	0.90	33	TxCU	2.0	Modified	0.02
Sample 7	1.50	10.31	0.91	-	K_0	2.0	Standard	0.008

3.3.3. Stresses and strains variables

All the experimental data have been elaborated by adopting the common triaxial stress variables, namely the mean effective stress p', the deviatoric stress q and the corresponding strain variables, volumetric strain, ε_p, and deviatoric strain, ε_q. Natural strains were adopted due to the large displacements typically reached when testing peats (Ludwik, 1909; Hencky, 1928). The deviatoric strain has been computed from ε_p and ε_a derived from the volume change and the axial displacement measurements:

$$\varepsilon_p = \varepsilon_a + 2\varepsilon_r = \ln \frac{V_0}{V} \tag{3.1}$$

$$\varepsilon_q = \varepsilon_a - \frac{\varepsilon_p}{3} = \ln\frac{H_0}{H} - \frac{1}{3}\ln\frac{V_0}{V} \tag{3.2}$$

where V_0 and H_0 are the initial volume and height of the sample, while V and H are the current values.

3.4. EXPERIMENTAL RESULTS

3.4.1. Deviatoric stress-strain response

Shear stresses at the interface between the sample and the porous stone constrain the lateral expansion of the sample upon axial compression, hence higher average axial stress and stiffness are expected. The impact on the calculated deviatoric response is reported in Figure 3.3(a), where the deviatoric stress is normalised with the mean effective stress at the beginning of shear, p'_0. In Figure 3.3(b) the calculated secant shear stiffness at 2% and 5% of deviatoric strain on the different samples are compared.

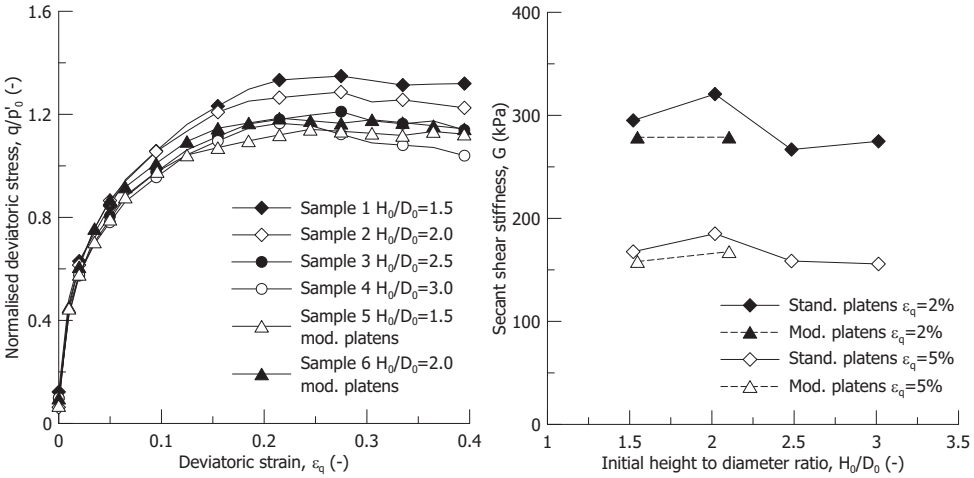

Figure 3.3: Deviatoric stress-strain response (a) and secant shear stiffness (b) upon undrained compression tests on samples with different height to diameter ratio tested with standard and modified end platens

The normalised deviatoric stress at failure decreases considerably with the height to diameter ratio towards the values calculated on sample 5 and sample 6, tested with modified end platens. The deviatoric stress levels off at about 25% of deviatoric strain, with the samples tested with modified end platens showing a more regular asymptotic response (Figure 3.3(a)). It is worth noting that the decrease in the deviatoric stress of sample 4 after $\varepsilon_q \cong 20\%$ is due to buckling occurring on the specimen. At small deviatoric strains, 2%-5% (Figure 3.3(b)), the modified end platens slightly reduce the overall secant shear stiffness for the same height to

diameter ratios compared to standard end platens, as in Duncan & Dunlop (1968) and Lade & Tsai (1985).

3.4.2. Excess pore pressure

The impact of end restraint on the excess pore pressure depends on the height to diameter ratio and on the friction between the sample and the end platens. In conventional undrained tests, rough end platens provide high resistance to the sample lateral expansion, inducing higher excess pore pressure at the top and bottom of the sample compared to the central portion (Rowe & Barden, 1964). Figure 3.4 depicts the excess pore pressure measured at the bottom of the samples, Δu_w, using standard and modified end platens. The values are normalised with p'_0.

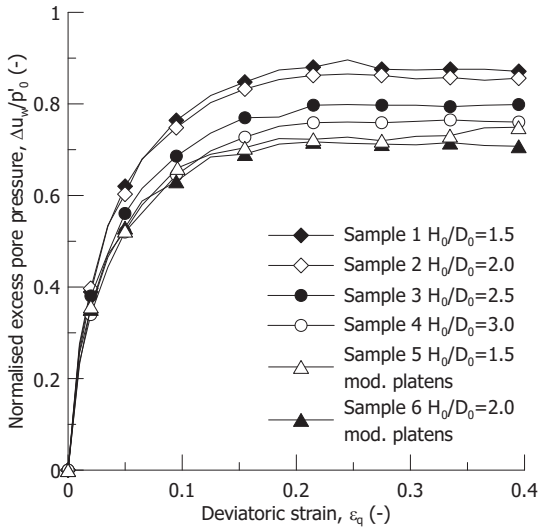

Figure 3.4: Excess pore pressure measured at the bottom of the samples with different height to diameter ratio tested with standard and modified end platens

The excess pore pressure measured at the bottom decreases with the height to diameter ratio, with the highest excess pore pressure measured for the shortest specimen, 18% higher than when modified end platens were used. Compared to the commonly adopted ratio H_0/D_0=2, significant benefit was already found for H_0/D_0=2.5. However, the findings in Figure 3.4 confirm that modified end platens are the most effective solution to avoid overestimation of the excess pore pressure, regardless the sample height to diameter ratio (sample 5 and sample 6). Benefits of low friction end platens on the pore pressure magnitude are well documented in the literature for classical inorganic soils (Olson & Campbell (1964) on sodium kaolinite, Barden & McDermott (1965) on Jackson boulder clay and Chelmarsh boulder clay, and Duncan & Dunlop (1968) on San Francisco bay mud, among others), but they had never been systematically investigated for peats.

3.4.3. Deformation mode and influence of the compressibility

Two aspects, among others, characterise the hydro-mechanical response of peats: a very high compressibility and relative low hydraulic conductivity, especially after the initial compression stage. The compressibility of peats has been traditionally investigated in oedometer (Landva & La Rochelle, 1983; Lefebvre et al., 1984; Den Haan & Edil, 1994; Den Haan, 1996; Mesri et al., 1997; Mesri & Ajlouni, 2007; Madaschi & Gajo, 2015b), while scarce attention has been paid in evaluating its implications during shear. Rough end platens in standard triaxial apparatuses restrain the lateral deformation at the top and bottom of the sample, creating two so-called dead zones, and confine the unrestrained part, the so-called free failure zone, to the central part of the sample. However, the existence and the extension of the free-failure zone depend on both the shear strength and the compressibility of the soil. If the dead zones are assumed to be inclined at $\beta = 45 + \varphi' / 2$ with respect to the horizontal for the sake of simplicity (Kirkpatrick & Belshaw, 1968), it is possible to estimate the extension of the free failure zone, L, over the sample height at failure, H_f, as reported in Figure 3.5 for different values of φ' and height to diameter ratio at failure, H_f/D_f.

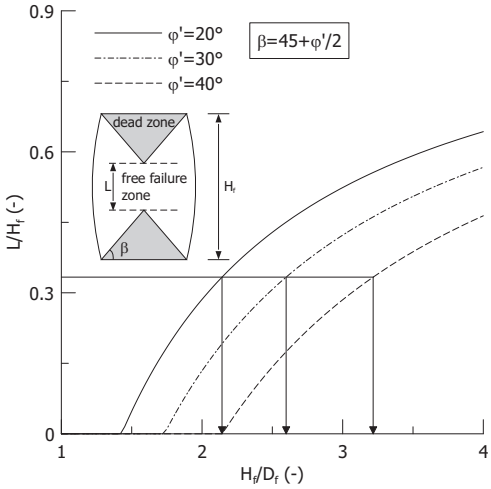

Figure 3.5: Extension of the free failure zone for different values of friction angle and height to diameter ratio

The commonly accepted hypothesis that with a sample having H_f/D_f=2, the middle third (i.e. L/H_f=1/3) will deform without restraint (Head & Epps, 2014a) does not hold already for φ'=30°. Despite the hypothesis on the inclination of the dead zone used in Figure 3.5 being the most unfavourable (Rowe & Barden, 1964; Roscoe, 1970; Arthur et al., 1977; Drescher & Vardoulakis, 1982), it is likely that the combination of high compressibility and high friction angle characterising peats, will rapidly reduce the "free failure" zone compared to any other stiffer soil (Figure 3.6). Eventually, at increasing axial strain the two dead zones merge and form connected dead wedges which force the lateral expansion of the external portion of the sample

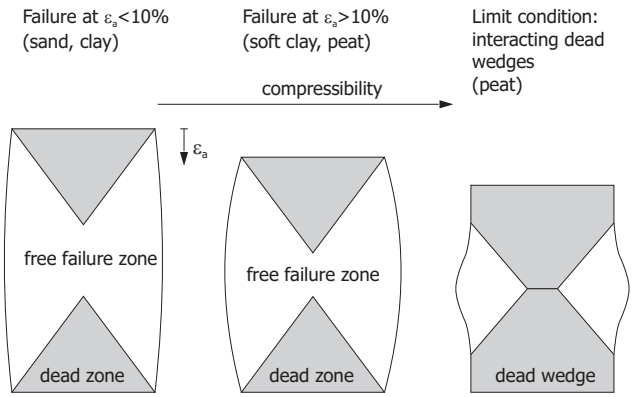

Figure 3.6: Influence of the compressibility on the extension of the free failure zone in samples with: (a) low compressibility, (b) high compressibility and (c) limit condition for peat

in the form of a localised bulging. This is schematically depicted in Figure 3.6 passing from a sand or clay sample to a soft clay and eventually to a peat sample. With the free failure zone reducing in size, the triaxial test loses representativeness as a soil "element" test. The evolution of the deformation mode can be appreciated in Figure 3.7 from a parallel test on a peat sample H_0/D_0=2 sheared with standard rough end platens under stress control. The deformation mode evolved towards the formation of two dead wedges penetrating into the central portion of the sample and enforcing the lateral expansion of the external parts.

3.4.4. Water content profile

The kinematic constraint imposed by the end restraint eventually results in a volume reduction of the soil within the dead zone, which is compensated by the expansion of the central portion of the sample. The result of a non-uniform pore pressure distribution within the sample is an internal water migration from the top and bottom of the sample towards the central portion, despite the external undrained conditions. At the end of the test, each sample was rapidly dismounted and cut into three or more segments, depending on the failure mode, for water content determination. The similarity between the deformed shape of the sample and the measured water content profile can be appreciated from Figure 3.8 for the case of sample 5 and sample 2, tested with modified and standard end platens respectively (w_{ave} is the average water content along the height of the sample measured at the end of each test). The deformed shape and the water content profile of sample 5 show significant uniformity thanks to the adoption of the modified end platens (Figure 3.8(a)). On the contrary, the water content profile of sample 2 replicates the non-uniform deformation mode shown in Figure 3.8(b), with higher water content in the central portion.

The water content ratio profiles w/w_{ave} of all the samples at failure, shown in Figure 3.9 clearly indicate that during the test water migrated from the top and bottom of the sample towards the central portion. When standard end plates are used,

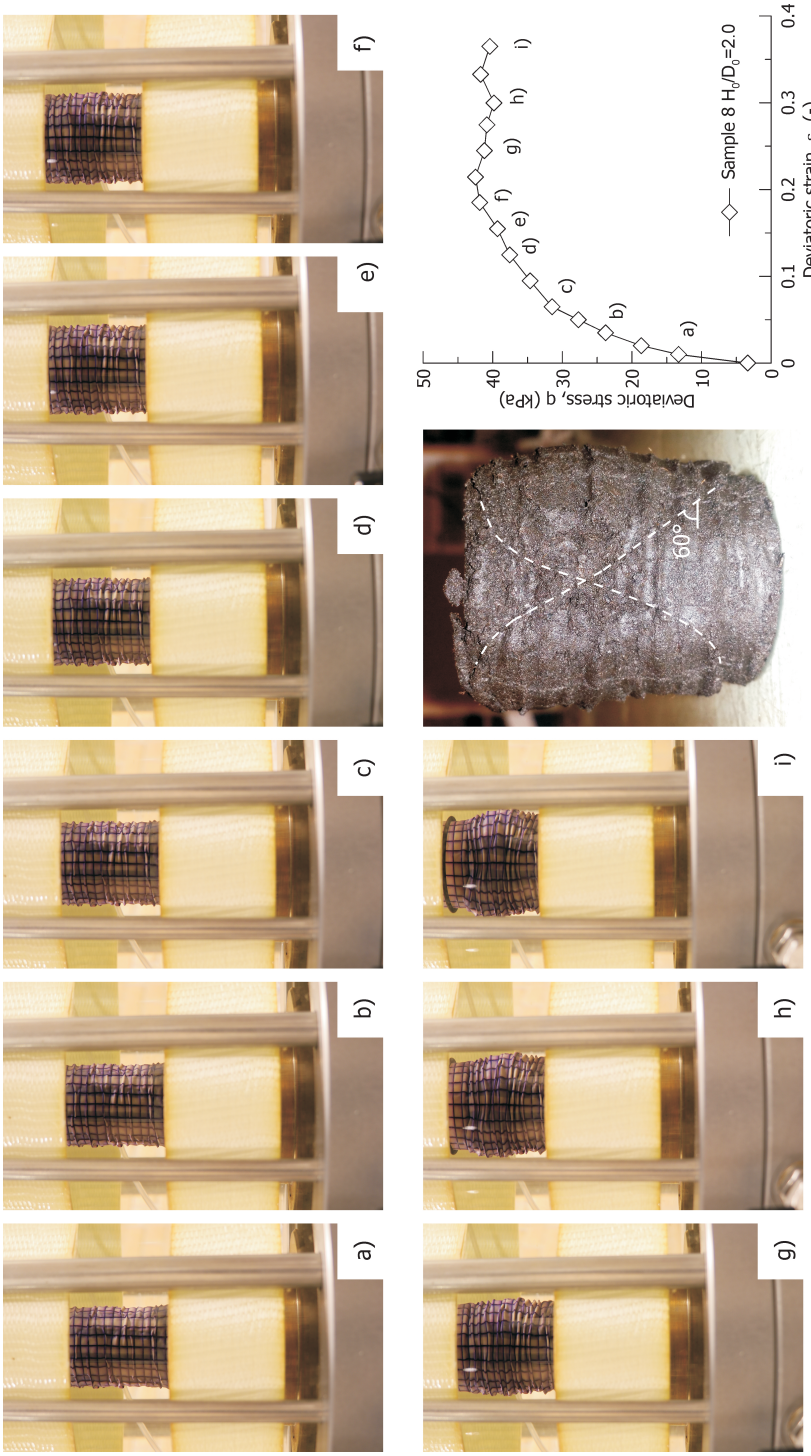

Figure 3.7: Evolution of the deformation mode for a sample with H_0/D_0=2 and standard rough end platens sheared under stress control

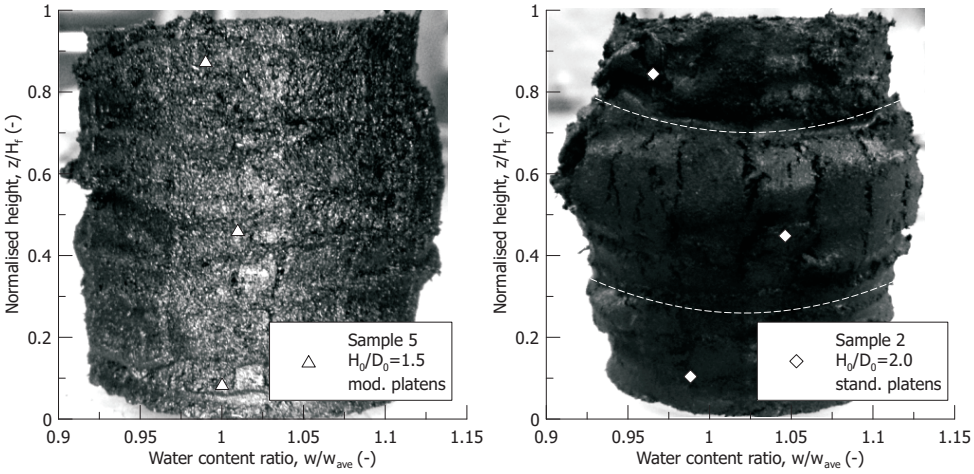

Figure 3.8: Analogy between the deformed shape and the water content profile in samples tested with (a) modified end platens and (b) standard end platens

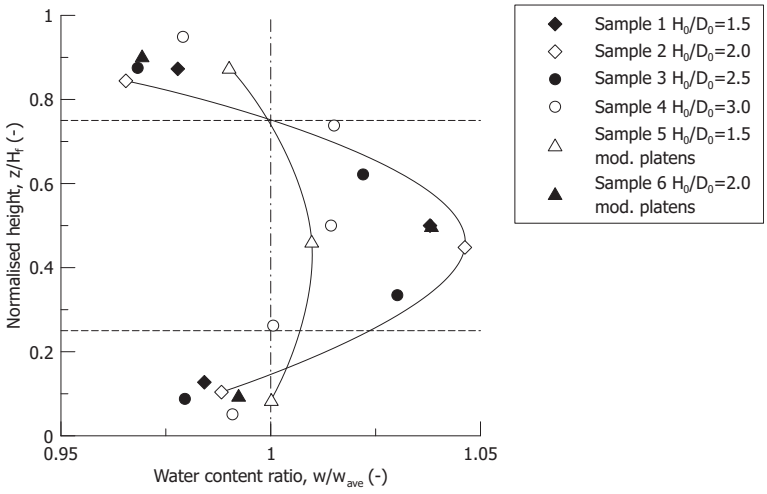

Figure 3.9: Water content profiles at the end of undrained compression tests on samples with different height to diameter ratio tested with standard and modified end platens

the final water content in the central portion of the sample is 5% higher than the average one. The highest difference is found for the sample with H_0/D_0=2 while the tallest tested sample, H_0/D_0=3 shows a lower deviation, namely 2%. Only with modified end platens and short sample H_0/D_0=1.5 the measured water content is almost uniform within the sample. It is worth noticing that despite the modified end platens, the water content in sample 6 shows a deviation due to the significant lateral expansion of the sample observed at the end of the test. However, this behaviour had no consequence on the measured excess pore pressure, similar to sample 5, also tested with modified end platens. A digital camera placed in front of sample 6 confirmed the formation of a localised lateral expansion only at the end of test when the excess pore pressure and deviatoric stress already levelled off. Based on the same considerations, Rowe & Barden (1964) and Barden & McDermott (1965) suggested the adoption of lubricated ends with samples H_0/D_0=1 to guarantee geometric stability.

3.4.5. Computed shear strength

The effects of end restraint on the excess pore pressure, and on the deviatoric stress both contribute in the calculation of the stress ratio, $\eta=q/p'$. Figure 3.10(a) reports the evolution of the calculated stress ratio plotted against the deviatoric stress increment normalised to p'_0, given by:

$$\frac{\delta q}{p'_0} = \frac{\delta F \cdot A - F \cdot \delta A}{p'_0 A^2} \tag{3.3}$$

where F is the axial force on the sample and A is the cross sectional area of the volumetrically equivalent cylinder.

Significant reduction in the ultimate stress ratio is observed with standard end platens by increasing the height to diameter ratio, from η_u=2.4 for H_0/D_0=1.5 to η_u=1.86 for H_0/D_0=3 (Figure 3.10(a)). However, samples with modified end platens reach failure for η_u=1.75, regardless the sample height. If the results are translated in terms of ultimate friction angle, Figure 3.10(b), the dramatic impact of end restraint on the estimated value becomes more evident. The overestimation for standard H_0/D_0=2 sample tested with conventional end platens compared to the samples tested with modified end platens is about 12°, passing from $\varphi' \cong 43°$ to $\varphi' \cong 55°$. The evolution of the stress ratio with the rate of the deviatoric stress deserves further attention. Samples tested with conventional end platens eventually show a steady increase in the stress ratio (i.e. mobilised shear strength) at a constant rate of deviatoric stress (vertical traits in Figure 3.10(a)). For natural fibrous peats deviatoric strain hardening is typically ascribed to the stretching of the fibres (Kanmuri et al., 1998; Cola & Cortellazzo, 2005; Zwanenburg et al., 2012; Hendry et al., 2012). However, these results show that there is a dominant effect of end-restraint which affects the observed response, even in the absence of big fibres. The vertical trait in the stress ratio with $\delta q \cong 0$ reduces as the height to diameter ratio increases, and eventually disappears when modified end platens are used.

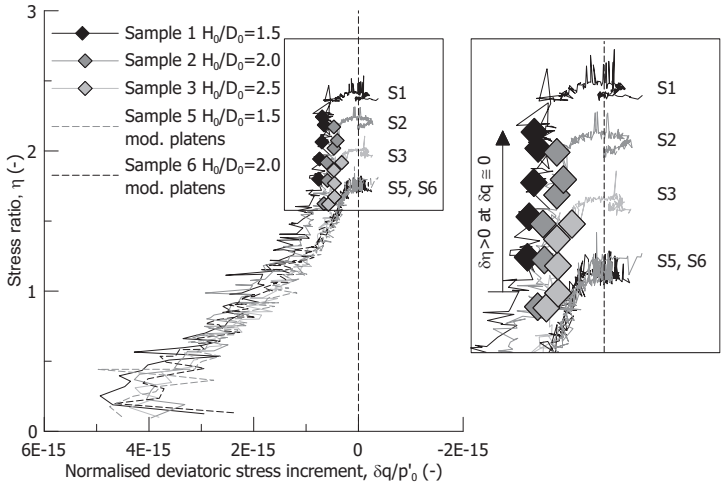

(a)

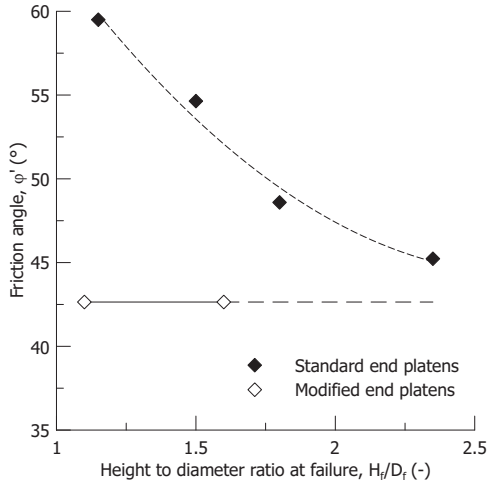

(b)

Figure 3.10: Stress ratio plotted against deviatoric stress rate (a) and (b) friction angle estimated from undrained compression tests on samples with different height to diameter ratio tested with standard and modified end platens

3.5. A PRACTICAL PROPOSAL TO REDUCE EXPERIMENTAL LIMITATIONS

The previous observations can be exploited to reduce some of the potential sources of error in the interpretation of the experimental data from standard triaxial tests with limited experimental effort.

3.5.1. K_0 at normally consolidated state

The implications of end restraint on the mobilised friction angle of peat are of great importance not only for ultimate limit states (i.e. shear strength), but also for serviceability limit states, where a correct determination of the field stress state is required. A long-lasting debate still holds about the validity of the empirical Jaky's simplified relationship (Jaky, 1948), $K_0 \cong 1 - sin\varphi'$, for estimating the coefficient of earth pressure at rest for normally consolidated peats. Several contributions reported that Jaky's relationship predicts values well below the ones obtained from K_0 apparatuses such as K_0-CRS or K_0 triaxial paths (Mesri & Ajlouni, 2007; Den Haan & Kruse, 2007; Leoni et al., 2010). Edil & Dhowian (1981) stated that "φ' is not adequate, as a single parameter, to reflect the lateral load transfer mechanisms due to the different nature of the microstructure in peat soils, in particular, due to the presence of fibres". Despite the differences between the fabric of peats and of inorganic cohesionless soils, for which the simplified Jaky's relationship was derived, the claimed inconsistency seems to come mostly from the uncertainty on the determination of the "true" friction angle. Satisfactory estimations of K_0 with Jaky's relationship were obtained in the literature by limiting the mobilised friction angle from standard undrained compression tests on natural fibrous peats either at subjective strain thresholds (Hayashi et al., 2012), or at the transition between contractive and dilatant response (Oikawa & Miyakawa, 1980; Mesri & Ajlouni, 2007). To clarify this aspect, a K_0-consolidation path was performed on sample 7 with rough end platens. The test was performed with an automated axial-radial stress ramp with volume change and axial displacement back measurements allowing for negligible radial strains. The calculated lateral pressure ratio K

$$K = \frac{3 - \eta}{3 + 2\eta} \tag{3.4}$$

where η is the current stress ratio, is reported in Figure 3.11.

The lateral pressure ratio decreases gently with the axial effective stress and levels off for K_0=0.33 in accordance with previous findings (Edil & Wang, 2000; Den Haan & Kruse, 2007; Hayashi et al., 2012). For the friction angle $\varphi' \cong 43°$ determined from samples with modified end platens, (sample 5 and sample 6, Figure 3.10(b)), Jaky's relationship gives K_0=0.32, in agreement with the result in Figure 3.11.

It is worth noting that over a K_0 stress path null radial strains theoretically rule out end restraint effects. The K_0 value obtained experimentally in this type of test well matches the value estimated from failure in TxCU tests with modified end platens. The evidence substantiates that Jaky's relationship can be used for peats, and sug-

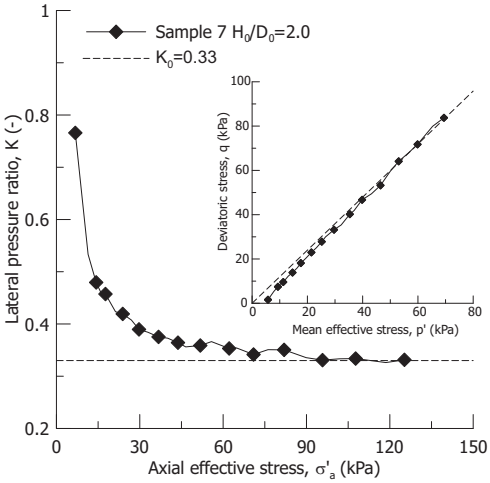

Figure 3.11: Lateral pressure ratio plotted against axial effective stress from a K_0 consolidation path

gests that K_0 determined on normally consolidated samples could be used to infer the "true" friction angle at failure of peats.

3.5.2. Estimation of the pore pressure difference within the sample

The difference in pore pressure between the bottom and the mid height of the sample affected by end restraint can be non-negligible, especially when small effective confining stresses are imposed on peats having low hydraulic conductivity (Kodaka et al. (2007) and Oka et al. (2005) on Fukakusa clay). If the only available measurement of pore pressure is located at the bottom or at the top of the sample, in the presence of significant end restraint, a non-negligible error is introduced in the estimation of the effective stress path followed by the central portion of the sample (Barden & McDermott, 1965; Blight, 1963).

The water content profiles in Figure 3.9 can be exploited to provide an estimation of the pore pressure difference between the bottom (B) and the mid height of the sample (M), $\Delta u_{w,BM}$, and to correct the apparent stress path for the effect of end restraint on the measured pore pressure. The different volumetric constraint at the extremities and at the central part of the sample promotes an internal water flow. The internal flow rate, q_w, is assumed to be one directional and on average measured by:

$$q_w = -\frac{k_v}{\gamma_w}\frac{\Delta u_{w,BM}}{H/2} \tag{3.5}$$

where k_v is the hydraulic conductivity in the vertical direction, γ_w is the unit weight of water and H is the current sample height. The corresponding mass of water flowing towards the central part of the sample in a time interval Δt can be estimated as:

$$\Delta M_w = 2\rho_w q_w A \Delta t \tag{3.6}$$

where ρ_w is the density of water and A is the cross sectional area of the volumetrically equivalent cylinder. Equation 3.5 and equation 3.6 give a mean to estimate the pore pressure difference between the bottom and the centre of the sample, which reads:

$$\Delta u_{w,BM} = -\frac{g}{4k_v}\frac{H}{A}\frac{\Delta M_w}{\Delta t} \tag{3.7}$$

where g is the gravity acceleration. Assuming a uniform distribution of water content at the start of shear, and knowing the water content profile at the end of the test, (Figure 3.9), the time evolution of the water mass change in the central part of the sample, ΔM_w, is estimated assuming a second order polynomial function, as depicted in Figure 3.12. The rate of the water mass change in Figure 3.12 increases with time as a result of the deformation mode of the sample affected by end restraint. The values are normalised with the initial mass of the water at the mid height of the sample, M_{w0}, and the time, t, with the time at failure, t_f.

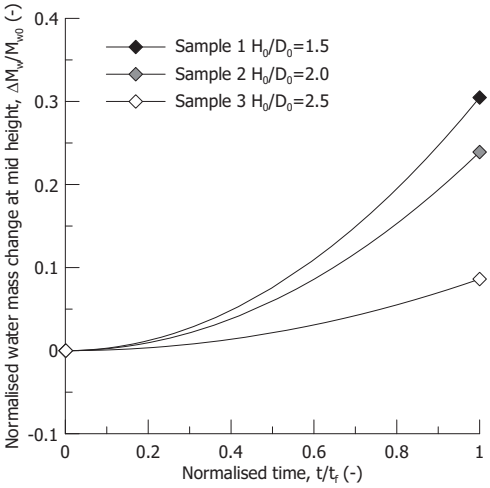

Figure 3.12: Estimated evolution of the water mass change at the mid height of each sample with the test time

The hydraulic conductivity, k_v, of the tested peat was determined from an oedometer apparatus equipped with pore pressure transducers (Zhao & Jommi, 2018). Hydraulic conductivity in the order of $k_v \cong$1e-09 m/s was obtained for a void ratio of about 7, attained on average by the samples during the undrained shear. The estimated pore pressure at the mid height of the sample over the shearing stage is compared with the measured one on samples 1, 2 and 3 respectively in Figure 3.13. The excess pore pressure measured at the bottom of sample 5 tested with modified end platens is also reported for the sake of comparison.

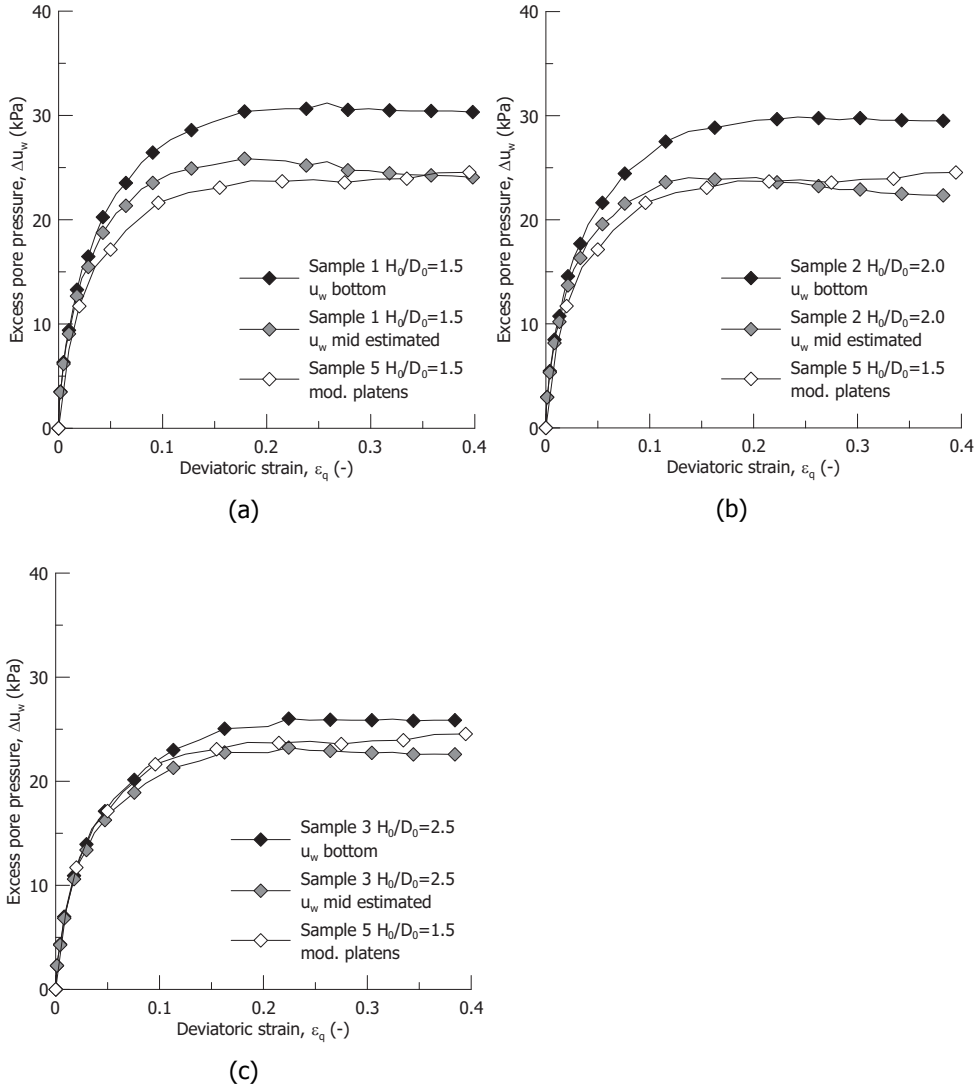

Figure 3.13: Excess pore pressure measured at the bottom and estimated at the mid height for (a) sample 1, (b) sample 2 and (c) sample 3 sheared with standard end platens and different height to diameter ratio

The estimated difference in the excess pore pressure between the bottom and the mid height of the sample at the end of the test is about 7 kPa for H_0/D_0=1.5-2, and 3 kPa for H_0/D_0=2.5. The corrected pore pressure for the sample tested with rough platens well matches the measured one at the bottom of sample 5 tested with modified smooth platens. The estimated pore pressure at mid height is used to correct the stress path followed by the samples. The results are shown in Figure 3.14, compared to the stress paths calculated with the measured pore pressure at the bottom.

The correction results in a horizontal translation of the calculated stress paths, which tend to become closer to the stress path calculated from the test with modified end platens (sample 5). The applied correction does not modify the computed deviatoric stress but allows to reduce significantly the error introduced by the overestimation of the excess pore pressure at the bottom of the sample on the derivation of the ultimate stress ratio when standard end platens are used. The benefits are visible in Figure 3.15 where the pore pressure parameter, a (Wood, 1990) is computed from the corresponding stress path as:

$$a = -\frac{\Delta p'}{\Delta q} \tag{3.8}$$

Over the entire stress path, the response moves from a contractive regime, a>0, asymptotically towards a dilatant regime, a<0 passing through the condition a=0 for a stress ratio which identifies the critical stress ratio, M_g. As displayed in Figure 3.15 if the pore pressure measured at the bottom of the sample is used to calculate the stress path, the result is a non-negligible overestimation of the critical stress ratio. Sample 1 and sample 2 attain the condition a=0 for a stress ratio η_u=2.4 and η_u=2.2 respectively. However, if the estimated pore pressure at the mid height of the sample is used in the attempt to remove end restraint effects, the new stress paths intersect a=0 for η_u=1.75=M_g which coincides with the ultimate stress ratio calculated from sample 5 and 6 tested with modified end platens (Figure 3.10(a)).

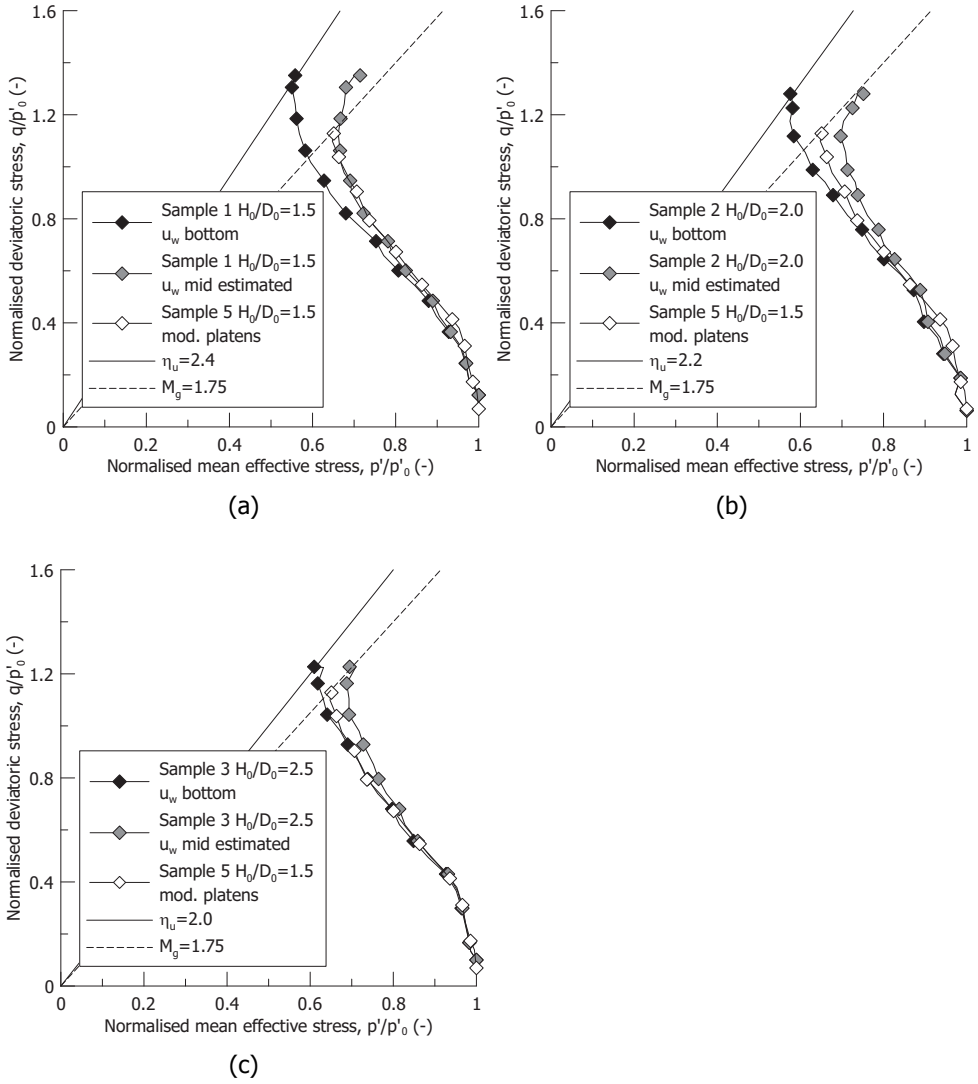

Figure 3.14: Stress path calculated with the measured pore pressure at the bottom of the sample and with the estimated one at the mid height for (a) sample 1, (b) sample 2 and (c) sample 3

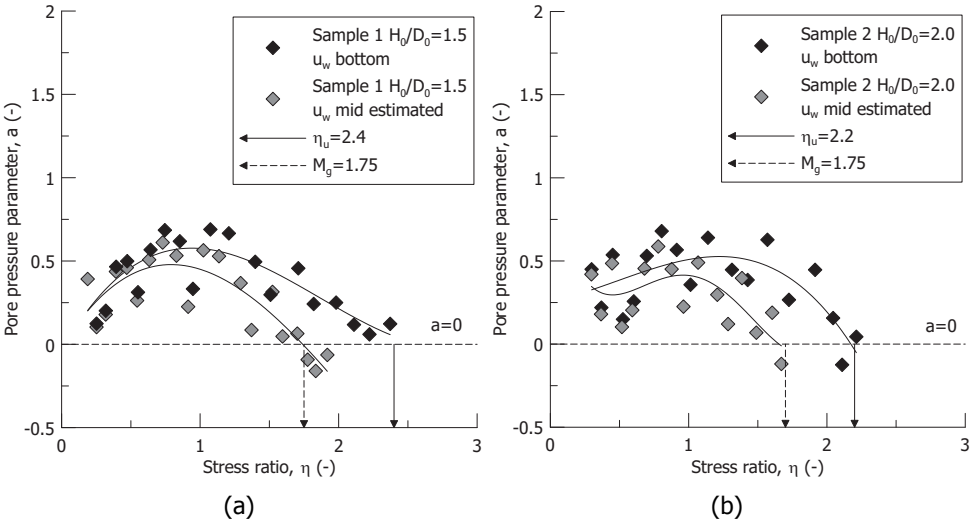

Figure 3.15: Pore pressure parameter a corresponding to the stress path calculated with the measured pore pressure at the bottom of the sample and with the estimated pore pressure at the mid height for (a) sample 1 and (b) sample 2

3.6. CONCLUSIONS

An experimental investigation on the end restraint effects was proposed to overcome a series of misconceptions on the derivation of shear strength parameters from undrained compression tests on peat. Paradoxically, despite the past efforts to study the end restraint effects on classic inorganic soils, scarce attention had been given to the implications of this issue in the elaboration of triaxial data from samples of soft soils such as peats. Exceptional compressibility combined with high friction angles increase the severity of non-uniformities in stresses and strains with potential relevant differences between the derived sample behaviour and true material behaviour. To reveal the end restraint influence on the results, repeatable reconstituted samples were tested. Big fibres were eliminated in order to rule out the additional confining effect, which is typically claimed to be responsible of the exceptionally high observed friction angle.

Experimental results from triaxial compression tests with standard rough and modified smooth end platens showed dramatic effects on both the volumetric and deviatoric response of the reconstituted peat. For specimens tested with rough end platens, the shorter the sample, the higher the excess pore pressure measured at the bottom of the samples. Only for slender specimens, with height to diameter ratio equal to 3, the results were close to the ones obtained with smooth end platens. The same result was found for the deviatoric stress-strain response with higher deviatoric stresses at failure for rough end platens, which demonstrates that end restraint must be cautiously accounted for when undrained shear strength values are derived from standard tests on peats. The implications in terms of the estimated ultimate friction angle are dramatic, with φ' passing from 43° for samples

tested with modified end platens to 55° for samples with the standard height to diameter ratio 2 and rough end platens.

A simple comparison with a K_0 triaxial path allowed to confirm the validity of the simplified Jaky's relationship, linking K_0 to the "true" friction angle of the tested reconstituted peat. The K_0 value derived from the test performed with active control of null radial strains well matches the value obtained by means of Jaky's formula from the undrained triaxial tests with smooth end platens. The same result holds for samples tested with rough end platens if the effects of end restraint on the pore pressure distribution are corrected for.

A simple procedure was outlined to estimate the excess pore water pressure at the mid height of the sample when the only pore pressure measurement is taken at the bottom of the sample and rough end platens are used. By calculating the representative stress path with the corrected pore pressure, most of the end restraint effect can be ruled out, with clear benefits on the estimated volumetric response and on the ultimate shear strength.

This study allows overcoming common doubts on the reliability of the triaxial tests for investigating the shear behaviour of peats. The peculiar characteristics of these soils require paying special attention in correcting the data for the drawbacks of standard experimental procedures. To obtain reliable information in a direct way from measured data, smooth end platens, which improve stresses and strains uniformity, and pore pressure measurements at mid height of the sample are highly recommended. When standard equipment with rough end platens is available, sample with an initial height to diameter ratio above 2 is strongly suggested. In addition, the simple procedure outlined in this work to correct the pore pressure measured at an end of the sample can be exploited to infer the correct stress path. The procedure requires an accurate measurement of the water content profile at the end of the test, and a reasonable estimate of the hydraulic conductivity of the peat in the relevant stress and strain range. Accompanying standard tests with an actively controlled K_0 stress path is recommended to clarify the "true" response of peats, as the kinematic constraint on null radial strains rules out end restraint effects.

LIST OF SYMBOLS

H	sample height
V	sample volume
H_0	initial sample height
D_0	initial sample diameter
V_0	initial sample volume
H_f	sample height at failure
D_f	sample diameter at failure
Gs	specific gravity
OC	organic content
e	void ratio
w	water content
w_{ave}	average water content along the sample height at the end of the test
M_w	mass of water
M_{w0}	mass of water at the mid height of the sample before shearing
ΔM_w	change of mass of water
ρ_w	density of water
γ_w	unit weight of water
g	gravity acceleration
k_v	hydraulic conductivity in the vertical direction
q_w	internal flow rate
A	cross sectional area
F	axial force
δA	increment of cross sectional area over deviatoric strain
δF	increment of axial force over deviatoric strain
ε_a	axial strain
$\dot{\varepsilon}_a$	axial strain rate
ε_p	volumetric strain
ε_q	deviatoric strain
σ'_v	vertical effective stress
K	lateral pressure ratio
K_0	coefficient of earth pressure at rest
G	secant shear stiffness
σ'_a	axial effective stress
p'	mean effective stress
p'_c	pre-consolidation mean effective stress
p'_0	mean effective stress at the beginning of shear
q	deviatoric stress
δq	increment of deviatoric stress over deviatoric strain
η	stress ratio
η_u	ultimate stress ratio
M_g	critical stress ratio
φ'	friction angle
Δu_w	excess pore pressure

$\Delta u_{w,BM}$ difference of pore pressure between the bottom and the mid height of the sample
$\Delta p'$ change in the mean effective stress
Δq change in the deviatoric stress
a pore pressure parameter
β inclination of the dead zone with respect to the horizontal
L extension of the free failure zone
t time
t_f time at failure
Δt time interval

4

Implication of end restraint in triaxial tests on the derivation of the stress-dilatancy rule for soils having high compressibility

호랑이에게 물려가도 정신만 차리면 산다

Even though a tiger is biting you, if you get a grip, you can live

Korean saying

The content of this chapter has been accepted as research paper in Canadian Geotechnical Journal. (Muraro & Jommi, 2018).

4.1. ABSTRACT

Constitutive models for soils are developed and validated against laboratory tests assuming these give representative information on the true material behaviour. However, data from standard laboratory tests reflect the sample response rather than the true material behaviour, due to non-uniformities in stresses and strains generated over the experimental test. The work examines the implications of end restraint on the definition of the stress-dilatancy rule of highly compressible soils with a finite element numerical approach. The numerical model replicates a reconstituted peat, typically characterised by a combination of high compressibility and high friction angle, which increases the severity of end restraint effects. Simulated results show that the global measurements from standard triaxial tests with rough end platens would not give the proper stress-dilatancy rule, if they were interpreted as the response of a single soil element at the constitutive level. Both overestimation and underestimation of the true dilatancy compared to the material response can be observed, depending on the deformation mode. To support the validity of the numerical results, experimental findings from drained triaxial tests on reconstituted peat are presented. Practical indications are given on how the standard interpretation of drained triaxial tests data on peats can be improved.

4.2. INTRODUCTION

Design and assessment procedures in many geotechnical applications require reliable constitutive models to describe the behaviour of the soil adequately. Constitutive models are usually developed and validated based on experimental laboratory tests, typically from triaxial tests. Passing from the laboratory scale to the constitutive equations, it is often assumed that the experimental test can be interpreted as a soil element test, thus representing the true material behaviour. This way of reasoning implicitly assumes that pore pressure, stresses and strains distributions are uniform within the sample. However, the boundary conditions imposed to the sample with standard laboratory devices may be far from being uniform.

Non-uniformities are introduced on the sample due to multiple factors. A first level of complexity and uncertainty comes from the assumption of uniform pore pressure both in drained and undrained tests when a finite loading rate is applied to soils with low hydraulic conductivity (Gibson & Henkel, 1954; Blight, 1965; Carter, 1982). The result is a spurious rate effect, which is not due to time-dependent behaviour (i.e. creep), but simply comes from the coupled hydro-mechanical response (Herle & Kolymbas, 2004). This problem is compounded when considering the effects of rough end platens usually employed in standard triaxial tests. Systematic attention has been given to investigate the effects of end restraint on the shear strength of both sands and clays since the 1960's, after the pioneering work of Taylor (1941). Despite the general agreement on that non-uniform conditions make the stress-strain quantities based on averaged external measurements hardly representative of the actual state of the soil in the shear zone, still some disagreement persists in quantifying their effect on the derivation of the shear strength parameters. Olson & Campbell (1964) and Bishop & Green (1965) came to the conclusion that a height to diameter ratio H/D=2 considerably minimises the effects of end restraint on the shear strength from tests on sodium-kaolinite and Ham river sand, respectively. However, the conclusion is not confirmed by the dedicated experimental work of Shockley & Ahlvin (1960) and Kirkpatrick & Belshaw (1968), who measured significant non-uniformities in the stresses and strains fields of sand samples having H/D ranging from 2 to 2.3. Significant end restraint effects leading to an overestimation of the shear strength were recently found by Kodaka et al. (2007) on normally consolidated rectangular specimens of Fukakusa clay tested in a triaxial apparatus with rough ends. More consensus is found on the influence of end platens on the volumetric behaviour upon shear. The shear stresses at the top and the bottom of the sample generated by rough end platens confine the lateral displacements to the central portion of the sample, thus preventing high degree of uniformity in stresses and strains. This typically results in higher tendency to dilate for samples tested with smooth end platens (Shockley & Ahlvin, 1960; Rowe & Barden, 1964; Lee & Seed, 1964). However, the experimental investigation to evaluate the effects of rough end platens on the volumetric strain gradient at failure for a quartzy sand and reconstituted loess by Feda et al. (1993) concluded that no significant effects could be observed.

The predominant attention to the effects of end restraint on the shear strength of soils from the experimental viewpoint is also reflected in several numerical con-

tributions to the problem. Non-uniformities in terms of pore pressure, stresses and strains distributions were observed from the results of FE analyses by Carter (1982), Airey (1991), Macari-Pasqualino et al. (1994), Asaoka et al. (1994) and Kodaka et al. (2007). The contributions of Schanz & Gussman (1994) and recently Jeremić et al. (2004) reported an increase in the shear strength with increasing end restraint for elastic-perfectly-plastic constitutive models. A noticeable step forward was done by Sheng et al. (1997), who discussed the implications of the end restraint on the global behaviour of soil samples. By comparing the response from global stresses-strains quantities with that at the element scale in FE analyses, Sheng et al. (1997) clearly showed the limitations in obtaining any information directly ascribable to the material behaviour from conventional triaxial tests. They also demonstrated that the effects of non-uniformities on the analysis of stress-strain and strength properties of the soil also depend on how the global stresses and strains are computed from triaxial tests data.

Despite the significant attention dedicated to the study of end restraint on the observed soil response and the numerical contributions which followed, the vast majority of these was devoted mainly to clarify their impact on the shear strength parameters and pore water pressure distribution. However, misconception introduced by disregarding the end restraint effects on the stress-dilatancy relationship of soils, hence on the description of the pre-failure behaviour, has not been tackled systematically. The importance of a correct description of the plastic deformation mechanism at failure in soils (i.e. flow rule) has been shown numerically by Potts & Gens (1984), Gens & Potts (1988) and Lagioia & Panteghini (2014), among others. However, the impact of different choices for the flow rule on the performance of constitutive models for soils can be extremely important especially in reproducing the pre-failure response.

The philosophy of the work is to provide an insight into the implications of end restraint on the standard derivation of the stress-dilatancy relationship for soils having very high compressibility together with high friction angle, such as organic clays and peats. To this end, a series of finite element analyses has been carried out by employing the simple modified Cam clay model, MCC (Roscoe & Burland, 1968). The analyses were run to support an experimental programme aimed to characterise the stress-strain behaviour of peat samples. The high compressibility, combined with high friction angles, makes the geotechnical description of peats extremely challenging (Adams, 1961; Oikawa & Miyakawa, 1980; Landva & La Rochelle, 1983; Yamaguchi et al., 1985b; Farrell & Hebib, 1998; Kanmuri et al., 1998; Edil & Wang, 2000; Cola & Cortellazzo, 2005; Hendry et al., 2012). Both these aspects magnify the effects of end restraint on the failure and pre-failure responses, with peat samples experiencing volumetric and deviatoric strains not comparable with any other classical soil (Den Haan & Feddema, 2013; Zhang & O'Kelly, 2014).

The effects of rough end platens are quantified in terms of stress-dilatancy rule for different radial paths at constant stress ratio η, involving both lateral contraction and expansion, by elaborating the results from FE analyses replicating actual triaxial tests. The difference between the pre-failure stress-strain behaviour derived from global measurements, as conventionally done with triaxial tests data, and the

"true" material response of the soil is highlighted. Results from reconstituted peat samples tested in triaxial apparatus with rough and smooth end platens are presented, to substantiate the relevance of this experimental aspect on the observed response, and to quantify the error introduced in the stress-dilatancy relationship by neglecting the stress inhomogeneities due to the geometrical constraint. Eventually, a suggestion is given to start reducing the error coming from the experimental constraint.

4.3. FINITE ELEMENT MODEL

The aim of this work is to investigate the direct effect of end restraint on the drained response of soils having high compressibility. Therefore, ideally drained analyses were performed, disregarding the issues possibly raised in the interpretation of experimental data by the low hydraulic conductivity typically shown by these soils. In the practice, unless low displacement rates are adopted during the test stages, significant pore pressure gradients are generated, which cannot be disregarded in the interpretation of drained as well as undrained tests (Barden & McDermott, 1965; Carter, 1982; Sheng et al., 1997).

4.3.1. Constitutive model of the soil

Coupled hydro-mechanical analyses were set up with the ABAQUS standard finite-element code (Hibbitt et al., 2009). In these analyses the available Modified Cam-Clay model was adopted to preliminary analyse the response of the soil sample. The properties used to describe the material behaviour are reported in Table 4.1, where λ and κ are the slopes of the normal consolidation and unloading-reloading lines respectively, e_0 is the void ratio at a mean effective stress p'_0=1 kPa, and M_g is the critical stress ratio. In the first set of analyses, M_f is set equal to M_g under the simplifying assumption of associated flow rule. The parameters are based on the results of triaxial tests performed on reconstituted peat samples adopting smooth end platens. A hypo-elastic law, with constant Poisson's ratio, ν, was adopted in order to avoid the unrealistic dilatant response given at low stresses by a constant shear modulus G. The shape of the yield surface on the deviatoric Π plane is chosen in order to properly reproduce the differences in the ultimate deviatoric stress experimentally observed along different stress paths, at the same time avoiding the tensile zones which would be encountered with a von Mises' criterion (K=1) for materials having high friction angle (Hibbitt et al., 2009). The resulting shape of the yield locus on the Π plane is sketched in Figure 4.1.

4.3.2. Boundary conditions and applied stress paths

The cross-section of the sample, having a radius equal to 19 mm (x coordinate) and a height of 76 mm (y coordinate), was discretized with 1444 8-node bi-quadratic axis-symmetric elements with bi-linear pore pressure interpolation and reduced integration (CAX8RP) (Figure 4.2(a)). Drainage is allowed from both the top and the bottom. To simulate conventional triaxial apparatus where rough porous stones are in contact with the sample, the horizontal displacements at these two

Table 4.1: Model parameters used in the numerical simulations

Parameter	Units	Numerical value
κ	(-)	0.3
λ	(-)	2.0
ν	(-)	0.2
p'_0	(kPa)	1.0
e_0 at p'_0	(-)	10.4
M_f=M_g (associated plasticity)	(-)	1.75
Shape factor K of the yield locus on the Π plane	(-)	0.778

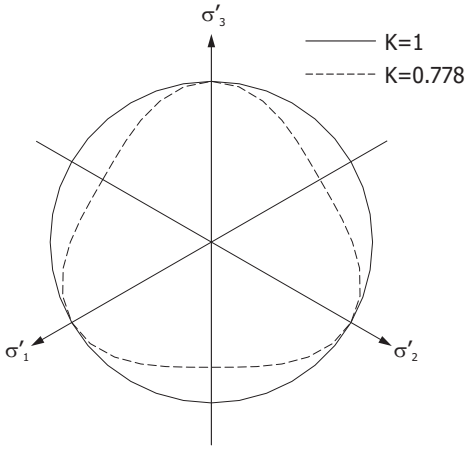

Figure 4.1: Shape of the yield locus on the deviatoric Π plane for K=0.778 (chosen value) and K=1 (von Mises)

boundaries were constrained. The hypothesis of null radial displacements at the top and bottom of the sample which may seem way too conservative for classical inorganic soils, was experimentally verified by Yamaguchi (1992) for natural peat samples in standard drained triaxial compression tests. However, significant constraint to the radial displacements is offered by O-ring sealing the rubber membrane at the extremities of the sample even if lubricated end platens, which have the same diameter as the specimen, are adopted (Sheng et al., 1997).

Different radial stress paths were imposed by defining stress time histories on the top and external boundaries. Seven radial paths, at constant stress ratio η=q/p', where q is the deviatoric stress and p' is the mean effective stress, were simulated, after isotropic compression up to p'_c=35 kPa followed by isotropic unloading to p'=15 kPa, giving an OCR=p'_c/p'=2.3. The deviatoric stress was then increased at constant p' until a pre-defined stress ratio. Eventually, radial stress paths were simulated up to p'=100 kPa (Figure 4.2(b)).

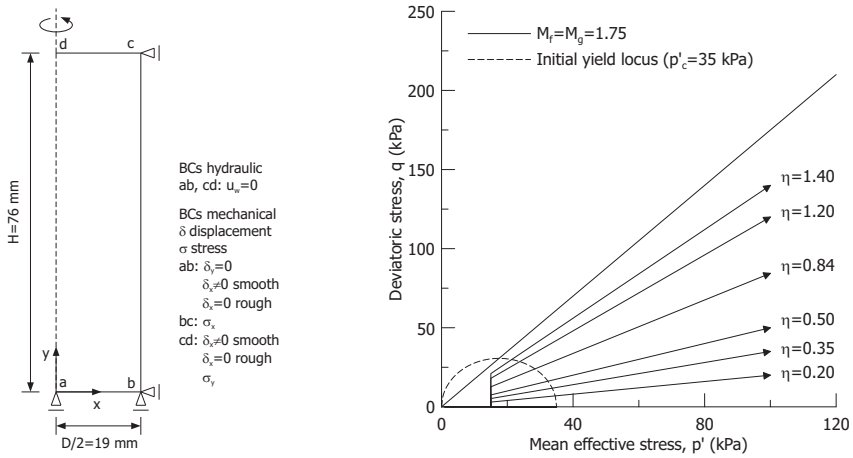

Figure 4.2: Sketch of the triaxial specimen and summary of the boundary conditions in the finite element model (a); (b) stress history imposed to the specimen in the numerical analyses

4.3.3. Stresses and strains variables

To provide a replica of the typical information coming from laboratory tests, global stress-strain quantities were calculated by elaborating the results of the FE analyses with the same corrections applied to the experimental data from triaxial tests. For the case of rough end platens the samples do not maintain their original aspect ratio (i.e. right cylinder), but either bulge or assume a hourglass shape depending on the imposed stress path. In both cases, in the absence of local measurements (i.e. local displacements transducers), different cross-sectional area corrections can be applied to compute the current axial stress and the representative radial strain. A detailed description of the possibilities for the area correction, depending on the available measurements, is provided by Ehrgott (1971). In this study the global radial stress is assumed to be equal to the applied cell pressure (Sheng et al., 1997; Praastrup et al., 1999), while the global axial stress has been computed by dividing the axial force measured at the top of the specimen by four different choices for the cross sectional area, namely:

a) nominal area: current contact area at the top of the specimen;

b) volumetrically equivalent right cylinder;

c) average between a) and b);

d) area at 9/10 of the height of the sample.

The latter two choices were suggested by Sheng et al. (1997) based on a careful comparison between the global stresses and the local stresses at the element scale, from the results of FE analyses of standard drained and undrained triaxial compression tests. In practice, the most appropriate area correction should be chosen on

the observed specimen geometry and measurements at the end of the test (Germaine & Ladd, 1988), which reduces the degree of arbitrariness on the possible choices. However, all the four possibilities were considered in the numerical exercise.

Geometrical non-linearities were accounted for in the FE model, and natural strains were used in the material description (Ludwik, 1909; Hencky, 1928). The inconsistency and severe shortcomings in elaborating triaxial tests by adopting linear engineering strains have been discussed by Praastrup et al. (1999), and great care must be taken in elaborating triaxial tests on peats, especially in drained conditions, due to the large displacements experienced by peat samples (Den Haan & Feddema, 2013; Zhang & O'Kelly, 2014). Natural strains were chosen as they imply the validity of the additive principle in equation 4.1 at large strains as well as at small strains. The global axial strain in equation 4.2 has been calculated from the current height of the sample while the volumetric strain from the volume change of the sample throughout the analyses. Positive compressive stresses and strains are assumed. As done in the current practice in the absence of direct measurement of radial displacements, the deviatoric strain has been computed from the measurement of the volume change, giving the volumetric strain ε_p, and of the axial displacement, related to the axial strain ε_a:

$$\varepsilon_p = \varepsilon_a + 2\varepsilon_r = \ln \frac{V_0}{V} \tag{4.1}$$

$$\varepsilon_q = \varepsilon_a - \frac{\varepsilon_p}{3} = \ln \frac{H_0}{H} - \frac{1}{3} \ln \frac{V_0}{V} \tag{4.2}$$

where H and V are the height and the volume of the sample (H_0, V_0 the initial values).

Dilatancy is defined as

$$d = \frac{\delta \varepsilon_p^p}{\delta \varepsilon_q^p} \tag{4.3}$$

or equivalently (Wood, 1990) by

$$\tan \beta = \frac{\delta \varepsilon_q^p}{\delta \varepsilon_p^p} \tag{4.4}$$

where $\delta \varepsilon_p^p$ and $\delta \varepsilon_q^p$ are the volumetric and deviatoric plastic strain increments, respectively. The plastic strains were calculated step by step as the difference between the total and the elastic strains. It is worth noting that the use of large strains introduces further non linearity in the elastic components of strains. However, the use of standard description for the elastic strain component albeit with a logarithmic measure of the strain is substantiated by literature data (Den Haan, 1996; Den Haan & Feddema, 2013).

4.4. NUMERICAL RESULTS

4.4.1. Representative cross sectional area

A possible way to discern the representativeness of the different methods for the area correction is to compare the resulting computed sample stress-strain response behaviour when rough end platens are adopted with the "true" material behaviour. Figure 4.4 presents the comparison in terms of deviatoric stress-axial strain for two radial paths at η=0.35 and η=1.40, respectively below and above the K_0 line (η_{K_0}=0.84 for the MCC with the parameters in Table 4.1).
It is often assumed that referring to the central portion of the sample, which is the farthest from the boundaries, minimises the effects of end restraint. Actually, this holds true for radial paths with $\eta<\eta_{K_0}$, where the lateral contraction results in a rather uniform deformation around the mid-height of the sample (Figure 4.3). However, for stress paths above K_0 this is not the case, due to the kinematic deformation mechanism showing significant bulging of the sample (Figure 4.3).

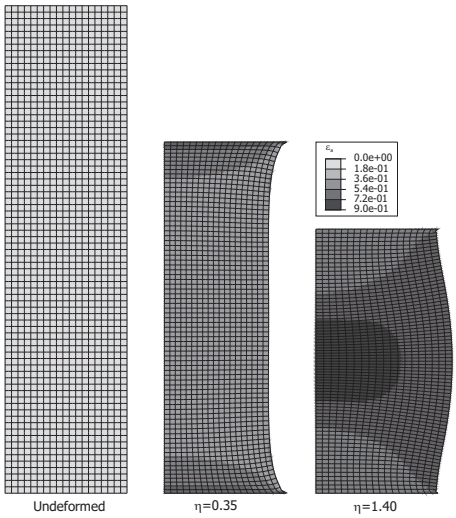

Figure 4.3: Contour plots of the axial strain from the numerical analyses: undeformed configuration and deformed configuration for radial paths with η=0.35 and η=1.40

The result is a lateral expansion of the external portions of the sample, around the mid height (Figure 4.3), which hardly participate to the axial load transfer mechanism. In the latter case, the significant stress gradient in the radial direction makes the assumption on the central portion of the sample close representing the material behaviour unrealistic.

The results in Figure 4.4(a) show that the traditional correction with a volumetrically equivalent right cylinder tends to overestimate the stress response for a given axial strain over radial paths lying below the stress ratio corresponding to K_0. Good agreement is found by using the average between the nominal area at the top of the sample and the equivalent cylinder. However, for radial paths above the

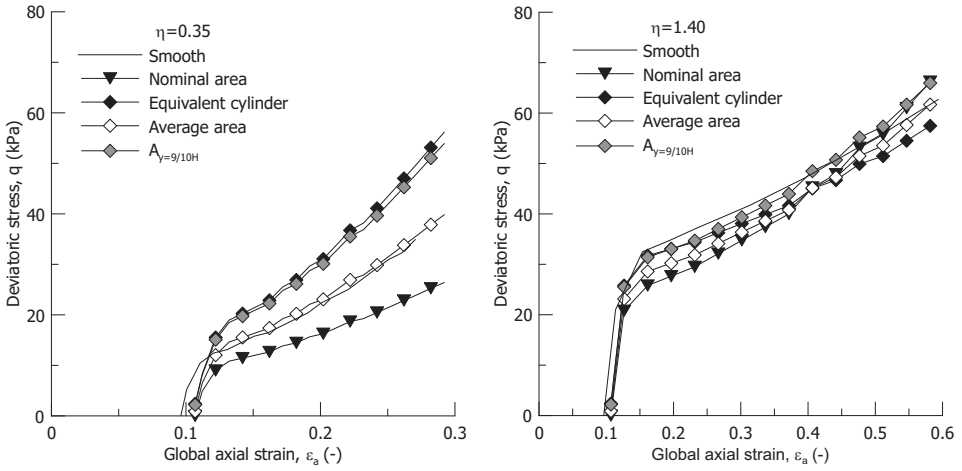

Figure 4.4: Comparison between the deviatoric stress-axial strain response after the four different cross sectional area corrections considered and the material response from smooth FE simulations for radial paths with (a) η=0.35 and (b) η=1.40

K_0 condition, the same correction suffers similar problems as the equivalent right cylinder correction, due to an overestimation of the effective cross section area. This drawback was pointed out already by Sheng et al. (1997) from the simulation of the shearing stage of standard undrained triaxial tests. For the radial path at η=1.40, above the stress ratio corresponding to the K_0 condition, choosing the cross sectional area at 9/10 of the height of the sample from the FE analyses results in the closest representation of the material behaviour (Figure 4.4(b)). Based on these observations, in the following discussion the results will be presented by correcting the area in two different ways, depending on the stress ratio, η:

a) average between the nominal area and the volumetrically equivalent right cylinder for radial paths with $\eta<\eta_{K_0}$;

b) area at 9/10 the height of the sample for radial paths with $\eta>\eta_{K_0}$.

4.4.2. Stress-dilatancy relationship

The stress-dilatancy relationship (equation 4.3) obtained by elaborating the FE analyses results at the sample level (global quantities) is reported in Figure 4.5. The "true" material behaviour, as modelled by the MCC, is displayed for the sake of comparison, together with numerical results of tests replicating the response of samples ideally tested with perfectly smooth bases. These allow validating the numerical model before analysing the effect of end restraint.

The shear stresses generated at the top and the bottom of the sample tend to reduce the lateral contraction and expansion compared to smooth conditions. For radial paths below K_0, higher deviatoric strains are expected at a given axial stress

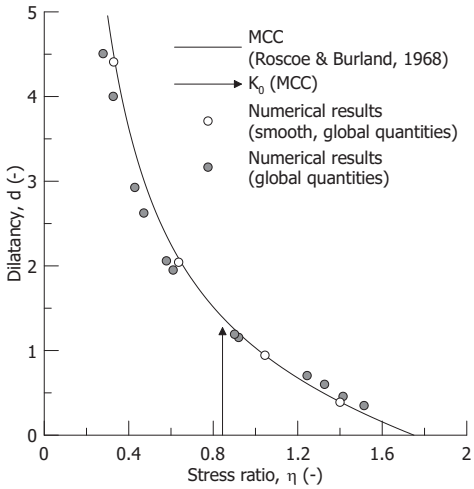

Figure 4.5: Stress-dilatancy relationship d-η from the FE results at the sample level (global quantities) for both smooth and rough end platens compared to the input MCC law

while the opposite occurs for radial paths above K_0. Consistently, the numerical results in Figure 4.4 underestimate the dilatancy for the stress paths below η_{K_0} and overestimate it for radial paths which imply lateral expansion. It is worth observing that the lowest discrepancy between the dilatancy derived at the sample scale and the material dilatancy occurs for a stress path corresponding to K_0 (η_{K_0}=0.84). Strictly speaking, it is only along a stress path implying zero lateral displacement that the end restraint effect is minimised and the true material behaviour is theoretically recovered. In Figure 4.5 the result for η=0.84 slightly differs from the expected one, due to the previous loading history simulated in the analyses (isotropic loading and unloading) which is responsible for the deviation due to a small irreversible end restraint effect.

4.5. A MODELLING EXERCISE

If the FE results in Figure 4.5 were processed as if they were representing the material behaviour, as typically done in processing experimental triaxial test data, the stress-dilatancy relationship would be obtained by interpolating the points displayed in Figure 4.6 referred to as sample behaviour. Figure 4.6(a) shows that by doing so, the derived stress-dilatancy relationship has a different shape compared to the true one (indicated in the figure as material behaviour), and also that it tends to overestimate the critical stress ratio M_g for which d=0. In Figure 4.6(a) the material behaviour obeys to the MCC with M_g=1.75 while the sample behaviour approaches null dilatancy for M_g=2. The difference between the inclination of the plastic strain increment vectors, $\Delta\beta$, predicted by the sample behaviour compared to the material behaviour is displayed in Figure 4.6(b) as a function of the stress ratio. Both overestimation and underestimation of the inclination were found for

low and high stress ratios respectively, in the order of 2° and -8°.

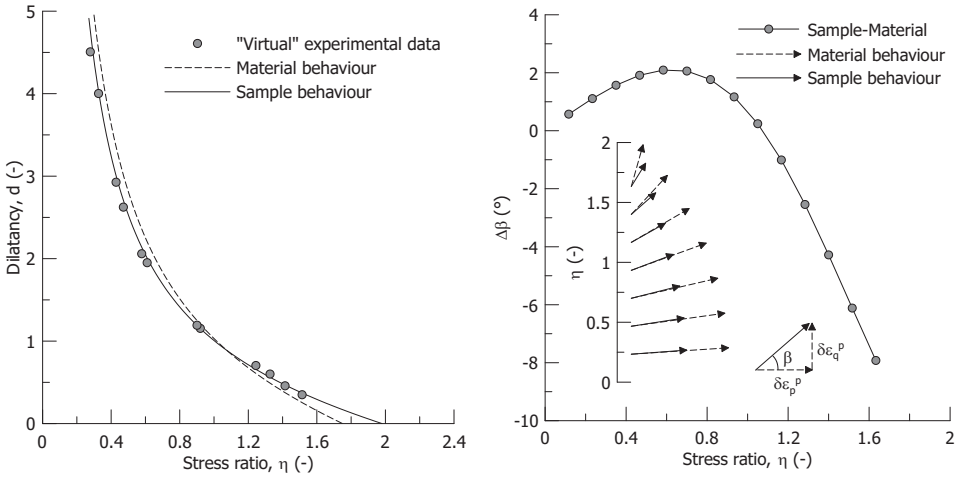

Figure 4.6: Stress-dilatancy relationship (a) and (b) inclination of the plastic strain increment vectors obtained by fitting the results of radial paths from conventional triaxial tests with rough end platens

Figure 4.7 reports the deviatoric stress-strain response along two radial paths at η=0.35 and η=1.40 predicted by using the stress-dilatancy relationship from the sample behaviour and material behaviour in Figure 4.6(a) on a soil element. For radial paths below the K_0 (Figure 4.7(a)), far from the failure conditions, misinterpreting the material flow rule results in overestimating the strains for a given stress level. On the contrary, for radial paths close to the failure state, and in general above K_0, (Figure 4.7(b)) the sample behaviour overestimates the deviatoric stress for a given strain level compared to the material behaviour. The difference may reach non-negligible values, with remarkable implications on the assessment of ultimate limit states. However, also a bias in the pre-failure deformation response below the K_0 line would be introduced by misinterpreting the stress-dilatancy relationship, which might influence serviceability limit states assessment.

4.6. EXPERIMENTAL EVIDENCE

The numerical results offer the possibility for a critical evaluation of experimental tests aimed to describe the failure and pre-failure response of peats. Dedicated experimental tests were performed to effectively quantify the influence of end restraint on the observed response of peat samples. Reconstituted samples were chosen to minimise the heterogeneity of natural peats. The reconstituted samples were prepared by mixing the natural material with demineralised water to a slurry with water content of 855%, corresponding to 1.4 times the liquid limit. The material was then consolidated in a floating consolidometer under a total vertical stress of 10 kPa for 48 hours and eventually mounted in a GDS triaxial apparatus.

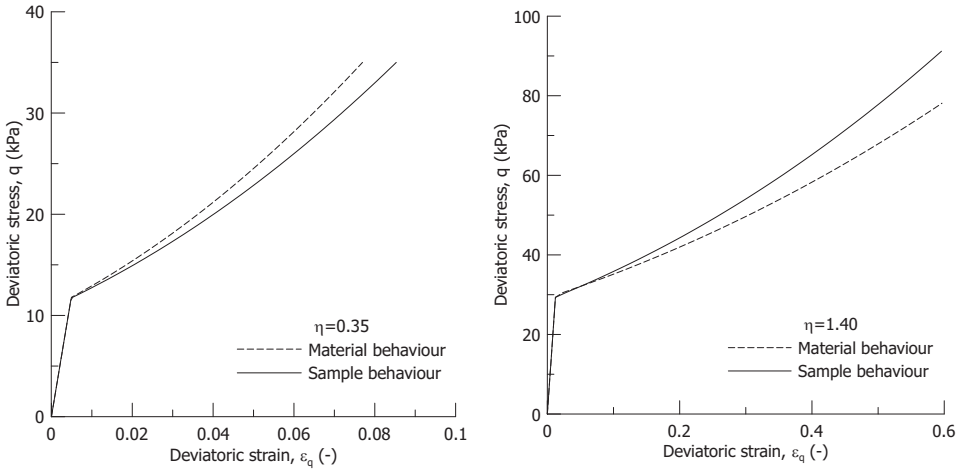

(a) (b)

Figure 4.7: Comparison between material and sample behaviour as predicted from a single element test based on the results from triaxial tests with rough end platens for two radial paths: (a) η=0.35 and (b) η=1.40

A suction cap was used to assure perfect contact between the load cell and the top cap. The volume change and the axial displacement were recorded with a digital pressure/volume controller and an external linear transducer. Relevant index properties of the samples are reported in Table 4.2, together with the isotropic preconsolidation stress at the start of the test, p'_0, the isotropic stress at the end of the test, p'_t, and an indication of the stress path followed during each test. The specific gravity, Gs, and the organic content, OC, were determined in accordance with the D5550-14 (2014) and the D2974-14 (2014).

Table 4.2: Index properties of the tested specimens and relevant stress levels

Sample	Gs (-)	e_0 (-)	OC (-)	p'_0 (kPa)	Path	p'_t (kPa)	$\dot{u}_a$ (mm/min)
Sample 1	1.52	9.80	0.91	8	Isotropic	74	0.003
Sample 2	1.51	10.41	0.92	8	Isotropic	100	0.002
Sample 3	1.50	10.31	0.91	8	K_0	70	0.008
Sample 4	1.46	9.65	0.91	32	Mixed	43	0.003

The testing programme consisted of a series of drained triaxial tests, including multiple stress paths which allowed to explore different loading conditions. The nominal dimensions of the specimens were 50 mm in diameter and 100 mm in height. All the tests were performed under stress control assuring limited excess pore pressure generation due to the loading rate. To accelerate the consolidation process, lateral filter paper strips were used, with free lower ends to avoid introduc-

ing lateral constraint. The resulting average axial displacement rate, $\dot{u}_a$, reported in Table 4.2, is approximately ten time lower than that required to guarantee a degree of dissipation of pore pressure of 95% (Blight, 1963).

Sample 1 and sample 2 were isotropically compressed up to p'_t=74 kPa and p'_t=100 kPa, while a K_0-consolidation test was performed on sample 3 up to p'_t=70 kPa (Figure 4.8(a)). The K_0 compression test was performed with a radial stress ramp with volume change and axial displacement back measurement allowing for automatic adjustment to guarantee negligible radial strains. Sample 4 was firstly isotropically consolidated up to a mean effective stress p'_0=32 kPa and subsequently isotropically unloaded to give an initial overconsolidation ratio $OCR=p'_0/p'$ of about 2. The final shearing stage consisted in a series of mixed isotropic and deviatoric loading steps as summarised in Figure 4.8(b). On the sample 2 the end restraint effects were limited by interposing a perforated plastic disk and a perforated nitrile membrane 0.1 mm thick between the filter paper and the sample.

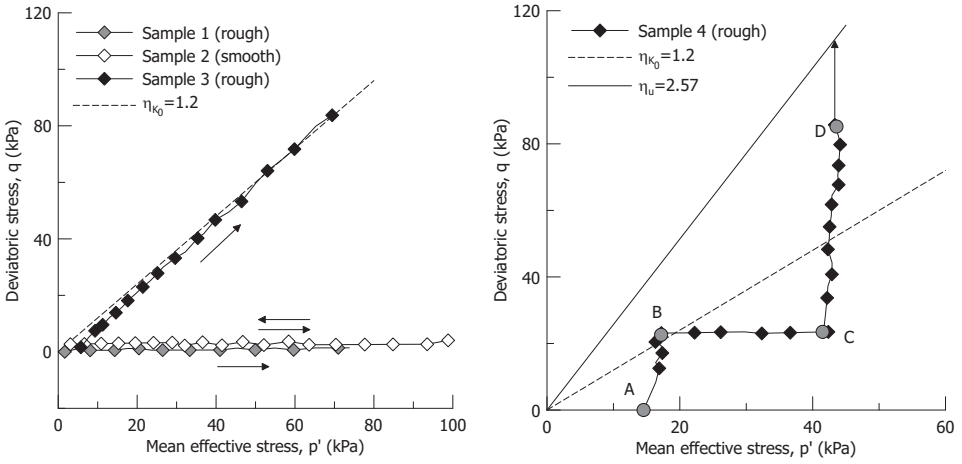

Figure 4.8: Experimental isotropic stress paths and K_0-consolidation (a) and (b) mixed isotropic-deviatoric path

4.6.1. Isotropic response

The results obtained from the isotropic compression on sample 1 and sample 2 are displayed in Figure 4.9(a) and Figure 4.9(b). To evaluate the deformation response of the samples, the isotropic compression was performed by controlling separately the axial and the radial stresses, and measuring the axial displacements and the volume change separately. In Figure 4.9(a) the incremental volumetric over axial strain ratio $\delta\varepsilon_p/\delta\varepsilon_a$, is given as a function of the mean effective stress.

If the sample response were perfectly isotropic, the incremental strain ratio would be equal to $\delta\varepsilon_p/\delta\varepsilon_a$=3. At the beginning of the compression stage the experimental ratio is higher due to the re-orientation of the initial fabric, created

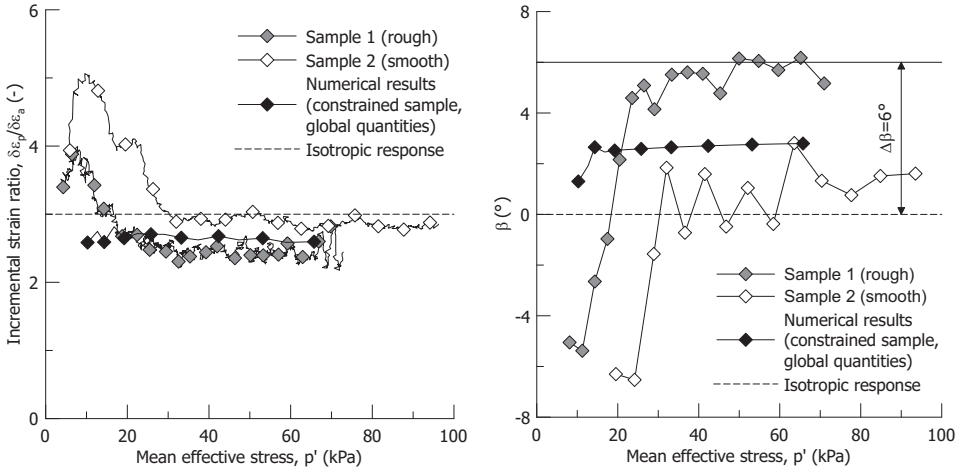

Figure 4.9: Incremental volumetric over axial strain ratio (a) and (b) inclination with respect to the horizontal of the plastic strains increment vectors during isotropic compression of reconstituted peat samples with rough and smooth end platens

during the 1-D preparation in the consolidometer tube under a small vertical stress and no lateral strain. However, the asymptotic ratio is of relevance to quantify the effect of the kinematic constraint imposed by the end restraint.

For sample 1, tested with rough end platens the incremental ratio between the volumetric and axial strain attains a value lower than that corresponding to the isotropic response. The result is due to the shear stresses between the soil sample and the porous stones, which constrained the lateral contraction during isotropic compression, hence inducing non-null deviatoric strain. The corresponding impact on the stress-dilatancy rule is reported in Figure 4.9(b), which shows that the inclination of the plastic strain increment vectors is about 6° to the horizontal. However, the observed inclination of the plastic strain increment vectors cannot be ascribed to an asymptotic anisotropic response, as the data on sample 2, tested with smooth end platens, demonstrate. At increasing stress, the incremental strain ratio tends to the expected value of 3 for the isotropic material response.

Previous tests in the literature (Yamaguchi et al., 1985a,b) indicate that natural fibrous peats may exhibit inherent anisotropy due to the orientation of the big fibres within the peat fabric (Landva & La Rochelle, 1983). However, the maximum length of the fibres in the tested peat was 3 mm, and they were randomly distributed during the 1-D preparation procedure. After re-orientation of the fabric from 1D to isotropic, the true material response appears to be isotropic as well (sample 2 Figure 4.9(a)). However, the sample response is affected by the kinematic constraint at the top and the bottom, and eventually appears anisotropic. It is worthwhile remarking that the FE simulation of the isotropic compression test on a constrained sample of a material obeying the MCC model with the parameters

reported in Table 4.1 gives a prediction of the incremental strain ratio which qualitatively reproduces the observed experimental response. The quantitative difference between the inclination of the calculated and observed vectors is mostly due to the choice for a MCC model to simulate the more complicated material behaviour of the peat. Possible concomitant constraint provided by the connection of the external membrane with the top cap may play a small role too, which was not accounted for in the numerical analyses.

4.6.2. Deviatoric response

The deviatoric response was investigated by means of the K_0 radial path (Figure 4.8(a)) and the mixed incrementally isotropic and deviatoric path on sample 4 (Figure 4.8(b)) where rough end platens were used. The experimental data from the different test stages were elaborated to give a comprehensive picture of the stress-dilatancy rule, as it appears from the sample behaviour (Figure 4.10).

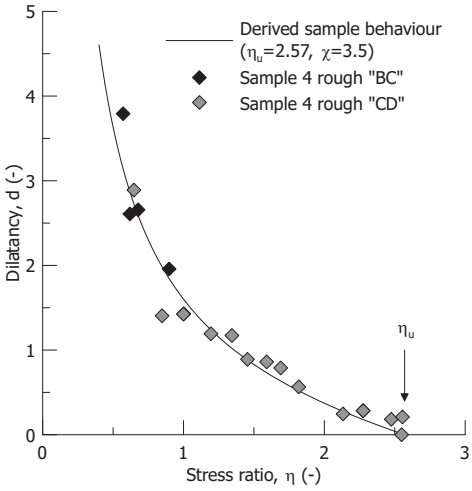

Figure 4.10: Stress-dilatancy relationship derived from the experimental results on sample 4 with rough end platens

Following the same approach described for the elaboration of the data in Figure 4.6(a), the experimental data from sample 4 are interpolated to give the sample d-η behaviour. To fit the experimental results in Figure 4.10, the generalised flow rule proposed by McDowell & Hau (2003) is adopted. The adopted equation allows high flexibility in the shape of the stress-dilatancy rule through the coefficient χ, though keeping the formulation extremely simple. It is worth remarking that the same formulation has been used by Ohmaki (1982), Alonso et al. (1990) and Yu (2007), among others. The stress dilatancy rule reads:

$$d = \frac{M_g^2 - \eta^2}{\chi \eta} \tag{4.5}$$

To interpolate the experimental data, the critical stress ratio was set equal to the asymptotic stress ratio reached by sample 4, M_g=η=η_u=2.57 (Figure 4.8(b)) and the shape factor to a value χ=3.5.

4.7. DISCUSSION

Based on the numerical results reported before, it is expected that the d-η values in Figure 4.10 lie below the true material response for η<η_{K_0} and above it for η>η_{K_0}. Also, the critical stress ratio of the material should be lower than the one elaborated from the triaxial tests with rough end platens. Despite the true d-η rule for the tested peat not being known, in principle it must satisfy three conditions:

i) $d\rightarrow\infty$ for η=0, due to the observed isotropic response in isotropic compression (Figure 4.9(a));

ii) d= observed d for η=η_{K_0}, as a K_0 path rules out the end restraint effect;

iii) d=0 for η=M_g, where M_g gives the critical stress ratio.

Based on these constraints and exploiting the fundamental information on K_0 coming from the experimental tests, the modelling exercise presented in the previous section is further exploited in an attempt to clean the experimental data from the effect of the end restraint. The calculated lateral pressure ratio derived from the experimental data along the radial path on sample 3 allows to define a value of K_0=0.33 for the tested peat, in the range indicated by previous findings (Den Haan & Kruse, 2007; Edil & Wang, 2000; Hayashi et al., 2012). The critical stress ratio determined from the undrained triaxial test with smooth end platens (TxCU) for this peat, M_g=1.75 (Table 4.1), gives a friction angle $\varphi'\cong$43°. According to the simplified Jaky's formula (Jaky, 1948), $K_0 \cong 1 - sin\varphi'$, the corresponding K_0 value would be K_0=0.32, which well matches the value determined from the K_0 triaxial test. If the ultimate stress ratio η_u=2.57 derived from sample 4 (Figure 4.8(b)) was used as critical stress ratio, a much lower value K_0=0.1 would be obtained, in contrast to the experimental result on sample 3.

Equation 4.5 is now used to propose a stress-dilatancy relationship which satisfies the three conditions above. The value of χ is chosen in such a way that the flow rule predicts zero lateral strain for a stress path corresponding to the K_0 condition expressed through the Jaky's simplified equation as

$$\eta_{K_0} = \frac{3M_g}{6 - M_g} \tag{4.6}$$

Along a η_{K_0} radial path, the constraint of null radial strain implies

$$d = \frac{3}{2}\frac{\lambda - \kappa}{\lambda} \tag{4.7}$$

if the elastic component of the deviatoric strain is neglected for the sake of simplicity (Alonso et al., 1990). Combining equations 4.5, 4.6, 4.7,

$$\chi = \frac{2}{9}\frac{\lambda}{\lambda-\kappa}\frac{M_g\left[(6-M_g)^2-9\right]}{6-M_g} \tag{4.8}$$

With the compression indexes (λ=2.0, κ=0.3) in Table 4.1 and the critical stress ratio M_g=1.75, a value of χ=0.98 is found. The resulting stress-dilatancy relationship is plotted in Figure 4.11(a), together with the experimental data from sample 3, sample 4 and the TxCU test with smooth end platens. The data from the constant deviatoric stress path "BC" and the portion of the path "CD" below the K_0 line (Figure 4.8(b)), lie below the model stress-dilatancy relationship. At increasing stress ratio along the path "CD" the experimental results move to the right hand side of the theoretical response consistently with the previous numerical findings.

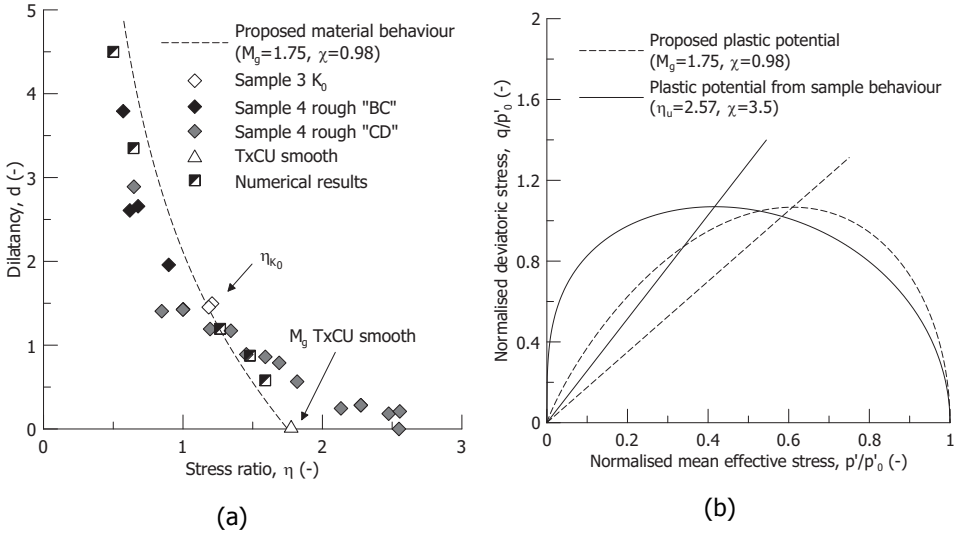

Figure 4.11: Proposed stress-dilatancy relationship for the tested reconstituted peat ruled out by the end restraint effect (a) and (b) plastic potential derived from the sample behaviour and proposed plastic potential

The experimental data on sample 4 intersect the proposed stress-dilatancy rule for a stress ratio of η_{K_0}=1.2, as expected. If the proposed stress-dilatancy law in Figure 4.11(a) were assumed to represent the "true" material behaviour and the experimental results were not corrected, an error on the inclination of the plastic strain increment vectors would occur. The difference in inclination between the "true" values and the values derived without correcting for the end restraint, $\Delta\beta$, is in the range of 7° to -15° for low and high stress ratios respectively. This is reflected in an appreciable change of the shape of the plastic potential, as shown in Figure 4.11(b).

In the attempt to verify the validity of the proposed "true" material stress-dilatancy function for the tested peat, the radial paths in Figure 4.2(b) have been reproduced numerically, by simulating the triaxial test and including end restraint. Compared

to the previous numerical results, only the d-η relationship was changed, by using equation 4.5 with M_g=1.75 and χ=0.98. All the other parameters were kept as in Table 4.1. As displayed in Figure 4.11(a), by using the proposed d-η relationship, the sample behaviour observed from the experimental triaxial tests with rough end platens was recovered. The agreement between the numerical results and the experimental data is more than satisfactory for $\eta<\eta_{K_0}$. For radial paths above the K_0 line, the numerical results predict a higher dilatancy than expected based on the material behaviour. However, the numerical results lie below the experimental ones, with the latter tending to a higher value of ultimate stress ratio, which could be ascribed to deviatoric hardening (Nova, 1977). By introducing the latter ingredient in a constitutive model higher ultimate stress ratio could be reproduced.

4.8. CONCLUSIONS

An experimental and modelling exercise was proposed to evaluate the effect of triaxial tests issues in the derivation of the stress-dilatancy law. The effects of the end restraint on the shear strength at failure obtained from triaxial compression tests have been intensively investigated in the past, both experimentally and numerically. However, inferring the correct stress-dilatancy relationship for the entire pre-failure range is essential in view of deformation analyses and of serviceability limit states assessment. So far, scarce attention has been given to the end restraint effects on this fundamental ingredient of any constitutive model. The consequences of end restraint on the derivation of the stress-dilatancy relationship are particularly relevant for soft organic soils such as peats, where the high compressibility combined with the high friction angle increases the non-uniformities in stresses and strains within the sample during a standard laboratory test.

Experimental results from triaxial compression tests with rough and smooth end platens showed the influence of the kinematic constraint on the deformation mode of peat samples. End restraint plays a role at any stage of the test, which clearly emerges from isotropic compression paths on isotropic samples. When rough end platens were used in the experimental test, the strain response appeared as if were anisotropic, with plastic strain increment vectors inclined of about 6° with respect to the horizontal.

A series of finite element analyses of triaxial tests were run to highlight the difference between the material behaviour at the constitutive level and the sample behaviour. The stress-dilatancy relationship reconstructed from global stress-strain variables in the numerical analyses differs substantially from the material flow rule, if rough end platens are introduced. In particular, the numerical results showed that for radial stress paths below the stress ratio which corresponds to the K_0 condition, the dilatancy is underestimated, while for radial path above K_0 it is overestimated. Moreover, when the stress-dilatancy relationship is derived from global stress-strain variables overestimation occurs of the critical stress ratio corresponding to null dilatancy. As a whole, the incorrect interpretation of the flow rule due to end restraint effects may have relevant engineering implications on both serviceability and ultimate limit states, by overestimating the displacements or the shear strength for loading paths below and above the K_0 condition, respectively.

The analysis of the experimental and numerical data including rough end platens allowed providing a practical approach to correct the interpretation of drained triaxial tests on peat, in an attempt to clean the observed data from end restraint effects. Based on simple observations coming from a K_0 test in the triaxial apparatus and undrained compression tests with smooth end platens, a corrected stress-dilatancy relationship for the reconstituted peat could be proposed and numerically validated.

LIST OF SYMBOLS

H	sample height
D	sample diameter
V	sample volume
H_0	initial sample height
D_0	initial sample diameter
V_0	initial sample volume
λ	slope of the isotropic normal compression line
κ	slope of the isotropic unloading-reloading line
ν	Poisson's ratio
G	shear modulus
Gs	specific gravity
OC	organic content
p'	mean effective stress
p'_c	preconsolidation mean effective stress
p'_t	maximum mean effective stress applied in the triaxial apparatus
q	deviatoric stress
OCR	overconsolidation ratio
K_0	coefficient of earth pressure at rest
η	stress ratio
η_{K_0}	stress ratio along a K_0 path
η_u	asymptotic stress ratio
M_f	stress ratio associated to the horizontal tangent of the yield locus
M_g	stress ratio at critical state
K	shape factor of the yield locus on the deviatoric Π plane
$\dot{u}_a$	axial displacement rate
ε_a	axial strain
ε_r	radial strain
ε_p	volumetric strain
ε_q	deviatoric strain
$\delta\varepsilon_a$	axial strain increment
$\delta\varepsilon_p$	volumetric strain increment
$\delta\varepsilon_p^p$	volumetric plastic strain increment
$\delta\varepsilon_q^p$	deviatoric plastic strain increment
d	dilatancy
β	inclination to the horizontal of the plastic strains increment vectors
χ	coefficient for the stress-dilatancy relationship
φ'	friction angle

5

Modelling the deviatoric behaviour of peat: between limitations and perspectives

The theory which fails to fit the soil behaviour is problematic, not the soil.

Professor Peter Vaughan

Part of this chapter was developed within the supervision of the MSc final project of Konstantinos Chatzis entitled "Advances in modelling the deviatoric response of peat" (Chatzis, 2018).

5.1. INTRODUCTION

Previous research on the geotechnical response of peat has mainly focused on the volumetric behaviour both from the experimental and the constitutive viewpoints. Only few attempts to model the deviatoric behaviour of peat are reported, despite this being crucial for most of the civil infrastructure as dykes and embankments where peats serve as foundation layers. The first attempt to develop an elastic-plastic model for the deviatoric behaviour of peat is due to Yamaguchi et al. (1985b), based on the Modified Cam clay (Roscoe & Burland, 1968) coupled with an experimentally based stress-dilatancy law. Following attempts include the application of the Soft Soil Creep model and its anisotropic version (Den Haan & Feddema, 2013; Den Haan, 2014), a kinematic bubble model (Boumezerane, 2014) and the elastic-plastic model by Li & Dafalias (2000) (Yang et al., 2016). All these different attempts were capable to capture the ultimate state of peat detected in the laboratory tests but with a significant overestimation of the stiffness in the deviatoric stress-strain response. The implications are not negligible considering that the design and the assessment criteria in many geotechnical applications where peats are encountered, are ruled by serviceability limit states rather than ultimate limit states. These considerations call for an adequate geotechnical description of the pre-failure response of peat.

The vast majority of the previous models for the deviatoric behaviour of peat have been developed and tested based on experimental results coming from triaxial undrained compression tests. However, undrained tests pose severe limitations to determine directly some of the main constitutive ingredients, such as the yield locus and the stress-dilatancy relationship which rule not only the failure but especially the pre-failure response of any elastic-plastic model. Another source of complexity comes from end restraint effects (Olson & Campbell, 1964; Barden & McDermott, 1965; Duncan & Dunlop, 1968). As demonstrated in Chapter 3 and Chapter 4, end restraint dramatically affects the apparent peat behaviour derived from standard laboratory tests as triaxial apparatuses. Shear stresses at the samples extremities when rough end platens are used contribute to increase the apparent shear strength and to alter the plastic deformation response. The high compressibility and shear strength of peats increase the severity of these problems with high non-uniformities in stresses and strains due to the high strain levels attained by peat samples before reaching failure (Rowe et al., 1984; Yamaguchi et al., 1987). From a modelling viewpoint, this limits the possibility to interpret and model experimental results on peats as element volume tests. Each experimental test should then be treated as a boundary value problem.

This chapter summarises the results of experimental and modelling efforts to interpret the observed experimental results from drained and undrained triaxial compression tests on reconstituted peat samples with a simple elastic-plastic model. To overcome the previous limitations, the constitutive ingredients of the model have been explicitly derived from the experimental results of drained tests with multiple loading directions. Particular attention has been given to the definition of yield surface and the stress-dilatancy relationship. The adopted elastic-plastic constitutive relationship was then introduced in a Finite Element code to model the experimen-

tal tests as boundary value problems. The model predictions are verified against triaxial tests which allow to highlight the current model capabilities and limitations. Despite the good qualitative agreement with the experiments, the results confirm the difficulty to describe the mechanical behaviour of peat in a constitutive framework which does not account implicitly or explicitly for the matrix-fibres interaction in the overall soil response. Rearrangement and realignment of the small fibres present in the peat matrix introduce a directional response in the plastic deformation response and contribute to the observed shear strength for high deviatoric strains.

5.2. EXPERIMENTAL PROGRAMME

5.2.1. Tested material and experimental methodology

Reconstituted samples were chosen to minimise the heterogeneity of natural peats. The reconstituted samples were prepared by mixing the natural material, collected from the Leendert de Boerspolder site in the Netherlands, with demineralised water to a slurry with water content of 855%, corresponding to 1.4 times the liquid limit. The material was then consolidated in a floating consolidometer under a total vertical stress of 10 kPa for 48 hours and eventually mounted in a GDS triaxial apparatus with back pressure and cell pressure volume controllers, and a submersible 1 kN load cell. A suction cap was used to assure perfect contact between the load cell and the top cap. Relevant index properties of the samples are reported in Table 5.1, together with the isotropic pre-consolidation mean effective stress before starting shearing, p'_c, the mean effective stress at the start of the shear, p'_0 and an indication of the stress path followed during each test. The specific gravity, Gs, and the organic content, OC, were determined in accordance with the D5550-14 (2014), D2974-14 (2014) and Den Haan & Kruse (2007). Fibre content determination from spare material gave an average value of 0.14 (D1997-13, 2013).

Table 5.1: Index properties of the tested specimens and specifics of the triaxial tests conducted

Sample	Gs (-)	e_0 (-)	OC (-)	p'_c (kPa)	p'_0 (kPa)	Path	H_0/D_0 (-)	$\dot{u}_a$ (mm/min)
Sample 1	1.51	10.41	0.92	-	8	Isotropic	2.2	0.002
Sample 2	1.50	10.31	0.91	-	8	K_0	2.0	0.008
Sample 3	1.48	7.38	0.91	34	17	Radial	2.1	0.001
Sample 4	1.51	7.99	0.91	37	14	Radial	2.1	0.002
Sample 5	1.49	6.87	0.90	34	34	TxCU	1.5	0.01
Sample 6	1.50	7.55	0.91	37	34	TxCD	2.1	0.001

The testing programme consisted of a series of drained triaxial tests with multiple stress paths which allowed exploring different loading conditions. The nominal dimensions of the tested specimens were 38 mm in diameter a part from sample 2, 50 mm in diameter. The initial height to diameter ratio is reported in Table 5.1. Thin membranes 0.25 mm thick were used. To accelerate the consolidation process,

lateral filter paper was placed around the samples. To prevent "short circuit" effects between the back pressure and the pore pressure transducers, 10 mm clearance were left between the lower edge of the lateral filter paper and the bottom of the samples (Head & Epps, 2014b). Each vertical drainage strip had free lower end to reduce the potential contribution offered by the lateral filter paper to the measured strength of the material. All the drained tested were performed under stress control assuring limited excess pore pressure generation due to the loading rate. The resulting average axial displacement rate, $\dot{u}_a$ reported in Table 5.1, is approximately ten time lower than that required to guarantee a degree of dissipation of pore pressure of 95% (Blight, 1963).

5.2.2. Stress paths

To investigate the volumetric behaviour, sample 1 was isotropically compressed up to p'=100 kPa, and isotropically unloaded to p'=7 kPa. A K_0-consolidation test was performed on sample 2 up to p'=70 kPa to determine the coefficient of earth pressure at rest for the tested peat. Sample 3 and sample 4 were firstly isotropically consolidated up to a mean effective stress p'_c=34 kPa and p'_c= 37 kPa and subsequently isotropically unloaded to p'_0 to give an initial overconsolidation ratio $OCR=p'_c/p'_0$ of about 2 and 2.6 respectively. The final shearing stage consisted in a series of mixed isotropic and deviatoric loading, unloading and reloading paths, as summarised in Figure 5.1(a) and Figure 5.1(b).

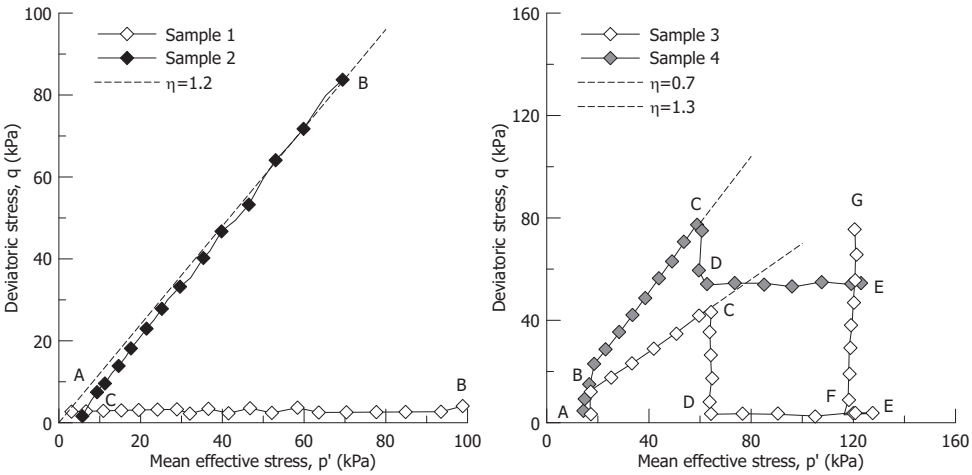

Figure 5.1: Experimental stress paths used for (a) isotropic volumetric behaviour and K_0-consolidation and for (b) deviatoric behaviour

5.2.3. Stresses and strains variables

All the experimental data have been elaborated herein by assuming axisymmetric test conditions and adopting the common triaxial stress-strain variables: mean

effective stress p', deviatoric stress q, volumetric strain, ε_p, and deviatoric strain, ε_q. Natural strains are adopted (Ludwik, 1909; Hencky, 1928) to account for the large displacements sustained by peat samples. The deviatoric strain has been computed from ε_p and ε_a derived from the volume change and the axial displacement measurements:

$$\varepsilon_p = \varepsilon_a + 2\varepsilon_r = \ln \frac{V_0}{V} \tag{5.1}$$

$$\varepsilon_q = \varepsilon_a - \frac{\varepsilon_p}{3} = \ln \frac{H_0}{H} - \frac{1}{3} \ln \frac{V_0}{V} \tag{5.2}$$

where V_0 and H_0 are the initial volume and height of the sample, while V and H are the current dimensions during the test. Compressive stresses and strains are assumed positive.

5.3. EXPERIMENTAL RESULTS

5.3.1. Compression behaviour

The isotropic compression path performed on sample 1 allows defining the position of the ISO-NCL and ISO-URL lines on the v-lnp' space, with λ=2.0 and κ=0.3 as reported in Figure 5.2(a). The obtained compression indexes agree with previous research on fibrous peat where a ratio κ/λ=0.1-0.3 is reported (Yamaguchi et al., 1985b; Mesri & Ajlouni, 2007). To evaluate the deformation response of peat sample upon isotropic compression, the test was performed by controlling separately the axial and the radial stresses, and measuring the axial displacement and the volume change separately. In Figure 5.2(b) the incremental volumetric over axial strain ratio $\delta\varepsilon_p/\delta\varepsilon_a$, is given as a function of the axial effective stress.

The previous stress history experienced by the sample in the 1D consolidometer tube justifies the initial soil anisotropic response observed at the beginning of the isotropic compression performed in the triaxial apparatus. However, the initial anisotropy is progressively erased over the isotropic loading path. Already for an axial effective stress of about 30 kPa (point P in Figure 5.2(a)) and Figure 5.2(b)), corresponding to about 2.5-3 times the one applied in the consolidometer tube the response turned to be isotropic with an incremental volumetric-axial strain ratio equal to 3. The exceptional compressibility of peats allows for very high irrecoverable strains (Landva, 2007), which are able to erase the initial anisotropy faster than for other soils tested previously (Mitchell, 1972; Lewin, 1973; Hueckel & Pellegrini, 1996; Romero & Jommi, 2008, among the others). As an example, Lewin (1973) found that stresses five times higher than those applied to the soil during the sample preparation were required on reconstituted silty-clay to reduce significantly the initial anisotropy. This result allows to consider the stress reached during isotropic compression by samples 3 and 4 after the sample preparation, p'_0=34-37 kPa, sufficient to assume the initial strain state for the radial paths in Figure 5.1(b) to be isotropic.

The 1D compression behaviour was investigated by the K_0-consolidation path on sample 2. The calculated lateral pressure ratio derived from the experimental data

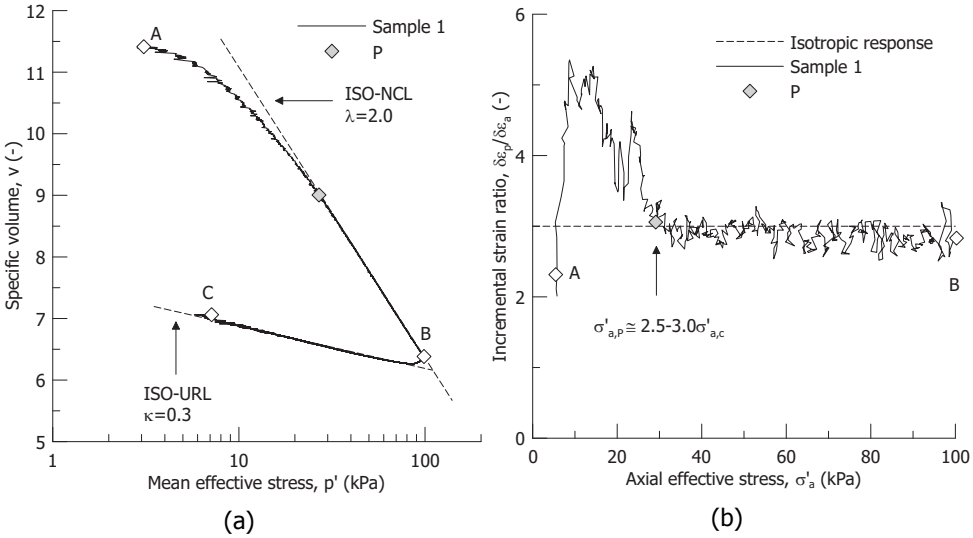

Figure 5.2: Specific volume (a) and (b) incremental volumetric over axial strain ratio during isotropic compression of reconstituted peat sample

allows defining for the tested peat a value of K_0=0.33, in the range indicated by previous findings (Den Haan & Kruse, 2007; Edil & Wang, 2000; Hayashi et al., 2012). As reported in Chapter 4, this result is consistent with the simplified Jaky's formula (Jaky, 1948), $K_0 \cong 1 - sin\varphi'$, assuming a friction angle $\varphi' \cong 43°$, obtained from undrained triaxial compression tests with modified end platens on the same reconstituted peat.

5.3.2. Yield locus

When the stress state of a soil sample overpasses the initial yield surface, the soil experiences a transition from the over-consolidated to the normally consolidated regime. A corresponding change in the stiffness of the stress-strain response occurs. It is well known that this transition is in general gradual and thus a degree of judgment must be exercised in selecting the yield stress (Wong & Mitchell, 1975), and this holds even more for peat due to its exceptional compressibility. To establish the position of the yield locus of the tested peat, the multiple stress paths applied on samples 3 and 4 in Figure 5.1(b) are exploited. Estimates of the yield points, Y, have been obtained by plotting the experimental data on different stress-strain planes (Wood, 1990). The cumulative work input per unit of volume versus the length of the stress path, $S=\sum \delta s$, is also used to support the estimates of the yield points (Becker et al., 1987):

$$W = \int p'\delta\varepsilon_p + q\delta\varepsilon_q \tag{5.3}$$

$$\delta s = \sqrt{\delta p'^2 + \delta q^2} \tag{5.4}$$

where the total increments of volumetric strain, $\delta\varepsilon_p$, and deviatoric strain, $\delta\varepsilon_q$, are used for the sake of simplicity.

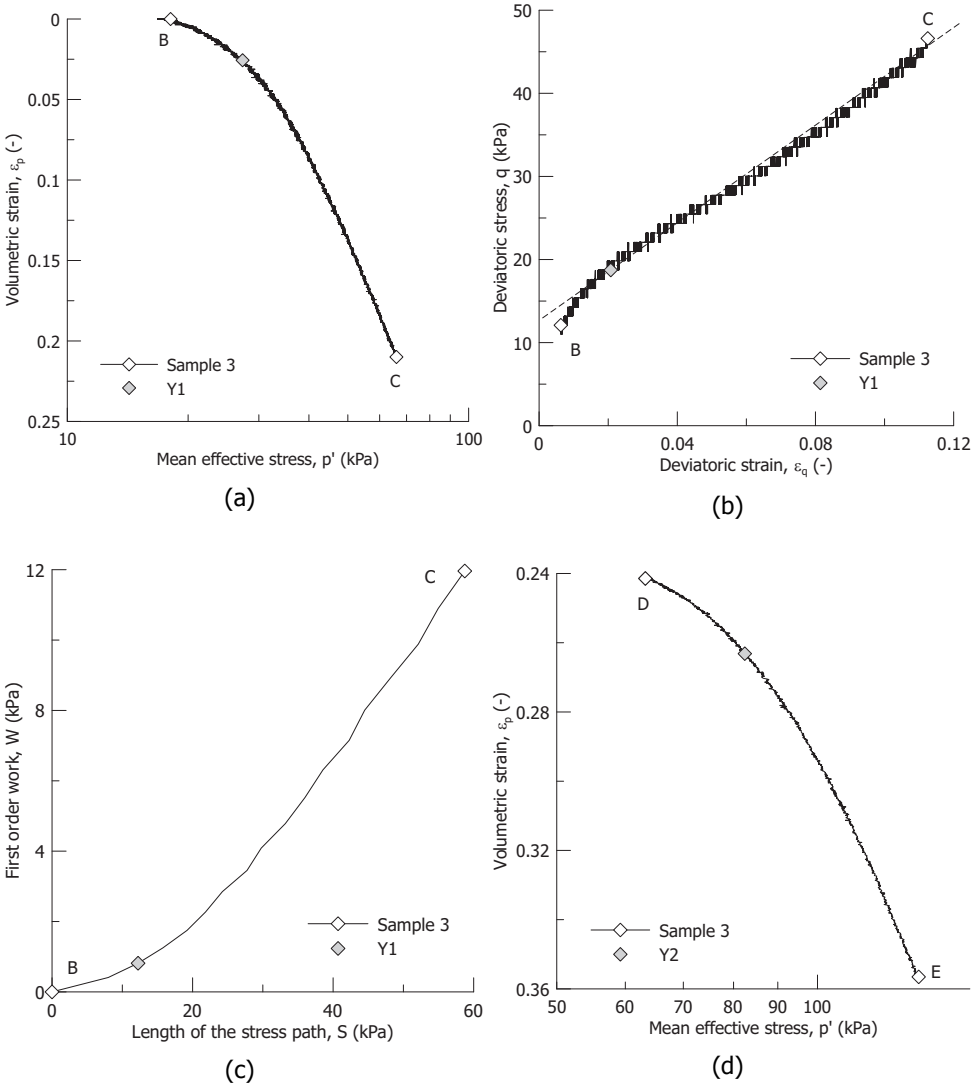

The yield points in Figure 5.3 and Figure 5.4 allow drawing an attempt of the yield locus, f=0, for the tested reconstituted peat. To this end, the generalised expression proposed by McDowell & Hau (2003) is used as reported in equation 5.5. It is worth remarking that the experimental results here presented are restricted to the wet side of the yield surface while no information is available for the dry side. The adopted equation allows high flexibility in the shape of the yield locus through the coefficient χ_f, though keeping the formulation extremely simple.

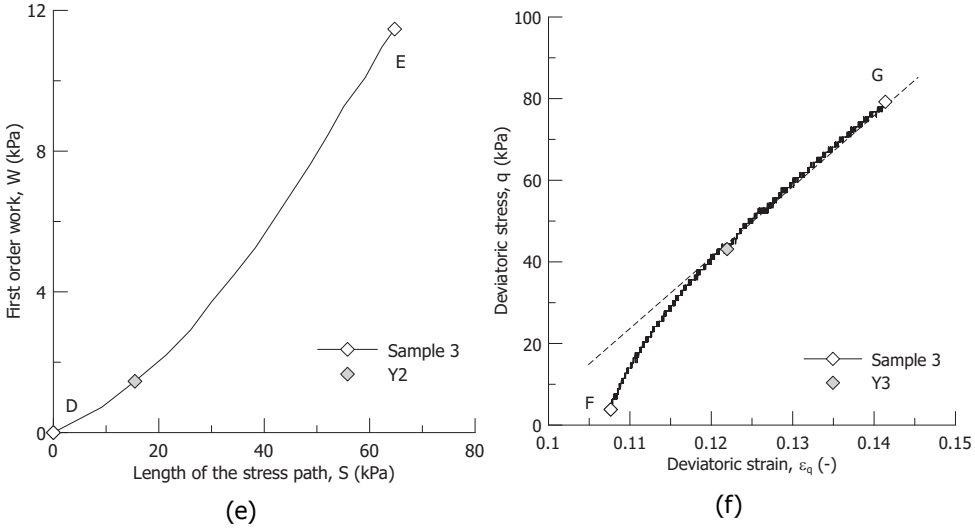

Figure 5.3: Estimates of the yield points for sample 3 along (a), (b), (c) the radial path BC, (d), (e) the isotropic loading DE and (f) the deviatoric path FG

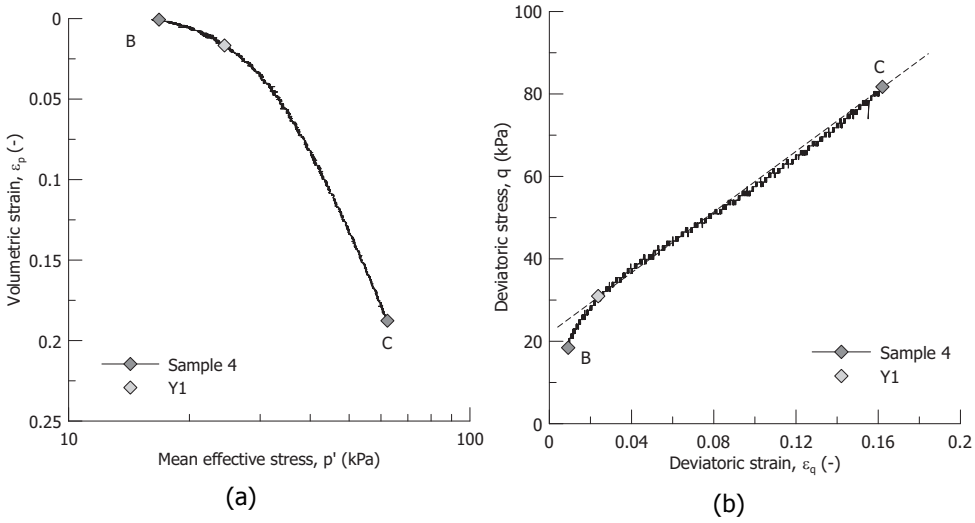

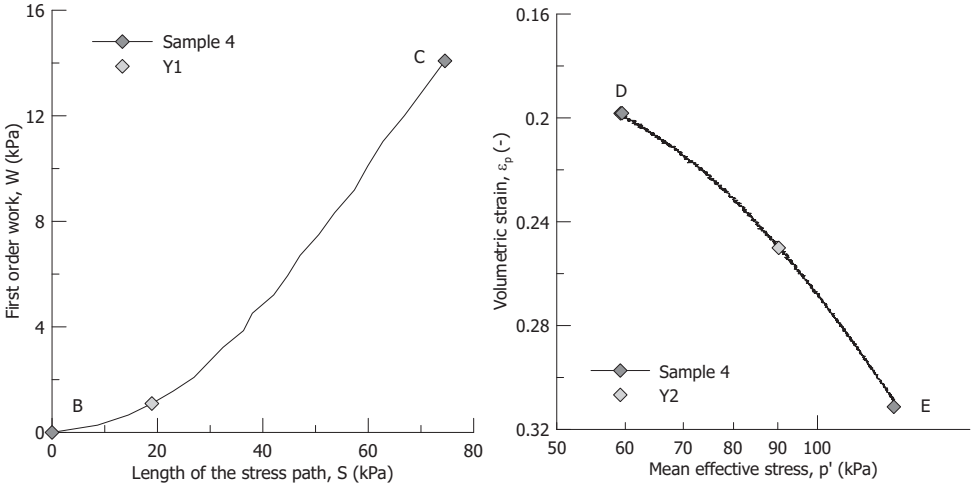

Figure 5.4: Estimates of the yield points for sample 4 along (a), (b), (c) the radial path BC and (d) the isotropic loading DE

$$f = 0 = q^2 + \frac{M_f^2}{1-\chi_f}\left(\frac{p'}{p_c'}\right)^{\frac{2}{\chi_f}} {p_c'}^2 - \frac{M_f^2 p'^2}{1-\chi_f} \tag{5.5}$$

In equation 5.5, M_f is the value of the stress ratio corresponding to a horizontal tangent to the yield locus in the p'-q plane and p_c' is the preconsolidation mean effective stress. Figure 5.5 displays the trace of the yield locus for the tested peat together with the Modified Cam clay which corresponds to χ_f=2.0 as reference (Roscoe & Burland, 1968).
The experimental yield locus fitted by equation 5.5 with M_f=1.5 and χ_f=3.0, lies slightly below the traditional Modified Cam clay. The evolution of the proposed yield locus during the tests on sample 3 and sample 4 is reported in Figure 5.6.
The results in Figure 5.6 seem to validate the choice for the shape of the yield locus over various non-standard stress paths. However, no direct experimental observations are available to support the assumption of a general homothetic expansion of the yield locus for the tested peat.

5.3.3. Hardening mechanism

Classical critical state models traditionally assume that the expansion of the yield locus (i.e. hardening of the soil) is controlled merely by the plastic volumetric strain and that this can be linked with the normal compression of the soils (volumetric hardening). However, it is well known that this assumption can be considered acceptable for fine grained materials as clays but not for granular materials as sands and for intermediate soils as silts. Information on the hardening of peat is

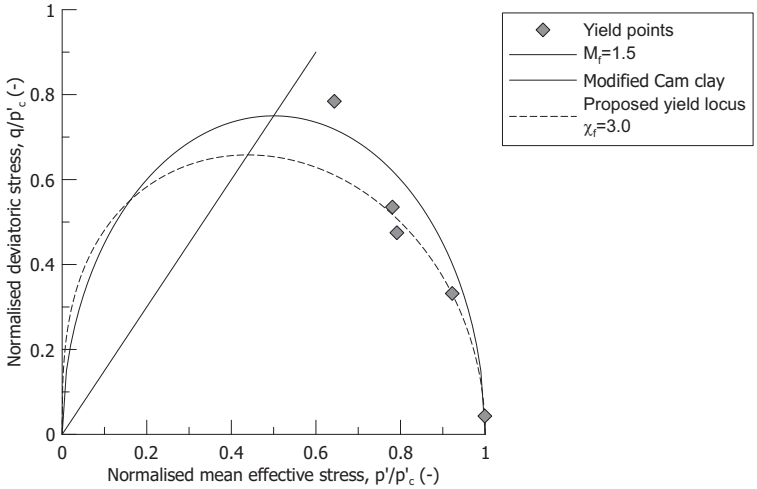

Figure 5.5: Trace of the yield locus on the p'-q space from the estimated yield points

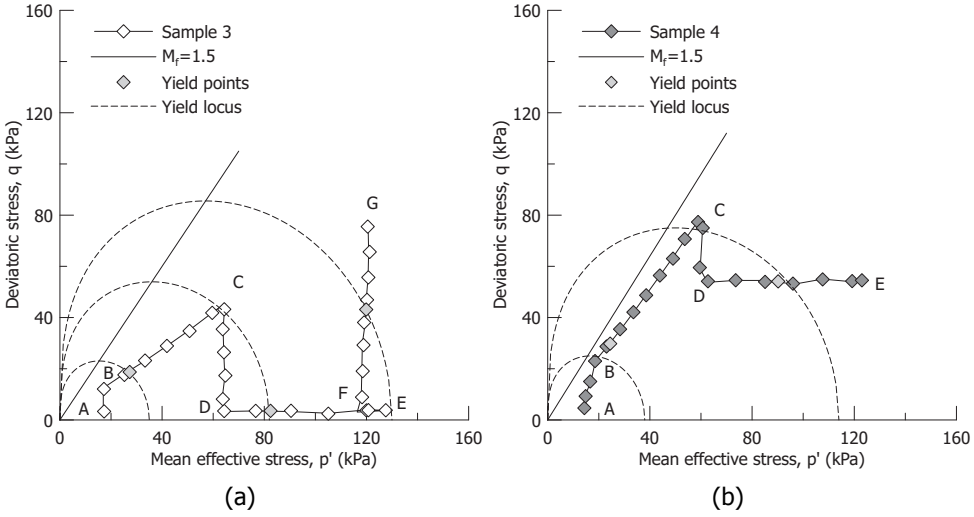

Figure 5.6: Proposed yield locus and estimated yield points for (a) sample 3 and (b) sample 4

scarce. Experimental evidence about the hardening mechanism for the tested peat are here presented first from drained triaxial tests and then from undrained triaxial tests. Throughout the entire work, plastic strains have been computed by adopting a hypo-elastic law with constant Poisson's ratio, ν=0.2, and κ=0.3 (Figure 5.2(a)) in order to avoid the unrealistic dilatant response given at low stresses by a constant shear modulus G.

Drained triaxial tests

The evolution of the preconsolidation mean effective stress p'_c (i.e. hardening variable) with the volumetric plastic strains, ε_p^p, computed for each radial path on sample 1, 3 and 4 is reported in Figure 5.7(a). Differently from sample 1 where the preconsolidation mean effective stress was controlled during the stress-controlled isotropic path, for sample 3 and sample 4 the preconsolidation mean effective stress has to be estimated based on the choice for the shape of the yield locus. The shape proposed in equation 5.5 with M_f=1.5 and χ_f=3.0 and displayed in Figure 5.5 is used. For each test, the current value of p'_c is normalised with the value at the onset of plastic strains.

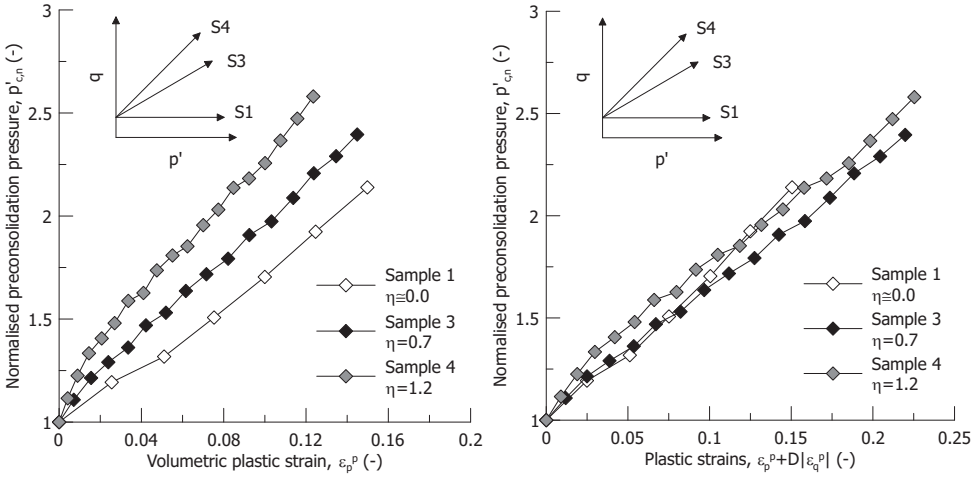

Figure 5.7: Evolution of the preconsolidation mean effective stress with (a) volumetric plastic strain and (b) the combination of volumetric and deviatoric plastic strains for radial paths on sample 1, sample 3 and sample 4

As displayed in Figure 5.7(a) the tested peat does not follow a simple volumetric hardening mechanism. The evolution of the hardening variable p'_c is not ruled by the plastic volumetric strain solely but seems to differ depending on stress path direction. In Figure 5.7(b) the same experimental data are plotted by adopting a simple linear combination of the volumetric and the deviatoric plastic strains $\varepsilon_p^p + D\left|\varepsilon_q^p\right|$ with D an empirical coefficient equal to 0.95. The results in Figure 5.7(b)

seem to suggest that both volumetric and deviatoric strains rule the hardening mechanism of the tested peat and that the relevance of the deviatoric component increases with the applied stress ratio

Undrained triaxial tests

Indirect information on the hardening of peats can also be found from undrained triaxial compression tests. To this scope it is convenient to calculate the pore pressure parameter a (Wood, 1990) defined as:

$$a = -\frac{\Delta p'}{\Delta q} \tag{5.6}$$

Figure 5.8 reports the evolution of the pore pressure parameter a with the stress ratio, η, computed from the sample 5 sheared in undrained conditions.

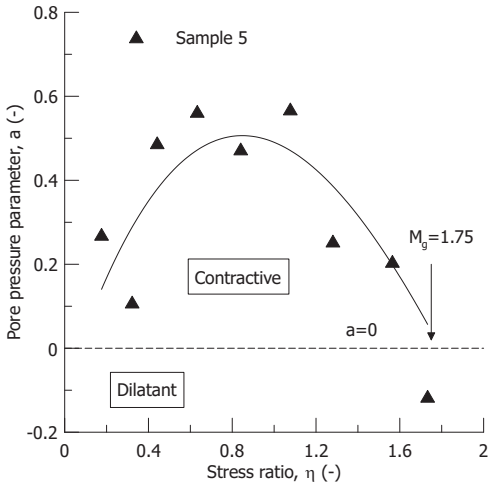

Figure 5.8: Pore pressure parameter a from undrained triaxial compression test on sample 5

Contractive behaviour is characterised by $a>0$ while dilatant response by $a< 0$ (Wood, 1990). The transition between these two regimes occurs in correspondence of the critical stress ratio with $a=0$ for $\eta=M_g$. For the tested peat, the pore pressure parameter firstly increases until a stress ratio of about 1 and then decreases approaching the zero line for a critical stress ratio $M_g=1.75$ (Figure 5.8). Stress ratios higher than M_g can be attained by the material in the dilatant regime. However, dilation is not accompanied by softening in the deviatoric response, but on the contrary, by hardening. The first indication of the occurrence of dilation during hardening from undrained compression tests on natural fibrous peat dates back to the 80's by Oikawa & Miyakawa (1980). However, the authors did not investigate the mechanical ground behind this behaviour.

Summing together the experimental results in Figure 5.7 for drained tests and in Figure 5.8 for undrained tests, it is possible to assert that for the first time there

is clear evidence to support the adoption of a hardening mechanism for peats not solely volumetric. A generalised mixed volumetric and distortional hardening rule, already proposed for granular soils (Nova, 1977; Nova & Wood, 1979), is here adopted in the form:

$$\frac{\delta p'_c}{p'_c} = \frac{v}{\lambda - \kappa}\left(\delta\varepsilon_p^p + D\delta\varepsilon_q^p\right) \tag{5.7}$$

In equation 5.7 v is the specific volume of the soil, λ and κ are the slope of the isotropic normal compression and unloading-reloading lines, respectively, and $\delta\varepsilon_p^p$ and $\delta\varepsilon_q^p$ are the volumetric and deviatoric plastic strain increments. The coefficient D accounts for the deviatoric strain dependent hardening. It is obvious that when D is set equal to zero, the usual volumetric hardening law is recovered. If not, D can be assumed either constant (Nova, 1977; Gens & Nova, 1993; Yu, 2007; Lagioia & Panteghini, 2014), or a function of the deviatoric plastic strain, to reduce the dilatancy at failure (i.e. saturating model). A possible expression is (Wilde, 1977):

$$D = D_0 exp\left(-D_1\varepsilon_q^p\right) \tag{5.8}$$

It is interesting to analyse the implication of the adopted hardening rule in a simple undrained compression test. Equation 5.7 together with the constraint of constant global volume (i.e. $\delta\varepsilon_p^p$=-$\delta\varepsilon_p^e$) gives

$$\kappa\frac{\delta p'}{p'} = -(\lambda - \kappa)\frac{\delta p'_c}{p'_c} + vD\delta\varepsilon_q^p \tag{5.9}$$

By introducing the definition of the pore pressure parameter, a (equation 5.6 in infinitesimal form), in equation 5.9 follows

$$a\frac{\delta q}{p'} = \frac{\lambda - \kappa}{\kappa}\frac{\delta p'_c}{p'_c} - \frac{vD}{\kappa}\delta\varepsilon_q^p \tag{5.10}$$

For a contractive soil response, the first term on the right hand side of equation 5.10 is always positive. The same holds for the second term considering that $D\geq 0$. Equation 5.10 shows that for a stable deviatoric response (i.e. $\delta q>0$), even in a contractive domain the pore pressure parameter firstly increases and then decreases, depending on the magnitude of the distortional term $D\delta\varepsilon_q^p$. As instructive case, Figure 5.9 reports the comparison between a classical associated Modified Cam clay with volumetric hardening rule (D=0), a mixed hardening rule with constant D (D=1.2) and with the saturating law of equation 5.8 (D_0=1.2 and D_1=15).
As displayed in Figure 5.9, depending on the magnitude of the distortional hardening coefficient D, the occurrence of dilation in the hardening regime is introduced with the possibility of reaching failure for a stress ratio, η_f, higher than the critical stress ratio, M_g, with non-null dilatancy, d_f. From equation 5.7 follows:

$$d_f = \frac{\delta\varepsilon_p^p}{\delta\varepsilon_q^p} = -D \tag{5.11}$$

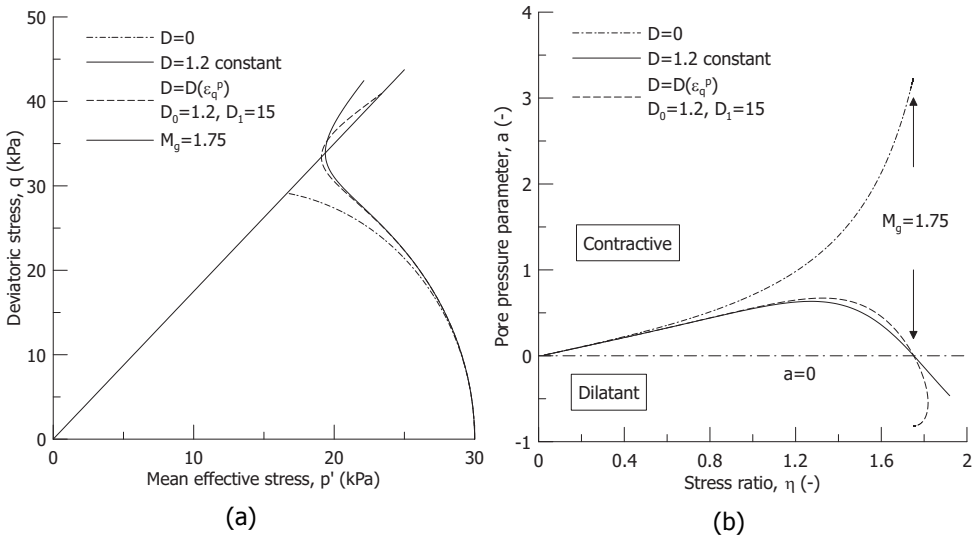

Figure 5.9: Implications of a mixed volumetric and distortional hardening rule on (a) stress path and (b) pore pressure parameter a

The results in Figure 5.9 compared with Figure 5.8 show clearly that a purely volumetric hardening is not adequate to capture the deviatoric response of peats. The geometrical rearrangement/realignment of the small fibrous network present in the fabric of the tested peat can provide the physical ground of equation 5.7 as the geometrical rearrangements or realignment of particles do for granular soils (Wood, 1990).

5.3.4. Stress-dilatancy relationship

The plastic response is analysed focusing on the stress-dilatancy relationship, with d defined in terms of volumetric and deviatoric plastic strain increments, $\delta\varepsilon_p^p$ and $\delta\varepsilon_q^p$

$$d = \frac{\delta\varepsilon_p^p}{\delta\varepsilon_q^p} \tag{5.12}$$

Drained and undrained triaxial tests are considered to provide a form of the stress-dilatancy rule for the tested peat. The flow rule for the tested peat should satisfy in principle the following conditions:

i) $d \to \infty$ for η=0, due to the observed isotropic response in isotropic compression (Figure 5.2(b));

ii) d= observed d for $\eta=\eta_{K_0}$, as a K_0 path rules out the end restraint effect as shown in Chapter 4;

iii) d=0 for $\eta=M_g$, where M_g gives the critical stress ratio.

The expression by McDowell & Hau (2003) already presented for the yield locus, is also used for the plastic potential g=0.

$$g = 0 = q^2 + \frac{M_g^2}{1-\chi_g}\left(\frac{p'}{p'_g}\right)^{\frac{2}{\chi_g}} {p'_g}^2 - \frac{M_g^2 p'^2}{1-\chi_g} \tag{5.13}$$

equation 5.13 gives a dilatancy

$$d = \frac{M_g^2 - \eta^2}{\chi_g \eta} \tag{5.14}$$

with M_g the stress ratio at critical state equal to 1.75 (Figure 5.8) and p'_g a dummy variable for the plastic potential. The value of the shape parameter χ_g was determined requiring zero lateral strain along the K_0 path, experimentally determined on sample 2 (Figure 5.2(a)) resulting in

$$\chi_g = \frac{2}{9}\frac{\lambda}{\lambda-\kappa}\frac{M_g\left[(6-M_g)^2-9\right]}{6-M_g} \tag{5.15}$$

where the elastic component of the deviatoric strain has been neglected for the sake of simplicity (Alonso et al., 1990). For the compression indexes λ=2.0 and κ=0.3 (Figure 5.2(a)) and the critical stress ratio M_g=1.75, a value of χ_g=0.98 is found. The resulting flow rule overcomes the well-known drawback of classical critical state models which overestimate the K_0 values (Gens & Potts, 1982). Figure 5.10(a) displays the resulting flow rule. The stress dilatancy data obtained from the undrained compression test on sample 5 is summarised in Figure 5.10(b).

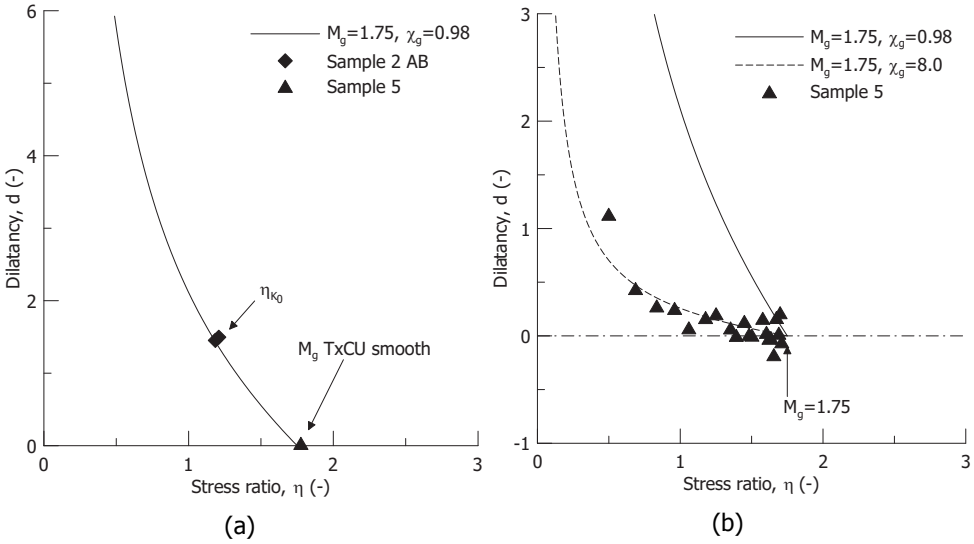

Figure 5.10: Stress-dilatancy rule based on (a) consideration on null radial strain along a K_0 path and (b) from undrained compression tests on sample 5

As displayed in Figure 5.10(b) the experimental data from undrained compression tests seem to provide a stress dilatancy rule far different from the one derived in Figure 5.10(a) based on the consideration on the K_0 path (χ_g=8 compared to χ_g=0.98). This difference cannot be explained by end restraint effects considering that sample 5 was tested with modified end platens and the K_0 path on sample 2 produced negligible radial strains. The results in Figure 5.10 are translated in two different shapes for the plastic potential as displayed in Figure 5.11.

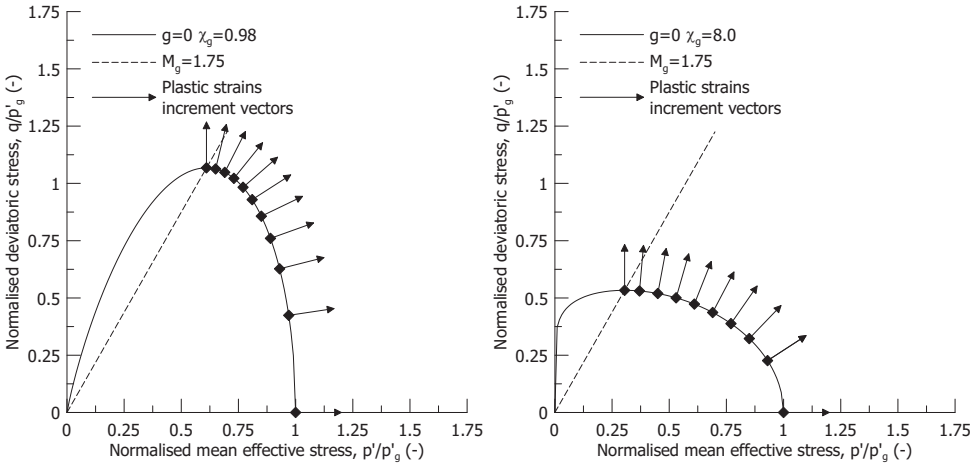

Figure 5.11: Plastic potential and plastic strains increment vectors for (a) χ_g=0.98 and (b) χ_g=8.0

The plastic potential in Figure 5.11(a) presents a rather classical dome shape with plastic strains increment vectors mainly ruled by volumetric strains for low stress ratios, and by deviatoric strains as the stress ratio increases. On the contrary, indications from the undrained triaxial test in Figure 5.11(b) seem to magnify the relevance of the distortional strains on the plastic deformation mechanism. The resulting plastic potential flattens down as χ_g increases with steeper plastic strains increment vectors. For the same imposed stress state, the resulting plastic strains increment vectors differ significantly as displayed in Figure 5.12.

5.4. DISCUSSION

Stress-path dependence of structural changes was advocated by Cotecchia & Chandler (1997) and Cotecchia & Chandler (2000) to interpret different stress-dilatancy relationship for drained and undrained triaxial tests on Pappadai clay. As for the tested peat, experimental results from undrained triaxial tests in Cotecchia & Chandler (1997) seem to magnify the distortional strain component in the plastic deformation mechanism. The apparent inconsistency may come from the role of fabric. The tested reconstituted peat was characterised by small fibres with a characteristic length smaller than 3 mm. Figure 5.13 displays a x-ray micro CT on the

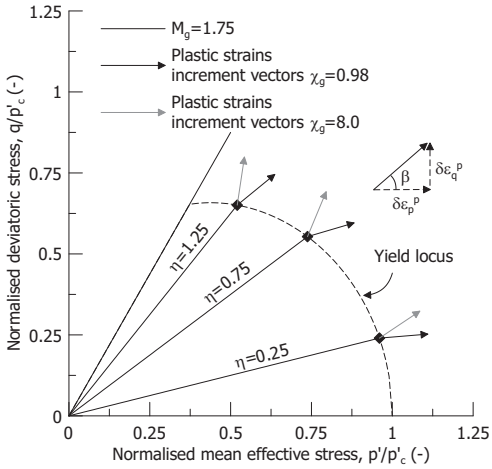

Figure 5.12: Plastic strains increment vectors for χ_g=0.98 and χ_g=8.0 in correspondence of three stress states along three radial paths

tested peat, left for 2 days to dry under air temperature 14°C and relative humidity 80%. Inorganic soil grains are visible with higher density (white spots) within the fibrous matrix.

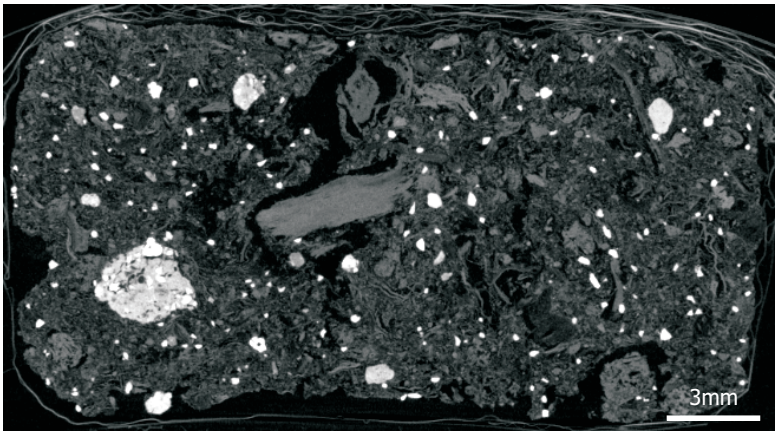

Figure 5.13: Micro CT scan of the reconstituted peat used in the present experimental investigation: inorganic grains (white spots) and small fibres are visible

Despite natural fibrous peat samples often exhibit inherent anisotropy related to the initial fibres orientation (Landva & La Rochelle, 1983; Yamaguchi et al., 1985a,b), for the tested peat the small fibres seem to be diffuse and randomly distributed without an initial preferential orientation. More likely, the results in Figure 5.12 seem to suggest a directional response of the plastic strains increment vectors during the loading path. Re-orientation of the fibrous network could dif-

fer depending on the stress-path direction. First experimental evidence of plastic strains increment vectors following the rotation of the stress increment vectors was reported by Le Lievre & Poorooshasb (1967) testing kaolin, Calabresi (1968) testing a silty clay, and Lewin & Burland (1970) testing a powdered slate dust. In the attempt to facilitate the interpretation of the experimental results, Figure 5.14 gives an insight into the plastic strains increment vectors for three different stress paths on three samples with the same isotropic compression up to p'_c=34 kPa before shear. On sample 6 a drained stress path was imposed in order to reproduce the stress path experienced by sample 5 during a standard undrained compression test.

A common stress state is chosen for each sample in correspondence of a stress ratio $\eta \cong 0.75$ (stress state A in Figure 5.14(a)). The deviatoric strains in correspondence of the stress state A attained similar values for each sample: 2% for sample 5 and 3% for sample 3 and sample 6. Also the void ratio for each sample at the stress state A were similar: 7.1 for sample 3, 6.9 for sample 5 and 7.6 for sample 6. Nevertheless, the plastic strains increment vectors resemble the loading direction with more vertical vectors for sample 5 and sample 6 (Figure 5.14(a)), confirming that the loading direction together with the stress path up to the current stress state seem to rule the plastic deformation response of tested peat. Furthermore, sample 6 confirmed the stress dilatancy data from sample 5 as displayed in Figure 5.14(b). Plausible physical reason for this directional response of the deformation response could lie in the interaction between the small fibrous network and the peat matrix. The results in Figure 5.14 can also be represented in terms of axial and radial strains paths. Figure 5.15 reports the axial-radial strains paths for all the samples here presented.

With reference to Figure 5.15(a), strain paths in the top right quadrant limit the fibres-matrix interaction. The fibres are not stretched due to compressive radial strains and the mechanical response is not affected by the fibres. Relevant cases are the isotropic compression path (ε_a=ε_r) and the K_0 path (ε_r=0) where the effect of fibres is substantially switched off. The former increases the fibres entanglement while the latter promotes both the fibres flattening or distortion (Figure 5.15(b)) depending on their initial orientation without any substantial stretching. On the contrary, strain paths in the top left quadrant promote the fibres-matrix interaction due to expansive radial strains. With the progressive radial expansion of the sample, fibres realignment is promoted (Figure 5.15(b)). Strong interaction between the soil matrix and the fibrous network takes place with consequent evolution of the peat fabric and alteration of the observed plastic deformation response. Isochoric test as the undrained compression test on sample 5 is expected to magnify the most this interaction. The substantial coincidence of the stress paths for sample 5 and sample 6 translates into similar stress dilatancy data and plastic strains increment vectors as verified in Figure 5.14. The small differences between these two samples in Figure 5.14(a) come from an initial volume contraction (3%) experienced by sample 6 due to an excess pore pressure of about 1-2 kPa present at the beginning of the shearing.

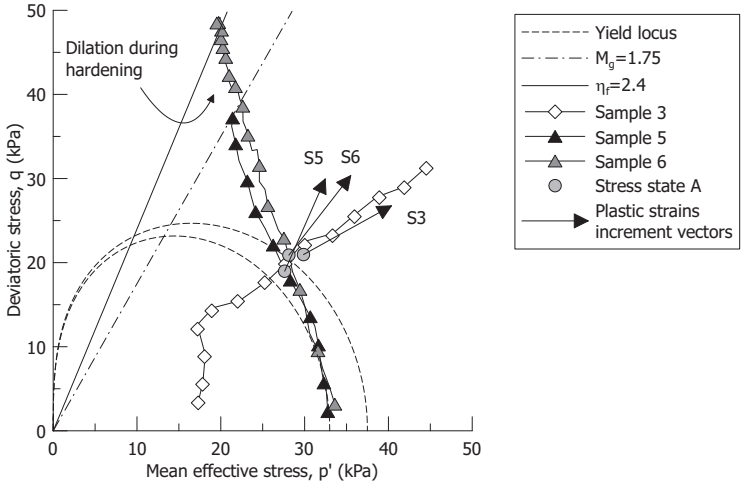

(a)

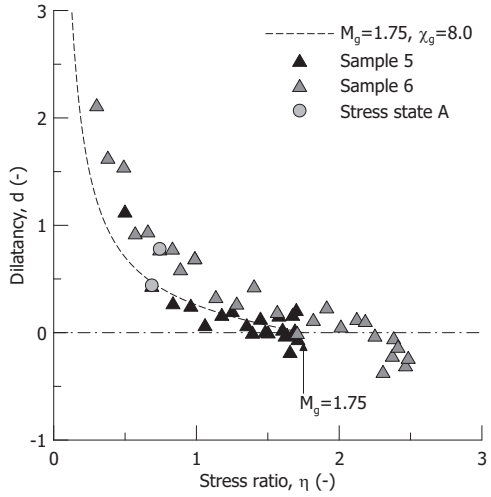

(b)

Figure 5.14: Stress paths (a) and (b) corresponding stress-dilatancy relationship for samples with two different loading directions

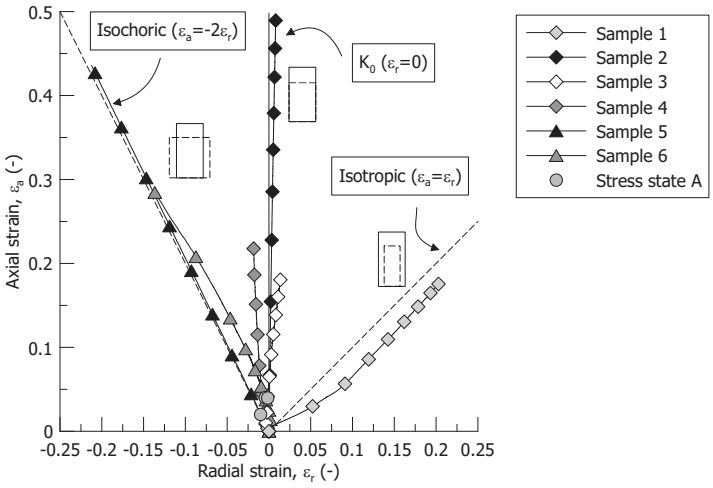

(a)

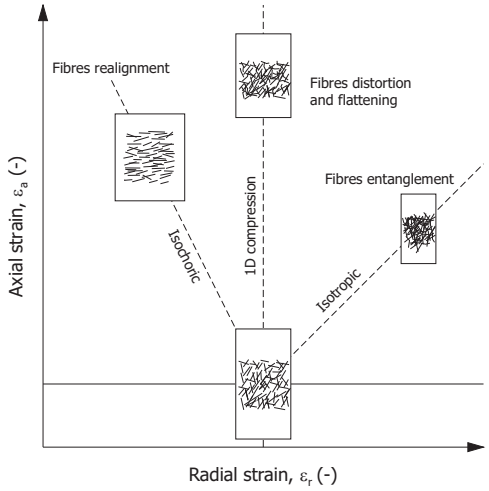

(b)

Figure 5.15: Experimental radial-axial strains paths (a) and (b) simplified scheme of the evolution of the small fibrous network along different strain directions

5.5. NUMERICAL SIMULATIONS

5.5.1. Model parameters

In the attempt to overcome the limitations of end restraint on the observed behaviour, the constitutive ingredients previously derived have been implemented in the Finite Element Code LAGAMINE (Charlier, 1987) and the experimental results have been modelled as boundary value problems as described in Chapter 4. The p'-q formulation has been extended to the general multi-axial stress space. The stress state of the material is described by the mean effective stress, p', the second invariant of the deviatoric stress tensor, J_2, and the Lode's angle, θ. The dependence of the critical stress ratio, M_g, on the Lode's angle was described by the Van Eekelen (1980) formulation. For the yield locus, a circular shape was adopted (McDowell & Hau, 2003). The model capabilities are tested by replicating the experimental results from selected drained triaxial compression tests. In the numerical analyses, the issues possibly raised in the interpretation of experimental data by the low hydraulic conductivity soils were disregarded. Table 5.2 reports the characteristics of each sample and the test prescriptions (e_0 is the void ratio at the beginning of shear in correspondence of p'_0). The model parameters are summarised in Table 5.3.

Table 5.2: Main characteristics and test prescriptions of drained triaxial tests

Sample	H_0/D_0 (-)	p'_0 (kPa)	e_0 (-)	OCR (-)	End platens
E	2.3	14.0	7.99	2.6	Modified (reduced friction)
F	2.1	15.0	6.93	2.2	Standard (rough)
G	2.0	14.0	7.79	2.3	Standard (rough)

Table 5.3: Parameters adopted in the constitutive model

λ (-)	κ (-)	ν (-)	M_f (-)	M_g (-)	χ_f (-)	χ_g (-)	D_0 (-)	D_1 (-)
2.0	0.3	0.2	1.5	1.75	3.0	0.98	1.2	30

5.5.2. Model results and discussion

The comparison between the numerical and experimental results are reported in Figure 5.16, Figure 5.17 and Figure 5.18 on different stress-strain spaces.
The numerical results for the case of sample E show good qualitative and quantitative agreement with the experimental results both in the volumetric and deviatoric response for wide range of strains up to 20%, encompassing representative strains levels for field applications where peats serve as foundation layers. While the qualitative response is still good for sample F and G, the quantitative agreement is less satisfactory especially for what concerns the deviatoric response. The numerical results are not able to capture the observed response with deviatoric stress overpassing the corresponding one at critical state, $\eta_f \cong 2.6$ compared to $M_g = 1.75$. The

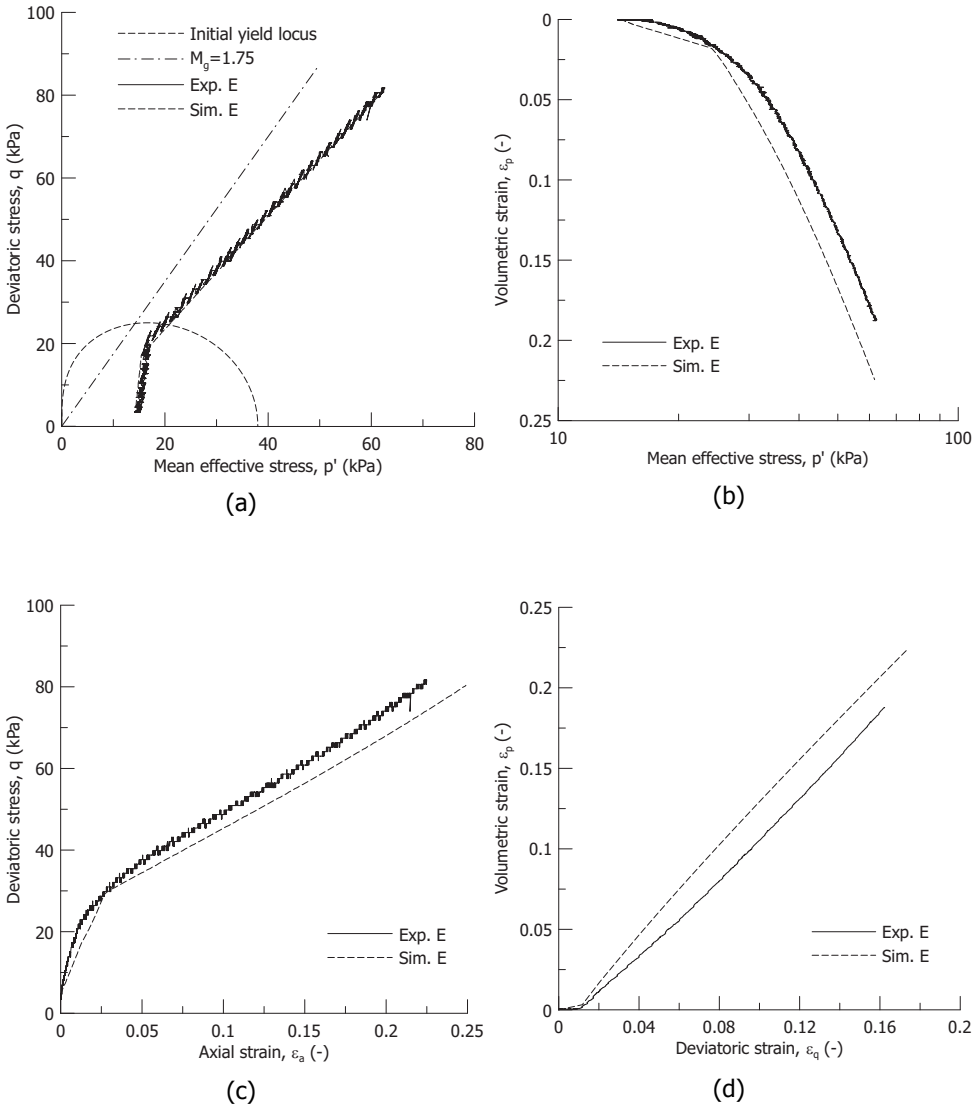

Figure 5.16: Comparison between experimental and numerical results for drained triaxial compression test on sample E in terms of: (a) stress path; (b) volumetric stress-strain response; (c) deviatoric stress-axial strain relationship; and (d) volumetric-deviatoric strains path

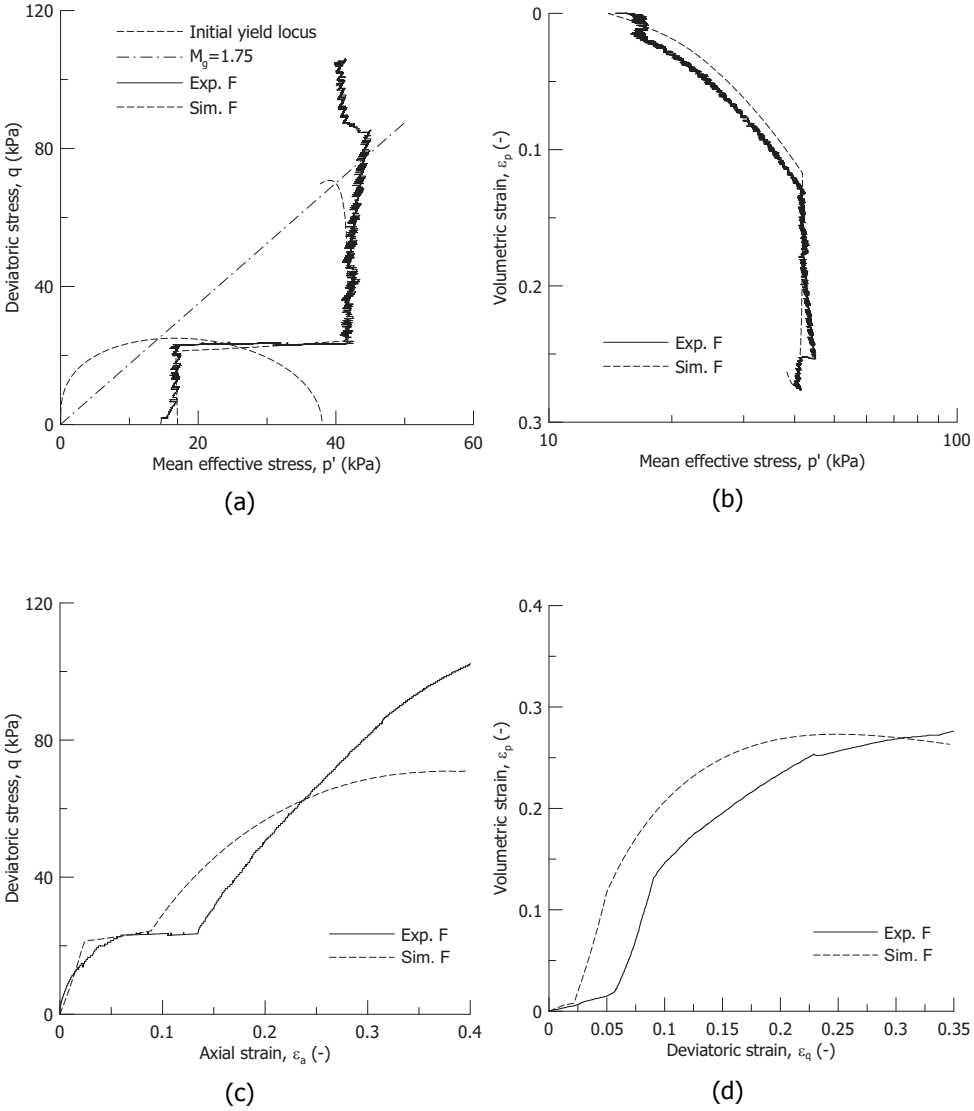

Figure 5.17: Comparison between experimental and numerical results for drained triaxial compression test on sample F in terms of: (a) stress path; (b) volumetric stress-strain response; (c) deviatoric stress-axial strain relationship; and (d) volumetric-deviatoric strains path

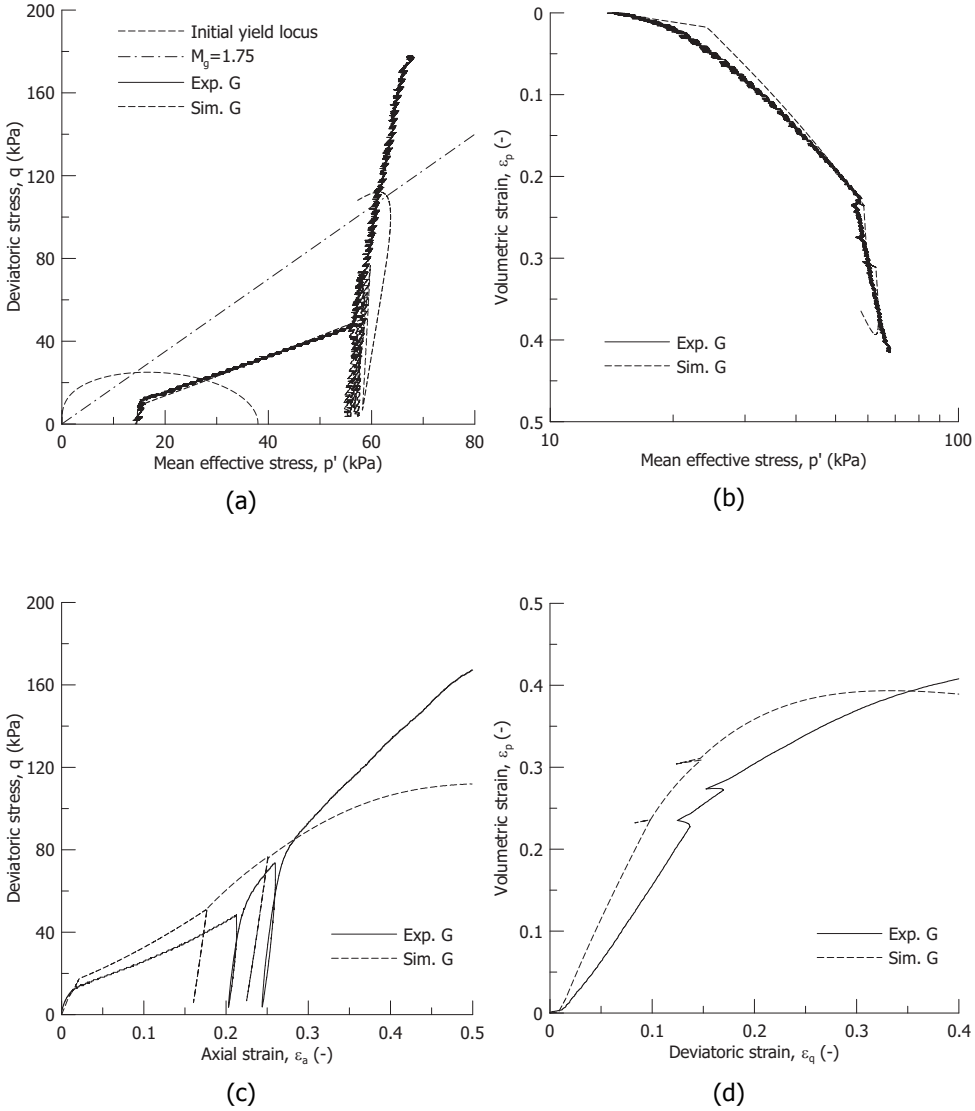

Figure 5.18: Comparison between experimental and numerical results for drained triaxial compression test on sample G in terms of: (a) stress path; (b) volumetric stress-strain response; (c) deviatoric stress-axial strain relationship; and (d) volumetric-deviatoric strains path

adoption of a mixed volumetric and distortional hardening allows the numerical stress paths attaining stress ratios above critical state but still well below the experimental ones (Figure 5.17(a) and Figure 5.18(a)). End restraint effects in the experimental results contributed to the observed behaviour for sample F and sample G which were tested with rough end platens contrary to sample E where platens with reduced friction were adopted. The complex stress history imposed to sample F and sample G brought the samples at failure with a height to diameter ratio equal to 1.1 hence magnifying the constraint applied at the top and bottom of the sample by the rough platens. The influence of the height to diameter ratio on the derived ultimate friction angle is summarised in Figure 5.19 where TxCU tests from Chapter 3 and the drained tests here presented are combined. Despite the numerical simulations of the experimental tests as boundary value problems, end restraint effects are not adequately captured by the finite element analyses especially for high axial strain levels.

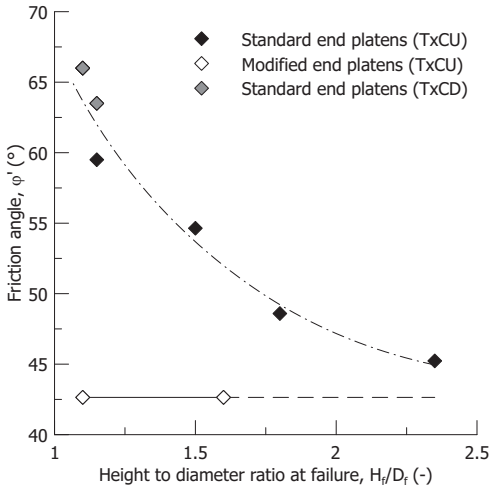

Figure 5.19: Influence of the height to diameter ratio on the friction angle from undrained and drained compression tests on samples with different height to diameter ratio tested with standard (rough) and modified (reduced friction) end platens

As displayed in Figure 5.19 drained tests magnify the end restraint effect on the derived friction angle due to the small height to diameter ratio at failure. Another contributing effect to the high shear strength of sample F and sample G may come from the additional confinement offered by the fibres stretching. Despite the tested reconstituted peat not including big fibres, for high axial compression as experienced by the samples F and G, small fibres stretching may have contributed to the observed behaviour. Extensive research on fibres reinforced soils showed that the additional confinement offered by fibres stretching allows the soil composite (soil matrix and fibres) to sustain higher stresses than the ones at critical state for the soil matrix and to a more pronounced compressive response (Diambra et al., 2013; Diambra & Ibraim, 2014). Despite the differences of the tested peat

(Figure 5.12) with traditional fibres reinforced soils (mainly granular soils with isolated polypropylene fibres), the high deviatoric stresses well above critical state observed in drained tests as displayed in Figure 5.17(a) and Figure 5.18(a) could reflect more a composite behaviour rather than the soil matrix behaviour. Differently from undrained compression tests, sample F and sample G tested in drained conditions, attained axial strains up to 40% and 50%. With significant axial compression, the initial isotropic fibres distribution evolves towards preferential horizontal distribution. This condition is the most favourable for the fibres, once stretched, to provide additional radial confinement to the sample. On the contrary, samples sheared under undrained conditions failed for axial strain of about 20% well below the strain level attained by samples sheared in drained conditions which may have contributed to reduce the contribution of the fibres stretching to the shear strength.

5.6. CONCLUSIONS

The capability of describing the behaviour of peats is of primary importance for many field applications where peats serve as foundation layers such as dykes and embankments. Contrary to the volumetric behaviour, modelling the deviatoric counterpart still poses significant difficulties and the available models are rather scarce. Despite the previous extensive experimental investigations dedicated to clarify the stress-strain response of peats upon deviatoric loading, still the vast majority of these studies were limited to undrained triaxial compression tests. Hence difficulties arise to provide experimental evidence supporting a rational development of a constitutive model for the deviatoric behaviour of peats.

An experimental investigation was proposed with the aim of revealing important constitutive aspects of the deviatoric behaviour of peats. Drained and undrained compression triaxial tests on reconstituted peat samples were presented. The experimental results allowed to reveal for the first time ingredients as the yield locus, the stress-dilatancy relationship and the hardening rule. The comparison between drained compression tests with different loading directions provided experimental evidence of a directional plastic deformation response. Stresses and strains path dependence of the evolution of the peat fabric which contains small diffuse fibres is suggested as responsible mechanism for the observed peculiar stress-dilatancy relationship. In particular, stress paths accompanied by radial contraction of the sample seem not to cause relevant fabric change and the plastic deformation response does not differ substantially from the classical response of fine grained materials. On the contrary, stress paths with significant radial expansion magnify the relevance of the deviatoric strain component in the plastic deformation response.

Rearrangement and realignment of the small fibres also affect the hardening mechanism. The experimental results revealed that the commonly assumed volumetric hardening rule does not reflect the observed behaviour especially for high stress ratios. A mixed volumetric and distortional hardening rule was introduced as the evolution of the hardening variable along radial paths with different loading direction is function of both volumetric and deviatoric strains.

All the experimental results were combined in a simple elastic-plastic non associative model with mixed volumetric and distortional hardening for the deviatoric

behaviour of peat. In the attempt of overcoming end restraint effects on both the shear strength and on the deformation mode of peat, the model has been formulated in the multi-axial stress space and implemented in a Finite Element code. The experimental tests were then simulated as boundary values problems. The numerical results showed reasonable qualitative and quantitative agreement with the experimental results from drained triaxial compression tests. The deviatoric stress-strain response was captured for a large interval of axial strains, up to 20%. This value is well above the shear strains attained by peat layers in field applications where failure occurs mainly due to the kinematic compatibility among different soils layers rather than for failure of the peat layer. Despite the possibility of attaining stress ratios above critical state thanks to the introduction of the mixed volumetric and distortional hardening, the numerical simulations failed to reproduce high deviatoric stress well above the critical state observed from samples tested with rough end platens. End restraint effects not properly captured by the numerical analyses and possible additional confinement offered by small fibres stretching for samples experiencing axial compression up to 40% and 50% appear of primary importance to reproduce the observed behaviour.

LIST OF SYMBOLS

H	sample height
V	sample volume
H_0	initial sample height
D_0	initial sample diameter
V_0	initial sample volume
λ	slope of the isotropic normal compression line
κ	slope of the isotropic unloading-reloading line
ν	Poisson's ratio
G	shear modulus
Gs	specific gravity
OC	organic content
e	void ratio
v	specific volume
p'	mean effective stress
p'_c	preconsolidation mean effective stress
p'_0	mean effective stress at the beginning of shear
$\delta p'_c$	preconsolidation mean effective stress increment
q	deviatoric stress
OCR	overconsolidation ratio
K_0	coefficient of earth pressure at rest
η	stress ratio
η_{K_0}	stress ratio along a K_0 path
M_f	stress ratio associated to the horizontal tangent of the yield locus
M_g	stress ratio at critical state
η_f	stress ratio at failure
χ_f	shape factor of the yield locus
χ_g	shape factor of the plastic potential
p'_g	dummy variable for the plastic potential
$\dot{u}_a$	axial displacement rate
ε_a	axial strain
ε_r	radial strain
ε_p	volumetric strain
ε_q	deviatoric strain
$\delta\varepsilon_a$	axial strain increment
$\delta\varepsilon_p$	volumetric strain increment
$\delta\varepsilon_p^p$	volumetric plastic strain increment
$\delta\varepsilon_q^p$	deviatoric plastic strain increment
ε_p^p	volumetric plastic strain
ε_q^p	deviatoric plastic strain
d	dilatancy
d_f	dilatancy at failure
W	first order work
D, D_0, D_1	coefficients of the distortional hardening

S	length of the stress path
a	pore pressure parameter
$\Delta p'$	change in the mean effective stress
Δq	change in the deviatoric stress
$\delta p'$	mean effective stress increment
δq	deviatoric stress increment
φ'	friction angle
J_2	second invariant of the deviatoric stress tensor
θ	Lode's angle

6

Natural and reconstituted peat: the role of fibres

등잔 밑이 어둡다

It's dark under the lamp

Korean saying

6.1. EXPERIMENTAL EVIDENCE

6.1.1. Introduction

The stress-strain behaviour of natural peats observed in triaxial tests is significantly affected by the fibrous network present in the peat fabric. Several contributions in the literature have already pointed out that part of the exceptional high shear strength of peat samples may come from the additional confinement offered by the fibres stretching (Yamaguchi et al., 1985b; Cola & Cortellazzo, 2005; Hendry et al., 2012). At the same time, Oikawa & Miyakawa (1980) firstly questioned the different effects the fibres have when moving from the laboratory scale (i.e. 10-20 cm) to the field scale (i.e. 1-2 m). In the attempt to clear out the effects of fibres, the authors proposed the adoption of the null increment in the mean effective stress, $\Delta p'=0$, as failure criterion for natural peat samples tested in undrained triaxial compression. The mechanical ground of this condition which marks the transition from a contractive to a dilatant behaviour was discussed by Nova (1977). The so defined failure line was called by Oikawa & Miyakawa (1980) *destructive envelope*, where "the shear strength of the peat is firstly mobilised and disruption of the soil fabric occurs". The additional portion of the stress path beyond $\Delta p'=0$ eventually approaching the Tension Cut Off line (TCO) results from the tendency of the sample to dilate (Oikawa & Miyakawa, 1980). In undrained conditions, this tendency is counterbalanced by an increase in the mean effective stress and thus shear strength. However, there is no guarantee that such a condition is representative of the actual field situation where the hydro-mechanical behaviour is neither perfectly undrained nor drained. Partial water intake or drainage from peat layers release the constant volume constraint and make every consideration after the $\Delta p'=0$ extremely uncertain (Asaoka et al., 1995). Based on the proposal by Oikawa & Miyakawa (1980), the following pages report a comparison between reconstituted and natural peat samples tested in undrained compression tests.

6.1.2. Material and experimental programme

The material for the reconstituted peat samples was collected 1.0 to 1.5 m below the ground surface at the Leendert de Boerspolder site in the Netherlands. Natural peat samples were retrieved between 1.0 and 2.5 m depth from the ground level in the subsoil of the Markermeer dykes at Katwoude. Reconstituted peat samples were prepared by mixing the wet peat with demineralised water to slurry with water content of 855%, which corresponds to 1.4 times the limit liquid. The material was then consolidated in a floating consolidometer under a total vertical stress of 9.5 kPa for 48 hours. The reconstituted sample was then extracted and mounted in the triaxial apparatus. For the natural peat samples, the in situ effective vertical stress of is around 10 kPa, typical of surficial peat layers in the Netherlands. Both samples were 50 mm in diameter and 100 mm in height. The most important index properties and tests specifics are summarised in Table 6.1 (e_0 is the void ratio at the beginning of shear in correspondence of a mean effective stress p'_0).

The specific gravity Gs, of the soil was measured with a helium pycnometer in accordance with D5550-14 (2014) and the organic content OC was assessed by

Table 6.1: Index properties and relevant information of the tested specimens

Sample	Gs (-)	e_0 (-)	p'_0 (-)	OC (-)	OCR (-)	Status
Sample 1-N	1.47	7.44	21	0.86	1.1	Natural
Sample 2-N	1.48	7.94	13	0.86	1.3	Natural
Sample 1-R	1.47	6.50	32	0.91	1.0	Reconstituted
Sample 2-R	1.45	6.70	21	0.92	1.5	Reconstituted
Sample 3-R	1.48	7.16	18	0.91	1.8	Reconstituted

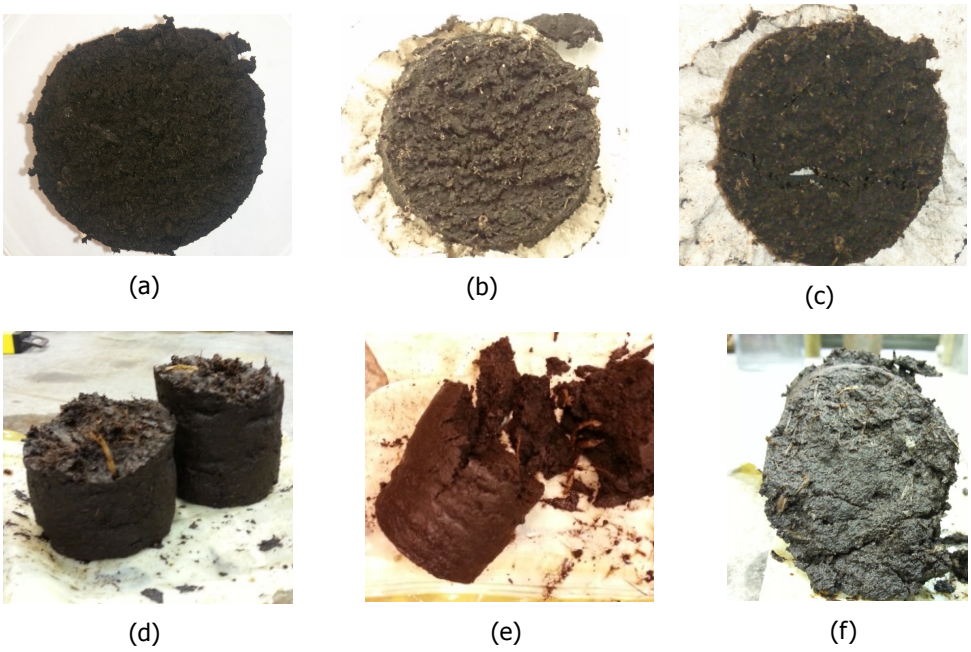

Figure 6.1: Reconstituted peat samples (a), (b), (c) at different drying periods (0-24-48 h) and (d), (e), (f) natural peat samples with the big fibres visible in the peat matrix

ignition in a furnace at 500°C (D2974-14, 2014). Reconstituted peat samples were characterised by a diffuse network of small fibres randomly distributed and with a maximum length of about 3 mm. No big fibres were present. On the contrary, natural peat samples presented not only a diffuse small fibrous network but also medium and big fibres with length of about 2-3 cm. Figure 6.1 reports a comparison of the different peats samples.

All the samples were firstly isotropic consolidated and then sheared under displacement control, with a constant axial displacement rate of 0.02 mm/min using a load frame type GDS triaxial system, with back pressure and cell pressure volume controllers, and a submersible 1 kN load cell. The accuracy of the controllers is ±1

kPa on pressure and ±300 mm^3 on volume (0.15% FSR). Thin membranes 0.25 mm thick were used. For the reconstituted samples, due to the significant lower hydraulic conductivity compared to the natural peat, lateral filter paper was placed. To prevent "short circuit" effects between the back pressure and the pore pressure transducers, 10 mm clearance were left between the lower edge of the lateral filter paper and the bottom of the samples. Each vertical drainage strip had free lower end to reduce the potential contribution offered by the lateral filter paper to the measured strength of the material (Head & Epps, 2014b). Standard rough end platens were used for all the samples.

6.1.3. Experimental results

The experimental data are presented by means of the typical triaxial stress-strain variables: p' mean effective stress, q deviatoric stress, η stress ratio, σ'_a axial effective stress, and ε_q deviatoric strain.

Figure 6.2 reports the normalised stress paths for all the samples. Normalised stress variables were obtained from the preconsolidation mean effective stress applied in the triaxial apparatus, p'_c.

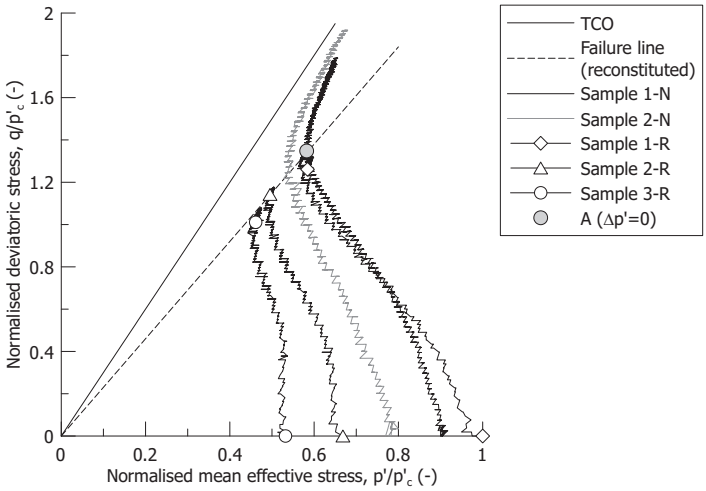

Figure 6.2: Normalised stress path from reconstituted and natural peat samples

As displayed in Figure 6.2 reconstituted peat samples failed for a stress ratio of about 2.3 which approximately coincides with the condition of $\Delta p'=0$ for natural peat samples (point A). The natural peat samples overpass this stress ratio, with a stress path approaching asymptotically the Tension Cut Off line (TCO) where the effective radial stress is equal to zero. For $\eta>\eta_{\Delta p'=0}$ any further increment in the deviatoric stress of natural peat samples is accompanied by dilation (Oikawa & Miyakawa, 1980). To clarify this transition from a contractive to a dilatant response, Figure 6.3 reports the pore pressure parameter a (Wood, 1990), defined as

$$a = -\frac{\Delta p'}{\Delta q} \tag{6.1}$$

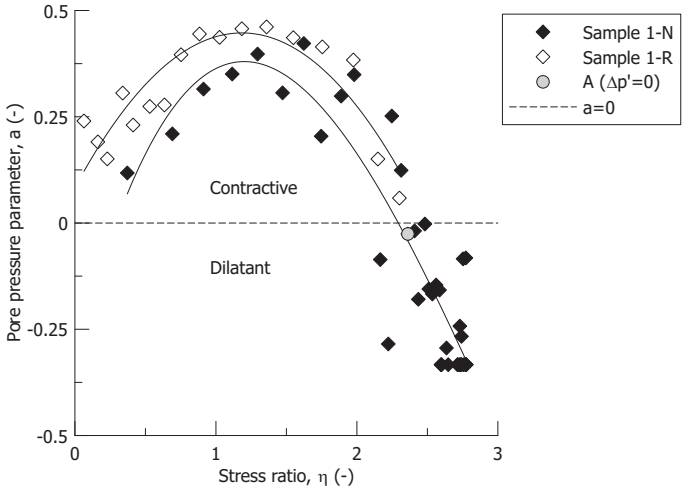

Figure 6.3: Pore pressure parameter a for reconstituted and natural peat samples

The failure stress ratio η=2.3 marks the transition between a contractive response (a>0) and a dilatant response (a<0). To elucidate the role of the fibres on the observed behaviour, it is worth comparing the deviatoric stress-strain response of natural and reconstituted peat samples in Figure 6.4(a). Samples 1-R and 1-N with OCR almost equal to 1 are considered.

The normalised deviatoric stress-strain response for both reconstituted and natural samples is comparable up to 5%–10% of deviatoric strain. At this stage the two responses start diverging with the reconstituted samples exhibiting a gentle plastic response eventually approaching the failure state. On the contrary, natural samples do not approach failure and in correspondence of the point A ($\Delta p'$=0) they enter in a strain-hardening regime, with a deviatoric stress increasing almost linearly with the imposed strain (Figure 6.4(a)). This response already observed by Oikawa & Miyakawa (1980) and Kanmuri et al. (1998) among the others, is associated to the additional confinement provided by the big fibres stretching. A nice comparison of the effect of fibres is reported by Andersland et al. (1981) testing kaolinite samples with different amount of pulp fibres in undrained compression triaxial tests. The authors found that "higher organic fibres fractions increasingly alter the deviatoric stress-strain behaviour, giving an almost straight line response for all fibrous samples". The comparison in Figure 6.4 confirms the role of big fibres in the peculiar strain-hardening behaviour of natural peat samples. In particular, the additional confinement offered by the big fibres is strain level dependent: only with progressive lateral bulging of the sample, the big fibres start being stretched and affect the sample stress-strain response. The same consideration holds for the

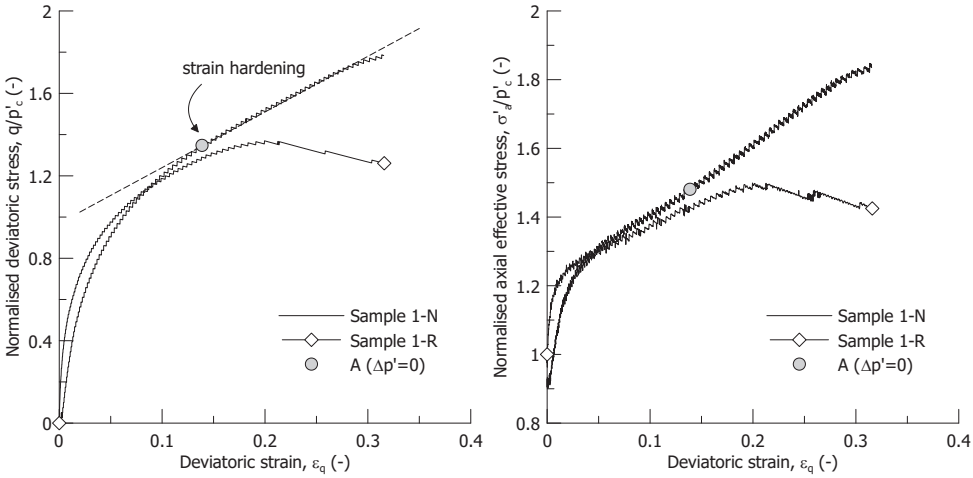

Figure 6.4: Normalised deviatoric stress-strain response (a) and (b) axial effective stress-strain response for reconstituted and natural peat samples

axial stress-strain response as displayed for the sake of clarity in Figure 6.4(b) and in terms of stress ratio in Figure 6.5.

6.1.4. Fibres-soil matrix interaction scheme

The results of the previous section support the idea that natural peat samples contain in general at least a two levels of fibrous structures as displayed in Figure 6.6:

- S_1 diffuse small fibres randomly distributed;
- S_2 big fibrous inclusions with preferential orientation, depending on the botanic species and depositional environmental conditions.

These two fibrous systems can be schematised through a superposition procedure as reported in Figure 6.6.
Accounting for the different length of the fibres for the two systems, it is possible to assume that the small fibres in the system S_1 are straight while the ones in the system S_2 are likely to be warped and twisted as visualised in Figure 6.7.

With reference to a standard undrained triaxial compression test, matrix-fibres interaction with fibres rearrangement and realignment are likely to occur for the small fibres S_1 since the beginning of the deviatoric loading. On the contrary, it is likely that only after significant axial strain applied to the sample, the S_2 fibres start being stretched either locally or globally, thus contributing to the observed behaviour. As reported in Figure 6.7, these fibres are normally twisted and warped within the peat matrix. Flattening and re-orientation are necessary for these fibres before exerting an effective reinforcement as reported by Li (2005) for the case of

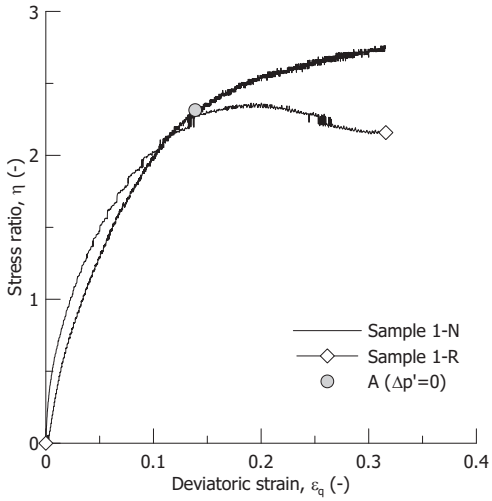

Figure 6.5: Stress ratio versus deviatoric strain for reconstituted and natural peat samples

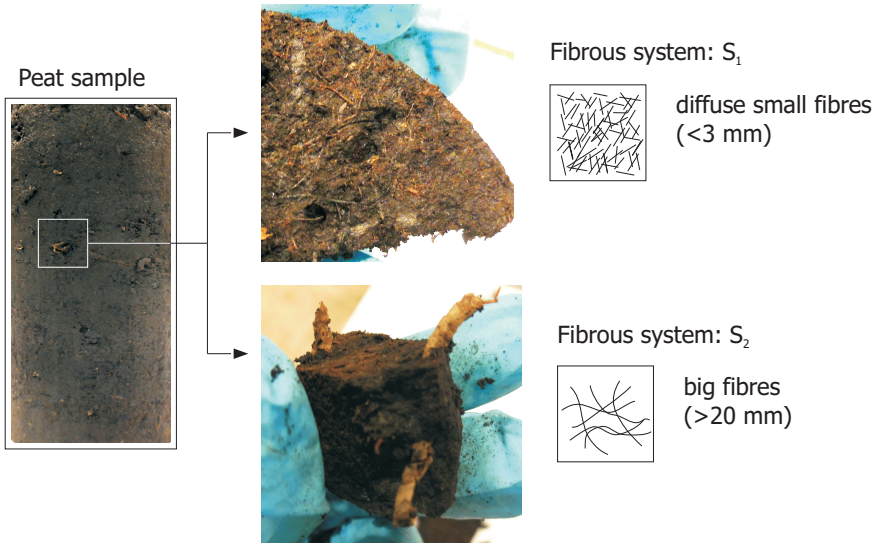

Figure 6.6: Simple scheme of the multiple levels of fibrous structures present in the peat fabric

Figure 6.7: Big fibres inclusions in natural peat sample where twisting and warping can be observed

silty-clay and sandy-silt specimens reinforced with polypropylene fibres. The result is a complex fibres-soil matrix interaction function of their initial special arrangement, progressive re-orientation and stretching (Anagnostopoulos et al., 2014).

6.2. MODELLING PEAT AS A FIBRES-REINFORCED SOIL: AN ILLUSTRATIVE CASE

6.2.1. Introduction

The following pages report an attempt to model the deviatoric behaviour of peats observed in undrained compression tests within the framework of fibres-reinforced soils. Previous attempts of accounting for the effects of the big fibres on the behaviour of natural peats were proposed by Molenkamp (1994) and Teunissen & Zwanenburg (2015) as overlay models and by Boumezerane et al. (2015) through a fabric tensor. All these attempts were more theoretical, rather than aiming at quantitative predictions. Within the framework of fibres-reinforced soils, several proposals have been reported in the literature mainly developed for the case of granular material reinforced with polypropylene fibres (Diambra et al., 2010). Superposition of the effects of the soil matrix and the fibres has been verified to be an efficient modelling approach for this kind of composite materials (di Prisco & Nova, 1993). The constitutive behaviours of the soil matrix and the fibres are defined separately and they are finally superimposed by volumetric homogenization procedure. Following the approach by Diambra et al. (2013), the proposed model represents a first attempt to model the behaviour of peat as soil matrix-fibres composite. With respect to the model by Diambra et al. (2013), more restrictive assumptions have been introduced hereby also due to the objective difficulty of distinguishing between the soil matrix and fibres for the case of peats with a much more complicated fabric than that of traditional fibres-reinforced soils. As a result, at this stage, the proposed model and its results must be considered more as illustrative case than as predictive tool.

6.2.2. Model formulation

The effective stress tensor of the composite, $\boldsymbol{\sigma'}_c$, can be derived from the stress state of the soil matrix, $\boldsymbol{\sigma'}_m$, and of the fibres $\boldsymbol{\sigma'}_f$ by using a volumetric averaging approach

$$\boldsymbol{\sigma'}_c = \mu_m \boldsymbol{\sigma'}_m + \mu_f \boldsymbol{\sigma'}_f \tag{6.2}$$

with μ_m and μ_f the matrix and fibres volumetric content. Despite the fibres being discrete elements, in equation 6.2 an equivalent stress state in assumed. The same strain tensor is assumed for the incremental strain of the composite and of the constituents (Teunissen & Zwanenburg, 2015). By doing so, no slippage between the fibres and the soil matrix is accounted for

$$\boldsymbol{\varepsilon} = \boldsymbol{\varepsilon}_m = \boldsymbol{\varepsilon}_f \tag{6.3}$$

The incremental form of the stress state of the composite reads

$$\dot{\boldsymbol{\sigma}}'_c = \dot{\mu}_m \boldsymbol{\sigma'}_m + \mu_m \dot{\boldsymbol{\sigma}}'_m + \dot{\mu}_f \boldsymbol{\sigma'}_f + \mu_f \dot{\boldsymbol{\sigma}}'_f \tag{6.4}$$

By limiting the application to the undrained case $\dot{\mu}_m$=0 and $\dot{\mu}_f$=0 and by substituting equation 6.3, and equation 6.4 in equation 6.2 it follows

$$\dot{\boldsymbol{\sigma}}'_c = \mu_m \left[\boldsymbol{M}_m\right] \dot{\boldsymbol{\varepsilon}} + \mu_f \left[\boldsymbol{M}_f\right] \dot{\boldsymbol{\varepsilon}} \tag{6.5}$$

where $[\boldsymbol{M}_m]$ and $[\boldsymbol{M}_f]$ are the stiffness matrixes of the soil matrix and the fibres, respectively. Equation 6.5 represents a unique constitutive stress–strain relationship for the composite material. Rewriting equation 6.5 in terms of axial and radial stress components, the stress-strain relationship for axis-symmetric conditions reads

$$\begin{bmatrix} \dot{\boldsymbol{\sigma}}'_{c,a} \\ \dot{\boldsymbol{\sigma}}'_{c,r} \end{bmatrix} = \mu_m \begin{bmatrix} \boldsymbol{M}_{11,m} & \boldsymbol{M}_{12,m} \\ \boldsymbol{M}_{21,m} & \boldsymbol{M}_{22,m} \end{bmatrix} \begin{bmatrix} \dot{\boldsymbol{\varepsilon}}_a \\ \dot{\boldsymbol{\varepsilon}}_r \end{bmatrix} + \mu_f \begin{bmatrix} \boldsymbol{M}_{11,f} & \boldsymbol{M}_{12,f} \\ \boldsymbol{M}_{21,f} & \boldsymbol{M}_{22,f} \end{bmatrix} \begin{bmatrix} \dot{\boldsymbol{\varepsilon}}_a \\ \dot{\boldsymbol{\varepsilon}}_r \end{bmatrix} \tag{6.6}$$

A basic assumption here adopted is that the fibres do not act in compression and they do not provide any resistance to bending (Diambra et al., 2013). As a result, they only contribute to the observed composite stress state when they are pulled in the radial direction. Fibres are assumed to be horizontal aligned herein and consequently $\boldsymbol{M}_{11,f}$=$\boldsymbol{M}_{12,f}$=$\boldsymbol{M}_{21,f}$=0. From the definition of mean effective stress, deviatoric stress, volumetric and deviatoric strains, equation 6.6 can be rearranged for the axisymmetric conditions as

$$\begin{bmatrix} \dot{p}'_c \\ \dot{q}_c \end{bmatrix} = \mu_m \begin{bmatrix} \boldsymbol{D}_{11,m} & \boldsymbol{D}_{12,m} \\ \boldsymbol{D}_{21,m} & \boldsymbol{D}_{22,m} \end{bmatrix} \begin{bmatrix} \dot{\boldsymbol{\varepsilon}}_p \\ \dot{\boldsymbol{\varepsilon}}_q \end{bmatrix} + \mu_f \begin{bmatrix} \boldsymbol{D}_{11,f} & \boldsymbol{D}_{12,f} \\ \boldsymbol{D}_{21,f} & \boldsymbol{D}_{22,f} \end{bmatrix} \begin{bmatrix} \dot{\boldsymbol{\varepsilon}}_p \\ \dot{\boldsymbol{\varepsilon}}_q \end{bmatrix} \tag{6.7}$$

Equation 6.7 only requires the definition of the stiffness matrix for the soil matrix and the fibres.

Peat matrix

The constitutive model proposed in Chapter 5 is adopted for the peat matrix which according to the scheme in Figure 6.6 also contains the small fibrous network S_1. The main constitutive terms are here recalled for the case of clarity.

- Hypo-elastic law with constant Poisson's ratio

$$\begin{bmatrix} \dot{p'}_m^e \\ \dot{q}_m^e \end{bmatrix} = \begin{bmatrix} K & 0 \\ 0 & 3G \end{bmatrix} \begin{bmatrix} \dot{\varepsilon}_p \\ \dot{\varepsilon}_q \end{bmatrix} \tag{6.8}$$

- Yield surface (McDowell & Hau, 2003)

$$f = 0 = q_m^2 + \frac{M_f^2}{1-\chi_f}\left(\frac{p'_m}{p'_{0,m}}\right)^{\frac{2}{\chi_f}} {p'_{0,m}}^2 - \frac{M_f^2 {p'_m}^2}{1-\chi_f} \tag{6.9}$$

- Plastic potential (McDowell & Hau, 2003)

$$g = 0 = q_m^2 + \frac{M_g^2}{1-\chi_g}\left(\frac{p'_m}{p'_{g,m}}\right)^{\frac{2}{\chi_g}} {p'_{g,m}}^2 - \frac{M_g^2 {p'_m}^2}{1-\chi_g} \tag{6.10}$$

- Hardening law

$$\frac{\delta p'_{0,m}}{p'_{0,m}} = \frac{v}{\lambda-\kappa}\left(\delta\varepsilon_p^p + D\delta\varepsilon_q^p\right) \tag{6.11}$$

$$D = D_0 exp\left(-D_1\varepsilon_q^p\right) \tag{6.12}$$

Fibres

Linear elasticity is used for the stiffness of the big fibres (S_2 Figure 6.6) with Young's modulus E_f. A part from the constitutive parameters for the peat matrix and the fibres, the model also requires the definition of volumetric content for the two constituents. Differently from artificially reinforced soils with synthetic fibres, peat samples are naturally reinforced with different amount of fibres and with different characteristics as shown in Figure 6.1 and Figure 6.7. Fibre content, f, is often used as index to describe the fibrous composition of the peat even if it does not provide any description about the different fibrous networks present. The fibre content is defined is terms of mass of dry fibres over the dry mass of peat. If the specific density of the peat is defined with Gs_p and of the fibres with Gs_f and the dry density with $\rho_{d,p}$ and $\rho_{d,f}$, the volumetric fabric content needed in equation 6.7 can be approximately estimated by

$$\mu_f = f\frac{\rho_{d,p}}{\rho_{d,f}} \tag{6.13}$$

The units of μ_f are volume of fibres over total volume of peat sample. The expression for the peat matrix volumetric fraction reads

$$\theta_m = 1 - \mu_f \tag{6.14}$$

For the case of peats, it is rather difficult to define $\rho_{d,f}$. For the sake of simplicity, the specific density of the organic matter of peat is assumed to represent the one of the fibres, slightly lower than the $\rho_{d,p}$ depending on the amount of organic matter (Kazemian et al., 2011; Madaschi & Gajo, 2015b). The definition of the dry density of the fibres also requires to know their void ratio. In this case if the fibres section can be schematized as a circular ring, the ratio between the void and the total cross section can be used as representative of the section porosity assumed to be uniform with the fibres length.

6.3. MODEL RESULTS AND DISCUSSION

The results of the proposed model are reported for illustrative scope with reference to the natural sample 1-N (Figure 6.2). To facilitate the discussion about the potential advantages of modelling natural peat sample as a composite soil, a comparison with the traditional approach of modelling peat as a single soil component is offered in Figure 6.8 and Figure 6.9. The corresponding set of parameters for the two cases are reported in Table 6.2 and Table 6.3.

Table 6.2: Parameters used in the constitutive model for peat as single soil component

Sample	λ (-)	κ (-)	ν (-)	M_f (-)	M_g (-)	χ_f (-)	χ_g (-)	D_0 (-)	D_1 (-)	E_f (kPa)	μ_m (-)
1-N	2.0	0.3	0.1	1.5	2.2	3.0	15.0	3.0	15.0	-	1.0

Table 6.3: Parameter used in the constitutive model for peat as soil composite

Sample	λ (-)	κ (-)	ν (-)	M_f (-)	M_g (-)	χ_f (-)	χ_g (-)	D_0 (-)	D_1 (-)	E_f (kPa)	μ_m (-)
1-N	2.0	0.3	0.1	1.5	1.8	2.0	2.0	7.5	8.5	50.0	0.3

The results are presented in terms of stress path, deviatoric stress-strain, excess pore pressure and stress ratio. Normalised values are obtained dividing the current value with the mean effective stress at the beginning of shear, p'_0.

From a first comparison of Figure 6.8 and Figure 6.9, it seems that the advantage of modelling peat as a fibres reinforced material is modest. Both approaches seem to agree with the experimental data related to the deviatoric response and to the excess pore pressure. However, a closer comparison of the results and of the parameters in Table 6.2 and Table 6.3 allow to highlight some important differences. Firstly, to capture the observed behaviour with a classical single-component model, the critical stress ratio M_g had to be set equal to 2.3 which corresponds to a very high friction angle equal to φ'=56°. This value is well above the one used

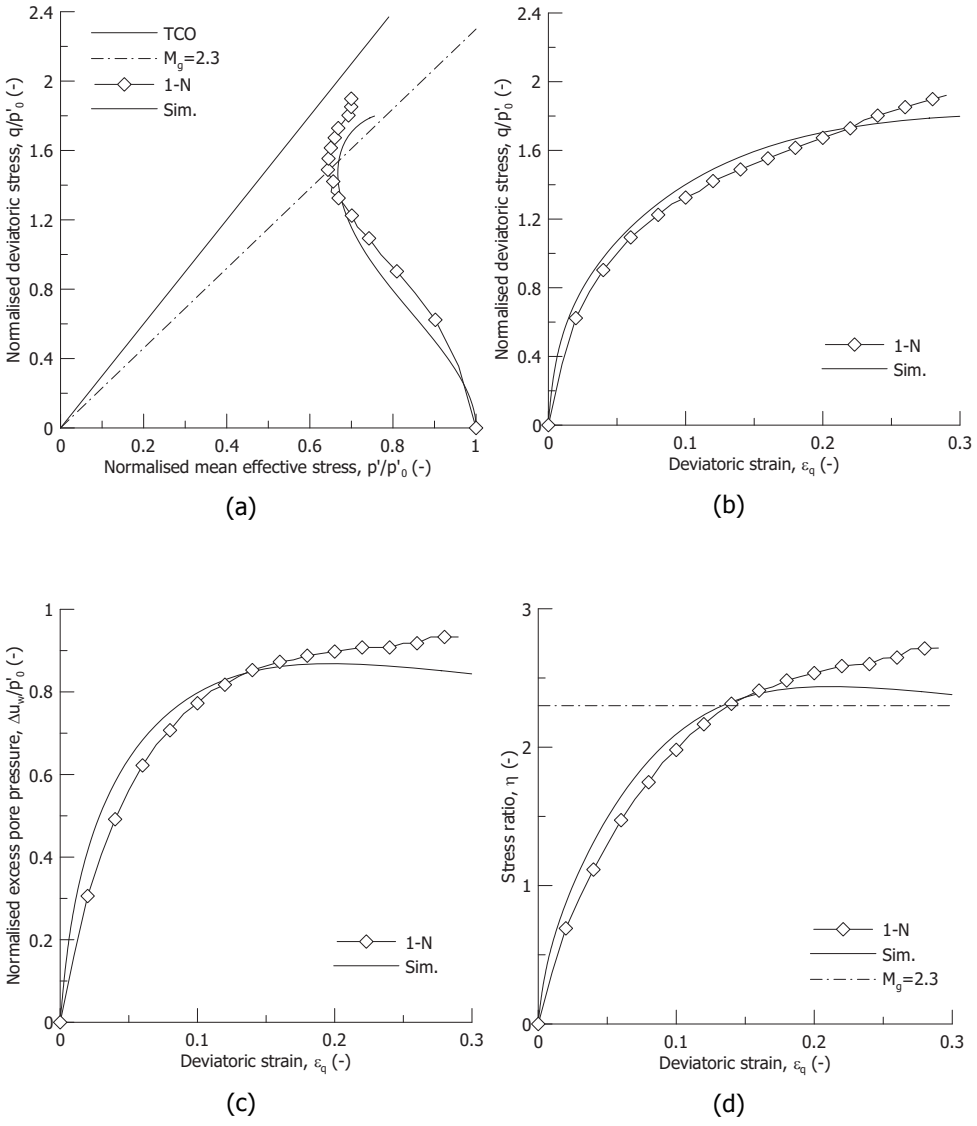

Figure 6.8: Comparison between the model results and the experimental data for sample 1-N as a single soil component: (a) stress path, (b) deviatoric stress-strain response, (c) excess pore pressure, and (d) stress ratio

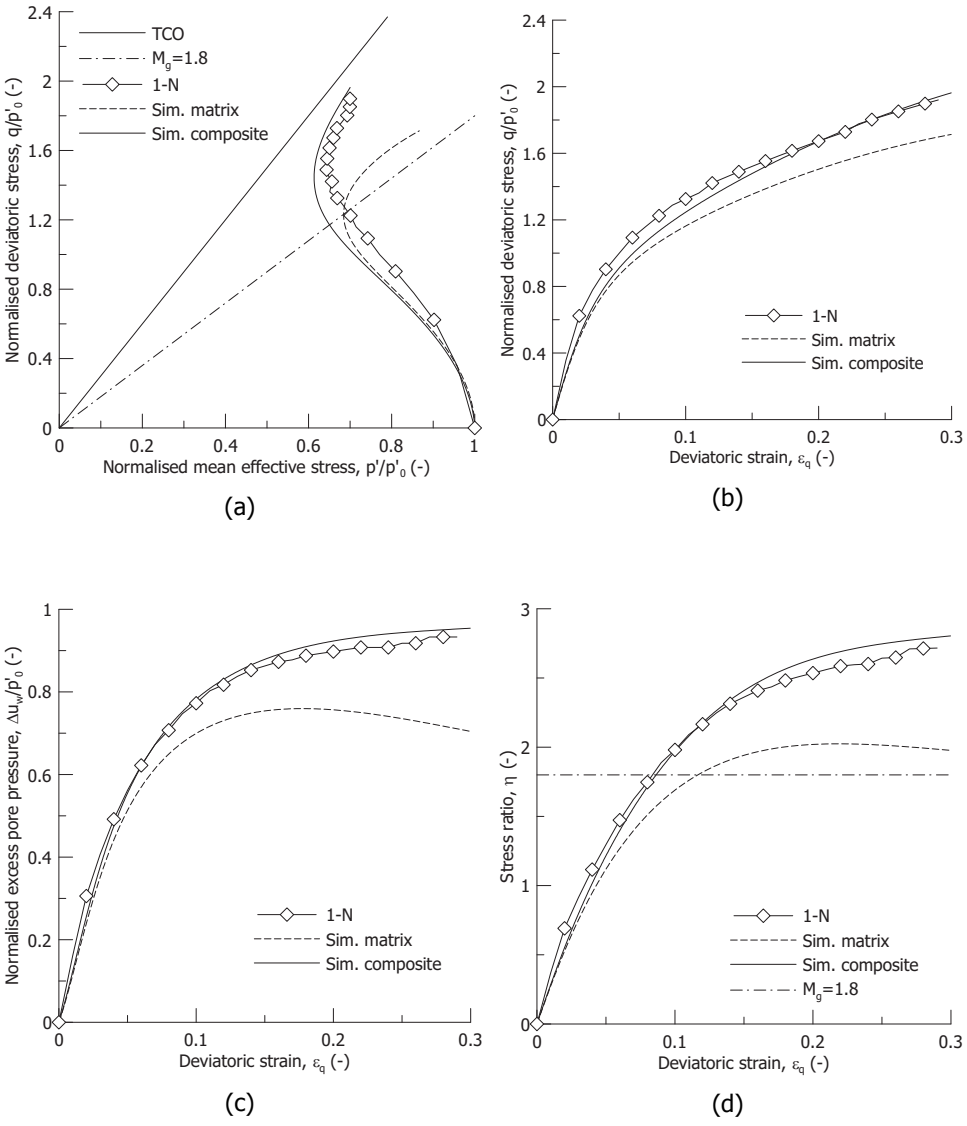

Figure 6.9: Comparison between the model results and the experimental data for sample 1-N as a soil composite: (a) stress path, (b) deviatoric stress-strain response, (c) excess pore pressure, and (d) stress ratio

in Table 6.3 for the composite model, M_g=1.8 which corresponds to 44°. More importantly, this value agrees with the friction angle determined from reconstituted samples sheared with modified end platens, φ'=43°, reported in Chapter 3. The proposed model predicts correctly the additional confinement of the fibres, which increases the observed shear strength without requiring to transfer the fibres effects into fictitious high shear strength parameters. As displayed in Figure 6.9(a) the matrix and the composite responses do not differ during the first part of the shear. With progressive radial expansion, the confinement provided by the fibres stretching contributes to decrease the mean effective stress and to increase the deviatoric stress for the composite. These two effects lead to a stress path asymptotically approaching the Tension Cut Off line (Figure 6.9(a)(d)). Even if less evident, improvements in the prediction of the excess pore pressure are also obtained with the adoption of the composite soil model. As displayed in Figure 6.8(c) the constitutive model for a single soil component predicts correctly the magnitude of the excess pore pressure but with a dilating response at high strain level which results from the adoption of a mixed volumetric and distortional hardening law. However, the experimental results show no decrease in the excess pore pressure in favour of a slight but still increasing trend. The composite confirms for the peat matrix a dilating response for deviatoric strains above 15%. However, accounting for the fibres stretching a counterbalancing contractive contribution is introduced and the composite behaviour observed experimentally is retrieved (Figure 6.9(c)). These two competing mechanisms hence govern the global response of the composite.

6.4. CONCLUSIONS

The influence of fibres on the hydro-mechanical response of natural peats has been matter of discussion for many decades. Despite the previous extensive experimental investigations which already showed the remarkable contribution of the fibres to the peat behaviour, still difficulties in modelling the experimental results are present. The deviatoric behaviour of natural peats tested in undrained triaxial compression is particularly challenging with peat samples exhibiting high excess pore pressure and very high deviatoric stress at the same time. Traditional constitutive models show evident difficulties in capturing this peculiar behaviour. The main limitation relies on assuming the observed behaviour as result of a unique soil component. In other words, no extensive attempts of modelling the peat response as result of soil matrix and fibres interaction have been reported so far. The present contribution represents an exploring attempt to model the deviatoric behaviour of natural peat samples by interpreting peat as a fibres-reinforced soil. The experimental background is firstly provided by comparing reconstituted and natural peat samples. The peat matrix for reconstituted sample contains small diffuse randomly distributed fibres, less than 3 mm long, while natural peat samples also contain big fibres, 1-3 cm long, with different preferential orientation. The experimental results clearly showed a matrix-fibres interaction mechanism which is strain level dependent. Up to deviatoric strains of about 5%–10% the deviatoric stress-strain response between normally consolidated reconstituted and natural samples did not differ significantly. With progressive axial compression and radial expansion, the

big fibres started to realign and to be stretched and the two responses began to diverge. While reconstituted samples approached failure with a gentle plateau in the deviatoric stress, the natural peat samples did not fail in favour of a strain-hardening response with progressive increase in the deviatoric stress and excess pore pressure. The resulting stress path approaches to the Tension Cut Off line with a continuous strain-hardening response.

Based on the experimental evidence, a simple constitutive approach within the framework of fibres-reinforced soils has been proposed. The behaviour of the peat matrix together with small diffuse fibres was described by a non-associative elastic-plastic model with a mixed volumetric and distortional hardening law. For the big fibres linear elasticity was adopted. The behaviour of the two components was eventually superimposed by a simple volumetric homogenisation procedure. With an illustrative perspective rather than with a predictive aim, the model capabilities have been compared with reference to the experimental results on natural peat samples. By taking into account the additional confinement offered by the fibres stretching it was possible assign to the peat matrix shear strength parameters considerably lower than the values reported for fibrous peat often considered "altered" by the fibres. The adopted value of friction angle used for the peat matrix, 44°, agrees with previous experimental results from reconstituted peat samples sheared with modified end platens. The observed stress path for natural samples asymptotically reaching the Tension Cut Off line was well reproduced by the superposition of the fibres effect, without the necessity of adopting fictitious high shear strength parameters. The comparison between the traditional single component model and the composite also shows the capabilities of the latter to reproduce the steady increase in the excess pore pressure measured experimentally for natural peats. The progressive tensile contribution of the fibres increases the confinement on the peat matrix and with an overall contractive response for the composite.

The results confirm the potentialities of a constitutive approach which interprets natural fibrous peats as fibres-reinforced soils. In particular such a model can help to overcome misconceptions on both shear strength and stress-strain response which still limit the possibility of using extensive experimental database from triaxial tests on natural peats. Having the possibility of using this vast database of experimental data for developing and validating advanced constitutive models for the deviatoric behaviour of peats represents a great step forward to model the behaviour of peats, even at the engineering scale.

LIST OF SYMBOLS

Gs	specific gravity
OC	organic content
e	void ratio
v	specific volume
λ	slope of the isotropic normal compression line
κ	slope of the isotropic unloading-reloading line
ν	Poisson's ratio
K	bulk modulus
G	shear modulus
σ'_a	axial effective stress
p'	mean effective stress
p'_c	preconsolidation mean effective stress
p'_0	mean effective stress at the beginning of shear
Δu_w	excess pore pressure
OCR	overconsolidation ratio
q	deviatoric stress
η	stress ratio
φ'	friction angle
ε_a	axial strain
ε_r	radial strain
ε_p	volumetric strain
ε_q	deviatoric strain
$\delta\varepsilon_p^p$	volumetric plastic strain increment
$\delta\varepsilon_q^p$	deviatoric plastic strain increment
ε_q^p	deviatoric plastic strain
a	pore pressure parameter
$\Delta p'$	change in the mean effective stress
Δq	change in the deviatoric stress
$\boldsymbol{\sigma'}_c$	effective stress tensor of the composite
$\boldsymbol{\sigma'}_m$	effective stress tensor of the soil matrix
$\boldsymbol{\sigma'}_f$	stress tensor of the fibres
$\boldsymbol{\varepsilon}$	strain tensor of the composite
$\boldsymbol{\varepsilon}_m$	strain tensor of the soil matrix
$\boldsymbol{\varepsilon}_f$	strain tensor of the fibres
$[\boldsymbol{M}_m]$	stiffness matrix of the soil matrix
$[\boldsymbol{M}_f]$	stiffness matrix of the fibres
μ_m	matrix volumetric content
μ_f	fibres volumetric content
f	fibre content
$\rho_{d,p}$	dry density of peat
$\rho_{d,f}$	dry density of fibres
M_f	stress ratio associated to the horizontal tangent of the yield locus
M_g	stress ratio at critical state

χ_f shape factor of the yield locus
χ_g shape factor of the plastic potential
D, D_0, D_1 coefficients of the distortional hardening

7

Experimental results on the influence of gas on the mechanical response of peats

If we knew what it was we were doing, it would not be called research, would it?

Albert Einstein

The content of this chapter has been published as research paper in Géotechnique. (Jommi et al., 2018).

7.1. ABSTRACT

Direct observation of gas in peat layers, generated by slow degradation in anoxic conditions, raised concern in the Netherlands about its potential impact on the geotechnical response of dykes founded on peat layers. To address this issue, an experimental investigation was initiated aimed at quantifying the main consequences of the presence of gas on the mechanical response of peats. The results of a series of triaxial tests on natural peat samples flushed with carbonated water are presented and discussed. Controlled amounts of gas were exsolved by undrained isotropic unloading, and the samples were sheared under undrained conditions. During gas exsolution, the samples suffered volumetric expansion, at a rate which is ruled by the relative compressibility of the fluid and the soil skeleton. The gas in the pore fluid dominates the stress-strain response upon undrained shearing, causing lower excess pore pressure compared to fully saturated samples. The experimental results suggest that local fabric changes occur during gas exsolution. However, for the amounts of gas investigated, these fabric changes seem to be almost reversible upon compression. Although the ultimate shear strength is hardly affected by gas, the reduction in the mobilised shear strength at given axial strain thresholds is dramatic, compared to fully saturated samples. The study suggests that the presence of gas must be cautiously accounted for at low stresses, when a reference stiffness is chosen for serviceability limit states, and when operative shear strength definitions, based on mobilised strength for given strain thresholds, are chosen in the assessment of geotechnical structures on peats.

7.2. INTRODUCTION AND MOTIVATION

Many flood defence embankments in the Netherlands have been built on peat layers (dykes on peat) or are made of peat (peat dykes). The assessment of these dykes is not straightforward, especially due to the lack of adequate geotechnical description of the behaviour of peats at the engineering scale. This often results in overly conservative assumptions, leading to high costs for maintenance and reinforcement. Several difficulties arise from the peculiar characteristics of this material, such as the exceptional high water content up to 800%-900% and the organic content reaching 80%-90%, multiple levels of fibrous structures and creep behaviour. Among these aspects, concerns on the stability and the serviceability of these dykes also arise from biodegradation of peat.

Oxidation of the organic fraction leads to significant modification of the soil skeleton compressibility, strength and retention capacity. In addition, the decomposition of organic matter produces gas species, typically CO_2 in aerobic environment and H_2S and CH_4 in deeper peat layers under anaerobic conditions. Dissolution of the available free gas and continuous degradation of the organic matter tend to saturate the pore fluid with gases. These are exsolved in the form of gas bubbles when their concentration exceeds the equilibrium solubility, because of atmospheric pressure changes, temperature oscillations, water table drop or total stress reduction (Dinel et al., 1988; Brown et al., 1989; Buttler et al., 1991). Previous research has addressed the role played by biogenic gas on buoyancy, retention, hydraulic conductivity, and volumetric expansion and contraction of peats, mostly from a hydrological perspective (Kellner et al., 2004, 2005; Waddington et al., 2009; Rosenberry et al., 2003; Tokida et al., 2005, 2007; Glaser et al., 2004; Strack et al., 2005). Only few contributions dealt with the possible geotechnical impact of gas in peats on the structural response of dykes or railway embankments (Vonk et al., 1994; Den Haan & Kruse, 2007; Acharya et al., 2016a,b). However, all these contributions just highlighted that local overpressure may occur due to gas pockets, but none of them included a systematic study on the consequences of gas entrapment on the mechanical behaviour of peats.

The effects of entrapped gas have been studied extensively in the past for marine sands and clays (Rad et al., 1994; Grozic et al., 1999, 2000; Amaratunga & Grozic, 2009; Nageswaran, 1983; Wheeler, 1988b; Hight & Leroueil, 2003; Sultan et al., 2007, 2012). In the case of sands, the predominant effect of gas is to increase the pore fluid compressibility, which affects the pore pressure development during shear, in turn increasing or decreasing the ultimate shear strength depending on the relative density of the sand (Rad et al., 1994; Grozic et al., 1999, 2000). More controversial results were found on clays, because of the role played by two competing mechanisms, depending on the combination of total stress and water pressure. On the one hand, the reduction in the fluid stiffness increases the mean effective stress and has a positive influence on the attainable undrained shear strength (Wheeler, 1988b; Grozic et al., 2005). However, the increase in the gas pressure during exsolution may damage the pore structure, and the formation of large gas filled pores eventually has a negative impact on the available shear strength (Nageswaran, 1983; Hight & Leroueil, 2003; Sultan et al., 2012).

Attention was raised on the influence of biogenic gas on the geotechnical response of flood defences in the Netherlands during a thorough field study of dykes founded on peat, where gas release was regularly observed (Zwanenburg, 2013). As the lack of systematic studies on the mechanical response of gassy peats increases the knowledge uncertainties on the short-term performance and the long-term durability of the embankments, an experimental investigation was initiated at TU Delft to start filling the knowledge gap (Jommi et al., 2017). To isolate the mechanical effects of gas on the soil skeleton from the direct consequences of biodegradation of the material, a series of triaxial compression tests has been performed on intact peat samples artificially charged with a controlled amount of gas. Some of the implications of the presence of gas in peat are discussed from the results of the triaxial compression tests, where attention has been given to the impact of gas on both volumetric and deviatoric response. The testing programme was designed to provide an answer to the following questions. How will the pore fluid pressure and the average stress acting on the soil skeleton be affected by the generation of gas? Is the amount of exsolved and entrapped gas dependent on the soil skeleton properties and on the external confinement? Will the gas volume and pressure affect the fabric of peat and will the modification be irreversible in this case? Will the deviatoric response be affected by gas, and will ultimate shear strength depend on the amount of gas?

7.3. EXPERIMENTAL PROGRAMME

7.3.1. Material

The experimental study has been conducted on undisturbed peat specimens sampled between 1.0 and 2.5 m depth from the ground level in the subsoil of the Markermeer dykes at Katwoude in the Netherlands (De Vries & De Bruijn, 2014). The soil profile is made of a 0.7-1 m thick silty clay cover above a peat layer with a variable thickness of 2-3 m, where the samples were retrieved. The water table is located 0.25 m below the ground level. The in situ effective vertical stress of the peat layer is around 10 kPa, typical of surficial peat layers in the Netherlands. After sampling, the material was stored in a climate controlled room at 10°C and 90% relative humidity to prevent oxidation of the organic matter. The water content was determined by oven drying at 60°C to avoid loss of organic mass (Head, 2014). The specific gravity of the soil, Gs, was measured with a helium pycnometer in accordance to D5550-14 (2014) and the organic content was assessed by ignition at 500°C (D2974-14, 2014; Den Haan & Kruse, 2007). Table 7.1 reports the index properties of the tested samples. Three tests assessing loss of ignition (N) following the standard D2974-14 (2014) gave an average organic content OC of 85.7% based on equation 7.1 (Skempton & Petley, 1970)

$$1 - OC = 1.04(1 - N) \tag{7.1}$$

The data reported in Table 7.1 show that the soil in the field is not completely saturated and that, on average, the lower the degree of decomposition (smaller values of specific gravity) the lower the in situ degree of saturation.

Table 7.1: Index properties of the tested specimens

Sample	z (ground) (m)	γ (kN/m^3)	Gs (-)	e_0 (-)	w_0 (-)	Sr (-)
Test 1	1.1-1.3	9.90	1.48	9.59	6.50	1.00
Test 2	1.1-1.3	10.1	1.47	9.21	6.20	0.99
Test 3	1.6-1.8	11.0	1.37	12.04	7.35	0.84
Test 4	1.7-1.9	10.4	1.40	9.89	6.63	0.94
Test 5	2.3-2.5	10.2	1.45	10.03	6.38	0.92
Test 6	1.7-1.9	10.4	1.43	10.78	6.53	0.87

7.3.2. Experimental set-up and procedure

A series of triaxial tests was carried out on samples 100 mm in height and 50 mm in diameter. A load frame type GDS triaxial system with standard back pressure and cell pressure volume controllers and a submersible 1 kN load cell was used (Figure 7.1). accuracy of the controllers is ±1 kPa on pressure and ±300 mm^3 on volume (0.15% FSR). Calibration of the system included the cell deformation during loading and unloading at the pressures used in the tests, using a steel sample replica. The calibration was essential to allow using the variations in volume recorded by the cell pressure volume controller, together with the volume change due to the piston displacement, to compute the volumetric strain of the sample, ε_p, during the undrained unloading (gas exsolution and expansion) and during the next shearing stage (gas compression and dissolution).

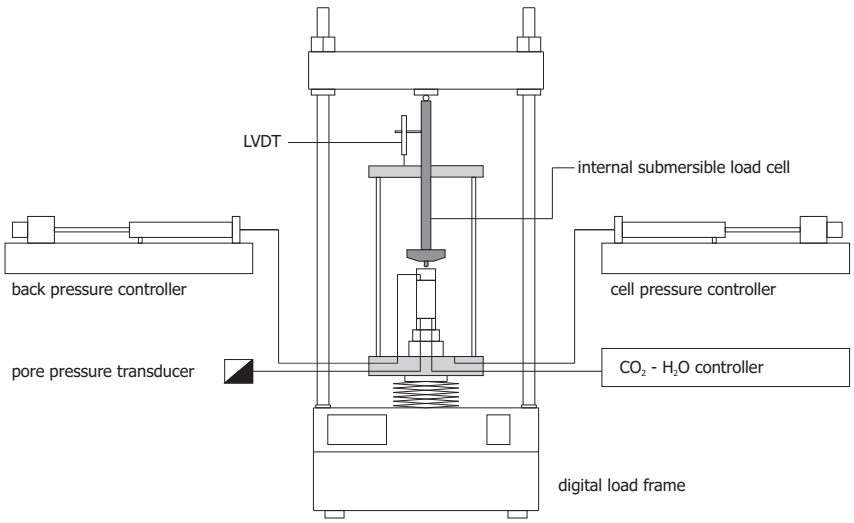

Figure 7.1: Triaxial testing system including the pressure/volume controllers and the carbonated water flushing system

All the tests were performed in a controlled environment, at temperature T=13°C

and relative humidity RH=68%. Carbonated water was prepared before each test in a Perspex cell, where CO_2 dissolution in de-aired water at a target pressure of 380 kPa was allowed for about 60 hours at 22°C (Van Der Putte, 2014). To generate a controlled amount of gas in the peat samples, the protocol suggested by Lunne et al. (2001), Amaratunga & Grozic (2009) and Sultan et al. (2012) was followed. After mounting in the triaxial apparatus, the samples were loaded isotropically to a cell pressure of about 400 kPa under undrained conditions, to dissolve the natural gas and air bubbles in the peat samples. Afterward, the pore water was replaced with carbonated water, by flushing the samples from a third pressure controller connected to the pedestal (Figure 7.1). A total volume of about 1.3 times the initial volume of voids was injected, under a small pressure difference of 2-4 kPa between the bottom and the top cap. Flushing was performed under a total isotropic stress between 400 and 420 kPa, while the effective confining mean stress ranged between 5-15 kPa. Before exsolving the gas previously injected in the samples, the effective stress was increased with a first short isotropic consolidation stage. Gas exsolution was triggered by decreasing the isotropic confining pressure under external undrained conditions. A second isotropic consolidation stage was performed on the gassy samples in order to re-adjust the confining stress to the target value after the gas exsolution, before the start of shearing. Undrained shearing was performed at controlled axial displacement rate of 0.02 mm/min, to replicate the one adopted in a previous extensive experimental study on saturated samples of peat coming from the same Markermeer area (De Vries & De Bruijn, 2014). As the behaviour of peat is rate sensitive, the same displacement rate was chosen to minimise the differences in the stress-strain response coming from rate dependency, and to allow isolating and evaluating the role played by the gas. However, in Test 6, stress controlled shearing was chosen to check the controllability of the mechanical response, which implied a variable strain rate, on average about five times higher than that experienced by the other samples. To limit gas diffusion towards the cell fluid, two latex membranes 0.25 mm thick with an intermediate grease layer in between were used. The choice seems to be substantiated by the results on sample 6, which was sheared five times faster than the others, though experiencing comparable volumetric strain. A reference test was performed on a sample fully saturated with demineralised de-aired water (Test 1). A second reference sample was tested after flushing with demineralised water saturated with nitrogen N_2 (Test 2). Flushing with N_2 charged water, allowed removing the small amount of oxygen that can remain in water even after de-airing process with a standard pump, and provides an alternative convenient reference for saturated conditions. Flushing was performed also on the saturated samples to minimise the differences in fabric changes between different samples, which could be due just to the saturation procedure. In Table 7.2, Table 7.3 and Table 7.4 the cell pressure (σ_c), the back pressure (u_b) and the pore fluid pressure measured at the bottom of the sample (u_f) are reported for each sample, for the different stages of the tests, until the start of shearing. It is worthwhile noting that the mean effective stress in the field can be estimated to be around 7 kPa. The confining stresses attained in the triaxial apparatus were slightly higher, to improve the accuracy of the results, still being

representative of the site conditions.

Table 7.2: Measured stress variables for Test 1 and Test 2 performed on saturated specimens (the values refer to the end of the steps unless otherwise specified)

	Test 1 H_2O			Test 2 N_2		
Stage	σ_c	u_b (kPa)	u_f	σ_c	u_b (kPa)	u_f
Flushing	421	407	411	407	397	398
1st consolidation	420	405	406	426	403	404
Undrained unloading	53	-	38	51	-	30
Undrained shear (start)	51	-	38	52	-	31

Table 7.3: Measured stress variables for Test 3 and 4 performed on gassy specimens (the values refer to the end of the steps unless otherwise specified)

	Test 3 CO_2			Test 4 CO_2		
Stage	σ_c	u_b (kPa)	u_f	σ_c	u_b (kPa)	u_f
Flushing	407	402	404	408	402	403
1st consolidation	404	383	383	406	382	382
Undrained unloading	51	-	49	63	-	58
2nd consolidation	68	50	51	79	55	55
Undrained shear (start)	69	-	50	80	-	53

7.4. EXPERIMENTAL RESULTS

Reporting and interpreting the stress-strain response of gassy peat samples requires a choice on the most convenient stress variables to describe the results. The choice is not straightforward as the samples may experience different states during the triaxial tests. At the start of the test, the peat is saturated with an almost incompressible fluid. Gas starts to be exsolved in the form of small bubbles, which are still surrounded by water. In these first two states, the measured pore pressure is the water pressure, and the solid skeleton response is likely to depend on the traditional effective stress, defined as the difference between the total stress and the water pressure. At increasing volume, the gas starts acting directly on the solid skeleton, and the mechanical response of the soil samples will start depending on both gas and water pressures. The latter state calls for a description of the soil state accounting explicitly for the volume fraction of gas and for the unsaturated state of the soil. Different choices could be equally made in the latter case, mostly depending on the available experimental information (Gens, 1996).

In previous investigations on gassy soils, the difference between total stress and water pressure has been used for any gas volume fraction. However, concern has been raised about the extension of the effective stress principle to the gassy state, which motivated naming "operative stress" the adopted stress variable (Sills et al.,

Table 7.4: Measured stress variables for Test 5 and 6 performed on gassy specimens (the values refer to the end of the steps unless otherwise specified)

	Test 5 CO_2			Test 6 CO_2		
Stage	σ_c	u_b (kPa)	u_f	σ_c	u_b (kPa)	u_f
Flushing	409	402	403	410	405	406
1st consolidation	408	387	387	409	383	384
Undrained unloading	52	-	50	65	-	64
2nd consolidation	70	50	51	98	*-	87
Undrained shear (start)	71	-	48	100	-	88

* For Test 6, the 2nd consolidation stage was substituted with a compression at closed drainage

1991; Sills & Gonzalez, 2001). In this work, it was assumed that the pressure measured at the bottom transducer is the average fluid pressure acting on the soil skeleton, and that the difference between the total stress and the measured pressure can be conveniently adopted to describe the relevant characteristics of the soil mechanical response. However, it is not proven that this difference can be identified with an effective stress, which alone would rule entirely the soil response (Jommi, 2000). For this reason, the definition "operative stress" is maintained in the presentation of the results. Accordingly, the mean operative stress is defined as

$$p'' = p - u_f = \frac{\sigma_a'' + 2\sigma_r''}{3} \tag{7.2}$$

where p is the total mean stress and σ_a'' and σ_r'' are the operative axial and radial stresses computed as difference between the axial and radial total stresses and the measured pore fluid pressure, u_f. In equation 7.2 the double apostrophe " is used to mark the conceptual difference between effective and operative stress for gassy soils (Sills et al., 1991).

7.4.1. Isotropic undrained unloading

The experimental results during the isotropic undrained unloading stage are reported in Figure 7.2. Normalised cell pressure was obtained by dividing the current cell pressure with the correspondent value at the start of unloading, $\sigma_{c0,u}$. Reduction of the cell pressure to about 50 kPa (Table 7.2,Table 7.3 and Table 7.4) was conducted in 2 hours for Test 1, Test 2 and Test 6, 4 hours for Test 4 and 5, while a slower step-by-step procedure was adopted in Test 3.

Based on the volumetric strains recorded in the tested gassy samples at the end of the unloading, the gas content attained a volumetric fraction between 4% and 16% of the initial sample volume. These values replicated the average gas volumetric fraction often encountered in peat layers (Landva & Pheeney, 1980; Reynolds et al., 1992; Beckwith & Baird, 2001; Baird & Waldron, 2003). As expected, fully saturated samples, Test 1 and Test 2, experienced null volumetric strains. The

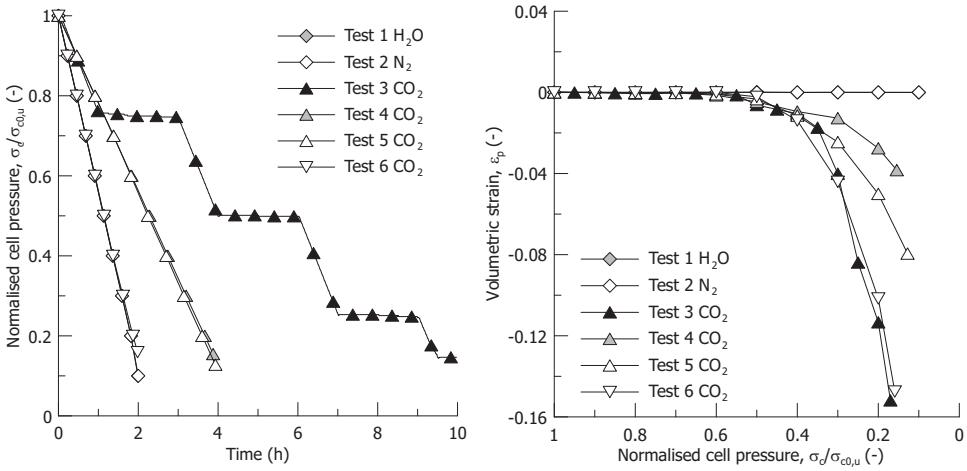

(a) (b)

Figure 7.2: Undrained unloading stage: (a) normalised cell pressure time sequence, (b) volumetric strains

rate at which the pore fluid pressure decreases during unloading is ruled by gas exsolution and expansion (Sobkowicz & Morgenstern, 1984), which are expected to start when the pore fluid pressure drops below the initial gas-liquid saturation pressure, $u_{l/g,0}$. The detail of the evolution of the measured pore fluid pressure during the isotropic undrained unloading is reported in Figure 7.3. Normalised pore fluid pressure was obtained by dividing the current pore fluid pressure with the correspondent value at the start of unloading, $u_{f0,u}$.

For an initial portion of the unloading stage in Figure 7.3, the pore fluid pressure for the gassy samples decreased as much as for the saturated samples. A closer examination of Figure 7.2(b) reveals that non-null volumetric strains started being observed only when the cell pressure reached a pressure of about 60% of the initial value (see Table 7.5). Starting from this point, the pore fluid pressure in the gassy samples remained higher than that in the saturated samples. For all the gassy samples, the pore fluid pressure corresponding to the onset of the gas exsolution, reported in Table 7.5, was below the initial gas-liquid saturation pressure, $u_{l/g,0}$, at which the carbonated water solution had been prepared. The main reason for this discrepancy can be ascribed to the different temperatures at which the water was saturated with gas (22° C) and the temperature of the room where the triaxial tests were run (13°C).

According to Henry's law, the gas solute mole fraction, χ, in the aqueous phase is proportional to the absolute gas pressure, u_g, through Henry's coefficient H^{xp} (Pa^{-1})

$$H^{xp} = \frac{\chi}{u_g} \tag{7.3}$$

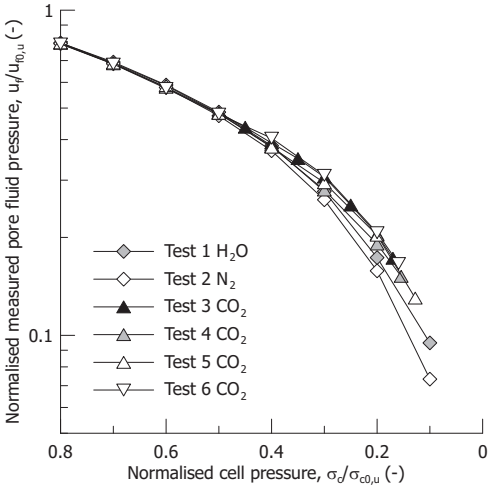

Figure 7.3: Evolution of the measured pore fluid pressure during undrained unloading

Table 7.5: Imposed gas-liquid saturation pressure, cell pressure and pore fluid pressure at the onset of gas exsolution

Test	$u_{l/g,0}$ (kPa)	σ_c (kPa)	u_f (kPa)
Test 3 CO_2	380	250	232
Test 4 CO_2	380	270	247
Test 5 CO_2	380	241	222
Test 6 CO_2	380	235	211

The dependence of Henry's coefficient on temperature is taken into account with the Van't Hoff's equation (Atkins & De Paula, 2014; Sander, 2015):

$$H^{xp}(T) = \frac{M_{H_2O}}{\rho_{H_2O}} H^{cp*} exp\left(\frac{-\Delta_{sol}H}{R}\left(\frac{1}{T} - \frac{1}{T^*}\right)\right) \tag{7.4}$$

where H^{cp*} is the Henry's coefficient (via concentration) at the reference temperature (T^*=298.15 K), equal to 3.3×10^{-4} mol/(m^{3}Pa), and M_{H_2O} is the molar mass of water and ρ_{H_2O} is its temperature dependent density. The term $\Delta_{sol}H$ is referred to as enthalpy of dissolution (Atkins & De Paula, 2014) and depends on the gas species, while R is the gas constant. The solubility in water of N_2, dry air and CO_2 are reported in Table 7.6 for the temperatures of interest, namely 22°C and 13°C. The dependence of CO_2 Henry's coefficient on temperature gives that the dissolved concentration at 22°C and relative pressure of 380 kPa corresponds to a relative liquid-gas saturation pressure $u_{l/g,13°}$=271 kPa at 13°C, at which the triaxial tests were performed. This change in the liquid-gas saturation pressure may account for most of the difference between the pressure at which the gas was dissolved into the water and the pressure at which it started exsolving during the undrained unloading.

Table 7.6: Molar solubility of relevant gases at different temperatures

Gas species	H^{cp} at 22°C (mol/(m^{3}Pa))	H^{cp} at 13°C (mol/(m^{3}Pa))
N_2	6.7×10^{-6}	7.7×10^{-6}
Air	9.2×10^{-6}	1.1×10^{-5}
CO_2	3.6×10^{-4}	4.6×10^{-4}

However, similar delay in gas exsolution was also observed on a soft marine clay (Sultan et al., 2012), although no difference in temperature was reported. Further influence on the gas exsolution pressure might have come from the presence of a small amount of air during the saturation of water with CO_2, which reduced the dissolved CO_2 fraction (Mori et al., 1977), or from the change in the pH of water when flushed into the organic soil material (Appelo & Postma, 2005).

7.4.2. Undrained shearing stage

The results of the shearing stage performed under undrained conditions are reported in terms of stress path in Figure 7.4(a), and excess pore fluid pressure, Δu_f in Figure 7.4(b). The symbols in the plots correspond to axial strain increments of 2%. Test 1 and Test 6 have an initial overconsolidation ratio, OCR, equal to 1.3 and 2.2, defined as

$$OCR = \frac{p''_{max}}{p''_{0,s}} \tag{7.5}$$

where p''_{max} is the maximum mean operative stress applied to the sample during the loading history and $p''_{0,s}$ is the mean operative stress at the beginning of the shearing stage.

As expected, the presence of free gas in the samples increases the pore fluid compressibility upon axial compression, promoting lower excess pore fluid pressure in comparison with fully saturated samples (Figure 7.4(b)) and non-null volumetric strain despite the external undrained conditions. The initial vertical traits in the stress paths in Figure 7.4(a) of the gassy samples resemble an initial elastic path. With further compression and dissolution of the free gas, the pore pressure rate increases, until the stress paths eventually become parallel to those of the saturated samples. Negligible consequences seem to be caused by the presence of gas on the ultimate shear strength of the peat, which occurred with a diffuse failure mode for all the samples, at an axial strain around 30%.

7.5. FABRIC EVIDENCE

To support the interpretation of the experimental results, a fabric investigation was performed, including micro-CT scans and polarisation microscope micrographs. Two CT-scans were performed on the same sample, the first one in the natural undisturbed state and the second one after gas exsolution. The comparison reported in Figure 7.5 reveals that gas exsolution results in the formation of

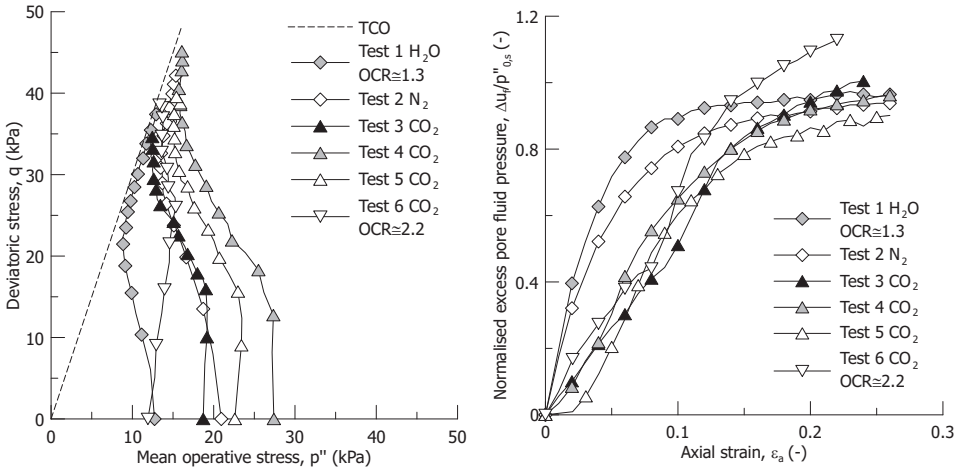

Figure 7.4: Undrained shearing stage for fully saturated and gassy samples: (a) stress path, (b) excess pore fluid pressure plotted against axial strain

new pores, with characteristic size of 1-2 mm, which are generated by gas expansion in undrained conditions. These are represented by the black spots in the micrographs, while denser elements have brighter appearance. Similar gas bubble radii were observed by Den Haan & Kruse (2007), Kettridge & Binley (2008) and Rezanezhad et al. (2010).

Due the low difference between the density of solids and that of the surrounding pore fluid, micro-CT scans do not allow to visualise in detail the fabric of wet peat, which could be revealed only after significant drying. To overcome this limitation and identify relevant fabric features of the wet peat, a companion sample was observed with a polarisation microscope equipped with a digital microscope camera. The peat fabric in Figure 7.6 appears to be organised in organic peds, made of organic components such as leaves, roots and stems, and some inorganic particles such as sand grains (white spots in Figure 7.5 and Figure 7.6). Fibres having different orientation and curvature crossing the organic peds are also evident in Figure 7.6. The visible pores in Figure 7.6 have a typical size in the range 0.1-2 mm, and they can be ascribed to the inter-particle (inter-peds) peat macro-porosity, which dominates the pore fluid response (Rezanezhad et al., 2016).

7.6. DISCUSSION

7.6.1. Pore fluid response during gas exsolution

There is clear evidence that the pore pressure evolution in a gassy soil depends both on the gas-liquid equilibrium and on the mechanical response of the soil skeleton, due to the coupled response being dominated by the relative stiffness of the pore fluid and the soil skeleton. A description of the gas exsolution pro-

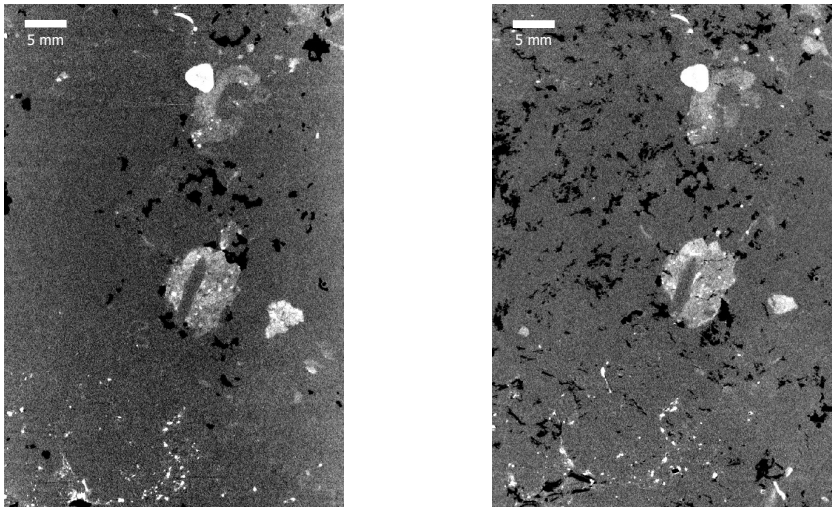

(a) (b)

Figure 7.5: Micro-CT scan of a gassy sample: (a) before gas exsolution, (b) after gas exsolution by undrained unloading (black spots correspond to gas filled pores)

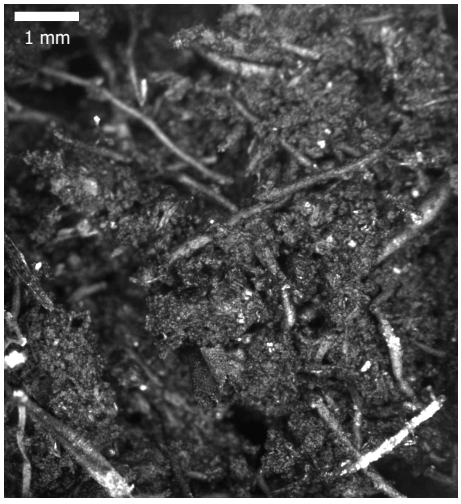

Figure 7.6: Micrograph of the tested peat fabric from polarised microscopy

cess is provided by analysing the time evolution of the cell pressure, σ_c, and pore fluid pressure, u_f, reported in Figure 7.7(a), Figure 7.8(a) and Figure 7.9(a). The corresponding time dependent mean operative stress and degree of saturation are displayed in the parallel series of figures (b).

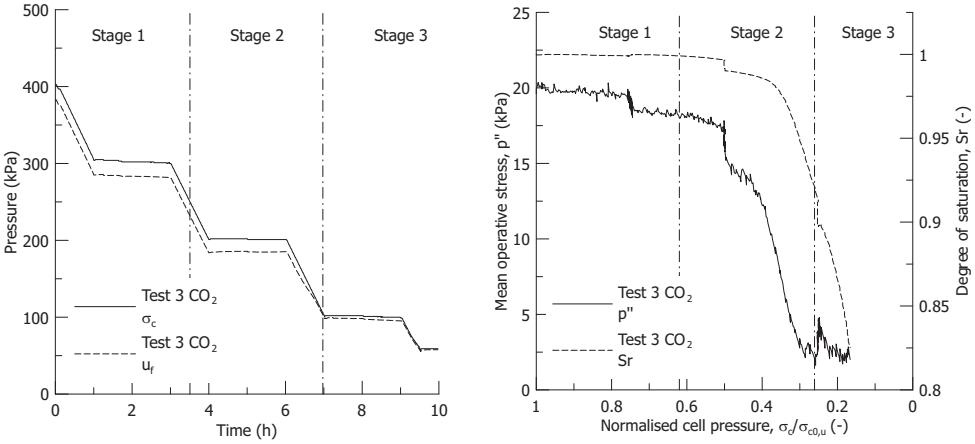

(a) (b)

Figure 7.7: Test 3 CO_2: (a) cell pressure and pore fluid pressure evolution, (b) mean operative stress and degree of saturation evolution during undrained unloading

A sequence of three stages can be clearly identified, namely:

- stage 1 $\dot{u}_f \approx \dot{\sigma}_c$, $\dot{p}'' \approx 0$ and $\dot{Sr} \approx 0$
- stage 2 $\dot{u}_f \ll \dot{\sigma}_c$, $\dot{p}'' \ll 0$ and $\dot{Sr} < 0$
- stage 3 $\dot{u}_f \approx \dot{\sigma}_c$, $\dot{p}'' \approx 0$ and $\dot{Sr} \ll 0$

During stage 1, the measured pore fluid pressure decreases commensurately with the cell pressure, almost no gas exsolution takes place, and the mean operative stress keeps nearly constant. Gas exsolution starts when the pore fluid pressure reaches values in the range 245-210 kPa, depending on the test (see Table 7.5), which increases the compressibility of the pore fluid. As a result, the total stress reduction is mainly transferred onto the soil skeleton, with a relevant decrease in the mean operative stress. In the final stage 3, the mean operative stress shows very small variation and keeps close to zero (Figure 7.7(b), Figure 7.8(b) and Figure 7.9(b)). The compressibility of the soil skeleton is largely increased and significant gas exsolution and expansion occur. The corresponding change in the ratio between the compressibility of the pore fluid and that of the soil skeleton is reflected in Figure 7.10 in terms of pore pressure parameter B (Skempton, 1954) for the case of Test 5 and Test 6.

During stage 1, the parameter B remains close to 1, as for the case of fully saturated sample. After the onset of the gas exsolution and expansion, during

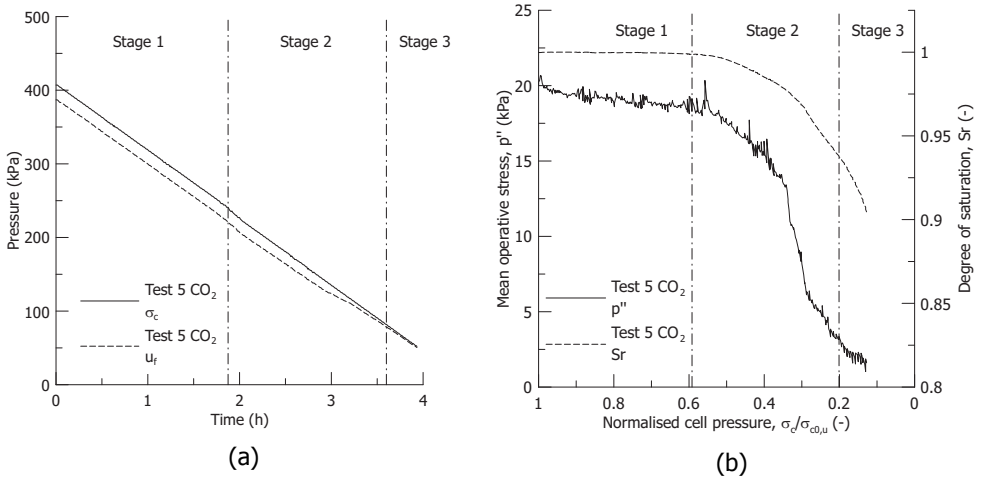

Figure 7.8: Test 5 CO_2: (a) cell pressure and pore fluid pressure evolution, (b) mean operative stress and degree of saturation evolution during undrained unloading

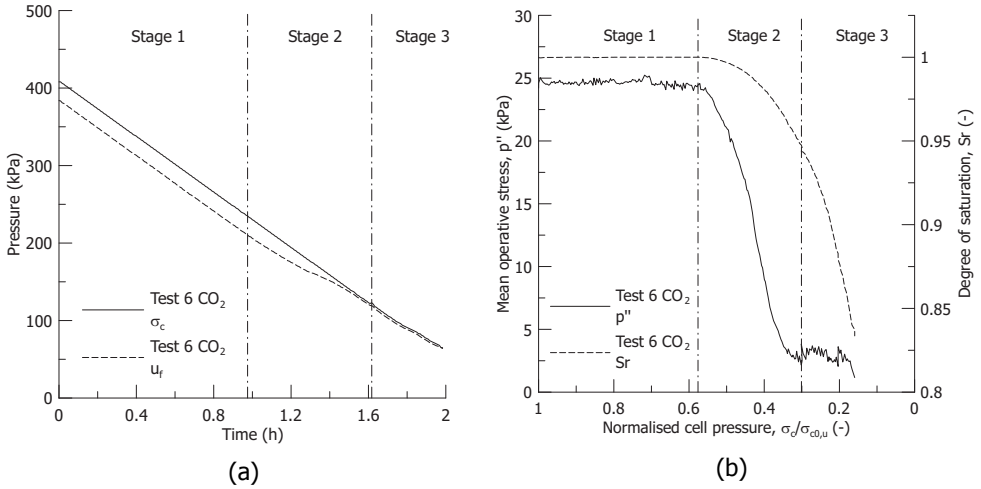

Figure 7.9: Test 6 CO_2: (a) cell pressure and pore fluid pressure evolution, (b) mean operative stress and degree of saturation evolution during undrained unloading

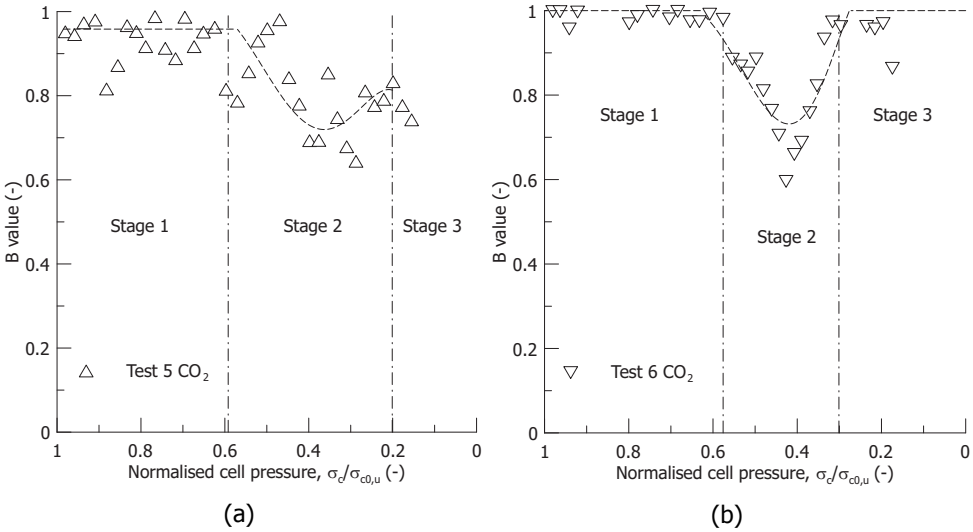

Figure 7.10: Evolution of the B value during undrained unloading for two gassy samples: (a) Test 5 and (b) Test 6

stage 2, the compressibility of the pore fluid increases and the B value decreases. The pore pressure parameter B starts increasing again, when a significant reduction in the mean operative stress occurs, which increases the compressibility of the soil skeleton.

7

7.6.2. Confining effects on gas exsolution and expansion

A description of the relative volume occupied by the gas bubbles within the porous space can be attempted making reference to the characteristics of the peat fabric visualised in Figure 7.5 and Figure 7.6, and using the simple schemes in Figure 7.11.

The sketched porous structure refers to the scale of the interparticles voids, where carbonated water replaced the natural water. For the sake of clarity, only the data from Test 6 are plotted. At the onset of gas exsolution, the bubbles can start growing in the pore space without interacting with the organic peds (isolated gas bubbles, sub-stage 2A in Figure 7.11). As long as the gas bubbles remain confined in the pore space, the response is typically that of a porous medium saturated with a compressible pore fluid. Over further unloading, the gas bubbles expand and coalesce, and they start interacting with the surrounding soil skeleton. The gas pressure starts acting directly on the organic peds in localized contact zones (sub-stage 2B in Figure 7.11), and full three phases interaction takes place between organic peds, pore fluid and gas bubbles (Wheeler, 1988a). Pores enlargement occurs, eventually reducing the contact forces between the soil particles. The transition between these two sub-stages occurs with a remarkable decrease in the mean operative stress, which is highlighted by a dramatic increase in the ratio $\Delta p''/\Delta\sigma_c$.

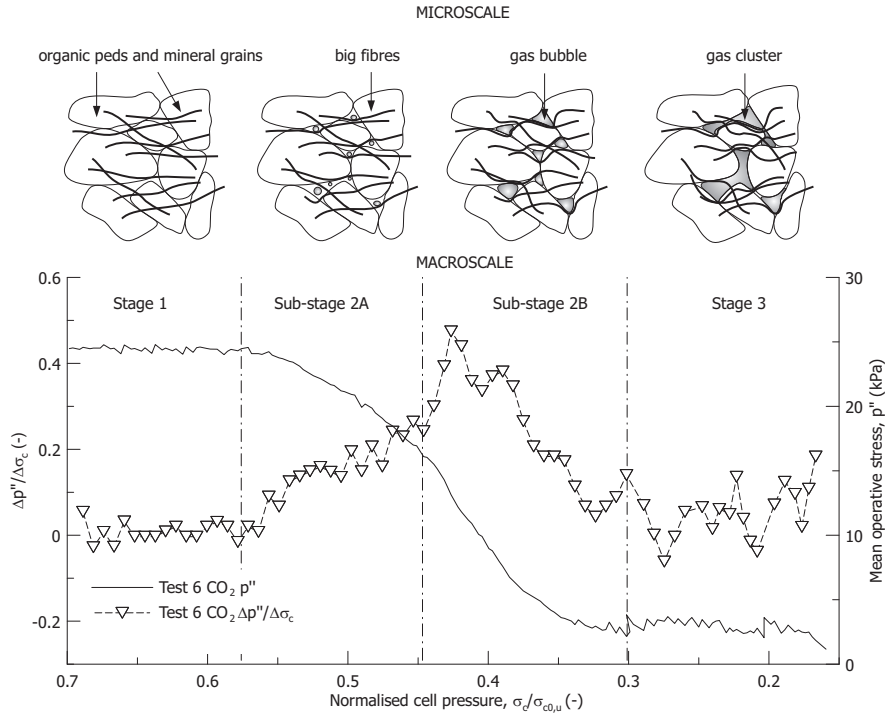

Figure 7.11: Interpretation at the micro–macro scale of the gas exsolution process

With a progressive reduction in the confining stress, gas exsolution and expansion bring to a rearrangement of the soil fabric (stage 3 in Figure 7.11), with gas bubbles locally interconnected in form of preferential cluster structures, as shown by Kettridge & Binley (2008) and by Rezanezhad et al. (2010) on different peat samples. The dependence of the volumetric strains on the confining stress can be appreciated with reference to Figure 7.12, where the results of all the tests on gassy samples are reported as a function of the current mean operative stress normalised with the value recorded at the beginning of unloading, $p''_{0,u}$.

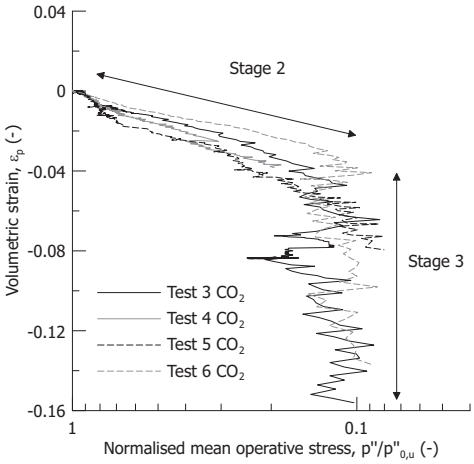

Figure 7.12: Volumetric strains plotted against the mean operative stress during undrained unloading for the gassy samples

Over stage 2, the volumetric strains are almost linearly dependent on the logarithm of the mean operative stress. At the end of this stage, the recorded volumetric strains range between 4%-6% for a relatively high change in the operative stress. The majority of free gas is generated only during stage 3, under nearly constant mean operative stress, when previous gas exsolution and expansion have softened the soil fabric. Possible local softening of the soil fabric was suggested during these tests by the observation of gas pockets developing at the boundaries of the samples during the last part of unloading. These were interpreted as the result of local expansion, which allowed preferential gas flow paths towards the external part of the samples (Jommi et al., 2017).

7.6.3. Deviatoric behaviour

The deviatoric response of fibrous peats is dominated by the fibres network. It is generally accepted that in a standard undrained triaxial tests the fibres tend to align horizontally, and provide an internal additional confinement to the sample, which is responsible for very high ultimate strength. The stress-strain curves for the saturated samples (Figure 7.13(a)) show continuously increasing deviatoric stress in the strain range investigated, as typically found on fibrous peats

(Oikawa & Miyakawa, 1980; Cola & Cortellazzo, 2005; Hendry et al., 2012). This feature complicates the definition of a failure criterion for the investigated material, because an asymptotic value for the deviatoric stress is not found, and the stress path approaches the Tension Cut Off (TCO) line (Figure 7.4(a)).

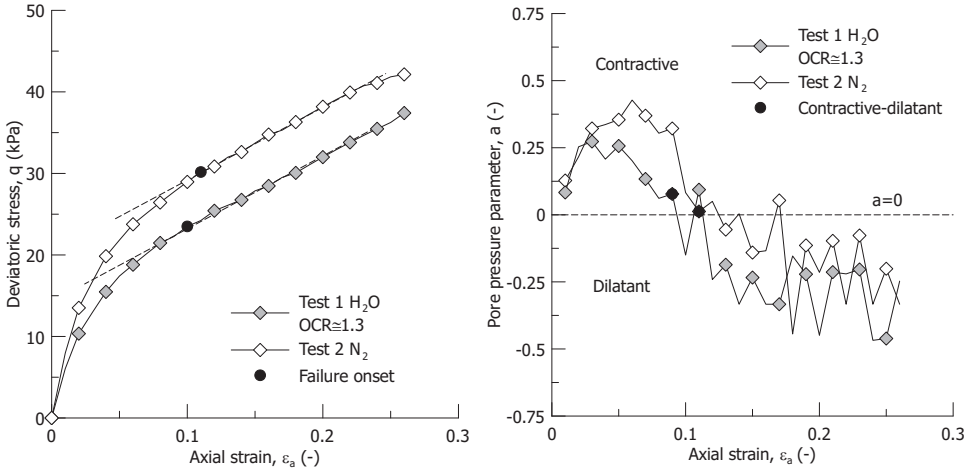

Figure 7.13: Failure onset on the deviatoric stress-strain response (a) and (b) evolution of the pore pressure parameter a for fully saturated samples during undrained shear

Among different possible choices, in this study failure is assumed to be triggered in correspondence of the start of the linear hardening portion of the q-ε_a stress-strain curve (Kanmuri et al., 1998). The rationale behind this choice is that this criterion corresponds to the transition between contractive and dilatant behaviour, which identifies the critical state for the peat matrix if the radial stretching effect of fibres is neglected. The transition between contractive and dilatant behaviour during an undrained deviatoric compression stage occurs when the pore pressure parameter a=-$\Delta p''/\Delta q$ becomes zero, passing from positive to negative values (contractive behaviour is characterised by a>0 while dilatant response by a<0, Wood (1990)). It is worth noting that this criterion was proposed for fibrous peats by Oikawa & Miyakawa (1980) and adopted by Mesri & Ajlouni (2007). The mechanical ground of this criterion had been discussed for dense sands in undrained compression by Nova (1977), who demonstrated that stress ratios higher than the critical stress ratio M can be reached after a=0 is overpassed due to dilation in the hardening regime. The evolution of the pore pressure parameter a for the saturated samples (Test 1 and Test 2) is reported in Figure 7.13(b). The transition from contractive to dilatant behaviour of the saturated samples occurred for axial strains of 7% and 12%, in Test 1 and Test 2 respectively, for an average stress ratio η=2.3. The evolution of the pore pressure parameter a for the gassy samples is reported in Figure 7.14. Significant higher axial strains, in the range 16%-20%, needed to be applied to the gassy samples in order to switch from contractive to dilatant be-

haviour. As this transition is associated to the start of significant confinement effect offered by the fibres, it can be concluded that the dominant effect of gas on the deviatoric behaviour is to delay the fibres stretching significantly.

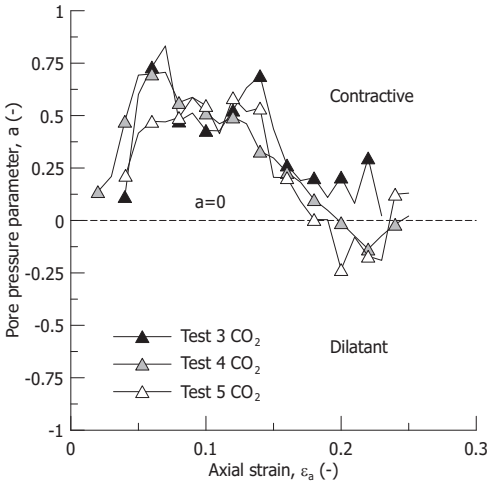

Figure 7.14: Evolution of the pore pressure parameter a for the normally consolidated gassy samples during undrained shear

To provide further insight into the deformation mechanism and to appreciate this delay in the fibres stretch contribution, the operative axial stress is reported in Figure 7.15(a) for the normally consolidated saturated sample and in Figure 7.15(b) for the gassy samples. The results are normalised for each test with the operative axial stress at the start of shearing, $\sigma''_{a0,s}$.

The fully saturated sample presents the typical response of saturated peats, with the operative axial stress increasing steadily with the axial strain. However, for gassy samples there is a significant intermediate portion of the response with almost constant operative axial stress, despite the increasing axial strain. The extension of this trait increases with the initial gas fraction previously exsolved, suggesting that significant rearrangement of the peat fabric must occur before stretching of the fibres starts being effective in contributing to the mobilised strength. Starting from the fabric evidence in Figure 7.6 and the sketch in Figure 7.11, it can be inferred that gas expansion causing an enlargement of the pores will be accompanied by distortion and bending of the fibres (stage 3 in Figure 7.11). This effect needs to be compensated by high strains during the deviatoric compression before the fibres start stretching. Eventually, the stress ratio corresponding to the onset of failure, detected by the condition a=-$\Delta p''$=0, is similar for the saturated and the gassy samples (Figure 7.16). Slightly higher values can be reached by gassy samples at the expenses of much higher axial strains, which increase with the volumetric gas fraction at the beginning of shear.

These results show that the shear strength of the tested peat is hardly affected by the presence of gas, or even slightly increased if the criterion a=-$\Delta p''$=0 is

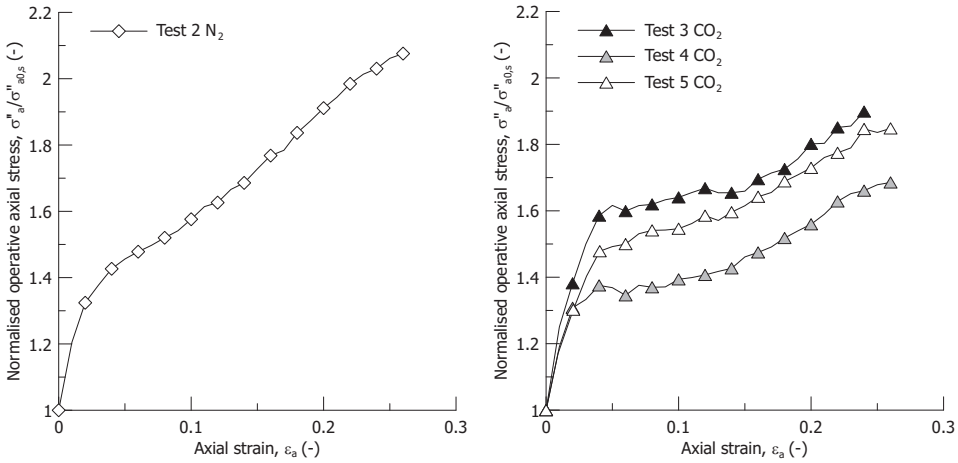

Figure 7.15: Normalised operative axial stress-strain relationship: (a) fully saturated sample and (b) gassy samples

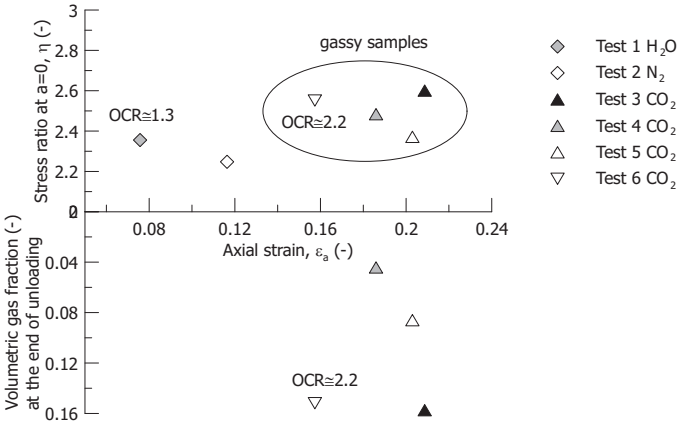

Figure 7.16: Stress ratio plotted against axial strain at the onset of failure together with the volumetric gas fraction generated at the end of undrained unloading

adopted to discriminate the onset of failure. However, the delay in mobilised shear strength due to gas compression and fibres stretching results in a dramatic effect on serviceability and ultimate limit states criteria based on mobilised shear strength at given axial strain thresholds. To quantify this remark, Figure 7.17 reports the mobilised friction angle, φ'_m, of the saturated and gassy samples in correspondence of typical reference axial strains of 2% and 5%, often used in traditional assessment approaches (Den Haan & Feddema, 2013). On average, a reduction of 30%-40% in the mobilised friction angle of gassy samples compared to saturated samples is observed at both axial strains of 2% and 5%.

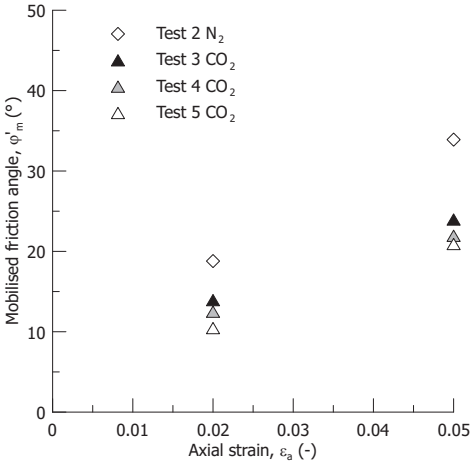

Figure 7.17: Mobilised friction angle at axial strains of 2% and 5% for normally consolidated fully saturated and gassy samples

7.7. CONCLUSIONS

Biodegradation of peat generates gases in the soil water, which can exsolve when the equilibrium pressure decreases due to changes in stress, temperature or water pressure. The potential consequences of these gases on the mechanical behaviour of peats have been systematically investigated by means of a series of triaxial tests on natural peat samples from Katwoude in the Netherlands. Controlled amounts of gas were generated by unloading the samples under undrained conditions, after flushing them with carbonated water. A gas fraction in the range 4% to 16% was generated, which replicates the typical amount of gas found in peat layers in the field.

The volumetric and the deviatoric stress-strain responses, as well as the strength have been investigated. During isotropic unloading, gas exsolution and expansion is ruled by the relative stiffness of the pore fluid over that of the solid skeleton. With respect to other gassy soils investigated in the past, the very high compressibility of peats decreases the rate of gas exsolution. Most of gas expansion takes place at very low stress, when the fabric can be locally softened, allowing for gas coalescence and migration. The mechanical response upon undrained unloading is characterised by gas-soil matrix interaction phenomena. As long as the gas bubbles remain confined in the pores space, the typical response of a porous medium saturated with a compressible pore fluid is observed. However, with further gas exsolution and expansion, gas bubbles start acting directly on the soil skeleton. The contact forces between the organic peds are reduced, which rapidly decreases the operative mean stress. Pore enlargement and significant soil matrix changes are expected to occur, until the gas bubbles become locally interconnected in gas clusters and the soil matrix is not able to contrast further gas expansion.

Volumetric strains due to gas compression and dissolution during shearing occur for gassy samples, despite the external undrained conditions. Both fully saturated and gassy samples showed diffuse failure mode. The stress ratio at the onset of failure, defined as the transition from contractive to dilatant response, is not significantly affected by the presence of the gas fraction. However, the pre-failure stress-strain relationship for gassy samples is remarkably different from that of fully saturated specimens, with a dramatic reduction in the mobilised shear strength and mobilised friction angle for given axial strain levels. The volumetric strains experienced by the soil matrix delay the peat fibres stretching, and their contribution to the shear strength.

The experimental study has been started to evaluate whether and how the presence of gas should be accounted for in the safety assessment of earth structures founded on peat, which are subjected to loading-unloading and thermal cycles, as well as changes in the atmospheric conditions, during their service life. The results suggest that the presence of gas should be carefully considered in the assessment of serviceability limit states. When total stress or pore pressure are reduced, for example due to excavation or dewatering, gas exsolution and expansion will occur, decreasing the operative stress and eventually increasing the soil skeleton compressibility. The effects appear to become dramatic at low total stresses, which is often the case for peat foundation layers at the toe of embankments. The presence

of gas becomes also extremely relevant when ultimate limit states are assessed by choosing an operative shear strength defined on strain thresholds. The compressibility of the gas phase and the delayed stretching of fibres largely reduce the mobilised friction angle for comparable strain thresholds.

LIST OF SYMBOLS

Gs	specific gravity
N	loss of ignition
OC	organic content
γ	unit weight
n_0	initial porosity
e_0	initial void ratio
Sr	degree of saturation
T	temperature
RH	relative humidity
σ_c	cell pressure
$\sigma_{c0,u}$	cell pressure at the beginning of unloading
u_b	back pressure
u_f	pore fluid pressure
$u_{l/g0}$	initial gas-liquid saturation pressure
$u_{l/g,13°}$	corresponding gas-liquid saturation pressure at 13° for concentration of dissolved CO_2 at $u_{l/g0}$=380 kPa and 22°
$u_{f0,u}$	pore fluid pressure at the beginning of unloading
Δu_f	excess pore fluid pressure
χ	gas solute mole fraction
u_g	absolute gas pressure
H^{xp}	Henry's coefficient of solubility (by way of mole fraction)
H^{cp*}	Henry's coefficient of solubility (by way of concentration) at the reference temperature T^*
T^*	reference temperature 298.15 K
M_{H_2O}	molar mass of water
ρ_{H_2O}	density of water
$\Delta_{sol}H$	enthalpy of dissolution
R	gas constant
p''	mean operative stress
p''_{max}	maximum mean operative stress pre-shear
$p''_{0,u}$	mean operative stress at the beginning of unloading
$p''_{0,s}$	mean operative stress at the beginning of shear
OCR	overconsolidation ratio
σ''_a	operative axial stress
σ''_r	operative radial stress
$\sigma''_{a0,s}$	operative axial stress at the beginning of shear
q	deviatoric stress
η	stress ratio
M	critical stress ratio
ε_a	axial strain
ε_p	volumetric strain
$\dot{\sigma}_c$	rate of cell pressure change
$\dot{u}_f$	rate of pore fluid pressure change

$\dot{p}$	rate of mean operative stress change
$\dot{S}r$	rate of degree of saturation change
$\Delta\sigma_c$	cell pressure increment
$\Delta p''$	mean operative stress increment
Δq	deviatoric stress increment
a	pore pressure parameter
B	pore pressure parameter
φ'_m	mobilised friction angle

8

Conclusions and recommendations

8.1. Observations and Conclusions

This work wants to advance the current knowledge of the deviatoric behaviour of peats by adopting a holistic research approach. Starting from the field stress-test on a historical rural dyke on peat at the Leendert de Boerspolder site, it is shown that the high deformability of peat rather than its shear strength dominates both the pre-failure and failure response of the entire geotechnical system. The role of each soil foundation layer is reconstructed to clarify the triggering mechanism and the critical soil layer which rule the response of the system. The necessity of investigating not only the failure but also and especially the pre-failure behaviour of peat is then transferred from the field to the laboratory scale.

The extensive experimental campaign is dominated by the desire to re-establish the use of drained and undrained triaxial compression tests on peat. However, a correct interpretation of the experimental data requires a clear distinction between the sample behaviour and the material behaviour. If this is true for classical inorganic soils, it is fundamental for peats. The high deformability and shear strength of peat magnify the impact of end restraint on the observed sample response, which can deviate significantly from the true material behaviour. Only when the true material behaviour is revealed, some of the long-lasting misconceptions on the shear strength of peat are overcome.

The experimental results are assisted by the development of a simple elastic-plastic model for the deviatoric behaviour of fully saturated reconstituted peat. For the first time, experimental evidence of the constitutive ingredients of an elastic-plastic framework as the yield locus, the plastic potential and the hardening law is provided. To overcome the difficulty of interpreting standard laboratory tests on peats as element volume tests, the model is implemented in a Finite Element code and validated against experimental results from laboratory tests modelled as a boundary value problem. The comparison with the experimental results allows to confirm the good qualitative and quantitative agreement of the simulated response for different stress paths with multiple loading directions and for a wide range of deviatoric strains, up to 20%. This range is well above the shear strains attained by rural dykes on peats as observed for the case of the Leendert de Boerspolder dyke, namely 5%. However, at the current stage the model does not have full predictive capabilities. The experimental results highlight important fabric effects, which introduce a directional response in the deformation mechanism and additional shear strength with the fibres stretching at high deviatoric strains. Further ingredients as induced anisotropy and matrix-fibres interaction should be added. With reference to the different aspects of the behaviour of peats covered in this work, the following specific conclusions are drawn.

8.1.1. Role of peat in the field applications

The pre-failure response and failure mechanism of the dyke at the Leendert de Boerspolder during the stress-test allow to clarify the role of different soils layers on the response of the geotechnical system.

- Peat layers which serve as foundation for dykes and embankments are not

necessarily the critical elements for the shear failure mechanism. Both the pre-failure and the failure responses of the system are ruled by the high deformability of the peat and by the kinematic compatibility at the interface between the peat and the soft soil underneath. As shown from the field monitoring, bulging and horizontal displacements of the peat at the toe of the dyke caused significant shear strains in the organic silt underneath which eventually failed for a shear strain of about 5%. At this strain level, the mobilised shear strength for the peat is well below its ultimate value, which can be reached only for shear strains three to four times higher.

- Neglecting the implications of the kinematic compatibility in the failure response of these dykes can lead to unsafe choices in the design and assessment procedures. For low total stresses, which is often the case for soft soils foundation layers at the toe of embankments, the stress-strain response of the soil is mainly dilatant but without a deviatoric softening. As a result, for assessment procedures based on the limit equilibrium methods, the undrained shear strength determined from laboratory tests cannot refer to large strains. The operative shear strength mobilised at failure in the field by taking into account the kinematic compatibility is much lower than the value at ultimate state from laboratory tests. On the contrary, ultimate state can be assumed as reference state in hydro-mechanical coupled analyses where the actual evolution of the stress state for each soil element is taken into account.

- The presence of gas bubbles should be carefully considered in the assessment of serviceability limit states of dykes founded on peat layers. Excavation or dewatering operations can exsolve gases previously dissolved in the pore fluid due to biodegradation of the organic matter. Gas exsolution and expansion cause a significant increase in the compressibility of the soil skeleton and of the pore fluid. The effects appear to become dramatic at low total stresses, which is often the case for peat foundation layers. The presence of gas becomes also extremely relevant during shear. Despite the ultimate shear strength of gassy peat samples being comparable with fully saturated samples, the compressibility of the gas phase reduces dramatically the mobilised shear strength and mobilised friction angle for given axial strain levels. When ultimate limit states are assessed by choosing an operative shear strength defined on strain thresholds, the influence of gas bubbles should not be disregarded.

8.1.2. Peat characterisation at the laboratory scale

The extensive experimental campaign conducted to characterise the behaviour of peat at the laboratory scale allows to overcome some of the previous knowledge gaps about the stress-strain response of peats.

- End restraint effects on the observed peat behaviour from conventional laboratory tests are magnified by the high deformability and high friction angle of peat. Large strains attained by peat samples at failure increase stresses and

strains non-uniformities thus precluding a correct interpretation of the tests results. Specific experimental precautions, like smooth end platens and pore pressure probes at mid height of the samples, must be adopted to have representative stresses and strains measurements. Without these specific precautions, great care must be taken in deriving shear strength parameters and constitutive model parameters from standard laboratory tests. In this case, the sample behaviour must be discerned from the true material behaviour.

- Experimental results from undrained triaxial compression tests with standard rough and modified end platens reveal dramatic end restraint effects on both the volumetric and the deviatoric response of reconstituted peat samples. Overestimation of the excess pore pressure at the extremities of the sample and of the deviatoric stress induce significant errors when deriving shear strength parameters from triaxial apparatus with rough end platens. The implication in terms of friction angle is dramatic passing from 43° for samples tested with modified end platens to 55° for sample with the standard height to diameter ratio 2 and rough end platens. End restraint effects are also expected when testing natural fibrous peat. However, in this case the higher hydraulic conductivity compared to the reconstituted samples, is expected to reduce the overestimation of the excess pore pressure at the bottom of the sample. On the contrary, the presence of big fibres in the samples can magnify the end restraint effect in the deviatoric response. Hence, end restraint effects and the representativeness of the volume tested must be carefully considered in each experimental campaign.

- The kinematic constraint at the extremities of the samples by the rough end platens also alters the deformation mode. The stress-dilatancy rule reconstructed from drained triaxial compression tests on peat samples where rough end platens are used, differs substantially from the true material flow rule. The incorrect interpretation of the material flow rule has important implications for both serviceability and ultimate limit states with overestimation of the displacements or of the shear strength, depending on the stress path direction. However, simple observations coming from a K_0-consolidation test in the triaxial apparatus and undrained compression tests with modified end platens offer a relatively simple approach to derive a more accurate flow rule with limited laboratory effort.

- Fabric effects with rearrangement and realignment of the small fibres in the peat matrix seem to introduce a directional response in the plastic deformation behaviour of the tested peat. The plastic deformation response is ruled not only by the current stress state but also by the loading direction. Loading directions accompanied by radial expansion magnify the deviatoric strain component to the volumetric counterpart as a result of an intense matrix-fibres interaction. On the contrary, loading directions accompanied by radial contraction tend to switch off the role of the fibres in favour of a more traditional deformation response. Induced anisotropy rather than inherent anisotropy seems to rule the deformation response of the tested peat.

8.1.3. Modelling the deviatoric behaviour of reconstituted peat

The extensive experimental results allow to propose a simple elastic-plastic modelling framework for the deviatoric behaviour of fully saturated reconstituted peat. Despite its simplicity, the model represents a step forward but not yet a predictive modelling tool for the deviatoric behaviour of peat. Induced anisotropy is not accounted for in the constitutive formulation. The most important advances are listed below.

- The adoption of a mixed volumetric and distortional hardening law allows to overcome well known limitations of previous models in capturing the pre-failure deviatoric stress-strain response and the excess pore pressure of peats tested in undrained triaxial compression tests. Rearrangement and realignment of the small fibres in the fabric of the tested peat are plausible reasons for the appearance of a distortional hardening component.

- The model shows good qualitative and quantitative agreement for drained triaxial compression tests with different loading directions. The agreement is more than satisfactory for a wide range of deviatoric strains up to 20%, hence including strain thresholds representative for the typical field applications where peat serves as foundation layer. For higher deviatoric strains the model predictions and the experimental results diverge. End restraint effects and possible additional confinement offered by small fibres stretching for samples experiencing compression with axial strains up to 40% and 50% increase the observed shear strength well above the model prediction. The experimental results from both undrained and drained triaxial tests suggest that geometrical effects are introduced in the observed deviatoric stress-strain response, which can be ascribed to the characteristic length of the small fibres present in the peat fabric and not accounted for in the implemented model.

- A constitutive approach at the element scale has been proposed to model natural peats as fibres-reinforced soils. By taking into account explicitly the additional confinement offered by the big fibres stretching in natural fibrous peat it is possible to quantify the role of the fibres on the observed behaviour. This approach allows to overcome conceptual difficulties when deriving shear strength parameters from triaxial compression tests on natural peat samples.

8.2. Limitations

Research advances are always accompanied by limitations. This work does not make an exception, with both conceptual and practical limitations.

- All the experimental effort is dedicated to characterise the fundamental behaviour of peats. To reduce the uncertainties introduced by fabric variability of natural peats, the research focuses on reconstituted peat without big fibrous inclusions which would compromise the representativeness of the soil volume tested.

- Time dependent behaviour in the experimental results is not accounted for. To minimise the differences in the stress-strain response coming from rate dependency, undrained triaxial tests were conducted by adopting a constant axial strain rate. Also for the drained tests, the resulting axial strain rate was uniform among the tests, despite one order of magnitude lower than for the undrained tests to assure negligible excess pore pressure. These choices allowed the experimental data not to be affected by significant time dependent effects.

- The effects of fibres on the observed behaviour is not taken into account either when elaborating the experimental results and in the constitutive model implemented in the Finite Element code. However, a simplified promising attempt to model natural fibrous peats as fibres reinforced soils is formulated in the final part of this work.

- To assure representative effective stress levels with respect to the field conditions, the experimental campaign adopted low effective confining stresses. However, the accuracy of the commercial triaxial apparatus used in this work limits the possibility of investigating the response of highly overconsolidated peat samples. All the experimental results and considerations are therefore limited to the wet side of the yield locus and mainly to normally or slightly overconsolidated samples.

- The experimental tests are limited to axisymmetric stress states, which do not cover entirely the possible strain-stress paths in the field.

8.3. Recommendations for future work

Based on the conclusions and the limitations of this work, the following research recommendations are suggested.

- Experimental efforts should be directed to determine the shape of the plastic potential and yield locus of reconstituted peats on the deviatoric plane. So far no information is available in the literature. Despite the evident difficulties with respect to traditional inorganic soils, attempts of testing peats samples in ad-hoc apparatuses, like hollow cylinder or axial-shear apparatus (Molenkamp, 1998) for soft soils should be pursed. This information is essential for a correct extension and validation of current constitutive models for peat to the multiaxial space and thus for correct simulations of field scenarios.

- In this work, gas exsolution and shear are limited to peat samples isotropically consolidated. Effects of gas bubbles on the hydro-mechanical behaviour of peat should be quantified with reference to anisotropic stress and highly overconsolidated states better representing actual field conditions.

- The sensitivity of the experimental results on the sample height to diameter ratio when rough end platens are used seems to suggest the presence

of a length scale. Therefore, end restraint effects on the observed hydro-mechanical response of reconstituted peat could be magnified in laboratory tests by the presence of the small fibres within the peat matrix. Non-local Finite Element methods and second gradient models seem to be promising techniques to introduce in the model predictions the influence of a characteristic length. This may replicate the effects of the small fibrous network present in the peat fabric.

- If peat is modelled with an homogenised approach, induced anisotropy should be added to translate the experimental evidence of a directional response of the plastic deformation response. However, constitutive approach which interprets peat as fibres-reinforced soil could represent a big step forward to model the behaviour of peat at the engineering scale. Such a model could overcome misconceptions at the laboratory scale due to the matrix-fibres interaction and the additional reinforcement offered by the fibres to the observed behaviour at high deviatoric strains. This possibility would open for a reappraisal of extensive database of laboratory data on natural peats not fully exploited yet. In this context, the proposed modelling approach for reconstituted peats could be used as reference for the peat matrix, introducing a superimposed effects of the fibres. Important indications could be obtained also for up-scaling the influence of the fibres from the laboratory scale to the field scale. However, conceptual difficulties in distinguishing multiple levels of fibres from each other in peats still remain, if compared to traditional artificially fibres-reinforced soils.

A

Applicability of hypoplasticity to reconstituted peat from drained triaxial tests

Restlessness is discontent and discontent is the first necessity of progress.
Show me a thoroughly satisfied man and I will show you a failure

Thomas Edison

The content of this appendix has been published as research paper in International Journal for Numerical and Analytical Methods in Geomechanics. (Muraro et al., 2018).

A

A.1. ABSTRACT

Proper understanding of the deviatoric behaviour of peats represents a challenge in soil mechanics. Exceptional high deformability together with extremely high friction angles distinguish peats from classical organic soils. Considerable amount of triaxial tests data on peats can be found in the literature, mostly coming from standard undrained triaxial compression tests. However, only a minor part was intended to describe their pre-failure behaviour. Also, limiting the investigation to the undrained response, reduces the information on those ingredients of constitutive models, which are necessary to describe the deformation behaviour. This contribution aims to provide better insight into the pre-failure deformation behaviour of peats, by analysing in detail the results of non-standard drained tests at various stress paths, and undrained tests performed on reconstituted peat samples. Based on the experimental findings, an existing hypoplastic model, originally developed for fine-grained soils, has been adapted to capture the behaviour of peats. The model is directly calibrated on selected experimental results and validated on a variety of different stress paths tests. The results reveal the merits of hypoplasticity in modelling the non-linearity of the pre-failure behaviour and the directional response of peats, which both are of great importance when assessing the serviceability limit states of geotechnical structures founded on peats.

A.2. INTRODUCTION AND MOTIVATIONS

Extensive experimental research has been carried out so far on peats, mainly using undrained triaxial compression tests. These tests have been focused mostly on the shear strength, and elucidated the frictional nature of the peat fabric with small apparent intercept cohesion and high friction angles in the range of 50°-70° (Adams, 1961; Landva & La Rochelle, 1983; Yamaguchi et al., 1985b; Farrell & Hebib, 1998; Edil & Wang, 2000; Cola & Cortellazzo, 2005; Cheng et al., 2007). The presence of multiple fibrous networks not entirely decomposed within the peat fabric is recognised to provide additional reinforcement to the material, hence justifying the high shear strength parameters (Landva & La Rochelle, 1983).

Despite the considerable amount of laboratory investigation on the shear behaviour of peats, only a minor part was intended to describe the mechanical behaviour before ultimate state conditions. However, the design and the assessment criteria in many geotechnical applications where peats are encountered, are ruled by serviceability limit states rather than ultimate limit states.

These considerations call for an adequate geotechnical description of the pre-failure response of these materials. The volumetric behaviour of peat, with particular attention to creep, has been widely investigated both from the experimental and the constitutive viewpoints (Berry & Poskitt, 1972; Berry & Vickers, 1975; Landva & La Rochelle, 1983; Lefebvre et al., 1984; Tsushima & Mitachi, 1985; Fox et al., 1992; Edil et al., 1994; Fox & Edil, 1996; Den Haan & Edil, 1994; Mesri et al., 1997; Den Haan & Kruse, 2007; Mesri & Ajlouni, 2007; Madaschi & Gajo, 2015b; Acharya et al., 2017; Den Haan, 1996; Madaschi & Gajo, 2015a). However, only few contributions focus on the modelling of the deviatoric behaviour of peats. The first attempt is due to Yamaguchi et al. (1985b), who developed an elastic-plastic model based on the Modified Cam clay (Roscoe & Burland, 1968), which was coupled with an experimentally based stress-dilatancy law. The model was capable to capture the ultimate state detected in undrained compression triaxial tests, but with a significant overestimation of the stiffness in the deviatoric stress-strain response. Recent attempts include the application of the Soft Soil Creep model, Den Haan & Feddema (2013), and its anisotropic version, Den Haan (2014), based on the original works by Leoni et al. (2008), Vermeer & Neher (1999) and Wheeler et al. (2003). A kinematic bubble model was proposed by Boumezerane (2014), based on Al-Tabbaa & Wood (1989) and Sivasithamparam (2012). More recently, Yang et al. (2016) adopted the elastic-plastic model by Li & Dafalias (2000) to reproduce undrained triaxial compression tests on reconstituted peat samples, while Boumezerane et al. (2015) suggested the use of an hyperplastic model.

The vast majority of the previous models have been calibrated and tested based on experimental results coming from undrained triaxial compression tests. However, undrained tests do not allow to determine directly some of the main constitutive ingredients, such as the yield locus and the stress-dilatancy relationship for the case of a general elastic-plastic framework. To overcome this limitation, a series of non-standard drained triaxial tests have been carried out on reconstituted peat samples, especially focussing on the pre-failure deformation behaviour. Based on the experimental results, a simple model for reconstituted peat is adopted starting from

an existing hypoplastic approach originally proposed for clays (Mašín, 2013, 2014). This choice is based on the capability of hypoplasticity to predict a smooth transition between overconsolidated and normally consolidated states and to account for the non-linear pre-failure response, which appears to be of great relevance for the case of peats. The constitutive ingredients of the hypoplastic model have been explicitly derived from the results of drained tests with multiple loading-unloading stress paths. Particular attention has been given to the definition of asymptotic states, namely the boundary surface and the corresponding asymptotic strain rate directions. The modelling effort has a twofold scope: it allows elucidating the hypoplastic modelling ingredients for peats, and it provides a reference hypoplastic model, on which further relevant features, such as anisotropy and creep can be added.

A.3. EXPERIMENTAL PROGRAMME

A.3.1. Stresses and strains variables

All the experimental data have been elaborated herein by assuming axisymmetric test conditions and full description of the soil stress state is accomplished by adopting the common triaxial stress variables: mean effective stress p', and deviatoric stress q. For the conjugate strain variables, volumetric strain, ε_p, and deviatoric strain, ε_q are considered. Large displacements typically reached when testing peat call for the adoption of the natural strains in the present work (Ludwik, 1909; Hencky, 1928). Natural strains imply the validity of the additive principle in equation A.1 at small as well as at large strain. In the absence of direct measurements of radial displacements, deviatoric strain has been computed from the measurement of volume change and axial displacement (i.e. ε_p and ε_a).

$$\varepsilon_p = \varepsilon_a + 2\varepsilon_r = \ln \frac{V_0}{V} \tag{A.1}$$

$$\varepsilon_q = \varepsilon_a - \frac{\varepsilon_p}{3} = \ln \frac{H_0}{H} - \frac{1}{3} \ln \frac{V_0}{V} \tag{A.2}$$

where V_0 and H_0 are the initial volume and height of the sample, while V and H are the current values throughout the test. The cross sectional area of the specimen has been corrected by assuming the specimen remained as a right cylinder (Head & Epps, 2014b). Comparison between the calculated diameters and the ones measured at the end of each test supported this choice.

A.3.2. Tested material and experimental methodology

The experimental study was conducted on peat collected from the Leendert de Boerspolder site in the Netherlands. The material was collected from a surficial peat deposit 1.5 m below the ground surface. To reduce bio-degradation, the material was stored in a climate controlled room at 10±1°C and 90% relative humidity. Reconstituted peat samples were prepared for all the tests according to the following procedure. Firstly, the material was mixed with demineralised water to slurry with water content of 855%, which corresponds to 1.4 times the limit liquid.

The material was then placed in a floating consolidometer tube to consolidate under a total vertical stress of 9.5 kPa for 48 hours. The reconstituted sample was then extracted and mounted in the triaxial apparatus. All the tests were performed under strict controlled air temperature 14±1°C and relative humidity 80%. To prevent loss of organic matter, the oven-drying procedures for the classification of the tested material were performed at a temperature of 60°C (Head, 2014). The specific gravity, Gs, of the soil was measured with a helium pycnometer in accordance with D5550-14 (2014). The organic content, OC, was assessed by ignition in a furnace at 500°C (D2974-14, 2014; Den Haan & Kruse, 2007). Table A.1 reports the index properties of the tested samples. The average fibre content was 0.14 (D1997-13, 2013). The nominal dimensions of the tested specimens were 50 mm in diameter and 100 mm high. All the tests were carried out using a load frame type GDS triaxial system, with back pressure and cell pressure volume controllers, and a submersible 1 kN load cell. Thin membranes 0.25 mm thick were used. To accelerate the consolidation process, lateral filter paper was placed around the samples. To prevent "short circuit" effects between the back pressure and the pore pressure transducers, 10 mm clearance were left between the lower edge of the lateral filter paper and the bottom of the samples (Head & Epps, 2014b). Each vertical drainage strip had free lower end to reduce the potential contribution offered by the lateral filter paper to the measured strength of the material.

Table A.1: Index properties and relevant stress variables of the tested specimens

Sample	Gs (-)	e_0 (-)	OC (-)	p'_0 (kPa)	$p'_{start-shear}$ (kPa)	OCR (-)	Drainage
Sample 1	1.52	9.80	0.91	74	18	4.1	Drained
Sample 2	1.49	9.76	0.91	32	14	2.3	Drained
Sample 3	1.46	9.65	0.91	32	15	2.1	Drained
Sample 4	1.47	9.50	0.91	32	14	2.3	Drained
Sample 5	1.47	9.54	0.91	33	33	1.0	Undrained
Sample 6	1.45	9.16	0.92	32	22	1.5	Undrained
Sample 7	1.48	9.43	0.91	33	18	1.8	Undrained

e_0 initial void ratio; p'_0 preconsolidation stress; $p'_{start-shear}$ stress at the beginning of shear

A.3.3. Stress paths

The testing programme consisted of a series of drained triaxial tests, including multiple stress paths which allowed to explore different loading conditions, and a series of standard undrained triaxial compression tests. A saturation ramp by back pressure was performed up to a cell pressure σ_c=200 kPa. The cell pressure was then increased to 400 kPa under undrained conditions. To determine the volumetric response upon loading and unloading, sample 1 was isotropically compressed up to p'_0=74 kPa (point b in Figure A.1(a)), and isotropically unloaded to $p'_{start-shear}$=18 kPa, ending with OCR≅4 (point c in Figure A.1(a)). The other samples were isotropically consolidated up to a mean effective stress p'_0=32-33 kPa (Figure A.1(a) and

Figure A.1(b)) and isotropically unloaded, to give an initial overconsolidation ratio $OCR=p'_0/p'_{start-shear}$ between 1.0 and 2.3 depending on the test (Table A.1). The initial preconsolidation pressure was decided in order to provide a representative data set in terms of stress levels for the typical field conditions of surficial peats in the Netherlands (σ'_v=10-40 kPa). For the drained tests, the shearing stage consisted in a series of mixed isotropic and deviatoric loading-unloading and reloading paths, as summarised in Figure A.1(a) and Figure A.1(b). For sample 1 and sample 2 the deviatoric stress was increased at nominally constant p', until the pre-defined stress ratio $\eta=q/p'$, equal to 1.92 and 0.78, respectively. For sample 3 and sample 4 multiple nominally constant p' and constant q traits were followed (note that the anticipated constant p' paths were not followed exactly due to difficulties in stress control). The remaining samples (5, 6 and 7) were brought to failure with a constant axial displacement rate of 0.02 mm/min and constant radial stress in undrained conditions. The radial stress paths imposed to sample 1 and sample 2 were exploited to update the existing hypoplastic formulation (Figure A.1(a)). The remaining stress paths on sample 3 and sample 4 (Figure A.1(b)) together with the undrained tests were used to evaluate the model performance.

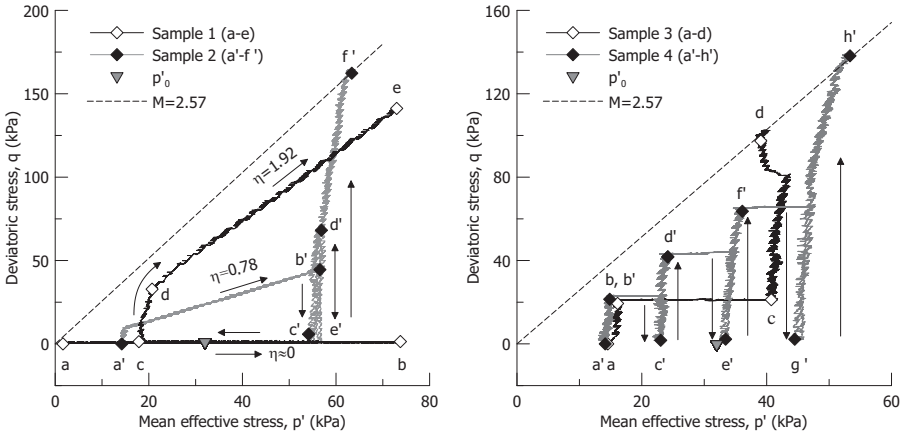

Figure A.1: Experimental drained stress paths used for (a) model calibration and for (b) model assessment (the applied stress history can be followed through the letters in the figures)

The results in Figure A.1(a) and Figure A.1(b) show that failure was reached for a critical stress ratio M=2.57 corresponding to a critical friction angle φ'_c=64°. Very high friction angles for peats are often reported in the literature (Oikawa & Miyakawa, 1980; Yamaguchi et al., 1985b; Farrell & Hebib, 1998; Cola & Cortellazzo, 2005). However, the end restraint at the boundaries of the sample is likely to contribute to the observed high values (Rowe et al., 1984; Drescher & Vardoulakis, 1982; Cheng et al., 2007).

A.4. HYPOPLASTIC FORMULATION

The hypoplastic formulation proposed by Mašín (2013) and Mašín (2014) was the starting point of this work. The main constitutive components are here recalled for the sake of clarity. The general non-linear hypoplastic formulation may be written as (Gudehus, 1996)

$$\mathring{\boldsymbol{\sigma}} = f_s(\boldsymbol{L} : \dot{\boldsymbol{\varepsilon}} + f_d \boldsymbol{N} \|\dot{\boldsymbol{\varepsilon}}\|) \tag{A.3}$$

where $\mathring{\boldsymbol{\sigma}}$ and $\dot{\boldsymbol{\varepsilon}}$ represent the objective (Zaremba-Jauman) stress rate and the Euler stretching tensor, respectively, $\boldsymbol{L}$ and $\boldsymbol{N}$ are fourth- and second- order constitutive tensors, f_s is the factor controlling the influence of mean stress (barotropy factor) and f_d is the factor controlling the influence of the void ratio (pyknotropy factor). Equation A.3 was further developed by Mašín (2013) allowing for the explicit incorporation of the asymptotic states. The complete set of equations of the final form employed in this study is given in the final Appendix. The experimental programme allowed to investigate explicitly the asymptotic states of the tested peat in terms of state boundary surface and strain rate directions, as reported in the following paragraph.

A.5. MODEL CALIBRATION AND ENHANCEMENT

The employed hypoplastic model had been originally proposed for fine-grained soils. As a consequence, the model parameters describing the asymptotic state boundary surface and the asymptotic strain rate directions had been validated for friction angles ranging between φ'_c=20°-35°. Straightforward applicability of the original model to peats is not guaranteed due to their higher friction angle, and no application of this type of hypoplastic models has been reported so far. Relevant drained stress paths from sample 1 and sample 2 (Figure A.1(a)) have been chosen to calibrate the constitutive formulation and to adapt some of its parts based on the experimental results. Asymptotic states are defined as those states achieved by the soil after a sufficiently long proportional stretching with a constant direction of the strain rate. Conceptual representation of asymptotic states has been proposed by Gudehus (2011) and Gudehus & Mašín (2009). For the case of radial compression stress paths at constant stress ratio, asymptotic states are traditionally defined as normal compression lines in the $ln\,(1+e)$-$ln(p'/p'_r)$ plane (Butterfield, 1979), where p'_r is a reference stress which was chosen equal to 1 kPa. Figure A.2 reports the compression lines from sample 1 and sample 2 with the corresponding asymptotic states. Sample 1 was isotropically loaded and unloaded. After unloading, it was further compressed along a radial direction, having a constant stress ratio η=1.92. Sample 2 was loaded along a radial direction having η=0.78 (see Figure A.1(a)).

The isotropic compression path and the isotropic unloading performed on the sample 1 (Figure A.1(a)) allow defining the ISO-NCL and the ISO-URL lines with λ^*=0.26 and κ^*=0.032, respectively (Figure A.2). The asymptotic states lie on compression lines parallel to the ISO-NCL, as reported in Figure A.2. The critical stress ratio is fixed at M=2.57, corresponding to a critical friction angle φ'_c= 64°, from the failure line reached by sample 2 (Figure A.1(a)).

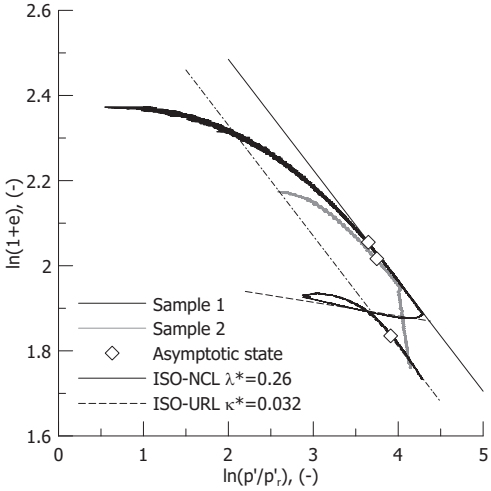

Figure A.2: Radial paths data from sample 1 and sample 2 and the corresponding asymptotic states

A.5.1. Asymptotic state boundary surface

The envelope of all the asymptotic states in the stress versus void ratio space is defined as the asymptotic state boundary surface (ASBS) (Mašín & Herle, 2005). The shape of its cross-section at constant void ratio is described from Mašín (2013) by

$$f = 0 = F_m + \left(\frac{p'}{p'_e}\right)^{\omega} - 1 \tag{A.4}$$

where p'_e is the Hvorslev's equivalent pressure on the isotropic normal compression line, given by:

$$p'_e = p'_r \exp\left[\frac{N - \ln(1+e)}{\lambda^*}\right] \tag{A.5}$$

with N defining the position of the normal compression line. The shape of the ASBS is controlled by the parameters ω and a, according to

$$\omega = -\frac{\ln\left(\cos\left(\varphi'_c\right)^2\right)}{\ln \vartheta^*_c} + a\left(F_m - \sin\left(\varphi'_c\right)^2\right) \tag{A.6}$$

in which ϑ^*_c defines the position of the critical state line on the ASBS and F_m is the Matsuoka-Nakai factor (Matsuoka & Nakai, 1974) defined as

$$F_m = \frac{9I_3 + I_1 I_2}{I_3 + I_1 I_2} \tag{A.7}$$

where I_1, I_2 and I_3 are the stress tensor invariants (recalled in the Appendix). For the tested peat, the intersection of the ASBS with the critical state line occurs for

$\vartheta_c^*=p'_e\ /\ p'_{cr}$=2.2 (with p'_{cr} the mean effective stress at critical state) slight higher than the original ratio of 2. Based on the asymptotic states and having fixed the critical state line, the final shape of the ASBS is reported in Figure A.3. The formulation ensures that the ASBS respects the tension cut off line (TCO) for η=3.

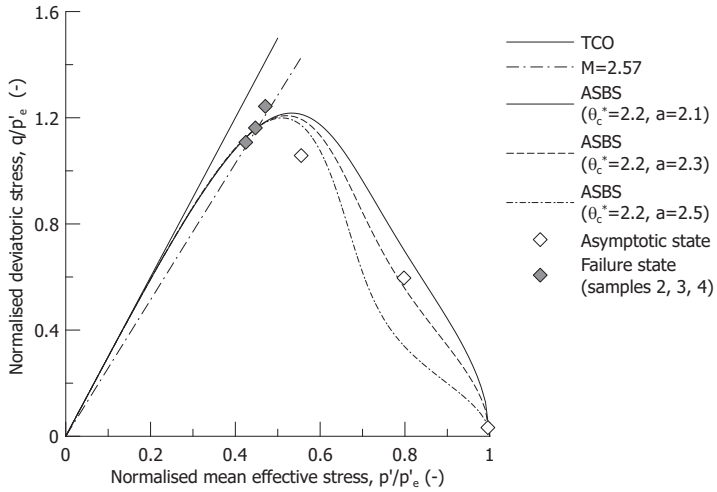

Figure A.3: Asymptotic state boundary surface used in the model compared to the experimental data

The ASBS can assume unrealistic shapes for high value of the parameter a in equation A.6 as displayed in Figure A.3. Despite this problem not limiting the applicability of hypoplastic formulations, the loss of convexity of the ASBS is not supported by any experimental evidence. In this study, to limit this problem and at the same time to match the experimental data, a=2.1 was assumed.

A.5.2. Asymptotic strain rate direction

The asymptotic behaviour of soils can be described in terms of a relationship between proportional deformation paths and the corresponding asymptotic stress states. With reference to Figure A.4(a) and Figure A.4(b), it is convenient to represent the strain rate obliquity and the stress obliquity with respect to the isotropic stress-strain state through the two angles $\psi_{\dot{\varepsilon}}$ and $\psi_{\sigma'}$, respectively. Relevant deformation paths on the $\dot{\varepsilon}_a$-$\sqrt{2}\dot{\varepsilon}_r$ plane and the corresponding asymptotic stress states on the Rendulic stress space σ'_a-$\sqrt{2}\sigma'_r$ are reported in Table A.2 and in Figure A.5. The asymptotic strain rate direction $\boldsymbol{d}$ is calculated as

$$\boldsymbol{d} = \frac{\boldsymbol{d^A}}{\|\boldsymbol{d^A}\|} \tag{A.8}$$

where

$$\boldsymbol{d^A} = -\hat{\boldsymbol{\sigma}}^* + \mathbf{1}\left[\frac{2}{3} - \frac{\cos 3\theta + 1}{4} F_m^{1/4}\right] \frac{F_m^{\xi/2} - \sin\left(\varphi'_c\right)^{\xi}}{1 - \sin\left(\varphi'_c\right)^{\xi}} \tag{A.9}$$

Table A.2: Values of the angles $\psi_{\dot{\varepsilon}}$ and $\psi_{\sigma'}$ at relevant states

State		Condition	$\psi_{\dot{\varepsilon}}$ (°)	$\psi_{\sigma'}$ (°)
Isotropic compression	i	$\dot{\varepsilon}_a = \dot{\varepsilon}_r$	0	0
Isochoric compression (critical state)	c	$\dot{\varepsilon}_p = 0$	90	$\tan^{-1}\left(\frac{2\sqrt{2}\sin\varphi_c'}{3-\sin\varphi_c'}\right)$
Isochoric extension (critical state)	-c	$\dot{\varepsilon}_p = 0$	-90	$-\tan^{-1}\left(\frac{2\sqrt{2}\sin\varphi_c'}{3+\sin\varphi_c'}\right)$
Axial splitting (tension cut off line)	d	$\dot{\varepsilon}_a = 0$ $\sigma_r' = 0$	144.7	54.7
Discing	-d	$\dot{\varepsilon}_r = 0$ $\sigma_a' = 0$	-125.3	-35.3

with θ the Lode's angle and $\hat{\boldsymbol{\sigma}}^*$ the normalised deviatoric stress (for the definition, see the Appendix). The coefficient ξ in equation A.9 controls the asymptotic strain rate direction, and was originally defined by Mašín (2013) as

$$\xi = 1.7 + 3.9 \sin\left(\varphi_c'\right)^2 \tag{A.10}$$

The asymptotic strain rate direction predicted by the original model (Mašín, 2013) is exemplified in Figure A.5 in terms of $\psi_{\sigma'}$ and $\psi_{\dot{\varepsilon}}$ relationship for a value of the critical friction angle φ_c'=30°.

The experimental asymptotic strain rate directions (ASRD) for the tested peat have been computed from the asymptotic states defined in Figure A.2 for each radial stress path. To allow proper representation of the experimental data the original model in Mašín (2013) (equation A.10) had to be modified through a coefficient ξ in equation A.9 as

$$\xi = \xi^{\zeta} \tag{A.11}$$

where the exponent ζ was assumed equal to 1.8 in order to fit the experimental data. The coefficient ξ rules the ratio between the deviatoric and the volumetric strain along any stress path. The adopted ζ higher than 1 increases the deviatoric strain increment for the same imposed stress ratio compared to the original model (equation A.10). Figure A.6 shows the predicted values for the original expression in Mašín (2013) and the one adopted in this study (equation A.11) together with the experimental results. For the sake of comparison the corresponding curved for the Original Cam clay (OCC, Roscoe et al. (1963)) and the Modified Cam clay (MCC, Roscoe & Burland (1968)) models are plotted too. It is worth noting that the last two models do not respect the limitation imposed by the tension cut-off line, differently from the original and the proposed hypoplastic formulations.

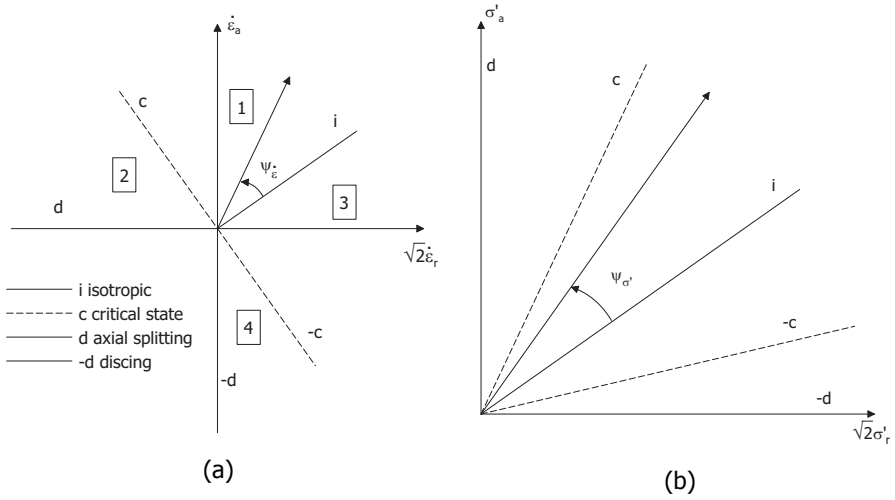

Figure A.4: Definition of the angles $\psi_{\dot{\varepsilon}}$ (a) and (b) $\psi_{\sigma'}$

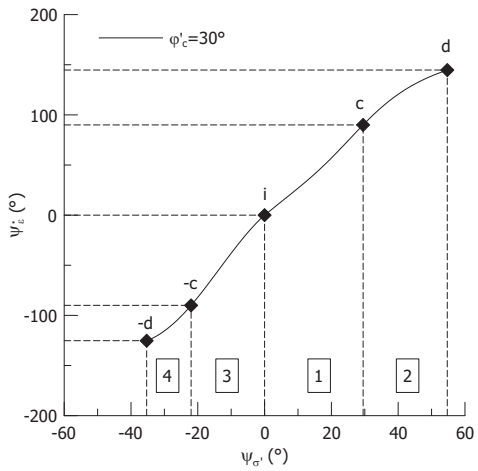

Figure A.5: Graphical representation of asymptotic strain rate-stress states for φ'_c=30°

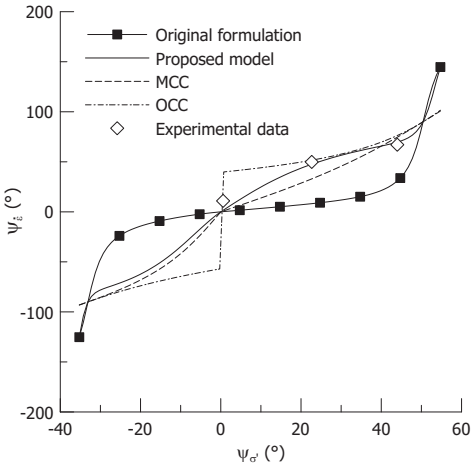

Figure A.6: Asymptotic strain rate directions for the proposed and original model compared with the experimental results

Significant improvement is obtained by adopting the equation A.11 for the asymptotic strain rate direction with respect to the original hypoplastic formulation, equation A.10, which was calibrated on clays. Having defined the asymptotic states through the ASBS and the ASRD, the hypoplastic model requires the calibration of the 5 basic parameters: φ_c', λ^*, κ^*, N, ν and of the additional parameters ϑ_c^*, ζ and α_f (see the Appendix).

A.6. MODEL RESULTS

The capabilities of the model have been tested in two steps. Firstly, the multiple stress paths performed on sample 1 and sample 2, other than the radial paths on which the asymptotic states had been determined, have been simulated to validate the formulation. Secondly, the model predictions have been compared to the experimental data from the other tested samples. The parameters used in the simulations are summarised in Table A.3. It is relevant to specify that the OCR in the model is defined with reference to the isotropic NCL line as $OCR{=}p_e'/p'$. A constant value of the parameter $\alpha_f{=}2$ has been used (instead of equation A.23 in the Appendix) as in Mašín (2013).

Table A.3: Parameters of the model used in the simulations

φ_c'	λ^*	κ^*	N	ν	ϑ_c^*	ζ	α_f
64°	0.26	0.032	3.005	0.2	2.2	1.8	2.0

It is worth noticing that in hypoplasticity the value of κ^* exactly represents the slope of the unloading line in the $ln\,(1+e)$-$ln(p'/p_r')$ plane upon unloading from the normally consolidated state. However, contrarily to classic elasto-plasticity, the

response is non-reversible inside the ASBS and the slope of the unloading line does not exactly correspond to κ^*. The value of κ^* adopted in the simulations (Table A.3) was thus calibrated back-analysing the results of the isotropic unloading path on sample 1 (Figure A.2).

A.6.1. Model performance

Simulations of the entire stress paths from sample 1 and sample 2 are shown in Figure A.7 and Figure A.8. The radial stress paths in Figure A.7(a) and Figure A.8(a) were used to define the asymptotic states, which implies the very good agreement between the experimental data and the model simulations. The agreement is also quite good on the subsequent stress paths, involving different deviatoric stresses. Over the final portion of the test, the model appears to respond stiffer than the soil tested. In general, the hypoplastic formulation allows a satisfactory prediction of the pre-failure behaviour over various loading directions.

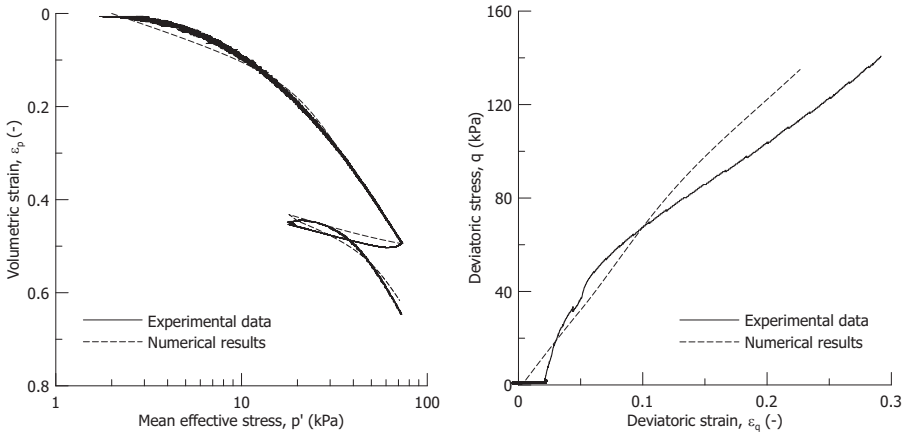

Figure A.7: Comparison between the experimental results and the model simulations for sample 1 in terms of (a) volumetric response and (b) deviatoric response

The underestimation of the deviatoric strain for a given deviatoric stress increases with the strain level. Furthermore, the hysteric behaviour observed in the experimental tests with cycles of isotropic (Figure A.7(a)) and deviatoric loading and unloading (Figure A.8(b)) is not properly captured by the adopted model. Intergranular strain concept developed by Niemunis & Herle (1997) could be introduced to account for this effect, but this is out of the primary scope of this paper.

A.6.2. Model predictions: drained triaxial compression tests

To further test the model capabilities, the results of the tests on sample 3 and sample 4 are analysed, where complex stress conditions have been applied with multiples traits of volumetric and deviatoric stress paths.

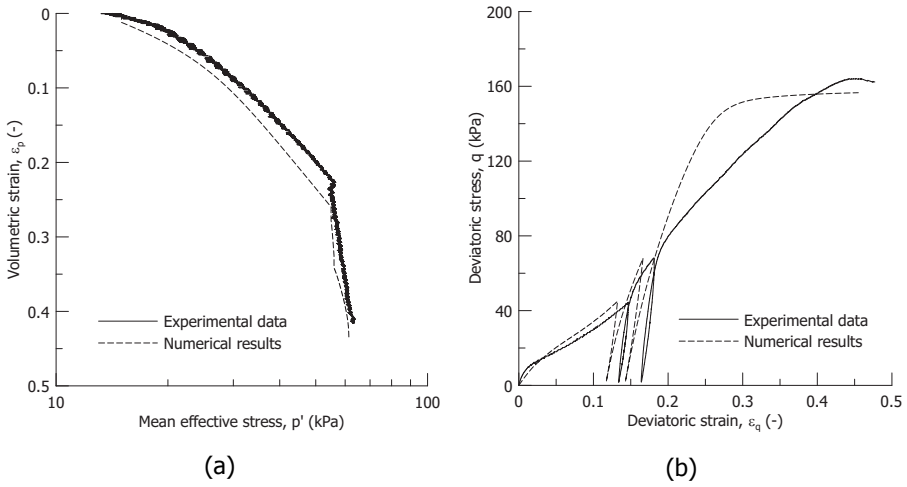

Figure A.8: Comparison between the experimental results and the model simulations for sample 2 in terms of (a) volumetric response and (b) deviatoric response

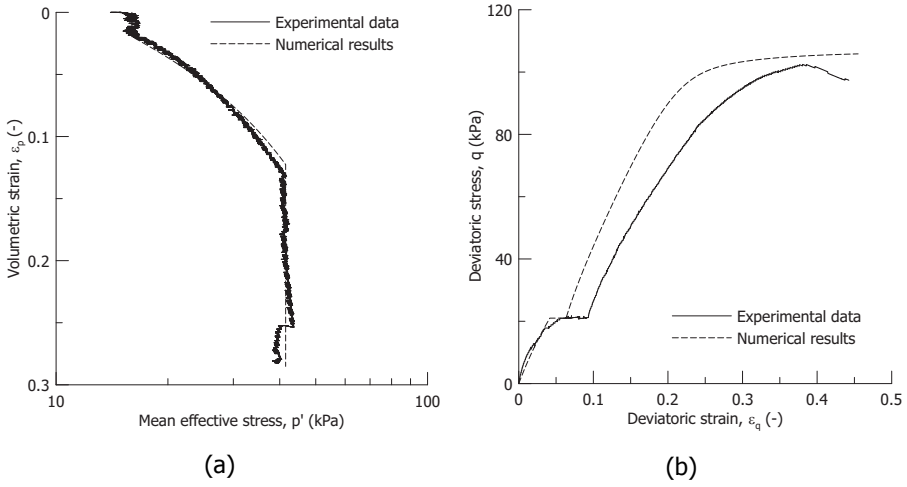

Figure A.9: Comparison between the experimental results and the model simulations for sample 3 in terms of (a) volumetric response and (b) deviatoric response

The comparisons in Figure A.9 and Figure A.10 confirm the previous considerations, with good agreement on the volumetric stress-strain response and less satisfactory simulation of the deviatoric response for high strain levels. The limitations of the adopted model in describing the cyclic response are magnified by the comparison on sample 4, with multiple cycles of deviatoric unloading-reloading.

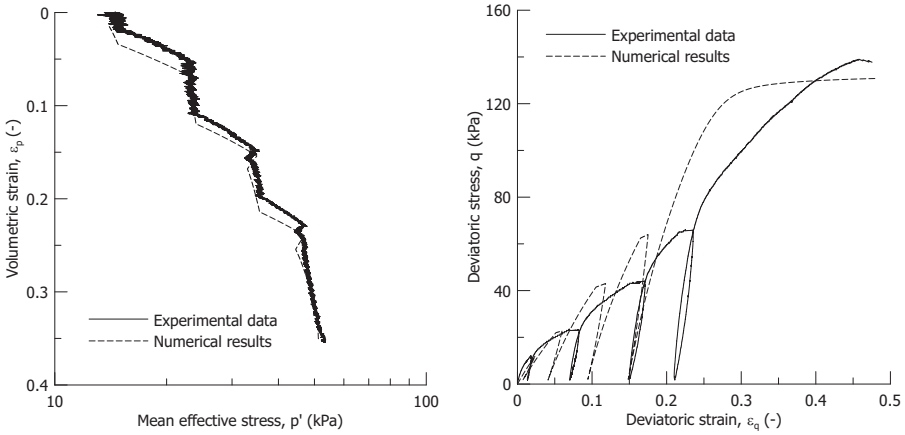

Figure A.10: Comparison between the experimental results and the model simulations for sample 4 in terms of (a) volumetric response and (b) deviatoric response

The experimental stress-dilatancy relationship is compared with the model predictions for non-proportional deformation paths in Figure A.11. Different stress paths are considered. Figure A.11(a) reports the comparison between the experimental data and the model prediction on the last p' constant trait applied to the sample 2, while Figure A.11(b) shows the same for the q constant and the p' constant traits for sample 3. Following the hypoplastic approach, the strain increment direction is defined in terms of total strain increments (and not in plastic strain increments as in elastic-plastic models) as

$$\tan\beta = \frac{\delta\varepsilon_q}{\delta\varepsilon_p} \tag{A.12}$$

where the $\delta\varepsilon_q$ and $\delta\varepsilon_p$ are the increment in the deviatoric and volumetric total strain respectively.
The adopted asymptotic strain rate direction relationship (Figure A.6) well matches the experimental results even for non-proportional strain paths as the ones in Figure A.11(a) and Figure A.11(b), and supports the adoption of the hypoplastic formulation for peat behaviour under complex loading conditions.

A.6.3. Model predictions: undrained triaxial compression tests

The model capabilities are further tested against the experimental results from undrained triaxial compression tests performed on sample 5, sample 6 and sam-

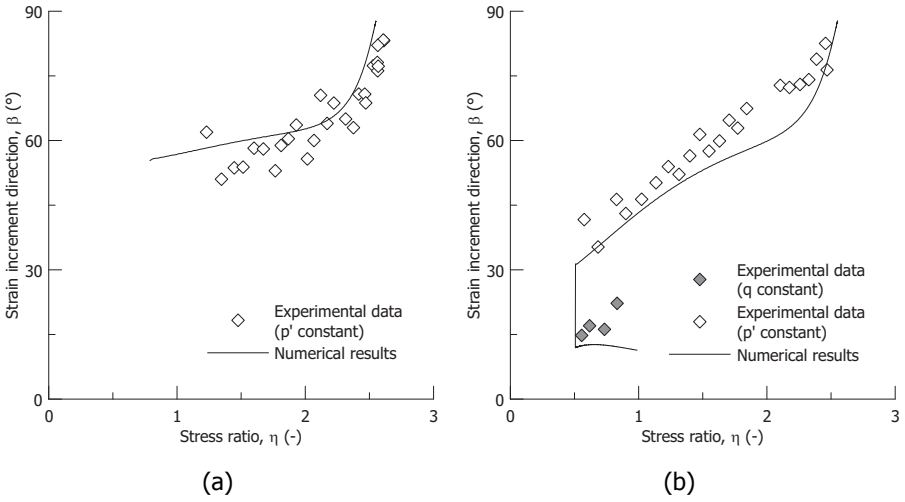

Figure A.11: Strain increment directions obtained from multiple stress paths from (a) sample 2 and (b) from sample 3 compared to the model simulations

ple 7, for three different values of OCR. The numerical predictions are compared with the experimental data in Figure A.12 in terms of stress-path and deviatoric stress-strain response. It is worth noting that the samples tested in undrained conditions, failed at a stress ratio slightly lower than the one reached in drained compression. This difference, already observed in Zhang & O'Kelly (2014), is most probably due to the different geometrical constraints imposed in the two types of tests (Drescher & Vardoulakis, 1982).

The agreement between the stress-strain curve is qualitatively good. However, the numerical results suffer of an incorrect prediction of the initial portion of the undrained stress path, particularly for tests on normally consolidated soils at isotropic stress states as already stated by Niemunis (2003), Huang et al. (2006) and Mašín & Herle (2007). To overcome this limitation, the approach proposed by Mašín & Herle (2007) has been adopted in the proposed model by rewriting equation A.3 as

$$\mathring{\boldsymbol{\sigma}} = f_s(\boldsymbol{L^D} : \dot{\boldsymbol{\varepsilon}} + w_y f_d \boldsymbol{N} \|\dot{\boldsymbol{\varepsilon}}\|) \tag{A.13}$$

where the weighting factor has been defined as

$$w_y = \left[\frac{\sin(\varphi'_m)}{\sin(\varphi'_c)}\right]^{\varsigma} \tag{A.14}$$

For mobilised friction angle higher than the critical state friction angle, $sin(\varphi'_m) > sin(\varphi'_c)$, w_y=1. The model requires an additional parameter ς which controls the shape of the initial portion of the undrained stress path. The new hypoelastic tensor $\boldsymbol{L^D}$ is reported in the Appendix. It is worth remarking that the effect of this correction

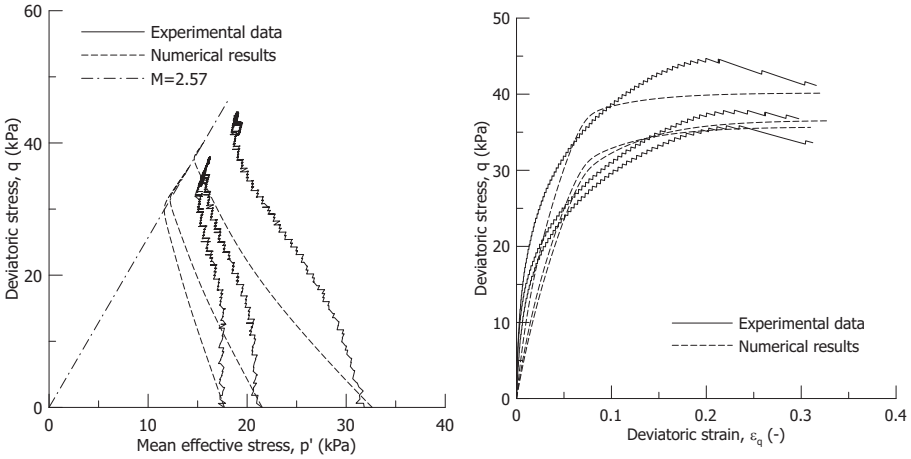

Figure A.12: Comparison between the experimental results and the model simulations for sample 5, 6 and 7 in terms of (a) stress path and (b) deviatoric response

vanishes for increasing deviatoric stress as for the drained tests and increasing OCR. Figure A.13 reports the numerical results for the case of undrained triaxial tests by adopting ς=1. The remaining parameters are the same as in Table A.3.
The results in Figure A.13 shows the benefit of the new approach in the predicted stress path thus resulting in a lower development of excess pore pressure upon undrained compression compared to the result in Figure A.12 despite a slightly more rigid stress-strain response.

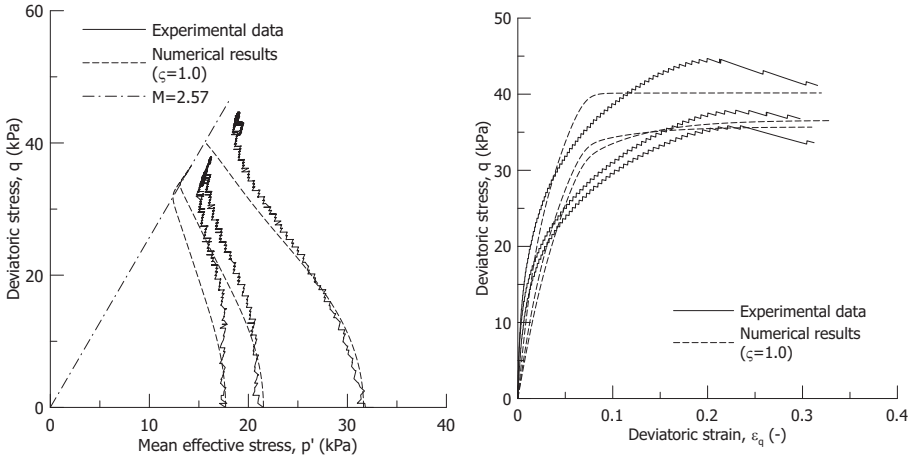

Figure A.13: Comparison between the experimental results and the model simulations for sample 5, 6 and 7 in terms of (a) stress path and (b) deviatoric response by adopting the new hypoelastic tensor $\boldsymbol{L^D}$ and ς=1

A.7. SUMMARY AND CONCLUSIONS

A first attempt of modelling the behaviour of reconstituted peat in the framework of hypoplasticity has been proposed. The formulation is based on an existing model originally developed for clays, which has been adapted to properly account for the peculiar characteristics of peat: a material with an extremely high deformability and exceptionally high friction angle. An advanced laboratory investigation was carried out to define explicitly the constitutive ingredients of the hypoplastic model. Non-standard drained triaxial compression tests were chosen, in which multiple stress paths were applied to the samples, allowing to validate the adopted model on a variety of loading directions. The results confirm the capability of hypoplasticity to capture fundamental aspects of the pre-failure behaviour of peats such as the non-linearity inside the state boundary surface and the directional response. The model represents a robust base suitable for further developments and enhancements, such as introduction of anisotropy and creep. The modelling exercise highlights that peats behave differently from clays, although they are frequently associated into the broad category of "soft soils". Both the shape of the ASBS and the ASRD indicate a predominant role of the deviatoric stress-strain components on the yielding of peats compared with their volumetric counterparts, which distinguish the behaviour of peats from that of clays.

A.8. APPENDIX

The entire set of equations needed in the model formulation are listed herein. Further details are reported in Mašín (2013) and Mašín (2014).

$$\mathring{\boldsymbol{\sigma}} = f_s \boldsymbol{L} : \dot{\boldsymbol{\varepsilon}} - \frac{f_d}{f_d^A} \boldsymbol{A} : \boldsymbol{d} |\dot{\boldsymbol{\varepsilon}}| \tag{A.15}$$

with

$$\boldsymbol{L} = \boldsymbol{I} + \frac{\nu}{1-2\nu} \mathbf{1} \otimes \mathbf{1} \tag{A.16}$$

$$\boldsymbol{A} = f_s \boldsymbol{L} + \frac{\boldsymbol{\sigma}}{\lambda^*} \otimes \mathbf{1} \tag{A.17}$$

$$f_d = \left(\frac{\vartheta_c^* p'}{p'_e} \right)^{\alpha_f} \tag{A.18}$$

$$f_s = \frac{3p'}{2} \left(\frac{1}{\lambda^*} + \frac{1}{\kappa^*} \right) \frac{1-2\nu}{1+\nu} \tag{A.19}$$

$$p'_e = p'_r \exp\left[\frac{N - \ln(1+e)}{\lambda^*} \right] \tag{A.20}$$

where $\mathbf{1}$ and $\boldsymbol{I}$ are the second and the fourth order unity tensors, λ^* is the slope of the isotropic normally consolidated line, κ^* is the slope of the isotropic unloading line for unloading starting from the isotropic normally consolidated state and ν is the parameter controlling the proportion of bulk and shear stiffness. p'_e is the Hvorslev's equivalent pressure on the isotropic normal compression line with N defining the position of the normal compression line and p'_r is a reference pressure of 1 kPa. The position of the critical state line on the asymptotic state boundary surface (ASBS) is specified as in Ragni et al. (2016) through

$$\frac{p'_e}{p'_{cr}} = \vartheta_c^* \tag{A.21}$$

Note that for ϑ_c^*=2 the original model is recovered. The non-linear response inside the ASBS is governed by the factor f_d. The value f_d^A needed in equation A.15 is computed by combining equation A.18 with the explicit ASBS formulation to give

$$f_d^A = \vartheta_c^{*\alpha_f} \left(1 - F_m\right)^{\alpha_f/\omega} \tag{A.22}$$

where α_f can be considered as a model parameter controlling the non-linear response inside the asymptotic state boundary surface. Mašín (2005) and Mašín (2014) suggested

$$\alpha_f = \frac{\ln\left[\frac{\lambda^* - \kappa^*}{\lambda^* + \kappa^*} \left(\frac{3 + a_f^2}{a_f \sqrt{3}} \right) \right]}{\ln \vartheta_c^*} \tag{A.23}$$

A

$$a_f = \frac{\sqrt{3}\,(3 - \sin\varphi_c')}{2\sqrt{2}\sin\varphi_c'} \tag{A.24}$$

The shape of the ASBS is controlled by the parameters ω

$$\omega = -\frac{\ln\left(\cos\left(\varphi_c'\right)^2\right)}{\ln\vartheta_c^*} + a\left(F_m - \sin\left(\varphi_c'\right)^2\right) \tag{A.25}$$

with a=2.1 for the case of the tested peat and with F_m the Matsuoka-Nakai factor defined as

$$F_m = \frac{9I_3 + I_1 I_2}{I_3 + I_1 I_2} \tag{A.26}$$

The stress invariants and the Lode's angle are defined as

$$I_1 = \mathrm{tr}\boldsymbol{\sigma} \tag{A.27}$$

$$I_2 = \frac{1}{2}\left(\boldsymbol{\sigma} : \boldsymbol{\sigma} - I_1^2\right) \tag{A.28}$$

$$I_3 = \det\boldsymbol{\sigma} \tag{A.29}$$

Finally, the asymptotic strain rate direction $\boldsymbol{d}$ is calculated as

$$\boldsymbol{d} = \frac{\boldsymbol{d^A}}{\|\boldsymbol{d^A}\|} \tag{A.30}$$

where

$$\boldsymbol{d^A} = -\hat{\boldsymbol{\sigma}}^* + \mathbf{1}\left[\frac{2}{3} - \frac{\cos 3\theta + 1}{4}F_m^{1/4}\right]\frac{F_m^{\xi/2} - \sin\left(\varphi_c'\right)^{\xi}}{1 - \sin\left(\varphi_c'\right)^{\xi}} \tag{A.31}$$

with θ the Lode's angle and $\hat{\boldsymbol{\sigma}}^*$ the normalised deviatoric stress defined as

$$\cos 3\theta = -\sqrt{6}\frac{\mathrm{tr}\left(\hat{\boldsymbol{\sigma}}^* \cdot \hat{\boldsymbol{\sigma}}^* \cdot \hat{\boldsymbol{\sigma}}^*\right)}{\left[\hat{\boldsymbol{\sigma}}^* : \hat{\boldsymbol{\sigma}}^*\right]^{3/2}} \tag{A.32}$$

$$\hat{\boldsymbol{\sigma}}^* = \frac{\boldsymbol{\sigma}}{\mathrm{tr}\boldsymbol{\sigma}} - \frac{1}{3} \tag{A.33}$$

The coefficient ξ in equation A.31, originally defined by Mašín (2013), has been modified by introducing the exponent ζ equals to 1.8 based on the experimental results

$$\xi = \left[1.7 + 3.9\sin(\varphi_c')^2\right]^{\zeta} \tag{A.34}$$

For the undrained triaxial compression tests, the hypoplastic formulation in equation A.14 has been modified according to the approach proposed by Mašín & Herle (2007) as

$$\mathring{\boldsymbol{\sigma}} = f_s(\boldsymbol{L^D} : \dot{\boldsymbol{\varepsilon}} + w_y f_d \boldsymbol{N} \|\dot{\boldsymbol{\varepsilon}}\|) \tag{A.35}$$

where the weighting factor has been defined as

$$w_y = \left[\frac{\sin\left(\varphi'_m\right)}{\sin\left(\varphi'_c\right)}\right]^{\varsigma} \tag{A.36}$$

The hypoelastic tensor $\boldsymbol{L^D}$ is now dependent on the direction of stretching (with respect to $\boldsymbol{d}$) through

$$\boldsymbol{L^D} = \begin{cases} f_s \boldsymbol{L} - \frac{f_d}{f_d^A}(1 - w_y)(\boldsymbol{A} : \boldsymbol{d}) \otimes \boldsymbol{d}, & \text{for } \boldsymbol{d} : \dot{\boldsymbol{\varepsilon}} > 0 \\ f_s \boldsymbol{L} + \frac{f_d}{f_d^A}(1 - w_y)(\boldsymbol{A} : \boldsymbol{d}) \otimes \boldsymbol{d}, & \text{for } \boldsymbol{d} : \dot{\boldsymbol{\varepsilon}} \leq 0 \end{cases} \tag{A.37}$$

B

Calibration of the triaxial equipment

B.1. CALIBRATION OF THE TRIAXIAL EQUIPMENT

Calibration of the triaxial equipment has been conducted before each laboratory campaign. The calibration involved:

- calibration of the pressure/volume transducers;
- deformability of the triaxial apparatus which includes the triaxial cell and all the connections.

B.1.1. 1st calibration cell 2

The cell 2 has been calibrated on the 21st May 2014 in correspondence with the beginning of the triaxial tests on gassy peat samples. The volume displayed from the cell pressure/volume controller during the loading and unloading pressure ramp with a steel dummy sample is reported in Figure B.1.

B.1.2. 2nd calibration cell 2

The pressure/volume controllers and the pore pressure transducer of the cell 2 have been calibrated on the 17th June 2015 in correspondence with the beginning of a series of triaxial tests on reconstituted peat samples as reported in Figure B.2.

B.1.3. 3rd calibration cell 2

The cell 2 has been calibrated on the 27th February 2017 in correspondence with the beginning of a second series of triaxial tests on gassy peat samples. The volume displayed from the cell pressure/volume controller during the loading and unloading pressure ramp with a steel dummy sample is reported in Figure B.3. The calibration of the cell pressure/volume controller, back pressure/volume controller and the pore pressure transducers is reported in Figure B.4.

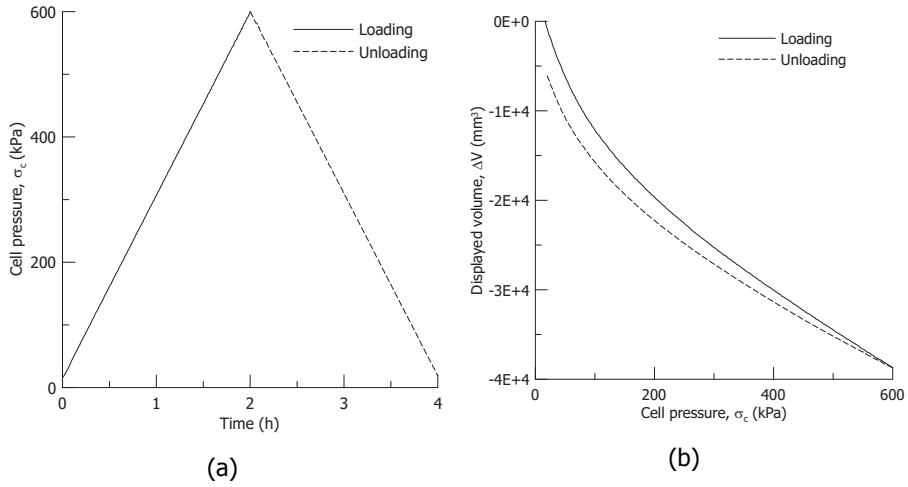

Figure B.1: 1st calibration cell 2: (a) imposed cell pressure history and (b) displayed volume change

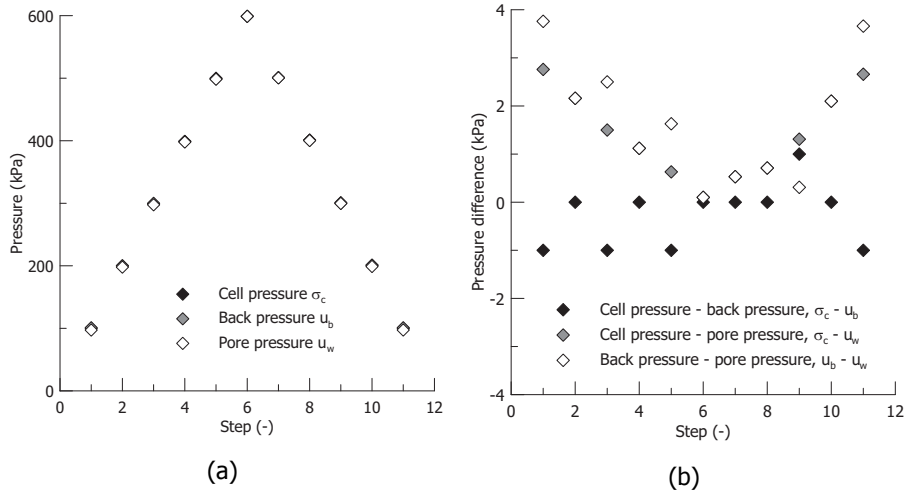

Figure B.2: 2nd calibration cell 2: (a) imposed cell pressure history and (b) displayed pressure differences

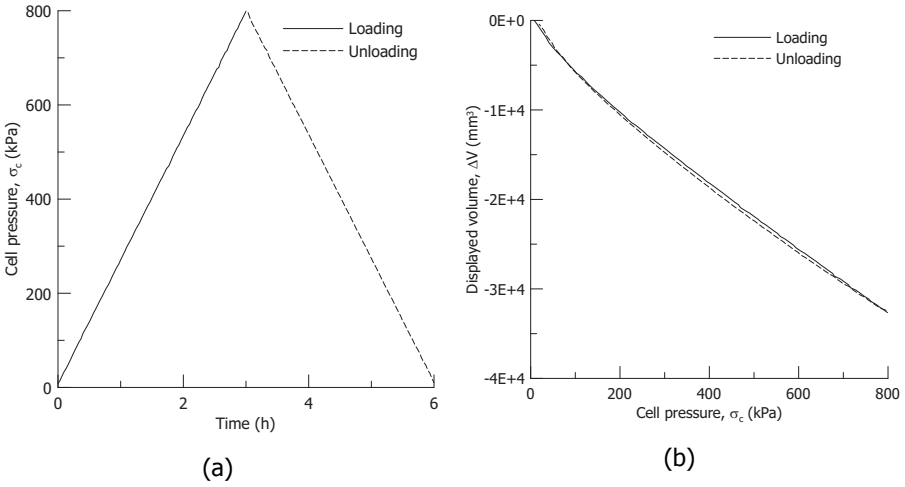

Figure B.3: 3rd calibration cell 2: (a) imposed cell pressure history and (b) displayed volume change

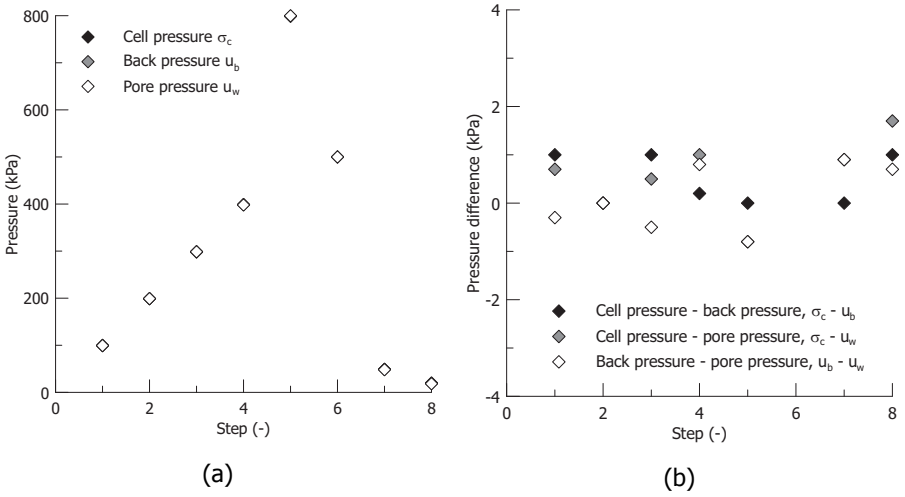

Figure B.4: 3rd calibration cell 2: (a) imposed cell pressure history and (b) displayed pressure differences

References

Acharya, M. P., Hendry, M. T., & Edwards, T. (2015). A case study of the long-term deformation of peat beneath an embankment structure. In *From Fundamentals to Applications in Geotechnics: Proceedings of the 15th Pan-American Conference on Soil Mechanics and Geotechnical Engineering* (pp. 438–446). IOS Press.

Acharya, M. P., Hendry, M. T., & Martin, C. D. (2016a). Effect of gas bubbles on pore pressure response in peat beneath a railway embankment. *Canadian Geotechnical Journal*, *53*, 765–772.

Acharya, M. P., Hendry, M. T., & Martin, C. D. (2016b). Thermally induced pore pressure response in peat beneath a railway embankment. *International Journal of Geotechnical Engineering*, *10*, 145–154.

Acharya, M. P., Hendry, M. T., & Martin, C. D. (2017). Creep behaviour of intact and remoulded fibrous peat. *Acta Geotechnica*, *13*, 399–417.

Adams, J. I. (1961). Laboratory compression tests on peat. In *7th Muskeg Research Conference* (p. 36–54). NCR volume 71.

Airey, D. W. (1984). *Clays in circular simple shear apparatus*. PhD thesis University of Cambridge.

Airey, D. W. (1991). Finite element analyses of triaxial tests with different end and drainage conditions. In Beer, Booker, & Carter (Eds.), *Proceedings of the 7th International Conference on Computer Methods and Advances in Geomechanics* (pp. 225–230). Balkema volume 1.

Al-Tabbaa, A., & Wood, D. M. (1989). An experimentally based bubble model for clay. In *Proceedings of the 3rd International Symposium on Numerical Models in Geomechanics NUMOG III* (pp. 91–99). Elsevier Applied Science.

Alonso, E. E., Gens, A., & Josa, A. (1990). A constitutive model for partially saturated soils. *Géotechnique*, *40*, 405–430.

Amaratunga, A., & Grozic, J. L. H. (2009). On the undrained unloading behaviour of gassy sands. *Canadian Geotechnical Journal*, *46*, 1267–1276.

Anagnostopoulos, C. A., Tzetzis, D., & Berketis, K. (2014). Shear strength behaviour of polypropylene fibre reinforced cohesive soils. *Geomechanics and Geoengineering: An International Journal*, *9*, 241–251.

Andersland, O. B., Khattak, A. S., & Al-Khafaji, A. W. N. (1981). Effect of organic material on soil shear strength. In *Laboratory shear strength of soil* (pp. 226–242). ASTM International STP 740.

Appelo, C. A. J., & Postma, D. (2005). *Geochemistry, groundwater and pollution*. (2nd ed.). CRC press.

Arthur, J. R. F., Dunstan, T., Al-Ani, Q. A. J. L., & Assadi, A. (1977). Plastic deformation and failure in granular media. *Géotechnique*, *27*, 53–74.

Asaoka, A., Nakano, M., & Noda, T. (1994). Soil-water coupled behaviour of saturated clay near/at critical state. *Soils and foundations*, *34*, 91–105.

Asaoka, A., Nakano, M., & Noda, T. (1995). Annealable behaviour of saturated clay: an experiment and simulation. *Soils and foundations*, *35*, 9–20.

Atkins, P., & De Paula, J. (2014). *Physical Chemistry: Thermodynamics, Structure, and Change*. (10th ed.). Oxford University press, UK.

Baird, A. J., & Waldron, S. (2003). Shallow horizontal groundwater flow in peatlands is reduced by bacteriogenic gas production. *Geophysical Research Letters*, *30*, 1–4.

Barden, L., & McDermott, J. W. (1965). Use of free ends in triaxial testing of clays. *Journal of the Soil Mechanics and Foundations Division*, *91*, 1–23.

Becker, D. E., Crooks, J. H. A., Been, K., & Jefferies, M. G. (1987). Work as a criterion for determining in situ and yield stresses in clays. *Canadian Geotechnical Journal*, *24*, 549–564.

Beckwith, C. W., & Baird, A. J. (2001). Effect of biogenic gas bubbles on water flow through poorly decomposed blanket peat. *Water Resources Research*, *37*, 551–558.

Berry, P. L., & Poskitt, T. J. (1972). The consolidation of peat. *Géotechnique*, *22*, 27–52.

Berry, P. L., & Vickers, B. (1975). Consolidation of fibrous peat. *Journal of the Geotechnical Engineering Division*, *101*, 741–753.

Bishop, A. W., & Green, G. E. (1965). The influence of end restraint on the compression strength of a cohesionless soil. *Géotechnique*, *15*, 243–266.

Blight, G. E. (1963). The effect of nonuniform pore pressures on laboratory measurements of the shear strength of soils. In *Laboratory shear testing of soils* (pp. 173–184). ASTM International volume ASTM STP 361.

Blight, G. E. (1965). Shear stress and pore pressure in triaxial testing. *Journal of the Soil Mechanics and Foundations Division*, *91*, 25–40.

Boulanger, R. W., Arulnathan, R., Harder Jr, L. F., Torres, R. A., & Driller, M. W. (1998). Dynamic properties of Sherman Island peat. *Journal of Geotechnical and Geoenvironmental engineering*, *124*, 12–20.

Boumezerane, D. (2014). Modeling unloading/reloading in peat using a kinematic bubble model. In Hicks, Brinkgreve, & Rohe (Eds.), *Numerical Methods in Geotechnical Engineering* (pp. 9–14). Taylor and Francis Group London volume 1.

Boumezerane, D., Makdisi, A., & Grimstad, G. (2015). A framework for peat behaviour based on hyperplasticity principles. In *Creep and Deformation Characteristics in Geomaterials* (pp. 1–4).

Brown, A., Mathur, S. P., & Kushner, D. J. (1989). An ombrotrophic bog as a methane reservoir. *Global Biogeochemical Cycles*, *3*, 205–213.

Budhu, M. (1984). Nonuniformities imposed by simple shear apparatus. *Canadian Geotechnical Journal*, *21*, 125–137.

Budhu, M. (1988). Failure state of a sand in simple shear. *Canadian Geotechnical Journal*, *25*, 395–400.

Butterfield, R. (1979). A natural compression law for soils. *Géotechnique*, *29*, 469–480.

Buttler, A. J., Dinel, H., Lévesque, M., & Mathur, S. P. (1991). The relation between movement of subsurface water and gaseous methane in a basin bog with a novel instrument. *Canadian Journal of Soil Science*, *71*, 427–438.

Calabresi, G. (1968). Deformazioni plastiche di una terra argillosa. *Riv. Ital. Geotec*, *12*, 27–35.

Carter, J. P. (1982). Predictions of the non-homogeneous behaviour of clay in the triaxial test. *Géotechnique*, *32*, 55–58.

Charlier, R. (1987). *Approche unifiée de quelques problèmes non linéaires de mécanique des milieux continus par la méthode des éléments finis (grandes déformations des métaux et des sols, contact unilatéral de solides, conduction thermique et écoulements en milieu poreux)*. PhD thesis Université de Liège.

Chatzis, K. (2018). *Advances in modelling the deviatoric response of peat*. MSc thesis Delft University of Technology.

Cheng, X. H., Ngan-Tillard, D. J. M., & Den Haan, E. J. (2007). The causes of the high friction angle of Dutch organic soils. *Engineering geology*, *93*, 31–44.

Cola, S., & Cortellazzo, G. (2005). The shear strength behavior of two peaty soils. *Geotechnical and Geological Engineering*, *23*, 679–695.

Cotecchia, F., & Chandler, R. (2000). A general framework for the mechanical behaviour of clays. *Géotechnique*, *50*, 431–448.

Cotecchia, F., & Chandler, R. J. (1997). The influence of structure on the pre-failure behaviour of a natural clay. *Géotechnique*, *47*, 523–544.

D1997-13 (2013). Standard test method for laboratory determination of fiber content of peat samples by dry mass. *American Society of Testing and Materials ASTM*, *PA, USA*.

D2974-14 (2014). Standard test methods for moisture, ash, and organic matter of peat and other organic soils. *American Society of Testing and Materials ASTM*, *PA, USA*.

D5550-14 (2014). Standard test method for specific gravity of soil solids by gas pycnometer. *American Society of Testing and Materials ASTM*, *PA, USA*.

De Vries, G., & De Bruijn, H. T. J. (2014). Dijken op veen II factual report laboratorium- engrondonderzoek. *Deltares*, *1208254-015*, 1–1466.

Den Haan, E. J. (1996). A compression model for non-brittle soft clays and peat. *Géotechnique*, *46*, 1–16.

Den Haan, E. J. (2014). Modelling peat with an anisotropic time-dependent model for clay. In Hicks, Brinkgreve, & Rohe (Eds.), *Numerical Methods in Geotechnical Engineering* (pp. 55–60). Taylor and Francis Group.

Den Haan, E. J., & Edil, T. B. (1994). Secondary and tertiary compression of peat. In D. Haan, Termaat, & Edil (Eds.), *Proceedings of Advances in Understanding and Modelling the Mechanical Behaviour of Peat* (pp. 49–60). Balkema, Rotterdam.

Den Haan, E. J., & Feddema, A. (2013). Deformation and strength of embankments on soft Dutch soil. *Proceedings of the Institution of Civil Engineers-Geotechnical engineering*, *166*, 239–252.

Den Haan, E. J., & Grognet, M. (2014). A large direct simple shear device for the testing of peat at low stresses. *Géotechnique Letters*, *4*, 283–288.

Den Haan, E. J., & Kruse, G. A. M. (2007). Characterisation and engineering properties of Dutch peats. In *Proceedings of the Second International Workshop of Characterisation and Engineering Properties of Natural Soils* (pp. 2101–2133). volume 29.

Diambra, A., & Ibraim, E. (2014). Modelling of fibre–cohesive soil mixtures. *Acta Geotechnica*, *9*, 1029–1043.

Diambra, A., Ibraim, E., Russell, A. R., & Wood, D. M. (2013). Fibre reinforced sands: from experiments to modelling and beyond. *International Journal for Numerical and Analytical Methods in Geomechanics*, *37*, 2427–2455.

Diambra, A., Ibraim, E., Wood, D. M., & Russell, A. R. (2010). Fibre reinforced sands: experiments and modelling. *Geotextiles and geomembranes*, *28*, 238–250.

Dinel, H., Mathur, S. P., Brown, A., & Lévesque, M. (1988). A field study of the effect of depth on methane production in peatland waters: equipment and preliminary results. *The Journal of Ecology*, *76*, 1083–1091.

Drescher, A., & Vardoulakis, I. (1982). Geometric softening in triaxial tests on granular material. *Géotechnique*, *32*, 291–303.

Duncan, J. M., & Dunlop, P. (1968). The significance of cap and base restraint in strength tests on soils. *Journal of the Soil Mechanics and Foundations Division*, *94*, 271–290.

Edil, T. B., & Dhowian, A. W. (1981). At-rest lateral pressure of peat soils. *Journal of Geotechnical and Geoenvironmental Engineering*, *107*, 201–217.

Edil, T. B., Fox, P. J., & Lan, L. T. (1994). Stress-induced one-dimensional creep of peat. In D. Haan, Termaat, & Edil (Eds.), *Advances in Understanding and Modelling the Mechanical Behaviour of Peat* (pp. 3–18). Balkema, Rotterdam.

Edil, T. B., & Wang, X. (2000). Shear strength and K0 of peats and organic soils. In *Geotechnics of high water content materials* (pp. 209–225). ASTM International.

Ehrgott, J. Q. (1971). *Calculation of stress and strain from triaxial test data on undrained soil specimens*. Report Army engineer waterways experiment station.

Farrell, E. R., & Hebib, S. (1998). The determination of the geotechnical parameters of organic soils. In Yanagisawa, Moroto, & Mitachi (Eds.), *Proceedings of International Symposium on problematic soils* (pp. 33–36). Balkema, Rotterdam, The Netherlands volume 98.

Feda, J., Boháč, J., & Herle, I. (1993). End restraint in triaxial testing of soils. *Acta Technica CSAV*, *38*, 197–220.

Fox, P. J., & Edil, T. B. (1996). Effects of stress and temperature on secondary compression of peat. *Canadian Geotechnical Journal*, *33*, 405–415.

Fox, P. J., Edil, T. B., & Lan, L. T. (1992). Cα/Cc concept applied to compression of peat. *Journal of geotechnical engineering*, *118*, 1256–1263.

de Gast, T. (2019). *Dykes and Embankments: a Geostatistical Analysis of Soft Terrain*. PhD thesis Delft University of Technology.

Gens, A. (1996). Constitutive modelling: application to compacted soils. In Alonso, & Delage (Eds.), *Proceedings of the first international conference on unsaturated soils* (pp. 1179–1200). Balkema: The Netherlands volume 3.

Gens, A., & Nova, R. (1993). Conceptual bases for a constitutive model for bonded soils and weak rocks. In Anagnostopoulos (Ed.), *Geotechnical Engineering of Hard Soils-Soft Rocks* (pp. 577–583). Balkema: Rotterdam.

Gens, A., & Potts, D. M. (1982). A theoretical model for describing the behaviour of soils not obeying Rendulic's principle. In *Proceedings of the International Symposium on Numerical Models in Geomechanics* (pp. 24–32).

Gens, A., & Potts, D. M. (1988). Critical state models in computational geomechanics. *Engineering Computations*, *5*, 178–197.

Germaine, J. T., & Ladd, C. C. (1988). Triaxial testing of saturated cohesive soils. In Donaghe, Chaney, & Silver (Eds.), *Advanced Triaxial Testing of Soil and Rock* (pp. 421–459). ASTM.

Gibson, R. E., & Henkel, D. J. (1954). Influence of duration of tests at constant rate of strain on measured "drained" strength. *Géotechnique*, *4*, 6–15.

Glaser, P. H., Chanton, J. P., Morin, P., Rosenberry, D. O., Siegel, D. I., Ruud, O., Chasar, L. I., & Reeve, A. S. (2004). Surface deformations as indicators of deep ebullition fluxes in a large northern peatland. *Global Biogeochemical Cycles*, *18*, 1–15.

Grozic, J. L. H., Nadim, F., & Kvalstad, T. J. (2005). On the undrained shear strength of gassy clays. *Computers and Geotechnics*, *32*, 483–490.

Grozic, J. L. H., Robertson, P. K., & Morgenstern, N. R. (1999). The behavior of loose gassy sand. *Canadian Geotechnical Journal*, *36*, 482–492.

Grozic, J. L. H., Robertson, P. K., & Morgenstern, N. R. (2000). Cyclic liquefaction of loose gassy sand. *Canadian Geotechnical Journal*, *37*, 843–856.

Gudehus, G. (1996). A comprehensive constitutive equation for granular materials. *Soils and foundations*, *36*, 1–12.

Gudehus, G. (2011). *Physical soil mechanics*. Springer Science and Business Media.

Gudehus, G., & Mašín, D. (2009). Graphical representation of constitutive equations. *Géotechnique*, *59*, 147–151.

Hayashi, H., Yamazoe, N., Mitachi, T., Tanaka, H., & Nishimoto, S. (2012). Coefficient of earth pressure at rest for normally and overconsolidated peat ground in Hokkaido area. *Soils and Foundations*, *52*, 299–311.

Head, K. H. (2014). *Manual of soil laboratory testing – Vol. I: Soil classification and compaction tests*. Dunbeath, UK: Whitteles Publishing.

Head, K. H., & Epps, R. J. (2014a). *Manual of soil laboratory testing – Vol. II: Permeability, shear Strength and compressibility tests*. Dunbeath, UK: Whitteles Publishing.

Head, K. H., & Epps, R. J. (2014b). *Manual of soil laboratory testing – Vol. III: Effective stress tests*. Dunbeath, UK: Whitteles Publishing.

Hencky, H. (1928). Über die form des elastizitätsgesetzes bei ideal elastischen stoffen. *Zeitschrift für technische Physik*, *6*, 215–220.

Hendry, M. T., Sharma, J. S., Martin, C. D., & Barbour, S. L. (2012). Effect of fibre content and structure on anisotropic elastic stiffness and shear strength of peat. *Canadian Geotechnical Journal*, *49*, 403–415.

Herle, I., & Kolymbas, D. (2004). Hypoplasticity for soils with low friction angles. *Computers and Geotechnics*, *31*, 365–373.

Hibbitt, D., Karlsson, B., & Sorensen, P. (2009). *ABAQUS standard user's manual, version 6.9-EF*. Pawtucket, RI, USA.

Hight, D. W., & Leroueil, S. (2003). Characterisation of soils for engineering purposes. In T. S. Tan, K. K. Phoon, D. W. Hight, & S. Leroueil (Eds.), *Characterisation and engineering properties of natural soils* (pp. 255–360). Balkema: The Netherlands volume 1.

Huang, W.-X., Wu, W., Sun, D.-A., & Sloan, S. (2006). A simple hypoplastic model for normally consolidated clay. *Acta Geotechnica*, *1*, 15–27.

Hueckel, T., & Pellegrini, R. (1996). A note on thermomechanical anisotropy of clays. *Engineering Geology*, *41*, 171–180.

Jaky, J. (1948). State of stress at great depth. In *Proceedings of the Second International Conference of Soil Mechanics and Foundation Engineering* (pp. 103–107).

Jeremić, B., Yang, Z. X., & Sture, S. (2004). Numerical assessment of the influence of end conditions on constitutive behavior of geomaterials. *Journal of engineering mechanics*, *130*, 741–745.

Jommi, C. (2000). Remarks on the constitutive modelling of unsaturated soils. In A. Tarantino, & C. Mancuso (Eds.), *Experimental evidence and theoretical approaches in unsaturated soils* (pp. 139–153). Balkema: Rotterdam.

Jommi, C., Muraro, S., Trivellato, E., & Zwanenburg, C. (2017). Evidences of the effects of free gas on the hydro-mechanical behaviour of peat. In Ferrari, & Laloui (Eds.), *Advances in Laboratory Testing and Modelling of Soils and Shales* (pp. 112–119). Springer.

Jommi, C., Muraro, S., Trivellato, E., & Zwanenburg, C. (2018). Experimental results on the influence of gas on the hydro-mechanical response of peats. *Géotechnique*, *https://doi.org/10.1680/jgeot.17.P.148*.

Kanmuri, H., Kato, M., Suzuki, O., & Hirose, E. (1998). Shear strength of K0 consolidated undisturbed peat. In E. Yanagisawa, N. Moroto, & T. Mitachi (Eds.), *Proc. of the Int. Symposium on Problematic Soils* (pp. 25–28). Balkema.

Kazemian, S., Prasad, A., Huat, B. B. K., & Barghchi, M. (2011). A state of art review of peat: geotechnical engineering perspective. *International journal of physical sciences*, *6*, 1974–1981.

Kellner, E., Price, J. S., & Waddington, J. M. (2004). Pressure variations in peat as a result of gas bubble dynamics. *Hydrological Processes*, *18*, 2599–2605.

Kellner, E., Waddington, J. M., & Price, J. S. (2005). Dynamics of biogenic gas bubbles in peat: potential effects on water storage and peat deformation. *Water Resources Research*, *41*, 1–12.

Kettridge, N., & Binley, A. (2008). X ray computed tomography of peat soils: Measuring gas content and peat structure. *Hydrological Processes*, *22*, 4827–4837.

Kirkpatrick, W. M., & Belshaw, D. J. (1968). On the interpretation of the triaxial test. *Géotechnique*, *18*, 336–350.

Kodaka, T., Higo, Y., Kimoto, S., & Oka, F. (2007). Effects of sample shape on the strain localization of water saturated clay. *International journal for numerical and analytical methods in geomechanics*, *31*, 483–521.

Koelewijn, A. R., Hoffmans, G. J. C. M., & Van Meindert, A. (2014). Lessons learned from a full-scale dyke failure test. In *International Conference on Case Histories in Geotechnical Engineering* (pp. 1–7).

Komatsu, J., Oikawa, H., Ogino, T., Tsushima, M., & Igarashi, M. (2011). Ring shear test on peat. In Chung, Hong, Langen, & Prinsenberg (Eds.), *The Twenty-first International Offshore and Polar Engineering Conference* (pp. 393–396). International Society of Offshore and Polar Engineers.

Ladd, C. C., & Edgers, L. (1972). *Consolidated-undrained direct-simple shear tests on saturated clays*. Report Department of Civil Engineering, Massachusetts Institute of Technology.

Lade, P. V. (2016). *Triaxial testing of soils*. Chichester, West Sussex, UK: John Wiley and Sons.

Lade, P. V., & Tsai, J. (1985). Effects of localization in triaxial tests on clay. In *11th International conference on soil mechanics and foundation engineering* (pp. 549–552). volume 2.

Lagioia, R., & Panteghini, A. (2014). The influence of the plastic potential on plane strain failure. *International Journal for Numerical and Analytical Methods in Geomechanics*, *38*, 844–862.

Landva, A. O. (2007). Characterisation of Escuminac peat and construction on peatland. In Tan, Phoon, Hight, & Leroueil (Eds.), *Proceedings of the Second International Workshop of Characterisation and Engineering Properties of Natural Soils* (pp. 2135–2191). Taylor and Francis Group volume 29.

Landva, A. O., & La Rochelle, P. (1983). Compressibility and shear characteristics of Radforth peats. In *Testing of peats and organic soils* (pp. 157–191). ASTM International.

Landva, A. O., & Pheeney, P. E. (1980). Peat fabric and structure. *Canadian Geotechnical Journal*, *17*, 416–435.

Le Lievre, B., & Poorooshasb, H. B. (1967). Strains in triaxial compression of normally consolidated clays. In *3rd Pan-American Conf. Soil Mech* (pp. 389–409).

Lee, K. L., & Seed, H. B. (1964). Discussion of "Importance of free ends in triaxial testing". *Journal of Soil Mechanics and Foundations Division*, *90*, 167–179.

Lefebvre, G., Langlois, P., Lupien, C., & Lavallée, J. G. (1984). Laboratory testing and in situ behaviour of peat as embankment foundation. *Canadian Geotechnical Journal*, *21*, 322–337.

Leoni, M., Karstunen, M., & Vermeer, P. (2008). Anisotropic creep model for soft soils. *Géotechnique*, *58*, 215–226.

Leoni, M., Karstunen, M., & Vermeer, P. (2010). Anisotropic creep model for soft soils (Discussion). *Géotechnique*, *60*, 963–966.

Lewin, P. I. (1973). The influence of stress history on the plastic potential. In *Proceedings of the Symposium on the Role of Plasticity in Soil Mechanics* (pp. 96–105).

Lewin, P. I., & Burland, J. B. (1970). Stress-probe experiments on saturated normally consolidated clay. *Géotechnique*, *20*, 38–56.

Li, C. (2005). *Mechanical response of fiber-reinforced soil*. PhD thesis University of Texas.

Li, X. S., & Dafalias, Y. F. (2000). Dilatancy for cohesionless soils. *Géotechnique*, *50*, 449–460.

Ludwik, P. (1909). *Elemente der technologischen Mechanik*. Springer-Verlag.

Lunne, T., Berre, T., Strandvik, S., Andersen, K. H., & Tjelta, T. I. (2001). Deepwater sample disturbance due to stress relief. In Aubeny, & Briaud (Eds.), *Proceedings of the 1st Annual Offshore Technology Conference* (pp. 64–85).

Macari-Pasqualino, E. J., Runesson, K., & Sture, S. (1994). Response prediction of granular materials at low effective stresses. *Journal of geotechnical engineering*, *120*, 1252–1268.

Madaschi, A., & Gajo, A. (2015a). Constitutive modelling of viscous behaviour of soils: a case study. *Geomechanics for Energy and the Environment*, *4*, 39–50.

Madaschi, A., & Gajo, A. (2015b). One-dimensional response of peaty soils subjected to a wide range of oedometric conditions. *Géotechnique*, *65*, 274–286.

Mašín, D. (2005). A hypoplastic constitutive model for clays. *International Journal for Numerical and Analytical Methods in Geomechanics*, *29*, 311–336.

Mašín, D. (2013). Clay hypoplasticity with explicitly defined asymptotic states. *Acta Geotechnica*, *8*, 481–496.

Mašín, D. (2014). Clay hypoplasticity model including stiffness anisotropy. *Géotechnique*, *64*, 232–238.

Mašín, D., & Herle, I. (2005). State boundary surface of a hypoplastic model for clays. *Computers and Geotechnics*, *32*, 400–410.

Mašín, D., & Herle, I. (2007). Improvement of a hypoplastic model to predict clay behaviour under undrained conditions. *Acta Geotechnica*, *2*, 261–268.

Matsuoka, H., & Nakai, T. (1974). Stress-deformation and strength characteristics of soil under three different principal stresses. In *Proceedings of the Japan Society of Civil Engineers* (pp. 59–70). Japan Society of Civil Engineers.

McDowell, G. R., & Hau, K. W. (2003). A simple non-associated three surface kinematic hardening model. *Géotechnique*, *53*, 433–437.

Mesri, G., & Ajlouni, M. (2007). Engineering properties of fibrous peats. *Journal of Geotechnical and Geoenvironmental Engineering*, *133*, 850–866.

Mesri, G., Stark, T. D., Ajlouni, M. A., & Chen, C. S. (1997). Secondary compression of peat with or without surcharging. *Journal of Geotechnical and Geoenvironmental Engineering*, *123*, 411–421.

Mitchell, R. J. (1972). Some deviations from isotropy in a lightly overconsolidated clay. *Géotechnique*, *22*, 459–467.

Molenkamp, F. (1994). Investigation of requirements for plane strain element tests on peat. In D. Haan, Termaat, & Edil (Eds.), *Advances in understanding and modeling the mechanical behaviour of peat* (pp. 181–202).

Molenkamp, F. (1998). Principle of axial shear apparatus. *Géotechnique*, *48*, 427–431.

Mori, Y., Hijikata, K., & Nagatani, T. (1977). Fundamental study of bubble dissolution in liquid. *International Journal of Heat and Mass Transfer*, *20*, 41–50.

Muraro, S., & Jommi, C. (2018). Implication of end restraint in triaxial tests on the derivation of the stress-dilatancy rule for soils having high compressibility. *Canadian Geotechnical Journal*, *https://doi.org/10.1139/cgj-2018-0343*.

Muraro, S., Mašín, D., & Jommi, C. (2018). Applicability of hypoplasticity to reconstituted peat from drained triaxial tests. *International Journal for Numerical and Analytical Methods in Geomechanics*, *42*, 2049–2064.

Nageswaran, S. (1983). *Effect of gas bubbles on the sea-bed behavior*. PhD thesis Oxford University, Oxford, England.

Niemunis, A. (2003). *Extended hypoplastic models for soils*. Thesis Habilitation, Inst. für Grundbau und Bodenmechanik, Bochum.

Niemunis, A., & Herle, I. (1997). Hypoplastic model for cohesionless soils with elastic strain range. *Mechanics of Cohesive and frictional Materials*, *2*, 279–299.

Nova, R. (1977). On the hardening of soils. *Archiwum Mechaniki Stosowanej*, *29*, 445–458.

Nova, R., & Wood, D. M. (1979). A constitutive model for sand in triaxial compression. *International Journal for Numerical and Analytical Methods in Geomechanics*, *3*, 255–278.

Ogino, T., Oikawa, H., Tsushima, M., & Mitachi, T. (2002). Strength characteristics of highly organic soil obtained by direct shear tests. *Doboku Gakkai Ronbunshu*, *715*, 277–285.

Ohmaki, S. (1982). Stress-strain behaviour of anisotropically, normally consolidated cohesive soil. In *Proc. 1st Int. Symp. Num. Mod. Geomech.* (pp. 250–269).

Oikawa, H., & Miyakawa, I. (1980). Undrained shear characteristics of peat. *Soils and foundations*, *20*, 91–100.

Oka, F., Kodaka, T., Kimoto, S., Ichinose, T., & Higo, Y. (2005). Strain localization of rectangular clay specimen under undrained triaxial compression conditions. In *Proceedings of the 16th International Conference on Soil Mechanics and Geotechnical Engineering* (p. 841–844). Millpress Science Publishers volume 16.

O'Kelly, B. C. (2015). Effective stress strength testing of peat. *Environmental Geotechnics*, *2*, 34–44.

O'Kelly, B. C. (2017). Measurement, interpretation and recommended use of laboratory strength properties of fibrous peat. *Geotechnical Research*, *4*, 136–171.

O'Kelly, B. C., & Zhang, L. (2013). Consolidated-drained triaxial compression testing of peat. *Geotechnical Testing Journal*, *36*, 310–321.

Olson, R. E., & Campbell, L. M. (1964). Discussion of "Importance of free ends in triaxial testing". *Journal of the Soil Mechanics and Foundations Division*, *90*, 167–173.

Ponzoni, E. (2017). *Historical constructions on natural silty soils accounting for the interaction with the atmosphere*. PhD thesis Università degli Studi di Brescia.

Potts, D. M., & Gens, A. (1984). The effect of the plastic potential in boundary value problems involving plane strain deformation. *International Journal for Numerical and Analytical Methods in Geomechanics*, *8*, 259–286.

Praastrup, U., Jakobsen, K. P., & Ibsen, L. B. (1999). Two theoretically consistent methods for analysing triaxial tests. *Computers and Geotechnics*, *25*, 157–170.

di Prisco, C., & Nova, R. (1993). A constitutive model for soil reinforced by continuous threads. *Geotextiles and Geomembranes*, *12*, 161–178.

Rad, N. S., Vianna, A. J. D., & Berre, T. (1994). Gas in soils. II: Effect of gas on undrained static and cyclic strength of sand. *Journal of geotechnical engineering*, *120*, 716–736.

Ragni, R., Wang, D., Mašín, D., Bienen, B., Cassidy, M. J., & Stanier, S. A. (2016). Numerical modelling of the effects of consolidation on jack-up spudcan penetration. *Computers and Geotechnics*, *78*, 25–37.

Reynolds, W. D., Brown, D. A., Mathur, S. P., & Overend, R. P. (1992). Effect of in-situ gas accumulation on the hydraulic conductivity of peat. *Soil Science*, *153*, 397–408.

Rezanezhad, F., Price, J. S., Quinton, W. L., Lennartz, B., Milojevic, T., & Van Cappellen, P. (2016). Structure of peat soils and implications for water storage, flow and solute transport: A review update for geochemists. *Chemical Geology*, *429*, 75–84.

Rezanezhad, F., Quinton, W. L., Price, J. S., Elliot, T. R., Elrick, D., & Shook, K. R. (2010). Influence of pore size and geometry on peat unsaturated hydraulic conductivity computed from 3D computed tomography image analysis. *Hydrological processes*, *24*, 2983–2994.

Romero, E., & Jommi, C. (2008). An insight into the role of hydraulic history on the volume changes of anisotropic clayey soils. *Water Resources Research*, *44*, 1–16.

Roscoe, K. H. (1970). The influence of strains in soil mechanics. *Géotechnique*, *20*, 129–170.

Roscoe, K. H., & Burland, J. B. (1968). On the generalized stress-strain behaviour of wet clay. In Heyman, & Leckie (Eds.), *Engineering plasticity* (p. 535–609). Cambridge: Cambridge University Press.

Roscoe, K. H., Schofield, A. N., & Thurairajah, A. (1963). Yielding of clays in states wetter than critical. *Géotechnique*, *13*, 211–240.

Rosenberry, D. O., Glaser, P. H., Siegel, D. I., & Weeks, E. P. (2003). Use of hydraulic head to estimate volumetric gas content and ebullition flux in northern peatlands. *Water Resources Research*, *39*, 1–13.

Rowe, P. W., & Barden, L. (1964). Importance of free ends in triaxial testing. *Journal of Soil Mechanics and Foundations Division*, *90*, 1–27.

Rowe, R. K., MacLean, M. D., & Soderman, K. L. (1984). Analysis of a geotextile reinforced embankment constructed on peat. *Canadian Geotechnical Journal*, *21*, 563–576.

Sander, R. (2015). Compilation of Henry's law constants (version 4.0) for water as solvent. *Atmospheric Chemistry and Physics*, *15*, 4399–4981.

Schanz, T., & Gussman, P. (1994). The influence of geometry and end restraint on the strength in triaxial compression in numerical simulation. In Smith (Ed.), *Numerical Methods in Geotechnical Engineering* (pp. 129–133). Balkema.

Sheng, D., Westerberg, B., Mattsson, H., & Axelsson, K. (1997). Effects of end restraint and strain rate in triaxial tests. *Computers and Geotechnics*, *21*, 163–182.

Shockley, W. G., & Ahlvin, R. G. (1960). Nonuniform conditions in triaxial test specimens. In *Research Conference on Shear Strength of Cohesive Soils* (pp. 341–357). ASCE.

Sills, G. C., & Gonzalez, R. (2001). Consolidation of naturally gassy soft soil. *Géotechnique*, *51*, 629–639.

Sills, G. C., Wheeler, S. J., Thomas, S. D., & Gardner, T. N. (1991). Behaviour of offshore soils containing gas bubbles. *Géotechnique*, *41*, 227–241.

Sivasithamparam, N. (2012). *Development and implementation of advanced soft soil models in finite elements*. PhD thesis University of Strathclyde.

Skempton, A. W. (1954). The pore-pressure coefficients A and B. *Géotechnique*, *4*, 143–147.

Skempton, A. W., & Petley, D. J. (1970). Ignition loss and other properties of peats and clays from Avonmouth, King's Lynn and Cranberry Moss. *Géotechnique*, *20*, 343–356.

Sobkowicz, J., & Morgenstern, N. (1984). The undrained equilibrium behaviour of gassy sediments. *Canadian Geotechnical Journal*, *21*, 439–448.

Stark, T. D., & Vettel, J. J. (1992). Bromhead ring shear test procedure. *Geotechnical Testing Journal*, *15*, 24–32.

Strack, M., Kellner, E., & Waddington, J. M. (2005). Dynamics of biogenic gas bubbles in peat and their effects on peatland biogeochemistry. *Global Biogeochemical Cycles*, *19*, 1–9.

Sultan, N., De Gennaro, V., & Puech, A. (2012). Mechanical behaviour of gas charged marine plastic sediments. *Géotechnique*, *62*, 751.

Sultan, N., Gaudin, M., Berne, S., Canals, M., Urgeles, R., & Lafuerza, S. (2007). Analysis of slope failures in submarine canyon heads: an example from the gulf of Lions. *Journal of Geophysical Research: Earth Surface*, *112*, 1–29.

Tashiro, M., Nguyen, S. H., Inagaki, M., Yamada, S., & Noda, T. (2015). Simulation of large-scale deformation of ultra-soft peaty ground under test embankment loading and investigation of effective countermeasures against residual settlement and failure. *Soils and Foundations*, *55*, 343–358.

Taylor, D. W. (1941). *Cylindrical compression research program on stress deformation and strength characteristics of soils*. Report Massachusetts Institute of Technology.

Teunissen, J. A. M., & Zwanenburg, C. (2015). An overlay model for peat. *Creep and Deformation Characteristics in Geomaterials*, (pp. 71–73).

Tokida, T., Miyazaki, T., & Mizoguchi, M. (2005). Ebullition of methane from peat with falling atmospheric pressure. *Geophysical Research Letters*, *32*, 1–4.

Tokida, T., Miyazaki, T., Mizoguchi, M., Nagata, O., Takakai, F., Kagemoto, A., & Hatano, R. (2007). Falling atmospheric pressure as a trigger for methane ebullition from peatland. *Global Biogeochemical Cycles*, *21*, 1–8.

Tsushima, M., & Mitachi, T. (1985). Influence of stress history on dilatancy characteristics of peat. *Soils and foundations*, *25*, 206–216.

Van Baars, S. (2005). The horizontal failure mechanism of the Wilnis peat dyke. *Géotechnique*, *55*, 319–323.

Van Der Putte, E. (2014). *An insight in the micro fabric of gassy and unsaturated peat*. MSc thesis Delft University of Technology.

Van Eekelen, H. A. M. (1980). Isotropic yield surfaces in three dimensions for use in soil mechanics. *International Journal for Numerical and Analytical Methods in Geomechanics*, *4*, 89–101.

Van Meindert, A., Zwanenburg, C., Van Esch, J. M., Sharp, M. K., & Mosher, R. L. (2008). Horizontal translational failures of levees due to water filled gaps. In *6th Int. Conf. on Case Histories in Geotechnical Engineering* (pp. 1–7).

Vermeer, P. A., & Neher, H. P. (1999). A soft soil model that accounts for creep. In Brinkgreve (Ed.), *Proceedings of the international symposium Beyond 2000 in Computational Geotechnics* (pp. 249–261). Balkema, Rotterdam.

Vonk, B. F., Den Haan, E., Termaat, R., & Edil, T. B. (1994). Some aspects of the engineering practice regarding peat in small polders. In E. Den Haan, R. Termaat, & T. B. Edil (Eds.), *Advances in understanding and modelling mechanical behaviour of peat* (pp. 389–402). Balkema.

Waddington, J. M., Harrison, K., Kellner, E., & Baird, A. J. (2009). Effect of atmospheric pressure and temperature on entrapped gas content in peat. *Hydrological processes*, *23*, 2970–2980.

Wheeler, S. J. (1988a). A conceptual model for soils containing large gas bubbles. *Géotechnique*, *38*, 389–397.

Wheeler, S. J. (1988b). The undrained shear strength of soils containing large gas bubbles. *Géotechnique*, *38*, 399–413.

Wheeler, S. J., Näätänen, A., Karstunen, M., & Lojander, M. (2003). An anisotropic elastoplastic model for soft clays. *Canadian Geotechnical Journal*, *40*, 403–418.

Wilde, P. (1977). Two invariants-dependent models of granular media. *Archives of Mechanics*, *26*, 799–809.

Wong, P. K. K., & Mitchell, R. J. (1975). Yielding and plastic flow of sensitive cemented clay. *Géotechnique*, *25*, 763–782.

Wood, D. M. (1990). *Soil behaviour and critical state soil mechanics*. Cambridge, UK: Cambridge University press.

Wood, D. M., Drescher, A., & Budhu, M. (1979). On the determination of stress state in the simple shear apparatus. *Geotechnical Testing Journal*, *2*, 211–221.

Yamaguchi, H. (1992). Consideration on method of triaxial test on highly organic soil. *Doboku Gakkai Ronbunshu*, *1992*, 13–22.

Yamaguchi, H., Ohira, Y., & Kogure, K. (1985a). Volume change characteristics of undisturbed fibrous peat. *Soils and foundations*, *25*, 119–134.

Yamaguchi, H., Ohira, Y., Kogure, K., & Mori, S. (1985b). Undrained shear characteristics of normally consolidated peat under triaxial compression and extension conditions. *Soils and Foundations*, *25*, 1–18.

Yamaguchi, H., Zushi, M., Ohira, Y., & Kogure, K. (1987). A few considerations on triaxial shear properties of peat. *The Japan Society of Civil Engineers, Doboku Gakkai Ronbunshu*, *1987*, 111–120.

Yang, Z. X., Zhao, C. F., Xu, C. J., Wilkinson, S. P., Cai, Y. Q., & Pan, K. (2016). Modelling the engineering behaviour of fibrous peat formed due to rapid anthropogenic terrestrialization in Hangzhou, China. *Engineering Geology*, *215*, 25–35.

Yu, H. S. (2007). *Plasticity and geotechnics* volume 13. Springer Science and Business Media.

Zhang, L., & O'Kelly, B. C. (2014). The principle of effective stress and triaxial compression testing of peat. *Proceedings of the Institution of Civil Engineers-Geotechnical Engineering*, *167*, 40–50.

Zhao, H., & Jommi, C. (2018). Consequences of drying on the engineering properties of fibrous peats: compression behaviour. *Engineering geology*, *(submitted)*.

Zwanenburg, C. (2013). Dikes on peat: analysis of field trials. Internal report. *Deltares*, *1203768-012*, 1–221.

Zwanenburg, C., Den Haan, E. J., Kruse, G. A. M., & Koelewijn, A. R. (2012). Failure of a trial embankment on peat in Booneschans, The Netherlands. *Géotechnique*, *62*, 479–490.

Zwanenburg, C., & Jardine, R. J. (2015). Laboratory, in situ and full-scale load tests to assess flood embankment stability on peat. *Géotechnique*, *65*, 309–326.

Summary

The geotechnical description of peats represents one of the main challenges in the Netherlands to assure the required safety standard and performance of the flood defence infrastructure. Almost a third of the country is situated below the sea and the rivers level with about 60% to 70% of the population and economic assets concentrated in low-laying areas prone to flooding. Flood protection in the Netherlands is assured by a vast system of primary and secondary dykes, of which 14000 km are regional dykes. Design and assessment procedure of these dykes is not straightforward, especially when peats layers are encountered. Adequate geotechnical description of the behaviour of peats at the engineering scale represents one of the biggest concerns that public water authorities and geotechnical engineers are currently facing.

The majority of the previous investigations have regarded the volumetric and time dependent behaviour of peat, both from the experimental and the modelling viewpoints. However, the information on the deviatoric counterpart is still scarce and contradictory. This has contributed to generate geotechnical uncertainties on the deviatoric behaviour of peats with severe overly conservative approaches in the current engineering practice and diffuse misconceptions within the research community on traditional experimental tests.

This thesis summarises a research effort to provide a fundamental description of the deviatoric behaviour of peat through field test, laboratory tests and numerical modelling. The importance of a correct description of the behaviour of peat is firstly outlined from a failure test on a historical rural dyke founded on a peat layer and organic silt layer. Contrarily to the common belief that peat is a weak soil, the field observations reveal that the dyke failure has not been initiated in the peat but in the organic clayey silt formation underneath. However, the exceptional deformability of the peat has been the trigger for the failure. The significant lateral bulging of the peat layer at the toe of the dyke has dragged the organic soil formation underneath to failure for shear strains well below the ones at ultimate state for the peat.

The necessity for investigating not only the failure but also and especially the pre-failure behaviour of peat is then transferred from the field scale to the laboratory scale. A first series of undrained triaxial compression tests has been carried out to define the shear strength of peat. The experimental results reveal that most of the long-lasting misconceptions on traditional experimental tests on peats, such as triaxial tests, come from dramatic end restraint effects on the observed behaviour imposed by traditional shear apparatuses. High deformability and shear strength of peat magnify the severity of end restraint on both the volumetric and deviatoric response resulting in non-negligible overestimation of shear strength parameters. Overestimation in the ultimate friction angle of 12° is found, passing from 43° to 55°, if the end restraint is not reduced or accounted for when performing triaxial

tests on peat. The influence of end restraint is not limited to the ultimate state but also extends to the pre-failure response. A second series of drained triaxial compression tests has been performed to quantify the error induced by end restraint in the derivation of the stress-dilatancy rule of peat. The experimental results combined with finite element analyses confirm that both overestimation and underestimation of the true dilatancy can be observed, depending on the deformation mode. As a whole, the incorrect interpretation of the flow rule due to end restraint effects may have relevant engineering implications on both serviceability and ultimate limit states, by respectively overestimating the displacements below K_0 condition and the shear strength for loading paths above it.

The extensive experimental results are assisted by the development of a simple elastic-plastic modelling approach for the deviatoric behaviour of reconstituted peat. For the first time, constitutive ingredients as the yield locus, the plastic potential and the hardening law have been derived directly from experimental evidence. The model has been implemented in a finite element program and the laboratory tests have been simulated as boundary value problems accounting for end restraint effects. The numerical results show qualitative good agreement with the experimental results for a wide range of loading directions and deviatoric strain up to 20% well above the deviatoric strain level relevant for serviceability and ultimate limit states in the field. However, in its current stage the model cannot be elevated as a predictive tool. The main limitation comes from the necessity of introducing matrix-fibres interaction phenomena. The experimental tests reveal a directional response in the plastic deformation mechanism for the tested peat. Previous stress history and loading direction seem to rule the plastic response for a given stress state, which translates into a non-unique relationship between the soil dilatancy and the stress ratio. Stress and strain path dependence on the evolution of the peat fabric is suggested as the responsible mechanism for the observed peculiar stress-dilatancy relationship. Stress paths accompanied by radial contraction seem not to cause relevant fabric change and the plastic deformation response does not differ substantially from the classical response of fine grained materials. On the contrary, for radial paths with radial expansion, the observed response seems to be dominated by the deviatoric strain component.

Going back to the field observations from the stress test at the Leendert de Boerspolder, the last part of the dissertation presents the results of the first experimental activity dedicated to quantify the consequences of gas bubbles on the geotechnical response of foundation peat layers. The presence of gas must be cautiously accounted for, when a reference stiffness is chosen for serviceability limit states, and when operative shear strength definitions, based on mobilised strength for given strain thresholds, are chosen in the assessment of geotechnical structures on peats. Gas exsolution and expansion decrease the average effective stress and eventually increase the soil skeleton compressibility. The compressibility of the gas phase and the delayed stretching of the fibres reduce the mobilised friction angle for comparable strain thresholds. The effects appear to become dramatic at low total stresses, which is often the case for peat foundation layers at the toe of embankments.

Samenvatting

De geotechnische beschrijving van veen is een van de belangrijkste uitdagingen bij het aantonen dat de waterkeringen van Nederland voldoen aan de vereiste veiligheidsniveaus en de beoogde functie vervullen. Bijna een derde van Nederland ligt onder de zeespiegel en de rivierpeilen. In dit laaggelegen deel is 60% tot 70% van de bevolking en het overgrote deel van de economische sector gevestigd. Dit gebied wordt tegen overstroming beschermd door een uitgestrekt netwerk van primaire en secundaire waterkeringen, waarvan 14000 km bestaat uit regionale dijken. Het ontwerp en de toetsing van deze dijken is niet eenvoudig, in het bijzonder waar veenlagen aanwezig zijn. Het grootste probleem dat momenteel wordt ervaren door geotechnische ingenieurs en desbetreffende waterschappen is het adequaat kunnen beschrijven van het geotechnisch gedrag van deze veenlagen.

Het overgrote deel van eerder onderzoek richt zich op het testen en modelleren van volumetrisch en tijdsafhankelijk gedrag van veen. Helaas is informatie over het gedrag onder deviatorische spanningen nog steeds schaars en bovendien tegenstrijdig. In de praktijk hebben geotechnische onzekerheden aangaande deviatorisch gedrag geleid tot aanzienlijk conservatieve aannames die door ingenieurs worden gehanteerd. Tevens bestaan er binnenin het geotechnisch onderzoeksveld veel misvattingen over de traditionele laboratorium proeven die meer inzicht zouden moeten bieden in deze onzekerheden.

In dit proefschrift wordt onderzoek gepresenteerd dat is uitgevoerd om aan de hand van veldtesten, laboratoriumtesten en numeriek modelleren bij te dragen aan een fundamentele beschrijving van het deviatorisch gedrag van veen. Ten eerste wordt het belang aangetoond van het hanteren van een correcte beschrijving van het gedag van veen door middel van een faaltest van een historische, landelijk gelegen dijk gepositioneerd op een veenlaag en onderliggende organische siltlaag. In tegenstelling tot de veelvoorkomende perceptie dat veen een zeer slappe grondsoort is, laten de observaties uit de veldtest zien dat het falen van de dijk niet is begonnen in de veenlaag, maar in de organisch kleiige siltlaag eronder. Echter heeft de uitzonderlijke hoge vervormingseigenschap van veen een grote rol gespeeld. De aanzienlijke vervorming van de veenlaag die optrad rondom de teen van dijk heeft aanzet gegeven tot falen van de organische siltlaag eronder, ondanks het gegeven dat de schuifspanningen in de veenlaag sterk onder de vastgestelde uiterste grenstoestand lagen. Vervolgens wordt in dit onderzoek de noodzaak uiteen gezet niet alleen het faalmechanisme te onderzoeken, maar ook het gedrag van het veen vóór het optreden van het faalmechanisme. Daarvoor wordt de stap gemaakt naar laboratoriumtesten.

Allereerst is een serie ongedraineerde triaxiaalproeven uitgevoerd om de schuifsterkte van veen vast te leggen. De resultaten bevestigen dat de veelvoorkomende misvattingen over experimentele proeven, zoals die van de traxiaalproef, ontstaan

door de sterke mate waarin het proefmonster begrensd is in de test opstelling wanneer het tot falen wordt gebracht. De invloed van deze begrenzing op zowel het volumetrisch als het deviatorisch gedrag resulteert in een significante overschatting van de parameters die de afschuifsterkte beschrijven. Zo kan voor de hoek van inwendige wrijving in plaats van 43° een hoek van 55° worden gevonden, een overschatting van 12°, als de invloed van de begrenzing niet wordt meegenomen bij het verwerken van de resultaten van de triaxiaalproef. Deze begrenzing is niet alleen van invloed op het vaststellen van de uiterste grenstoestand, maar ook op de bepaling van het gedrag voor het falen van de veenlaag. Een tweede serie van gedraineerde triaxiaalproeven is uitgevoerd om de fout te kwantificeren die wordt veroorzaakt door begrenzing van het proefmonster en die voortvloeit uit de spanning-dilatantie relatie van veen. In combinatie met een eindige elementen analyse wordt met de resultaten van deze tweede serie aangetoond dat, afhankelijk van het type vervorming, de dilatantie zowel kan worden overschat als onderschat. Het is mogelijk dat de incorrecte afleiding van de spanning-dilatantie relatie, die wordt veroorzaakt door de begrenzing van het proefmonster, gevolgen heeft voor zowel de bruikbaarheidsgrenstoestand als de uiterste grenstoestand. Bij spanningen lager dan de neutrale gronddruk K_0 worden vervormingen overschat, bij spanningscondities erboven wordt de afschuifsterkte overschat.

De resultaten van de proevenseries worden vergeleken met een eenvoudige elastisch-plastische benadering voor het deviatorisch grondgedrag. Voor het eerst zijn constitutieve componenten, zoals de de vloeigrens, de plastische potentiaal en de sterktetoename door deformatie, afgeleid vanuit experimentele proefresultaten. Deze zijn verwerkt in een eindige elementen programma en de laboratoriumproeven zijn gesimuleerd als grenswaarde problemen om het effect van de begrenzing te beschouwen. De numerieke resultaten komen goed overeen met de experimentele uitkomsten. Dit geldt voor een breed scala aan belastingpaden en deviatorische spanningen, tot wel 20% boven de spanningen relevant voor de bruikbaarheids en uiterste grenstoestanden in het veld. Echter is het model in de huidige staat nog niet bruikbaar voor het maken van predicties. De voornaamste belemmering hiervoor is de benodigde beschrijving van matrix-vezel interacties. De experimenten laten voor het plastisch vervormingsmechanisme een richtingsafhankelijk resultaat zien. Bij een bepaalde spanningstoestand zijn de eerder opgetreden spanningen en bijbehorende spanningsrichtingen van voornaamste invloed op de optredende plastisch vervormingen. Dit vertaalt zich in een niet eenduidige relatie tussen dilatantie van het veen en de spanningsratio. Dit gesuggereert dat het samenspel tussen eerdere spanning-rek toestanden en de opbouw van het veenmateriaal de oorzaak is van de geobserveerde spanning-dilatantie relatie. Het lijkt alsof spanningstoestanden die gepaard gaan met radiale contractie geen aanzienlijke veranderingen teweegbrengen in de structuur. De plastische vervorming is niet substantieel anders dan bij gangbaar fijnkorrelig materiaal. Daarentegen is het waargenomen dat de reactie van het veen op spanningstoestanden die gepaard gaan met radiale expansie voornamelijk bepaald wordt door deviatorische rek componenten.

Om terug te komen op de observaties bij de veldtest in de Leendert de Boerspolder, gaat het laatste deel van het onderzoeksrapport in op de resultaten van

de experimentele activiteiten om de invloed van gas bubbels op het geotechnisch gedrag te kwantificeren. De aanwezigheid van gas dient op een voorzichtige wijze te worden meegenomen bij de bepaling van een referentie stijfheid voor de bruikbaarheidsgrenstoestand. Ook is voorzichtigheid geboden bij het vaststellen van gangbare schuifspanningsdefinities die worden gehanteerd bij het toetsen van geotechnische constructies op veenlagen, gebaseerd op een gemobiliseerde kracht voor gegeven rektoestanden. Het uittreden en uitzetten van gas verlaagt de waarde voor de gemiddelde effectieve spanning en verhoogt uiteindelijk de samendrukbaarheid van het grondskelet. De samendrukbaarheid van het gas en de vertraagde uitrekking van de vezels verminderen de gemobiliseerde hoek van inwendige wrijving bij vergelijkbare rekgrenzen. Bij lage totaalspanningen, zoals typisch aanwezig bij de teen van een dijk, kunnen deze effecten van dramatische omvang zijn.

Acknowledgements

I express my gratitude to my promotor-supervisor-daily supervisor Prof. Cristina Jommi for her support and freedom she gave me during all my PhD.
The research presented in this thesis had the financial support of the Dutch Technology Foundation STW, part of the Netherlands Organisation for Scientific Research (NWO) under the project Reliability-Based Geomechanical Assessment Tools for Dykes and Embankments in Delta Areas (Reliable Dykes, project number 13864). It was also partly founded by Deltares through the project "Gasvorming", in the framework of the "Dijken op Veen II" financed by Rijkswaterstaat and by the FP7-PEOPLE-2012-IAPP-Marie Curie Action: "Industry-Academia Partnerships and Pathways" under the project "Monitoring systems to Assess Geotechnical Infrastructure subjected to Climatic hazards" (MAGIC, project number 324426).
Special thanks to Dr. Dominique Ngan-Tillard for her true interest and encouragement expressed during all my research and to Dr. David Mašín for his research support during my visiting period at Charles University in Prague.
I want to thank Arno Mulder, Han de Visser and Wim Verwaal for their assistance during the entire experimental activity.
Thanks to Prof. Frans Molenkamp, Dr. Anne-Catherine Dieudonné, Dr. Federico Pisanò and Tom de Gast for the nice conversations, interests and laughs during these years. Thanks to Inge and Dr. Broere for their precious help with Dutch translation. Thanks to Kostantinos for having being my research companion during my last period in Delft.
Thanks to all the colleagues and staff members of the Geo-Engineering section, and also friends and colleagues from other sections and places, in particular: Divya, Arash, Monica, Weiyuan and Haoyuan.

To you, a special thank

Roderick: my life guru;
Elisa: my experimental buddy, always in a good mood;
Edoardo: plano come un condor sulla testa di ...;
Guglielmo: my Veneto twin;
Gianfranco: my Southern counterpart;
Marco: per il postulato Muraro-Bertè.

Hongfen. Four years ago, the first time I came to pick you up at the train station, you treated me as a stranger. One year after, I became your housemate, partner and Zhouhan's father on the same day. I am wondering now what will happen in the coming years. My deepest gratitude to you and Zhouhan for your presence, help, support during every single day as only a family can do.

Papà, Mamma, Romina e Simone. Grazie per il vostro amore e per il silenzioso ma costante appoggio duranti tutti questi anni. Siete la migliore famiglia che potessi desiderare. Grazie Papà e Mamma per la vostra saggezza specialmente in questo ultimo anno.

Cristina. I used to call you boss but actually, looking backwards I was wrong. Leader suits you the most.

Is there any difference?

"The leader leads, the boss drives" (T. Roosevelt)

Were you a good leader?

"A good leader takes a little more than his share of the blame, a little less than his share of the credit" (A. H. Glasow)

Definitely yes.

Jinju

내 얘길 들어주는 단 한 사람 그대
그대가 있어 나는 살아갈 수 있어
내 생에 단 하나의 이유일수 있어
그대는
나에게 고마운 사람
살아가는 힘이 돼줘서
나 다시 꿈을 꿀 수 있게 해줘서

사랑해

Curriculum Vitæ

Stefano MURARO

13-01-1987 Born in Marostica, Italy.

Education

Since 2018 Research Assistant
Politecnico di Milano

2014-2018 PhD student
Delft University of Technology

2010-2012 Master Degree in Environmental and Land Engineering
Università degli Studi di Trento

2006-2010 Bachelor Degree in Environmental Engineering
Università degli Studi di Trento

Funded research fellowship

2012-2013 Università degli Studi di Trento, Italy

Work experience

2013 SWS Engineering, Trento, Italy

2012 Province of Vicenza: Office of Soil Protection, Italy

Awards

2018 Seal of Excellence, Marie Sklodowska-Curie actions call
H2020-MSCA-IF-2017, Proposal project 795201

List of Publications

Journal Publications

6. **Muraro, S.** and Jommi, C. (2019). Beyond misinterpretation of shear failure of peats from standard undrained triaxial tests. An experimental study. *Géotechnique*, (submitted).

5. Jommi, C., **Muraro, S.**, Trivellato, E. and Zwanenburg, C. (2018). Experimental results on the influence of gas on the mechanical response of peats. *Géotechnique*, https://doi.org/10.1680/jgeot.17.P.148.

4. **Muraro, S.** and Jommi, C. (2018). Implication of end restraint in triaxial tests on the derivation of the stress-dilatancy rule for soils having high compressibility. *Canadian Geotechnical Journal*, https://doi.org/10.1139/cgj-2018-0343.

3. **Muraro, S.**, Mašín, D. and Jommi, C. (2018). Applicability of hypoplasticity to reconstituted peat from drained triaxial tests. *International Journal for Numerical and Analytical Methods in Geomechanics* 42(17): 2049-2064, https://doi.org/10.1002/nag.2840.

2. **Muraro, S.**, Madaschi, A. and Gajo, A. (2015). Passive soil pressure on sloping ground and design of retaining structures for slope stabilization. *Géotechnique* 65(6): 507-516, https://doi.org/10.1680/geot.14.P.211.

1. **Muraro, S.**, Madaschi, A. and Gajo, A. (2014). On the reliability of 3D numerical analyses of passive piles used for slope stabilization in frictional soils. *Géotechnique* 64(6): 486-492, https://doi.org/10.1680/geot.13.T.016.

Conference proceedings

2. Jommi, C., **Muraro, S.**, Trivellato, E. and Zwanenburg, C. (2017). Evidence of the effects of free gas on the hydro-mechanical behaviour of peat. *Advances in Laboratory Testing and Modelling of Soils and Shales*, 112-119, Springer, Cham, Switzerland.

1. Jommi, C., **Muraro, S.** (2014). The geotechnical response of levees to hydraulic loads. *XXV Convegno Nazionale di Geotecnica*, 4-6 June 2014, Baveno (VB), (in Italian).

More importantly

"Remember to look up at the stars and not down at your feet. Try to make sense of what you see, and wonder about what makes the universe exist. Be curious and however difficult life may seem, there is always something you can do and succeed at. It matters that you don't just give up. Be brave, be determined, overcome the odds.
Thank you for listening"

Professor Stephen Hawking